UNIVERSITY OF SOUTHAMPTON

FACULTY OF PHYSICAL AND APPLIED SCIENCES

School of Electronics and Computer Science

AUTONOMOUS OPERATION OF A TUNABLE VIBRATION BASED ENERGY HARVESTER

By

Ivo Neftali Ayala Garcia

Thesis for the degree of Doctor of Philosophy

February 2012

UNIVERSITY OF SOUTHAMPTON

ABSTRACT

FACULTY OF PHYSICAL AND APPLIED SCIENCES
SCHOOL OF ELECTRONICS AND COMPUTER SCIENCE

Doctor of Philosophy

AUTONOMOUS OPERATION OF A TUNABLE VIBRATION BASED ENERGY HARVESTER

by Ivo Neftali Ayala Garcia

Vibration-based energy harvesters transduce kinetic energy into electrical energy, which is then utilized to power small electronic systems, like wireless sensor nodes. Vibration-based harvesters are designed with high Q-factor to maximize their power generation capability; however, this results in low bandwidth of operation. Different tuning mechanisms have been previously presented, but none is integrated as an autonomous system. The work described in this thesis outlines the development of a tunable vibration-based energy harvester that adjusts its resonant frequency to coincide with the base frequency and it is powered exclusively by the harvester.

This work builds upon an electromagnetic vibration-based energy harvester and a non-contact tuning mechanism previously developed in this research group. This thesis presents the integration of the different mechanical and electronic components required to operate the tuning mechanism with the lowest overhead power feasible; an optimal range of operation for the harvester, where the frequency bandwidth is maximized while the power used for tuning is minimized, is proposed. A closed loop frequency tuning system is presented that identifies when the base frequencies have changed and adjust the harvester resonant frequency in consequence, using the mathematical model of the harvester and the period difference between the harvester voltage and the base acceleration. Analysis of the operation of the harvester when exposed to a real application was performed. The system was modified to allow its operation under this condition.

The optimization of the power extraction and conversion was also evaluated. The flexibility of the tunable harvester to adjust its resonant frequency increases by increasing the power available to perform this adjustment. Passive extraction and conversion is preferred due to the reduced overhead power compared to active conversion.

The combined result of tuning and power extraction is a fully functional tunable energy harvester that operates autonomously. Its use as a power source for a wireless sensor node is demonstrated in this thesis.

Contents

Chapter 6 Harvester performance at high and real environmental acceleration 159

List of Figures

List of Tables

Declaration of Authorship

I, Ivo Neftali Ayala Garcia declare that the thesis entitled **Autonomous Operation of a Tunable Vibration Based Energy Harvester** and the work presented in it are my own. I confirm that:

- this work was done wholly or mainly while in candidature for a research degree at this University;
- where any part of this thesis has previously been submitted for a degree or any other qualification at this University or any other institution, this has been clearly stated;
- where I have consulted the published work of others, this is always clearly attributed;
- where I have quoted from the work of others, the source is always given. With the exception of such quotations, this thesis is entirely my own work;
- I have acknowledged all main sources of help;
- where the thesis is based on work done by myself jointly with others, I have made clear exactly what was done by others and what I have contributed myself;
- parts of this work have been published as listed in section 1.4 of the thesis.

Signed: ………………………………………………………………………..

Date:……………………………………………………………………………

Acknowledgments

I am deeply grateful to my advisors, Prof. Steve P. Beeby and Dr. M. John Tudor, who have always supported and guided my research since the earliest stages of my work as a MSc student at the University of Southampton. I would like to express my gratitude for his technical advice and friendship to Dr. Dibin Zhu. Also to my internal examiners Dr. Nick R. Harris and Prof. Michael Brennan.

I acknowledge the support of the Mexican government through the National Council on Science and Technology (CONACYT) for the scholarship awarded to pursue my PhD.

To all my colleagues and friends at ESD who made this a much better place to work day after day. Russel Torah for his advice on technical matters and for passing on his experiences as a new father. Neil Grabham, Elena Koukharenko, Alex Weddel, Leran Wang, Cheryl Metcalf, Geoff Merret. Likewise, I want to thanks all the people who have contributed with their friendship and support to complete this journey, my friends from bay 5: Noreha, Stephen, Somphop, Yang, Ahmed, Asmahan, Kiwi, Adam, Hamed, Anton, Joseph. To Peter and Steve for their friendship and support during our life in Southampton.

Finally, this work would not be possible without the constant support, care and encouragement of my beloved wife Miriam. To whom I owe all my appreciation and endless love. To my dear son Emilio whose light has given me the energy to finish my research.

Nomenclature

a	Acceleration
F	Axial load
F_b	Compressive axial force
c	Damping coefficient
g	Earth acceleration
ε	Electromagnetic force
ω	Excitation frequency
ω_n	Natural frequency
Φ_B	Magnetic flux
m	Mass
N	Number of wire turns in a coil
λ	Output voltage to input voltage ratio
ϕ	Phase of the displacement with respect to the exciting force
f_r	Resonant frequency
k	Spring stiffness
h_o	Stopper position
ζ_T	Total damping

Abbreviations

ATVA	Adaptive tuned vibration absorbers
ADC	Analogue to digital converter
BeCu	Berilium copper alloy
ESR	Equivalent series resistance
FEA	Finite element analysis
HUMS	Health and usage monitoring
CMOS	Metal oxide semiconductor
MOSFET	Metal oxide semiconductor field effect transistor
NdFeB	Neodymium, iron and boron alloy magnet
PSD	Power spectral density
RF	Radio frequency
SSHI	Synchronised switch harvesting on inductor
VM	Voltage multiplier

Chapter 1

Introduction

1.1 Research Objectives

Advances in low power electronics technology, radio frequency transmission, data computation, sensing and microelectromechanical systems have led to a broad range of wireless sensing applications and the development of wireless sensor nodes. The life span of such a system is constrained to the battery life. Energy harvesting offers a solution for this limitation by either expanding the battery life or completely replacing it.

Vibration-based micro-generators produce power levels of hundreds of microwatts to several milliwats [1] which is sufficient to power modern low power circuits. There is a major challenge that such systems must comply; their resonance frequency must coincide with that of the driving force. Numerous vibration-based energy harvesters have been demonstrated that operate on the principle of resonance with a high-Q factor, effectively multiplying the source amplitude and increasing the energy output. However their performance drops significantly when the resonant frequency of the harvester and the source frequency do not coincide, thus limiting the practical application of vibration-based harvesting to those environments where the ambient frequency remains constant. There are examples in the literature that address this limitation by tuning the harvester [2], but none presents a fully functional system.

They rely on manual adjustment or an external power source to adjust the harvester resonant frequency.

This research focuses on the development of an autonomous tunable energy harvester system based upon a magnetically tuned harvester [3]. The aim is to maximize the power generated while increasing the bandwidth of operation of the harvester. The harvester resonant frequency is adjusted to match the source frequency, whilst the tuning mechanism and control system are powered exclusively by the energy generated by the harvester. Additionally the power extraction and conversion are optimized to increase the power available for the application electronics, e.g. wireless sensor node.

1.2 Statement of Novelty

Novelties in this thesis include:

- Development of an autonomous tunable energy harvester that uses a closed loop control system to adjust the resonant frequency of the harvester to match the base frequency, relying exclusively on the energy harvested.
- Design and validation of an over acceleration protection mechanism that prevents the physical contact between the harvester and its frame.
- Operation of a tunable energy harvester when exposed to a real environment excitation.
- Experimental analysis of a tuning mechanism based on the variation of magnetic flux by inserting a flux guide between tuning magnets.

1.3 Document structure

Chapter 2 presents a literature review on previous work in the field of vibration-based energy harvesting. The strategies to increase the bandwidth of operation and the methods to extract energy from these devices are discussed.

Chapter 3 describes the development of a tunable energy harvesting. The mechanical and electrical components of the system are presented and evaluated.

Chapter 4 presents the characterization of the tunable energy harvester. The optimal frequency band of operation is discussed and two control strategies are proposed and evaluated. This chapter finishes with the evaluation of the autonomous operation of the tunable energy harvester.

Chapter 5 builds on the results of chapter 4 and details the further optimization of the tunable energy harvester by improving the performance of the energy extraction and conversion. The optimized operation of the autonomous tunable energy harvester and its function as a power source for an autonomous wireless sensor node are presented.

Chapter 6 describes the design of a protection mechanism that prevents the physical contact between the harvester and its frame at high acceleration. It then looks at the operation of the tunable energy harvester for a real environmental frequency spectrum and details on the modifications required to adjust the harvester resonant frequency under this condition.

Chapter 7 introduces an alternative tuning method based on the variation of the magnetic flux between the tuning magnets by inserting a flux guide. Experimental tests of the tuning mechanism for three different designs are presented and the optimal design and range of operation are proposed. Numerical simulations of the magnetic flux are detailed and discussed.

This thesis concludes in Chapter 8, which summarises the conclusions that have been drawn from this thesis and outlines further opportunities in the research field.

1.4 Published Papers

1. I. N. Ayala-Garcia, D. Zhu, M. J. Tudor, and S. P. Beeby, "A tunable kinetic energy harvester with dynamic over range protection," Smart Materials and Structures, vol. 19, 2010.

2. L. Wang, T. Kazmierski, B. Al-Hashimi, A. S. Weddell, G. V. Merrett, and I. N. Ayala-Garcia, "Accelerated simulation of tunable vibration energy harvesting systems using a linearised state-space technique," in Design, Test and Automation in Europe, Grenoble, France, 2011.

3. I. N. Ayala, D. Zhu, M. J. Tudor, and S. P. Beeby, "Over Range Protection for a Tunable Kinetic Energy Harvester," in Technical Digest PowerMEMS 2010, Leuven, Belgium, 2010, pp. 9-12.

4. I. N. Ayala, D. Zhu, M. J. Tudor, and S. P. Beeby, "Autonomous Tunable Energy Harvester," in Technical Digest PowerMEMS 2009, Washington, USA, 2009, pp. 49-52.

5. R. N. Torah, M. J. Tudor, K. Patel, I. N. Garcia, and S. P. Beeby, "Autonomous Low Power Microsystem Powered by Vibration Energy Harvesting," IEEE Sensors, pp. 264-267, 2007.

Chapter 2

Tunable energy harvesting

2.1 Introduction

This chapter presents an overview of the technologies and strategies related to the increase in performance of vibration-based energy harvesters. Energy harvesting principles are introduced in Section 2.2. The model for vibration-based energy harvesting is presented in Section 2.3. Section 2.4 discusses strategies to increase their bandwidth of operation. Power management schemes to maximize the energy harvested are presented in Section 2.5.

2.2 Energy harvesting

Energy harvesting is defined as the process of converting or transducing energy from an ambient energy source into electrical energy to power an electronic device [4]. This ambient energy is freely available within the environment where the harvester is deployed, either as an excess or by-product of a process, e.g. vibration, heat; or naturally available, e.g. solar radiation.

The interest in energy harvesting arises from its potential use in applications of small size, stand-alone electronics systems with low power consumption, like environmental sensing nodes. Energy harvesting in sensor nodes will augment the life cycle of the finite power source, e.g. battery, or eliminate it completely. It could also save the economic costs related to a wired power connection or the periodic replacement of the finite power source and the potential risks associated to human activity.

The removal of the human factor during the operation of these sensors brings a new range of opportunities for applications where the costs and risks related to their operation previously surpassed the benefits. Areas like healthcare [5, 6], health and usage monitoring (HUMS) [7], and machinery and structural monitoring [8], to mention just a few.

A first consideration when using energy harvesting techniques is the availability and type of an energy source in the surroundings of the sensing node to which the harvester has to be adapted in consequence. The most common sources exploited for energy harvesting are photovoltaic, thermoelectric, electromagnetic radiation and kinetic energy [1]. Photovoltaic is the most commonly exploited source of energy. Solar radiation and indoor illumination provide sufficient energy to power calculators and wristwatches [9]. Thermal harvesters rely on a thermal gradient to generate energy, for example the temperature difference between the human body and ambient [10-12]. Inductive scavengers make use of the energy associated with electromagnetic radiation from sources like radio and microwave communications to produce energy; e.g. passive radio frequency (RF) tags for automatic identification and surveillance [13]. Kinetic energy is present in any object in motion including flowing fluids like air [14] water [15], and solids that are exposed to vibrational or oscillatory motion [1]. Kinetic energy is regarded as the most versatile and ubiquitous [16], therefore offering the greatest potential for energy harvesting use. For this reason, the research presented here focuses on kinetic energy, in the form of energy harvesting from mechanical vibration, i.e. vibration-based energy harvesting.

A second consideration is the continuous availability of such an energy source. If the original source of energy is not available all the time, some sort of storage should be included to collect energy for future use. A third consideration, and the most important, is the energy levels available for harvesting. The power that can be harvested from harvester with a volume lower than 10 cm^3 is in the order of tens of microwatts to tens of milliwatts [16]. The increasing interest in energy harvesting not only comes from the new strategies to transduce energy, but mainly from the reduction in energy consumption on the electrical devices that can be powered. The development of low power electronics including radio frequency transmission, data computation, sensing and microelectromechanical systems have reduced enormously the energy required for their operation. For example, a heartbeat monitor can potentially consume between 10 to 20 μW [16]. The joint use of energy harvesting techniques and low power electronics has created an increasing number of self-powered systems, or autonomous wireless sensor nodes [4].

An autonomous wireless sensor nodes is comprised of three main elements: transduction mechanism, power conditioning and storage, and electric load [17]. The transduction mechanism converts the energy from one type to electric energy. The power conditioning compromises all the elements required to rectify, adjust and store the energy extracted from the transduction mechanism to be used by the electric load. Finally, the electric load relates to the electric components that sense the environment, process and transmit the information collected, and the control entity that operates the entire node.

2.3 Vibration-based energy harvesting

A vibration-based harvester subject to base excitation is modelled as a second-order spring-mass inertial resonator with a linear damper. Figure 2-1 shows the model for the inertial resonator where m is the seismic mass, k the spring stiffness, c_T damping coefficient (mechanical and electrical in the generator), z displacement of the seismic mass relative to the base, y displacement of the base, and x absolute displacement of the seismic mass. Assuming and harmonic base excitation, the differential equation of motion [1, 18] is described in equation (2-1), where m is the seismic mass, c is the damping constant and k is the linear spring constant.

$$m\ddot{z}(t) + c\dot{z}(t) + kz(t) = -m\ddot{y}(t) \tag{2-1}$$

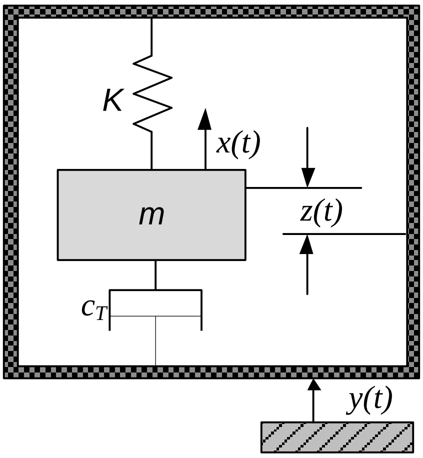

Figure 2-1. Model of a linear, inertial resonator [1]

The power dissipated in the generator is given by equation (2-2) [19], where ω_n is the natural frequency, ζ_T is the total damping ratio and ω is the excitation frequency

$$P_d = \frac{m\,\zeta_T\,Y^2 \left(\frac{\omega}{\omega_n}\right)^3 \omega^3}{\left[1-\left(\frac{\omega}{\omega_n}\right)^2\right]^2 + \left[2\,\zeta_T\,\left(\frac{\omega}{\omega_n}\right)\right]^2} \tag{2-2}$$

The maximum power occurs when the generator operates at resonance, i.e. $\omega = \omega_n$. The theoretical maximum power dissipated in the damper, which include the power transduced and the parasitic mechanical damping, is given by:

$$P = \frac{m\,Y^2 \omega_n^3}{4\,\zeta_T} \tag{2-3}$$

It is found from equation (2-3) that the power can be maximized by increasing the seismic mass, operating the generator at resonance and, as will be discussed next, having a high quality factor (Q-factor). The quality factor Q_T is defined as the ratio between the relative displacement of the mass z and the displacement of the base y, it is given by equation (2-4).

$$Q_T = \frac{1}{2\,\zeta_T} \tag{2-4}$$

It is found that the power at the generator is inversely proportional to the damping, i.e. proportional to the Quality-factor. Hence more power can be generated if the generator is designed with a high Quality-factor. However this has the inverse effect on the bandwidth, reducing the frequency range of operation of the harvester, as shown in figure 2-2.

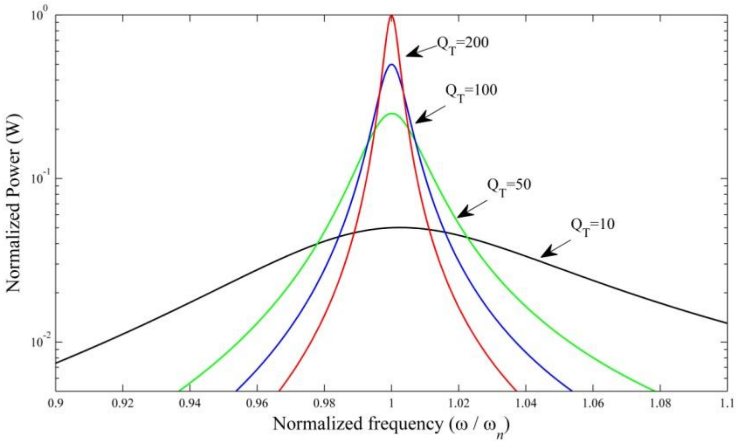

Figure 2-2. Power spectrum of generator at various Quality-factors

2.4 Strategies to increase the frequency range of energy harvesters

Most of the research groups investigating energy harvesting technology have considered the optimal case of operation, where the base acceleration and frequency levels are constant and invariable in time. Vibration-based energy harvesters are designed with a high Q-factor, which results in high levels of amplification of the seismic mass displacement, increasing the power generation [20]. For the ideal case of operation, the harvester can be designed with a high Q-factor, maximizing its power generation. However, it is important to consider that the kinetic energy transduced by the harvester is a subproduct of the normal operation of the subject under inspection, e.g. machinery. Therefore its excitation, either displacement or frequency, may vary over time.

Variations on the acceleration level do not represent a disadvantage by itself, as long as the level is high enough to generate energy for the operation of the node. The challenges reside on the joint effect that high acceleration and high Q-factor have on the harvester. The displacement of the seismic mass is a multiple of the Q-factor. Hence as the acceleration increases, the displacement increases even more for high Q-factor harvesters. This could result in the harvester crashing against its frame or stressing the harvester’s structure beyond its yield strength, resulting in permanent damage. While high Q-factor is advantageous to generate more energy for a given acceleration level, it has the inverse effect on the bandwidth of operation. The Q-factor is inversely proportional to the frequency bandwidth. For a harvester with a high Q-factor, a small variation between its resonant frequency and the base frequency will result in a drastic drop in its displacement, hence, its power generation. A low Q-factor structure can be used to widen the bandwidth of operation, but this reduces the power generated [18], as shown in figure 2-2.

A practical vibration-based energy harvester must address these two fluctuations and act in consequence to generate the maximum power feasible without exceeding its maximum amplitude. Also, it must compensate for any variations in the building process of the harvester itself that can alter the mechanical and electrical characteristic of the harvester, e.g. its resonance frequency.

Different methodologies have been proposed by research groups to improve the performance of the vibration-based harvester under a wider range of frequencies. Zhu, et al [2] presented a recent review on these techniques, categorizing them into two groups. The first group focuses its attention on widening the bandwidth of the generator, while the second attempts to adjust the resonant frequency of the harvester. Both approaches will be discussed next, comparing the benefits and weaknesses. The present research also reports on the first mechanism designed to protect the harvester from over acceleration.

2.4.1 Widening bandwidth of the harvester

Methods to widen bandwidth, as the definition implies, use structures that have a wider bandwidth due to their mechanical design and do not require further adjustment during operation. Different methods are reported in the literature: array of structures, amplitude limiter, bi-stable structures, large inertial mass and non-linear springs. Some examples are presented next.

2.4.1.1 Array of structures

These designs comprise an array of structures, each structure designed with a particular resonance frequency. The frequencies overlap widening the bandwidth of operation of the harvester.

Shahruz [21] presents an analysis on the design of an array of cantilevers with the same dimensions but different masses at the free end, hence different natural frequencies. Similarly Ferrari, et al. [22] present a design of a multiple frequency converter array formed by three cantilevers. Each cantilever has a distinctive natural frequency. The structure and frequency response of the converter is shown in figure 2-3. The combined output power was not given by the authors but it was shown that it produces enough power to operate a RF transmitter intermittently every 6 to 21 s, depending on the excitation frequency. The excitation level was maintained at 9.81 $ms^{-2}{}_{(rms)}$ and the output voltage from each cantilever was conditioned using a 2 stage voltage multiplier (VM), and then connected to a storage capacitor.

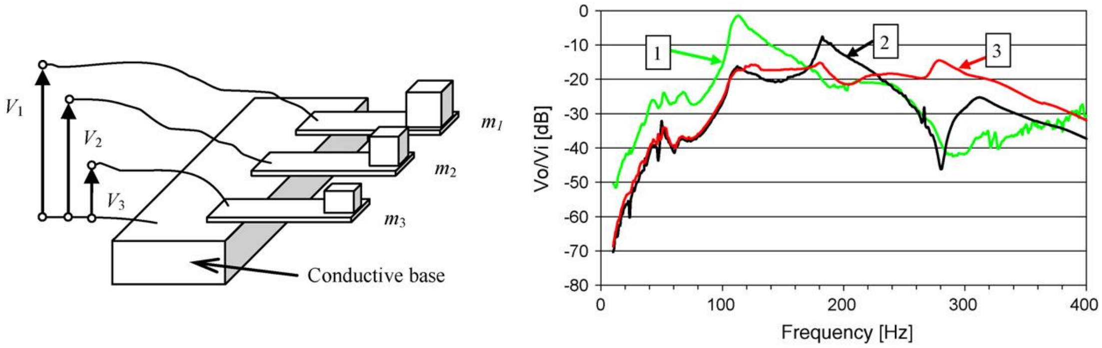

a. Structure of the piezoelectric energy array

b. Frequency response of the piezoelectric cantilevers. The number represents each particular cantilever in the array.

Figure 2-3. Multifrequency converter array [22]

Sari, et al. [23-25] reported an electromagnetic generator for wideband vibrations, shown in figure 2-4. The generator has multiple cantilevers, each with different length, and therefore natural frequency. The cantilevers are connected in series overlapping their frequency spectrum. The peak power of each individual cantilever is in close range with the neighbour cantilever resulting in an increasing power generation as shown in figure 2-4. Experimental analysis shows a steady power generation, delivered into its optimal load, of 0.4 μW at an excitation average level of 490 ms^{-2}. The frequency band expands from 4.2 to 5 kHz using 35 cantilevers, achieving a bandwidth of operation of 800 Hz.

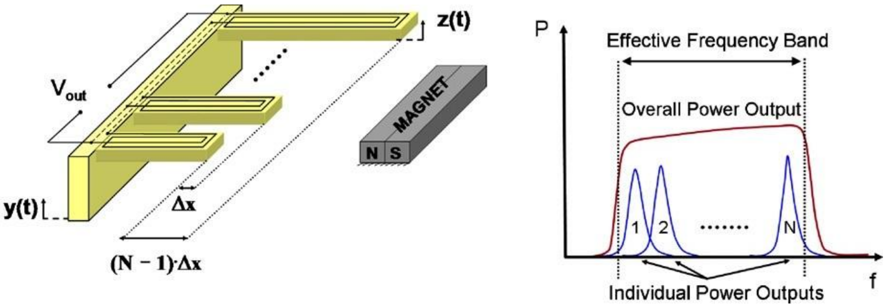

a. Muticantilever structure b. Power bandwidth

Figure 2-4. Electromagnetic generator for wideband vibrations (modified from [24])

Liu, et al. [26] also present an energy harvester comprising an array of piezoelectric cantilevers, as shown in figure 2-5. Each cantilever is designed with a different length, width and mass; hence a different resonance frequency. This effectively broadens the frequency response of the entire device. Experimental tests were performed using only three cantilevers from the entire array; no information on the bandwidth of operation is presented. The output voltage was 3.06 V if the cantilevers are connected in series without previous rectification; while connecting them after AC-DC rectification brings the voltage to 3.93 V. In the first case, the phase difference between each individual voltage reduces the total output voltage of the array. Meanwhile, for the series connection case, each individual voltage is added to generate a higher output voltage.

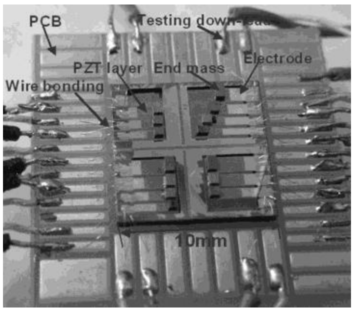

Figure 2-5. Power generator array prototype [26]

Shaofan, et al. [27] also proposed a multi cantilever structure. The cantilevers are mounted on a beam which is clamped at both ends as shown in figure 2-6. Unlike the previous designs, in this case the transduction element, in the form of a piezoelectric composite is located directly on the beam, not in the cantilevers. The energy is harvested by the strain produced on the beam when the cantilevers are excited at their resonant frequency.

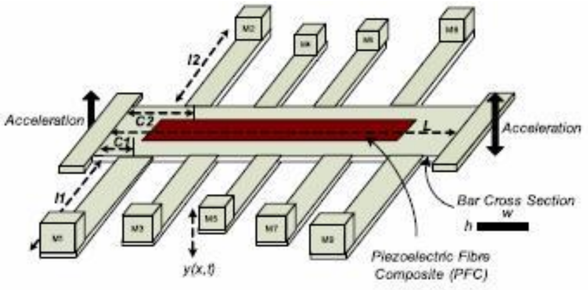

Figure 2-6. Multiple cantilever structure(modified from [27])

While the use an of array of structures for vibration-based energy harvesting can increase the bandwidth of operation in comparison to those using a single structure, a number of limitations have to be considered, as follows:

1. There is a physical limit in the number of cantilevers that the harvester can accommodate. It is not possible to expand its bandwidth indefinitely.
2. A reduced number of cantilevers will be generating power at any given time; the rest will be out of resonance not producing energy, wasting physical space.
3. The resonant frequency spacing and the number of structures affects the bandwidth and overall power generation. For a fixed number of

cantilevers, increasing the frequency spacing increases the bandwidth but results in discontinuous power output, as shown in figure 2-7a. Reduction in the spacing reduces the bandwidth but produces a higher and more uniform power generation, as shown in the example in figure 2-7b and figure 2-7c.

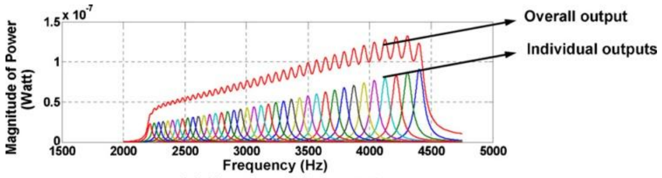

(a) 10 μm length increment

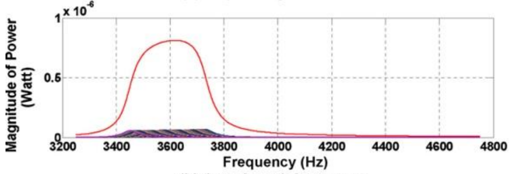

(b) 1 μm length increment

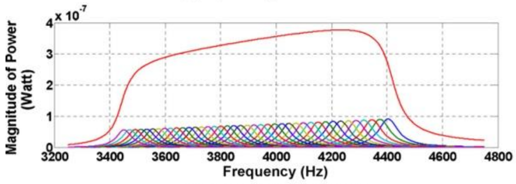

(c) 3 μm length increment

Figure 2-7. Multicantilever power.
Simulated output power of 40 cantilevers with different length increment [24]

2.4.1.2 Amplitude limiter

Soliman, et al. [28, 29] present a design comprising a single cantilever with the addition of an external stopper. Figure 2-8a shows a schematic of the harvester with stopper. The stopper is placed within the stroke of the cantilever. When the cantilever moves, it engages the stopper, increasing its stiffness, hence its resonance frequency, widening its bandwidth in comparison to a standard un-impeded cantilever. However, this effect only occurs in a frequency up-sweep. The down-sweep bandwidth is equal to the standard cantilever, as presented in figure 2-8b.

The power generated is also affected by the presence of the stopper. As the position of the stopper increases (h_0 in figure 2-8a), the power increases. However, the up-sweep bandwidth reduces. If h_0 is further increased, the bandwidth profile approaches that where the stopper is not present, as shown in figure 2-9.

The constant contact between the cantilever and the stopper raises questions regarding the physical damage that this could produce over time and the possible repercussion in the lifetime of the generator and its performance. The authors do not provide information regarding this effect.

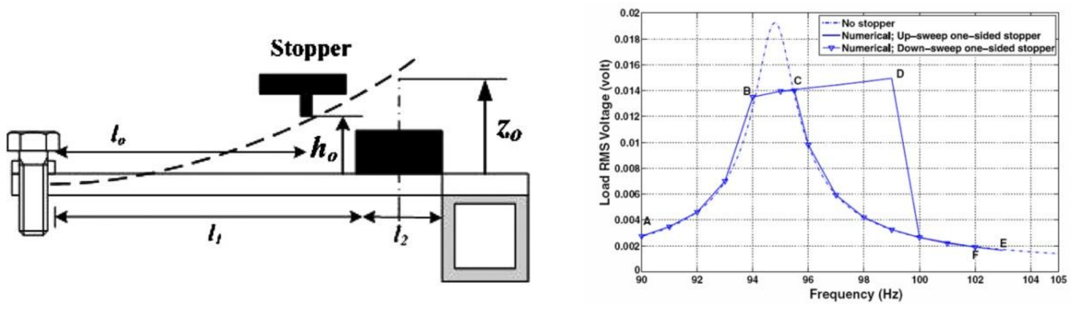

a. Schematic b. Numerical frequency-response

Figure 2-8. Harvester with stopper (modified from [28])

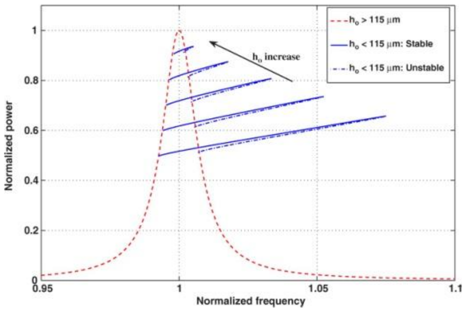

Figure 2-9. Frequency-response curves.
Harvester with stopper as the stopper height increases [29]

2.4.1.3 Bistable structures

Bistable structures alter their displacement between two possible stable conditions as a function of a mechanical excitation. Dogheche, et al.[30, 31] report on an ultrasonic transducer for energy harvesting that generates energy when a membrane is deformed by inertial excitation, shown in figure 2-10. A piezoelectric material, acting as the transduction mechanism, is placed on one side of the membrane. As the membrane moves between opposite stable positions, the piezoelectric is stressed generating energy.

Simulations show two mechanical behaviours on the membrane. The first is the linear or elastic behaviour where the membrane does not reach a minimum displacement threshold to move to the opposite stable state. The second is the bistable behaviour where the membrane moves from one stable position to its opposite as is observed when the output voltage from the device produces two opposite and equal voltages. In both cases the transducer can generate energy, but only the bistable state power is reported as 2 nW.

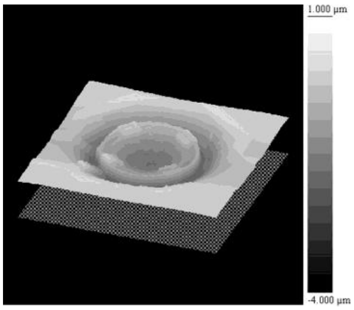

Figure 2-10. Surface profile of piezoelectric ultrasonic transducer [31]

Ramlan, et al. [32, 33] describes a bistable mechanism that has the effect of increasing the displacement of the mass resulting in a higher velocity for a given input excitation. The mechanism, also called "snap-through", consists of two linear springs at an angle θ, as shown in figure 2-11. This arrangement results in a non-linear restoring force in the x-direction.

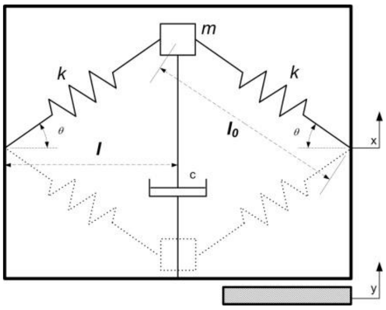

Figure 2-11. Snap-through mechanism (modified from [32])

If the amplitude of excitation is small, the mechanism oscillates about one of its stable states. As the amplitude increases, the mechanism starts to oscillate between its two stable states. Figure 2-12 shows the harvested power comparison between a linear device and the snap-through harvesters, where γ is defined as $\gamma = \frac{l}{l_0}$ in figure 2-11. The snap-through mechanism exceeds the performance of the linear device at lower frequencies than its resonance frequency. This is because the power generation in the linear system drops rapidly as the frequency moves away from resonance, Ω=0 in figure 2-12. However, the snap-through mechanism presents a linear response, even at low frequencies, when γ is small because more force is required to oscillate between its stable positions. This effect can be seen in figure 2-12, the power generated by the snap-through mechanism has a similar performance than that of a linear harvester when Ω is lower than 0.2.

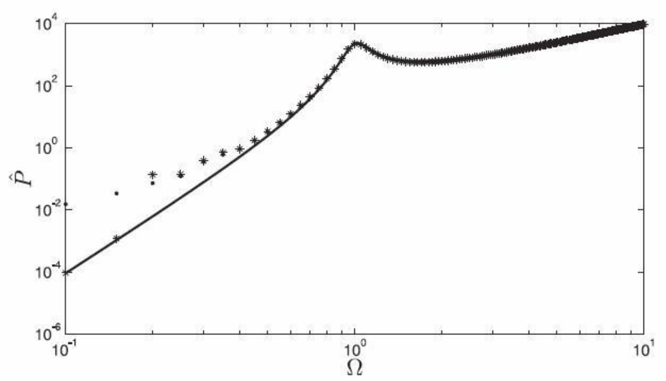

Figure 2-12. Harvested power comparison.
Linear mechanism (--), snap-through mechanism with $\gamma = 0.1$ (∗) and $\gamma = 0.5$ (•) [33].

Ramlan, et al. [34] outlines that if optimally tuned, the theoretical maximum power that the snap-through mechanism can produce is at most 4/π times greater than the linear case. However this case may not be achievable because the rise time, which is the time taken by the mechanism to move from one stable position to its counterpart position must be much shorter than a quarter of the period of oscillation. The rise time is further limited by the presence of the mass and the damping. As the frequency increases, the system produces a sinusoidal wave that results in a similar amount of power than that produced by the linear device, as shown in figure 2-12.

Andó, et al. [35] present a bistable mechanism compromising a cantilever shaped piezoelectric energy harvester with a permanent magnet attached to the tip end. A second external permanent magnet is aligned to the tip end with the same polarity on each side, as shown in figure 2-13a. The non-linear behaviour of the cantilever increases as the distance between the cantilever and the external magnet decreases, creating two stable positions, described as x_1 and x_2 in figure 2-13b. Experimental tests show that the displacement of the bistable mechanism surpasses that of the linear system, especially for frequencies below the resonant frequency of the device at 400 Hz, as depicted in figure 2-14.

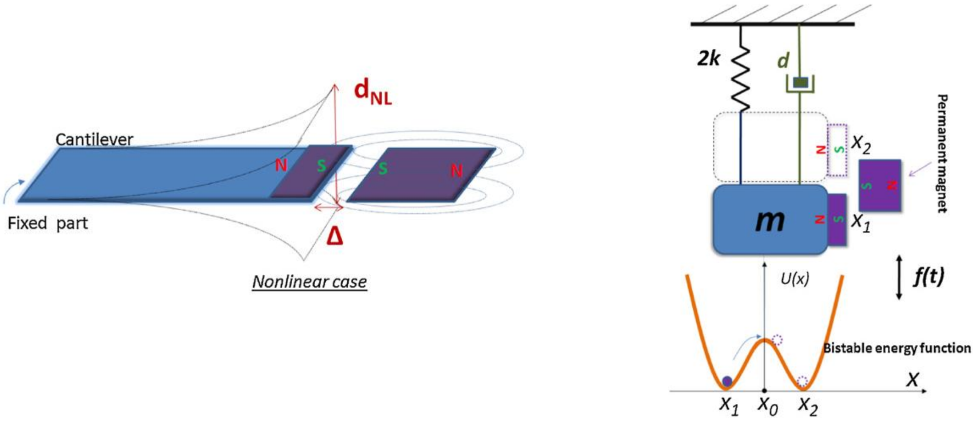

a. Schematic b. Model

Figure 2-13. Bistable MEMS energy harvester (modified from [35])

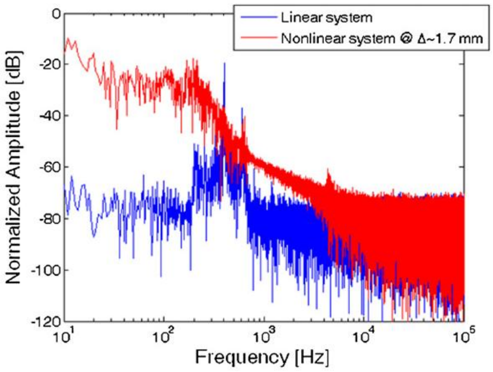

Figure 2-14. Bistable mechanism displacement spectrum at an acceleration of 7.7 ms^{-2} [35]

2.4.1.4 Non-linear spring-mass harvester

Non-linear behaviour appears on resonant structures, as the spring-mass harvester, when the excitation amplitude increases. The restoring forces become a non-linear function of the displacement, as detailed by Beeby, et al [36]. Non-linear harvesters have advantage over linear harvesters due to their effect of shifting the resonance frequency as the amplitude of vibration increases with the potential for a wider bandwidth response compared to the linear case.

Inertial-based harvesters are commonly modelled as a second-order spring-mass systems, as presented in section 2.3. The addition of the non-linearity requires the inclusion of the third-order term in equation (2-1). The equation of motion for a non-linear spring-mass system can be written in the form of the Duffing equation [37] as presented in equation (2-5), where k_1 is the linear spring constant and k_3 is the third-order spring constant.

$$m\ddot{z}(t) + c\dot{z}(t) + k_1 z(t) + \ k_3 z(t)^3 = -m\ddot{y}(t) \tag{2-5}$$

When the third-order term has a positive coefficient, the peak in the mass amplitude displacement versus frequency bends toward a higher frequency, then the spring system is referred as "hard spring". When the third-order term has a negative coefficient, the peak bends towards lower frequency, the spring is considered as a "soft spring". Finally, when the third-order term is zero, the spring shows a linear response. Figure 2-15 shows a schematic with the three different cases.

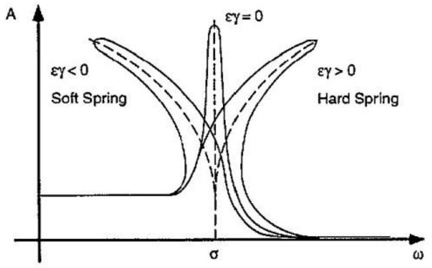

Figure 2-15. Schematic illustration of non-linear frequency response.
γ corresponds to the third-order spring constant [38].

However there are limitations for non-linear systems. They can produce more than one stable solution, or state, depending on the initial conditions. This translates into an energy harvester with the potential to generate more power for a given set of conditions, but also it may fall on the low energy solution, where it will produce less power than its linear counterpart.

The non-linear effect on the amplitude can be observed in figure 2-16. The jump phenomenon, as named in [39], is the sudden discontinuous jump in amplitude near resonance. For the hard spring in figure 2-16, with the increase in frequency, the amplitude gradually increases until point “a”. It suddenly drops to a lower value on point “b”, or low energy state and diminishes along the curve to its right. In decreasing frequency from point “c”, the amplitude decreases passing point “b”, increasing until point “d”. It then suddenly jumps to a larger amplitude in point “e”, and continue decreasing along the curve to the right.

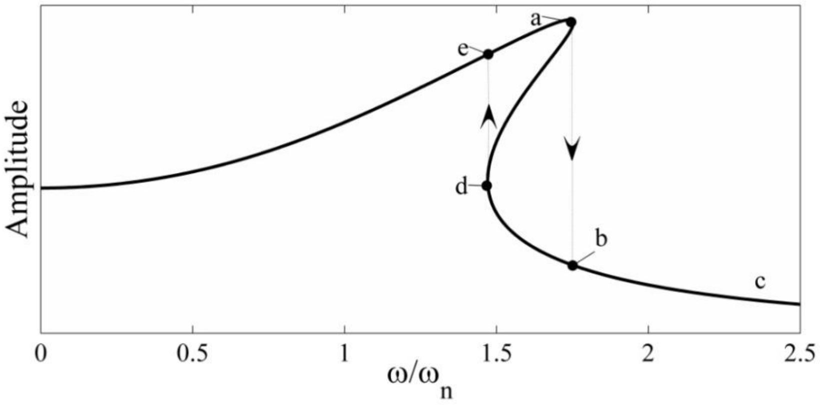

Figure 2-16. Effect of non-linearity on the response of resonant structures, hard spring.(modified from [39])

Ramlan, et al. [40] investigate the benefits of a hard-spring harvester for energy harvesting. This type of non-linear system provides a wider bandwidth than the linear system by shifting the resonance frequency as the amplitude increases. The power generation is the same as for the linear system although this may occur at a different frequency, as shown in the numerical analysis in figure 2-17.

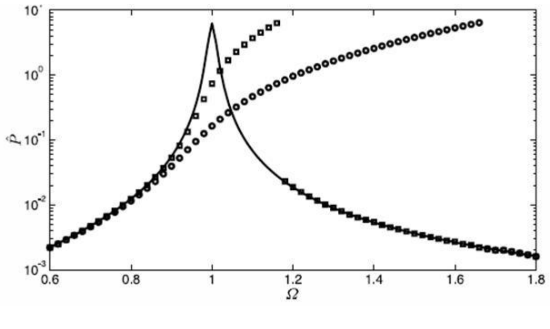

Figure 2-17. Numerical solution for non-dimensional power harvested [40]. Linear system (solid line), hardening system α = 0.001 (☐) and α = 0.01 (°)

Burrow, et al. [37, 41] present a resonant generator with a non-linear response due to the addition of reluctance forces. The generator is formed by two opposite polarized "c" cores attached to the free-end of a cantilever, formed from NdFeB magnets and iron in a manner that forces the magnetic flux through the stator in alternate directions as the cantilever moves, as shown in figure 2-18a. The measured frequency response of the generator, figure 2-18b, shows possible stable states that the generator can produce depending on whether the frequency increases or decreases.

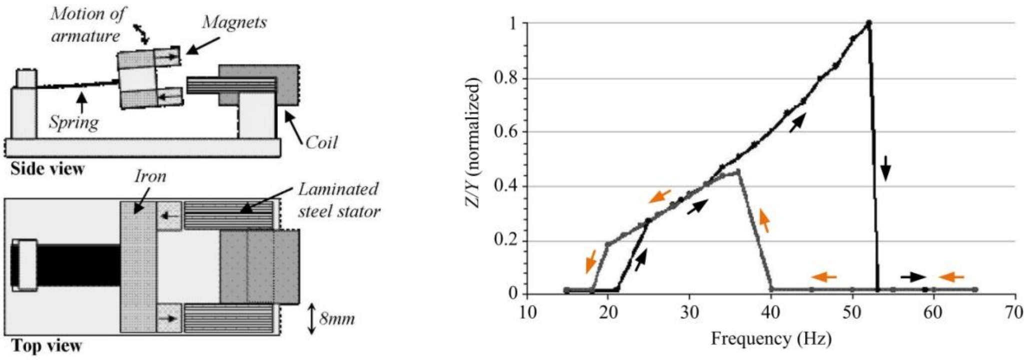

a. Layout

b. Frequency response

Figure 2-18. Resonant Generator with non-linear compliance
(modified from [41])

Burrow, et al. [42] further investigated the effects of sinusoidal excitation and narrow-band random signal excitation on the non-linear oscillator. In the first case, the harvester operates in a near-linear regime when the amplitude of excitation is small. For large excitations, the non-linear response greatly increases the bandwidth of the harvester, resulting in a large hysteresis loop. For the case of narrow-band excitation, the behaviour of the oscillator appears increasingly linear as the frequency rises. This is explained due to shortage of force from the random excitation to bring the harvester to the high-energy level.

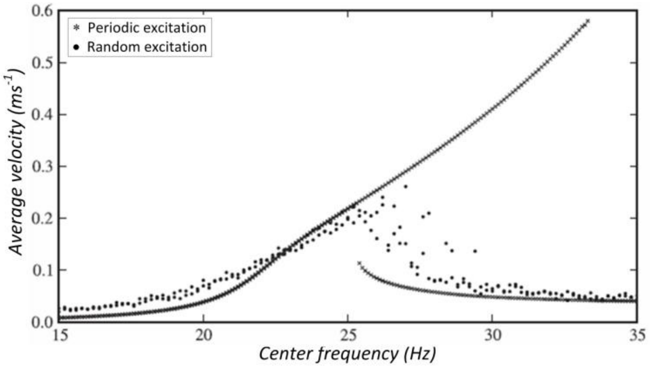

Figure 2-19. Frequency response to pure-tone excitation and a narrow-band random signal (2Hz bandwidth) [42]

Stanton, et al. [43] reported on a reversible hysteresis energy harvesting. The harvester consists of a spring-mass harvester with a magnet attached to its free-end. Two stationary magnets are manually placed either behind or ahead of the mass, as shown in figure 2-20. This arrangement produces a hardening or softening response respectively as shown in figure 2-21. The harvester's linear resonance is 12 Hz and it produces around 4.8 mW at 2.943 ms^{-2}, delivered into a resistive load, and -3dB bandwidth of 1 Hz, approximately. The reversible hysteresis mechanism has the potential to increase the bandwidth to 3 Hz when using the softening configuration and 1.2 Hz using the hardening configuration. In both cases, the position of the magnet was not optimized and the authors considered only the cases where the harvester occupies the high-energy level. Stanton discusses the advantage of a mechanical or electrical perturbation if the harvester takes a low-energy level that could bring the harvester back to the high-energy, but no further details are provided.

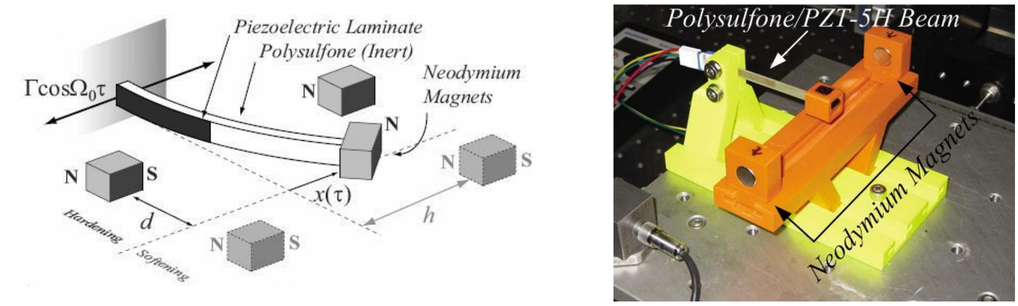

a. Schematic

b. Experimental setup

Figure 2-20. Reversible hysteresis energy harvester (modified from [43])

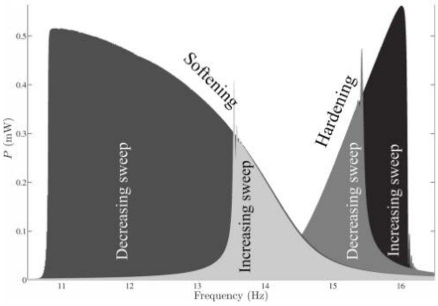

Figure 2-21. Reversible hysteresis energy harvester, experimental results (modified from [43])

Sebald, et al. [44] recently proposed to overcome this problem by the use of fast burst voltage perturbations applied to a piezoelectric on an energy harvester. This technique would bring the non-linear harvester from the low-energy to the high-energy level. However there is a frequency limit beyond which the perturbation cannot force the harvester to jump to the high state. Equally, large acceleration levels would require higher voltages that would not be feasible. The practical implementation of such mechanism would presents challenges regarding power management and energy consumption required for the perturbation mechanism that were not considered by the authors, and represent a future area of development.

Nguyen, et al. [45] present an electrostatic energy harvester that integrates non-linear springs with softening effect, shown in figure 2-22. The characteristic softening response can be seen when the device is subject to narrow band vibrations, as shown in figure 2-23a, with the aforementioned double energy levels. The response of the harvester when excited by broadband random vibrations shows an increase in the bandwidth of the power spectral density (PSD) of the output voltage, figure 2-23b, as the level of vibration increases, while the upper frequency range of the harvester remains fixed.

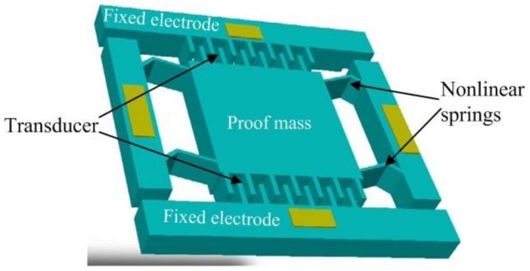

Figure 2-22. Schematic of electrostatic energy harvester with non-linear springs (modified from [45])

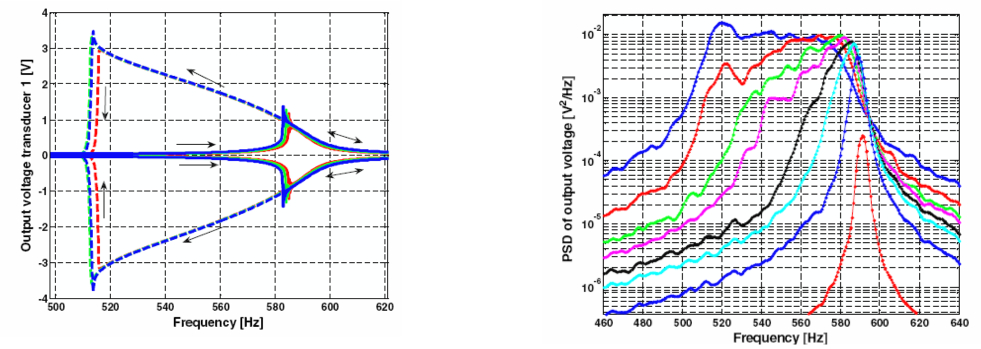

a. Peak voltage for narrow bandwidth at peak accelerations of 1.55, 1.79 and 2.20 ms^{-2} (from lower to upper curve)

b. Output power for broadband random vibrations.

Figure 2-23. Frequency response of electrostatic energy harvester with non-linear springs [45]

Tvedt, et al. [46] analysed an electrostatic energy harvester which displayed properties of softening spring at low levels of acceleration. As the acceleration increases, a mixture of softening and hardening spring can be observed. This creates a region of single stable response of the harvester that can be utilized to extend the bandwidth of operation of the device without the limitations regarding high and low energy levels associated with the non-linearity, as shown in figure 2-24. Five regions can be identified in the response of the harvester: i) unique low amplitude for low frequencies, ii) unique low amplitude response for high frequencies, iii) unique high amplitude response at intermediate frequencies, iv) and v) corresponds to the range just below and above the high amplitude response where the harvester can either fall in high or low amplitude depending if the frequency increases or decreases. Similar behaviour can be observed in figure 2-18a.

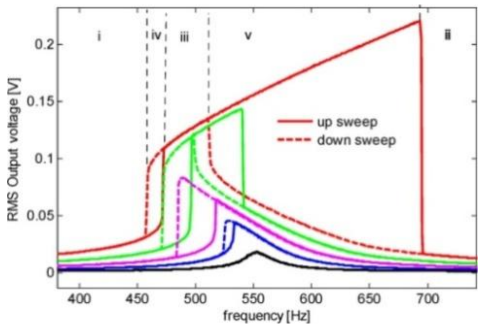

Figure 2-24. Non-linear electrostatic energy harvester output voltage response at 0.098, 0.245, 0.539, 0.981 and 1.569 ms^{-2} (from lower to upper curve) [46].

Cottone, et al. [47] present an energy harvester in the form of an inverted pendulum. A small permanent magnet is added at the top of the pendulum which, in conjunction with and external magnet, is used to introduce an additional force on the cantilever, figure 2-25a shows a schematic of the harvester. The magnets are placed with opposed polarities. When the distance between magnets is large, more than 11.2 mm, the harvester behaves as a linear oscillator. As the distance decreases, the swing of the oscillator becomes more complex and two equilibrium positions appear. The harvester swings from one position to the other, but also shows small oscillations around each equilibrium position. The harvester is excited with random vibration. Experimental results show an increase in power generation when the distance between magnets is below 11.2 mm, where the harvester has a more complex oscillation, see figure 2-25b.

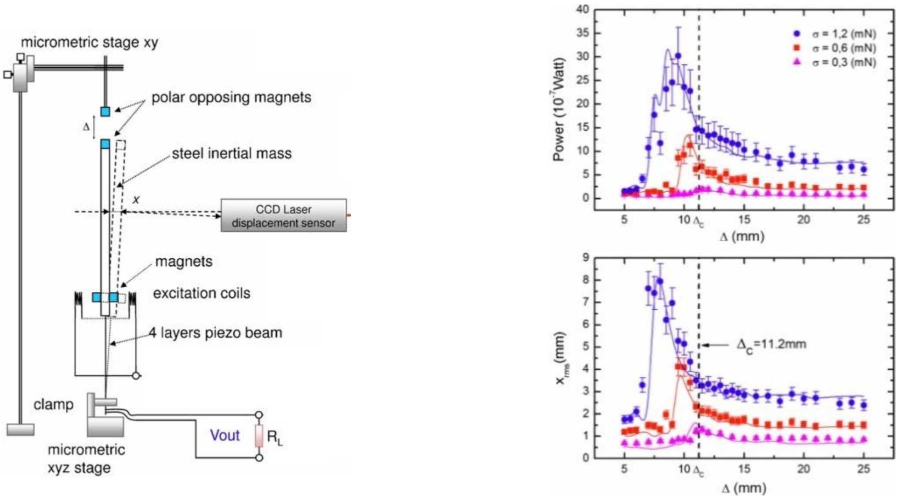

a. Schematic

b. Electric power (upper panel) and harvester position (lower panel) as function of the distance between magnets Δ for three different values of the noise standard deviation σ.

Figure 2-25. Non-linear energy harvester [47].

Erturk, et al [48] introduce a piezoelectric energy harvesting that exploits the non-linear behaviour of a magnetoelastic structure to increase its frequency band of operation. The structure compromises a ferromagnetic cantilever with two permanent magnets located symmetrically near the cantilever’s free end, see figure 2-26a. The structure is subject to harmonic excitation. The system has two stable positions at either side of the shaker towards the permanent magnets. If the initial harvester position is at one of these stable positions and is excited with a harmonic excitation of 4.905 ms^{-2} at 8 Hz, the open-circuit voltage shows a chaotic response. If the acceleration is increased to 7.848 ms^{-2}, the voltage changes to a large-amplitude periodic motion increasing its output voltage. The same response can be forced if the harvester is disturbed by a hand impulse even at 4.905 ms^{-2}. Experimental tests presented in figure 2-26b show that the piezomagnetoelastic harvester only has a lower output voltage than the piezoelastic case, close to the resonance frequency of the piezoelastic harvester of 7.4 Hz (where the permanents magnets are removed), while generating up to more than 3 times higher voltage for the rest of the range.

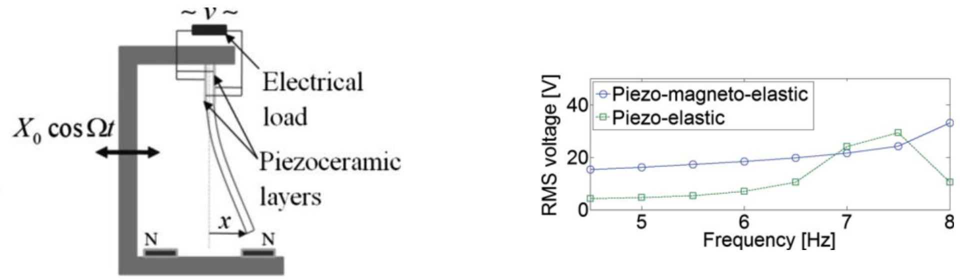

a. Schematic

b. Open-circuit rms voltage output

Figure 2-26. Piezomagnetoelastic energy harvesting (modified from [48])

2.4.2 Tuning methods for energy harvesting

Tuning methods for energy harvesting comprise a single transduction structure whose resonant frequency is altered to match the environment excitation frequency. They can be divided according to the strategy employed to accomplish tuning, into electrical and mechanical [2]. Electrical methods rely on adjusting the electrical damping of the harvester shifting its power spectrum. The resonance frequency tuning by mechanical methods is achieved by changing the dimensions, moving the centre of gravity of mass, varying the spring stiffness or straining the structure. Both designs are presented next.

2.4.2.1 Electrical methods

The resonant frequency of the harvester can be modified by adjusting its stiffness through a piezoelectric element implanted in the cantilever. Wu, et al. [49, 50]

propose the use of a bimorph structure where one piezoelectric element transduce kinetic energy into electrical, while the second piezoelectric is connected to a capacitive load to adjust the resonance frequency of the cantilever to match that of the environment. Experimental results were only presented for two operating cases: tuning piezoelectric in open and closed circuit. The frequency operation range goes from 91.5 to 94.5 Hz with a maximal power generation of 2 mW.

Peters, et al. [51, 52] present a tunable resonator for energy harvesting using two piezoelectric actuators, one clamped and one free. They are joined together by three hinges, one in the centre and one at each side of the structure. The resonant frequency of the structure is adjusted by applying an operation voltage to the actuators, causing a change in the mechanical stiffness. The operation voltage varies from -5 to 5 V, and should be maintained once the desired resonance frequency is reached.

The control system is based on the phase characteristic of the resonance system. At resonance, the phase shift between the displacement of the beam and the base excitation tends to 90°. This brings the necessity of sensing both displacements. The beam displacement was measured directly from signal output from the transducer, while the base excitation was measured using a piezoelectric buzzer. Figure 2-27 shows the tunable harvester. The control system was externally powered during performance tests with a total power consumption of 150mW. The authors suggest that a purpose built CMOS control circuit would require 30μW to operate. The resonance frequency band was expanded 30% from its non-tuned frequency of 78 Hz, from 65 to 89 Hz with base excitation amplitude of 20μm, or 4.8 ms^{-2} at 78 Hz. The harvester produced 1.4mW, but there is no detail of the load at which this power is generated.

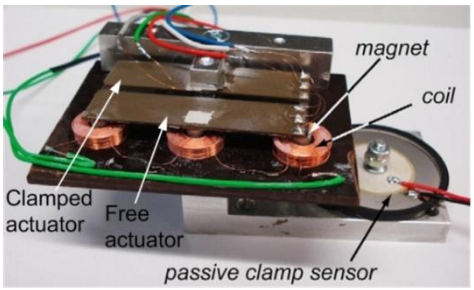

Figure 2-27. Tunable inductive energy harvester with additional clamp sensor (modified from [52]).

A similar tuning approach is presented by Wischke, et al. [53]. A cantilever shaped piezoelectric is used as an oscillatory structure. Two magnets are bonded to its free end, while a pick-up coil is fixed to the base, as show in figure 2-28. The resonant frequency is adjusted by applying a voltage to the piezoelectric, adding an axial stress on the cantilever. Under ideal conditions the voltage would remain constant after adjustment. However due to the internal resistance of the piezoelectric material, the voltage reduces gradually over time. Therefore the system must periodically re-charge the piezoelectric to maintain the desired resonant frequency.

The tuning range expands over 25 Hz, from 275 to 300 Hz approximately. This range requires a tuning voltage from -65 to 130 V. The author estimates that 200 μJ is the charge required on the piezoelectric over the frequency range proposed, which can be harvested in 20 sec given a 50μW power generation and 20% circuit efficiency. However, there is no mention on the power used by the control system or power efficiency on bringing the voltage to such ample range of voltages on the piezoelectric. The tuning system was not autonomously operated, nor operated from the harvested power.

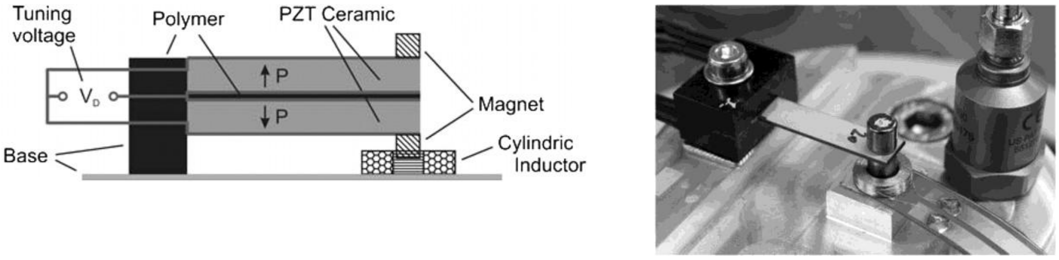

a. Schematic b. Test rig

Figure 2-28. Vibration harvester (reproduced from [53]).

Lallart, et al. [54], also report on a tuning mechanism for a piezoelectric energy harvester. The tunable energy harvester compromises a cantilever-shaped bimorph piezoelectric and an additional piezoelectric disc to measure the deflexion of the cantilever, as shown in figure 2-29. The stiffness of the cantilever, hence its resonant frequency, is controlled by switching one of the layers in the bimorph piezoelectric into a controlled electrical network every time the deflection crosses a zero value. This technique increases the bandwidth from 4.1 to 8.1 Hz for the device presented.

The control system relies on the observation of the product of the signals from the cantilever deflexion and an additional accelerometer attached to the base according to equation (2-6) [54]. The structure is at resonance when the phase ψ is π/2. Under such condition, the first term in equation (2-6) becomes zero. If the resonant frequency is lower than the excitation, the result would be positive. And negative when the resonant frequency is higher than the excitation.

$$sin(\omega t)sin(\omega t+\psi)=\frac{1}{2}\left(cos(\psi)-cos(2\omega t+\psi)\right) \qquad \textbf{(2-6)}$$

Under this strategy the power required to tune the harvester is proportional to the difference between the natural, or uncontrolled, frequency of the harvester and the excitation frequency. This is a consequence of the tuning mechanism based on a piezoelectric element, which requires more energy to adjust the stiffness of the cantilever as it shifts away from its natural frequency. The experimental results show that the -3dB bandwidth increases from 4.1 Hz for the not tuning case, to 17 Hz when tuned. This represents an overall increase of 12.9 Hz. Once the power used to maintain the resonance frequency is accounted for, the bandwidth reduces to only 4 Hz. A decrease of almost 70%. The power consumption was only estimated, it was considered that the power for processing the data was in the order of microwatts and that most of the tuning power would be used during the adjustment of the voltage at the piezoelectric. The tuning control system was implemented on a digital signal processing and powered externally.

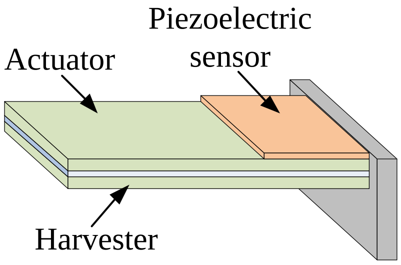

Figure 2-29. Energy harvesting schematic (not at scale).

Cammarano, et al. [55] presents an approach to tune an electromagnetic energy harvester by adjusting the electric load. The results show that the resonant frequency can be altered by selecting the load connected to the harvester. The experimental results confirm an increase of 3.5 times in the bandwidth for the harvester, compared to the untuned case. The optimal load for each particular resonant frequency, apart from the natural frequency, is a complex impedance. It varies from capacitive to inductive as the resonant frequency increases. In the example presented, the impedance was manually adjusted using a variable inductance and a configurable capacitor bank. The authors recognize that there are important challenges that must be met before a fully automatic load impedance tuning harvester can be developed; among them, the control and the power consumption for such system.

An additional electrical method to tune or adjust the resonance frequency of a spring-mass system is by using an electrostatic force. Cabuz, et al. [56] present a resonant infrared sensor with the capability to fine tune its resonant frequency. The structure includes two electrodes that interact with the resonator inducing compressive or tensile stress, effectively modifying its resonant frequency, as presented in figure 2-30. Similar design is investigated by Piazza, et al. [57] that integrates a single electrode to tune the resonant frequency of a silicon resonator. The resonator can only be tuned for frequencies below the resonant frequency of the cantilever, from 719 to 713 kHz. Scheibner, et al. [58] explore the use of tunable micromechanical resonators for spectral vibration detection system. The resonance tuning is performed by the addition of an electrostatic-softening structure shown in figure 2-31.

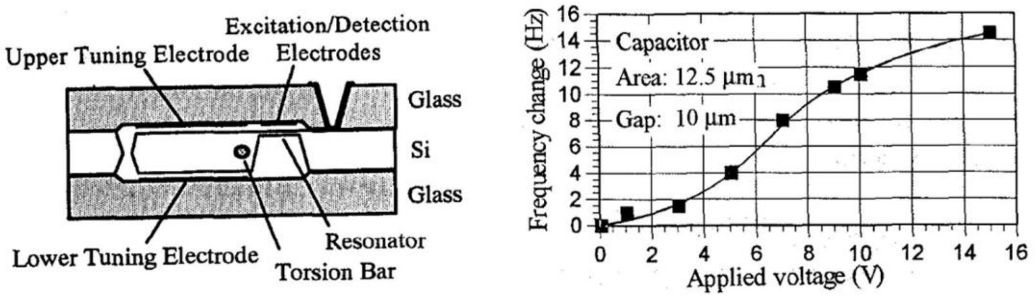

a. Structure

b. Frequency change as voltage at lower electrode is applied.

Figure 2-30. Fine resonance frequency tuning (modified from [56])

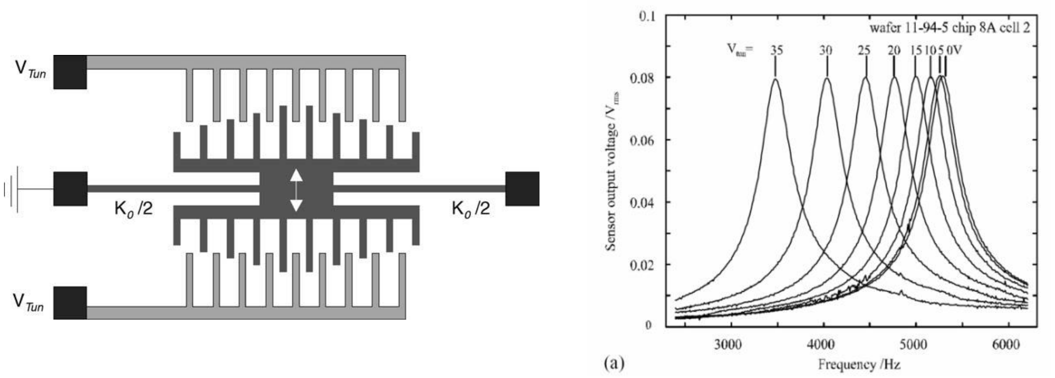

a. structure

b. Resonance tuning as function of voltage at tuning capacitor.

Figure 2-31. Resonance tuning by electrostatic-softening [58]

2.4.2.2 Mechanical methods

Leland, et al. [59] present a tunable piezoelectric harvester where a compressive axial force is applied to the harvester's structure to modify its stiffness, hence its resonant frequency. Picture figure 2-32 shows the harvester setup. It has a natural frequency of 250 Hz and can be altered by exerting an axial preload down to 200 Hz, at which point the axial force is 64 N. The force is manually adjusted throughout the test and no control mechanism was utilized. The maximum power generated at 9.8 ms^{-2} is 400μW.

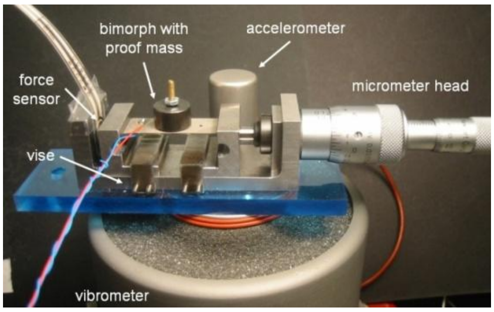

Figure 2-32. Experimental apparatus. [59]

Challa, et al. [60] proposed a magnetic tuning mechanism for a piezoelectric harvester. Two tuning magnets are positioned in the cantilever while another two are mounted on the enclosure of the device. One pair is aligned to create an attractive force while the second pair creates a repulsive force, as shown in figure 2-33. The cantilever is mounted in a structure that can be vertically adjusted. Using this tuning mechanism the frequency can be adjusted from 22 to 32 Hz, with a maximum adjustment on the position of the cantilever of 3 cm. The tuning mechanism was manually adjusted, however the researchers assumed that 85 mJ are required by an actuator to adjust the cantilever 3 cm.

The maximum power generated by the harvested was 250 μW at 0.8 ms^{-2}, there is no information regarding the load into which this power is delivered. At this level of generation, they estimated that the harvester requires 320 sec to harvest the energy lost during the adjustment. However, the power consumption for an autonomous tunable harvester is not exclusively drawn by the actuator; also, a control system is required to operate the actuator and to recognize when the harvester requires adjustment. Such activities will add power consumption on the harvester tuning.

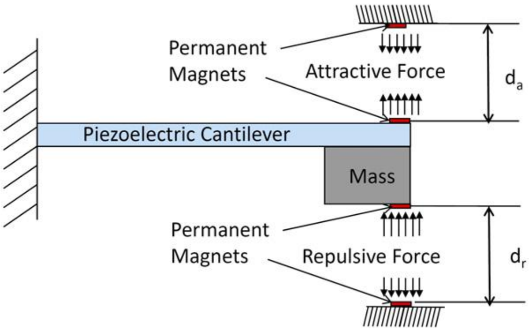

Figure 2-33. Magnetic tuning mechanism [60].

Eichhorn, et al. [61, 62] propose a tuning mechanism that preloads a cantilever beam to adjust its resonant frequency. The design compromises a cantilever beam with additional arms to apply an axial force using a spring. The spring is compressed by a screw. The spring pushes the generator base creating a counterforce. Using this mechanical tuning design the resonant frequency expands from 292 to 380 Hz, requiring a tuning force up to 23 N. The system is manually adjusted using a screw, as shown in figure 2-34.

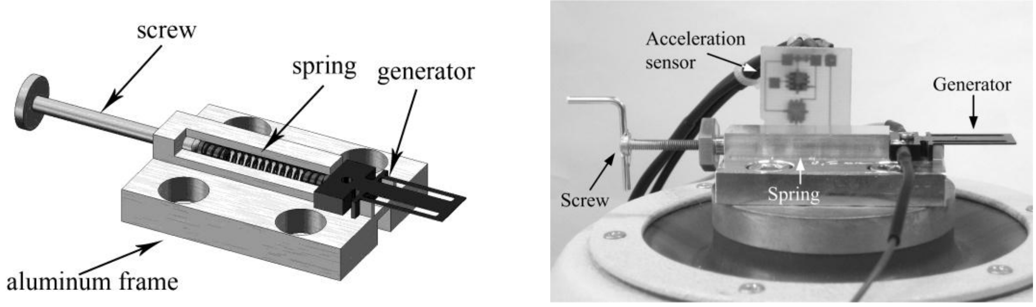

a. Schematic

b. Converter situated on a shaker with accelerometer

Figure 2-34. Tunable piezoelectric converter. (modified from [61]).

Wu, et al. [63] presents the design of a tunable harvester that alters its centre of gravity to adjust the resonant frequency. The frequency range extends from 130 to 180 Hz. The adjustment is manually performed and there is no mention of any control system.

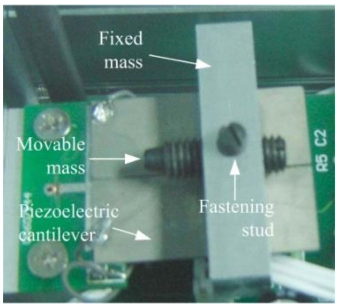

Figure 2-35. Piezoelectric generator with gravity centre movable mass, (modified from [63]).

The preload mechanism of the extensional mode resonator presented by Morris, et al. [64] exploits the extension effect on the piezoelectric transduction mechanism, rather than bending. The harvester is formed by two piezoelectric sheets linked by a rigid element. The resonant frequency is changed by manually adjusting the tension on both sheets using the preloading screw. The resonant frequency can be adjusted between 80 to 235 Hz, with a total displacement of approximately 1.25 mm.

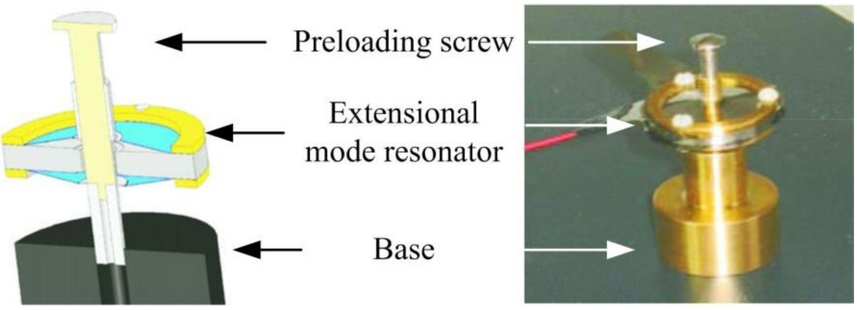

a. Cross-sectional drawing

b. Photograph of the assembled extensional mode resonator

Figure 2-36. Extensional mode resonator.
(modified from [64]).

A magnetic tuning mechanism is presented by Ji-Tzuoh, et al. [65]. The harvester compromises a cantilever shaped piezoelectric with a tuning magnet mounted at the superior tip end of the cantilever. A second tuning magnet is positioned above the cantilever, aligned to the first magnet as shown in figure 2-37. The magnet polarization is selected to create an attractive force between them. The separation between tuning magnets can be adjusted to increase or reduce the force between them, hence the harvester resonant frequency. The bandwidth of a tunable piezoelectric harvester using this mechanism expands from 17 to 25 Hz, for a distance between magnets from 7 to 40 mm. The adjustment of the separation was manually performed. The force and the power generated were not reported.

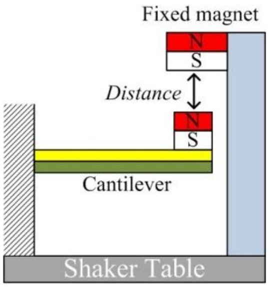

Figure 2-37. Experimental setup
(modified from [65]).

Zhu, et al. [3, 66] present a tunable electromagnetic energy harvester. The harvester design is shown in figure 2-38a. The electromagnetic transducer is formed by four magnets attached to the beam and a pick-up copper coil fixed to the base of the harvester. An additional tuning magnet is positioned at the tip end of the beam while a second tuning magnet is mounted on a movable platform, as shown in figure 2-38b. The distance between tuning magnets can be adjusted to vary the axial force exerted on the beam, effectively varying its spring stiffness, hence its resonant frequency. The resonant frequency of the harvester can be tuned from 67.6 to 98 Hz by adjusting the distance between tuning magnets from 5 to 1.2 mm, respectively. A closed loop system was developed that automatically tuned the resonant frequency to match the ambient excitation. The tuning electronics and the actuator adjusting the distance between magnets were powered by an external source to the harvester. This is the device upon which the present research is based, as described in Chapter 3.

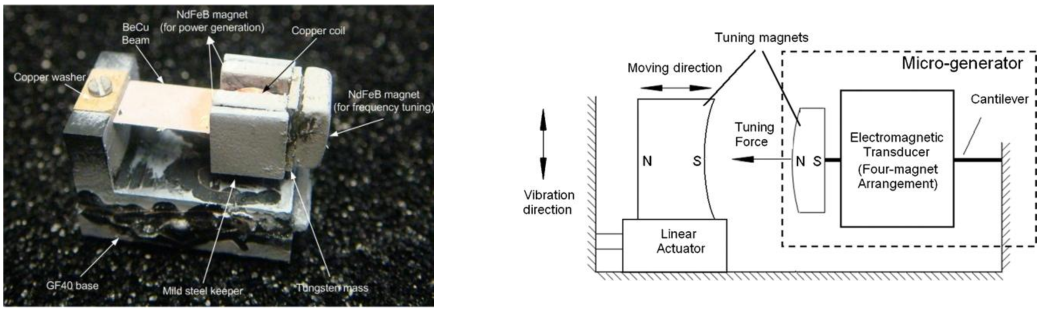

a. Harvester photograph b. Tuning design schematic

Figure 2-38. Tunable electromagnetic micro-generator [3]

Mansour, et al. [67] presents a magnetic tuning mechanism for a piezoelectric energy harvester, shown in figure 2-39. The permanent magnets exert a compressive force over the piezoelectric cantilever affecting its stiffness, consequently its resonant frequency. In this solution the resonant frequency was adjusted from 3.19 to 12 Hz, corresponding to a compressive force of 0 to 3.35 N and a distance between magnets from more than 60 mm to approximately 15 mm. The tuning mechanism was manually operated.

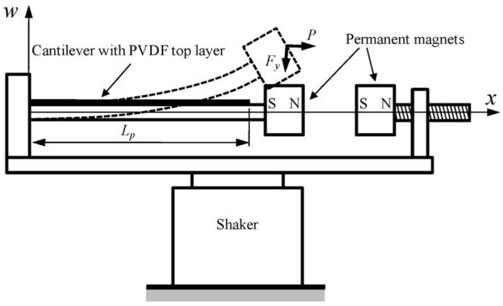

Figure 2-39. Schematic illustration design.
(reproduced from [67])

2.4.3 Discussion

Widening the bandwidth of operation of a vibration energy harvester presents some challenges for its final application in an autonomous sensor node. The *array of structures* technique is limited by the maximum physical volume that the harvester can occupy. The *amplitude limiter* is restricted by the fatigue that may occur in the material due to continuous contact with the stopper. *Non-linear harvesters* present a major challenge due to the hysteresis frequency response, an effect also shared by the *amplitude limiter* technique. The *bistable structure* for energy harvesting has a better performance than the standard cantilever-shaped energy harvester, only if the excitation frequency is below the resonance frequency, provided that the excitation is high enough to force the structure to move between its two stable positions. The great advantage of these techniques is that they do not require any additional power to operate, which is the main drawback of the tuning methods for energy harvesting.

The mechanisms presented here to tune the harvester rely on manual adjustment or on an external power supply to operate, and in most cases the overhead power is not considered. Those tuning devices that adjust the stiffness by means of varying the charge on a piezoelectric or a capacitive load require a control system with the ability to drive high voltage levels, and even change polarity. Mechanical tuning techniques require an actuator to adjust the stiffness of the harvester. The power used during tuning varies depending on the force necessary for adjustment of the harvester.

2.5 Power management

The advances in energy harvesting have surpassed the initial stage where the concept was evaluated as a feasible competitor to assist or eliminate conventional power sources to provide energy to sensor nodes. The next stage is to integrate the harvester with a real electric load to evaluate its performance. A resistive load is commonly used to evaluate the behaviour and power generation of the harvester, however practical applications seldom have a resistive behaviour.

The power management for energy harvesting systems not only refers to the use of the energy available, it also comprises the extraction, conversion and storage of the energy generated by the harvester. In order to achieve high levels of energy extraction some form of impedance matching must be considered [68]. Next the output voltage and current from the spring-mass energy harvester is typically not compatible with the load electronics, hence regulation is required. Finally, the intermittent nature of the energy available for conversion or its low level, oblige the inclusion of an storage element that can save the energy and supply the electric load when necessary, provided that the average power generated is higher or equal to the power consumed by the load.

Three different power management topologies for energy harvesting have been identified in the literature. The three differ in the approach taken to interface with the transducer and extract power, see figure 2-40. The first design utilizes a diode rectifier, the second uses switching capacitor technique to rectify and conditioning the power. The third approach uses active switching techniques with the same purpose. The advantages, disadvantages and uses of each topology will be presented next, with special consideration towards their efficiency and overhead power.

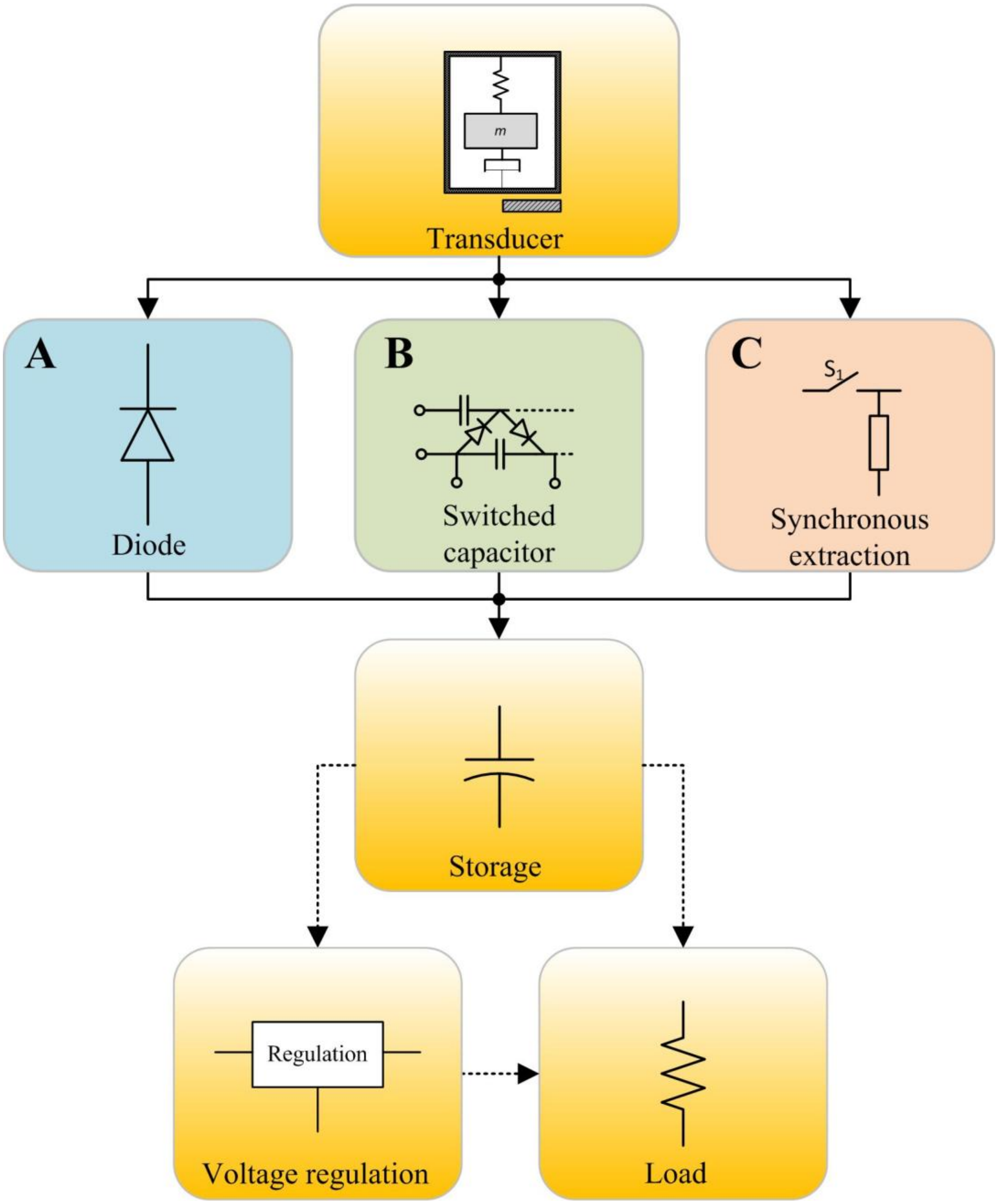

Figure 2-40. Power electronics topology for energy harvesting systems

2.5.1 Diode rectification

Diode rectifier is the most common method of rectification in the form of a full bridge rectifier; however its behaviour is not the most desirable for maximum power transfer for energy harvesting. Clare, et al. [69] consider that the diode voltage drop is a limitation for this topology considering that electromagnetic energy harvesters have commonly low output voltage at high current level [70]. Electrostatic and piezoelectric harvesters are characterized by relatively high output voltages with large ripples and low output current that may not be affected by the voltage drop. Furthermore, poor power factor due to the presence of the storage capacitor reduces the peak power at the load.

Clare, et al. [69] substituted the diodes by switching elements, in this case MOSFET, which are externally controlled. This synchronous rectification results in a lower voltage drop than when diodes are used, but adds power losses inherent to the MOSFET operation and control. Experimental tests using an electromagnetic energy harvester show that more power can be extracted when using this technique for loads drawing power in the range of 1.6 to 100 mW. Below this range, the efficiency reduces due to the increasing proportion of power used for control in relation to the power extracted, although no further details are given on the power consumed by the control, see figure 2-41.

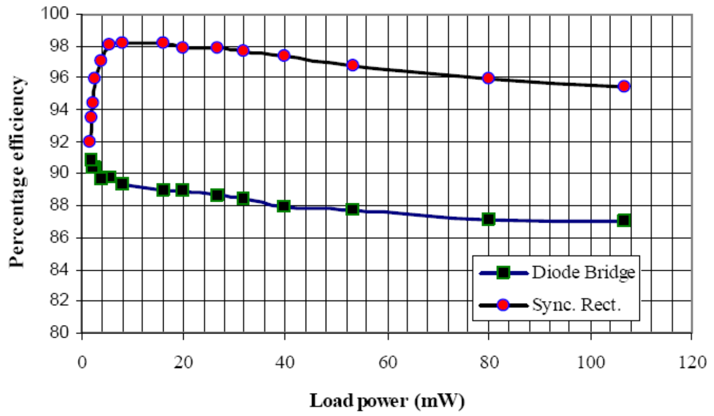

Figure 2-41. Measured performance of synchronous full wave rectification [69]

2.5.2 Switched capacitor

Switched capacitor converters transfer energy by controlling the charging and discharging sequence of a bank of capacitors, either using a diode as the switching element or transistors. The AC voltage generated by the energy harvester is increased, or multiplied by the switched capacitor converter and at the same time is rectified. Dickson charger pump [71, 72] and Villard voltage multiplier [73] are examples of these configurations, presented in figure 2-42.

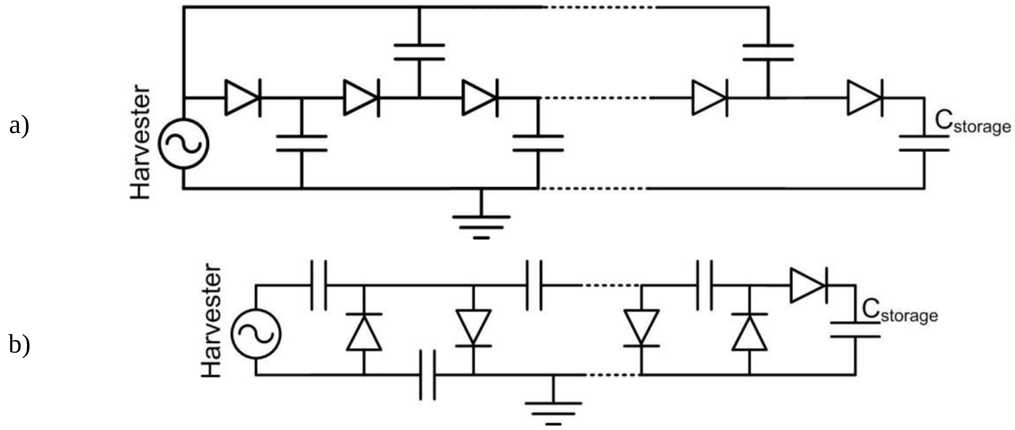

Figure 2-42. Switched capacitor converters
a. Dickson charge pump, b. Villard voltage multiplier.

The use of these techniques for energy harvesting has been demonstrated by Torah, et al. [74]. The electromagnetic harvester has an optimum output voltage of 450 mV_{rms} when excited at 0.6 ms^{-2} at 50 Hz, hence the need to increase the voltage for later use of the electric load. Two topologies were evaluated; Dickson charge pump and Villard voltage multiplier. A 5 stage Dickson charge pump showed a faster charging time of a 0.22 F storage capacitor. It reaches 2.2 V in 8.5 hours. The authors selected Schottky diodes due to their fast switching time and low forward bias voltage, but compromising a higher leakage current compared to standard diodes. The topology cannot be reconfigured to increase or decrease the number of stages; hence, the impedance seen by the harvester cannot be adjusted.

Saha, et al. [75] present a 4 stage Villard voltage multiplier. The diodes were replaced by switches driven by comparators. The authors compare the performance of the voltage multiplier (VM) when attached to two similar harvesters, micro and macro harvester. The second is simply a larger version of the first. It is shown that this VM circuit is best suited for the micro harvester version than for the macro. This can be observed by the mismatch between the theoretical optimal load when the VM is attached. Considering that the VM not only steps up the voltage, it also modifies the impedance seen by the harvester by a factor of λ^2; where λ is the ratio between output voltage from the VM and the input voltage from the harvester. Thus, a 4 stage VM would result in impedance seen by the harvester of 1/16th the actual load. For the micro harvester the maximum power generation occurs close to the theoretical value of 48 kΩ, while for the macro harvester, the maximum power is generated more than 3 times above the theoretical. The authors conclude that the 4 VM is better suited for the micro harvester with an overall efficiency of 80% at a power level of 18 μW.

Table 2-1**.** Load power with and without voltage multiplier

	without VM		with VM		Theoretical
	Max. power (μW)	Load (Ω)	Max. power (μW)	Load (Ω)	Load (Ω)
micro	18	3000	15.75	50000	48000
macro	256	100	210	5500	1600

Maurath, et al.[76-79] substitute the diodes by CMOS transistors and include two configurable banks of capacitors. This topology eliminates the drawbacks related to the use of diodes while giving the freedom to adjust the impedance to optimize the power generation and output voltage level. The output voltage from the harvester is rectified by a transistor bridge. The rectified signal is then connected to one of the bank of capacitors, charging the capacitors in parallel as show in figure 2-43a. As the voltage at the bank reaches a limit voltage (*Vopt*), which corresponds to the optimal generation voltage plus a small overdrive voltage *(ΔV)*, the bank is disconnected from the harvester and the capacitors are connected in series to generate a higher voltage according to the number of capacitors stacked, as show in figure 2-43b. At the same time, the second bank of capacitors is connected to the harvester charging the capacitors. The stacked capacitors transfer their energy into a storage capacitor until their individual voltage reduces its voltage by *ΔV* below *Vopt*.

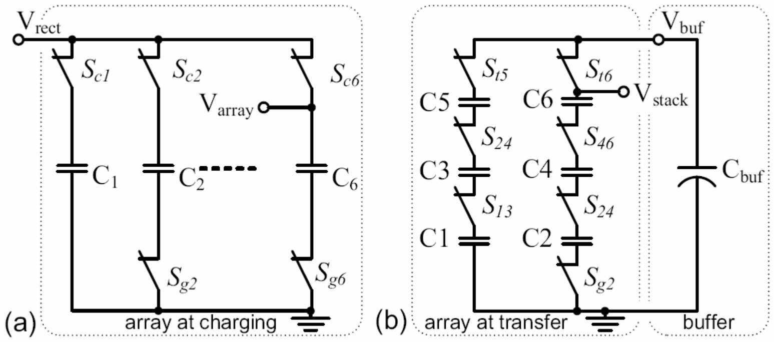

Figure 2-43. Capacitor array charging (a) and in stacking configuration (b).

The proposed design was implemented on a 0.35 μm CMOS process. The overhead power consumed by this design varies according to the voltage level required by the electric load, V_{buf} in figure 2-43 and are presented in table 2-2.

Table 2-2. Power consumption

V_{buf} (V)	Power (μW)
0.9	25.3
1.5	40.8
3.3	103.3

Taithongchai, et al. [80] reported an electromagnetic energy harvester using induced voltage on a toroidal core. The transduction mechanism is the same as for the spring-mass based harvester, the output voltage is similar, an AC signal, hence the same challenges are present. The voltage induced on the harvester output ranges from 1.5 to 3 V, at currents through the primary transmission line of 65 to 130 A. The voltage is amplified and rectified using a 4 stage Villard voltage multiplier, and then is conditioned using a DC-DC boost converter to charge a battery. The boost converter duty cycle is controlled by a microcontroller. The overall power harvested is 58 mW at 65 Amp, but there is no mention of the power consumed by the microcontroller.

2.5.3 Switching conversion

"Switching conversion" refers to the processing of energy from the harvester into the storage system using active elements, e.g. transistors. The input voltage from the harvester can be increased or decreased as required, and the apparent impedance can be adjusted to maximize the energy generation. These improvements can be achieved using adaptive controls which must be energy efficient so that the power they consume does not surpass the power generated by the harvester.

The first consideration for synchronized rectification is the transduction mechanism. As previously explained, electromagnetic energy harvesters have low-voltage and high-current; while piezoelectric harvester are characterized by high-voltage and low-current with a capacitive output. For this reason, each case will be discussed separately.

2.5.3.1 Electromagnetic energy harvester

Processing separately the positive and negative half cycle of the output voltage from the electromagnetic harvester is proposed by Mitcheson, et al. [68]. Two boost converters connected in parallel to the harvester are enabled alternatively avoiding the requirement for AC-DC rectification. Figure 2-44 presents the dual polarity boost converter. Simulation results indicate that an efficiency of 44% is feasible when using this technique and it is suitable for electromagnetic harvesters with output power in the range of 50 mW.

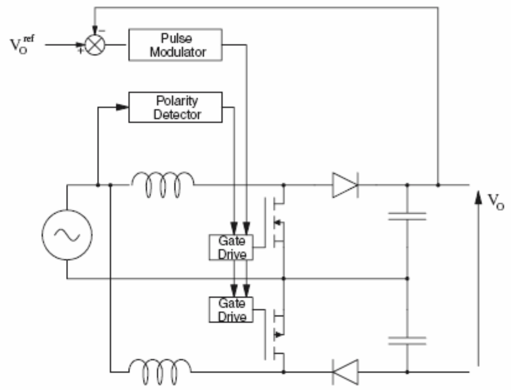

Figure 2-44. Dual polarity boost converter [68]

Dwari, et al. [81] demonstrated an AC-DC converter that also utilized a boost converter to bring the output voltage from an electromagnetic energy harvester from 400 mV to 3.3 V. Two topologies are presented: secondary switch and split-capacitor. The difference between them is the mode in which the energy stored in the inductor is transferred into the storage capacitor. The first topology, figure 2-45a, performs this operation by enabling transistor S3, or S4, according to the input voltage polarity. S3 is enabled during the negative cycle and S4 for in the positive. This topology requires a gate controller to enable the charge of the inductor and a polarity detector to select the transistor at each cycle. The second topology substitutes S3 and S4 by a pair of capacitors as shown in figure 2-45b. This modification eliminates the need for a polarity detector. Once the inductor is charged and S1 is disabled the voltage through the inductor forward biases D1, or D2, during the positive, or negative, half cycle.

Both topologies were implemented using discrete components and evaluated using an ideal voltage source of 400 mV. Controller circuits were also implemented using discrete components, no reference was made of the power source employed to operate them, nor the power consumed. The estimated efficiency of the secondary-switch topology was 60.7%, while for the split-capacitor 60%. The advantage of the split-capacitor relies on the lower number of controls required to operate.

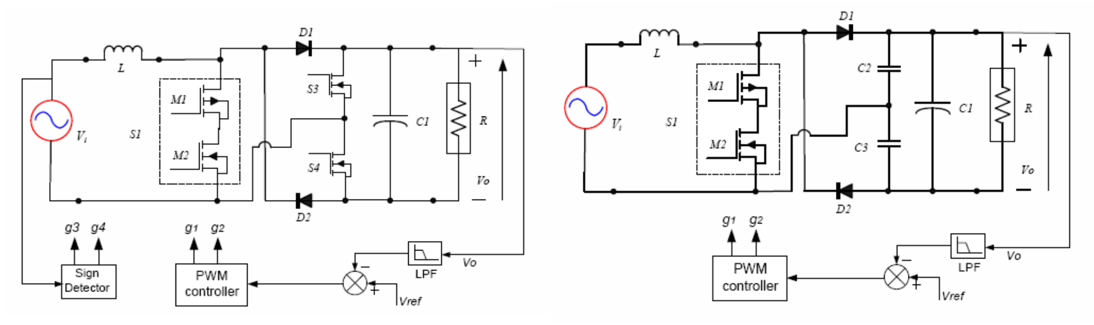

a. Secondary switch b. Split capacitor

Figure 2-45. AC-DC converters topology [81].

An electromagnetic energy harvesting with a boost converter is presented by Xinping, et al. [82]. The harvester generates 35 mW at an acceleration of 208 ms^{-2}. The boost converter is optimized by the inclusion of a feedback and feedforward control that adjusts the duty cycle of the converter. The converter is presented in figure 2-46. It was implemented using discrete components and on 0.35 μm CMOS IC technology. The performance comparison between both cases shows a higher output power for the first case, 35 mW, than for the IC design, at 4 mW. The authors do not provide an explanation for this discrepancy, or their efficiency.

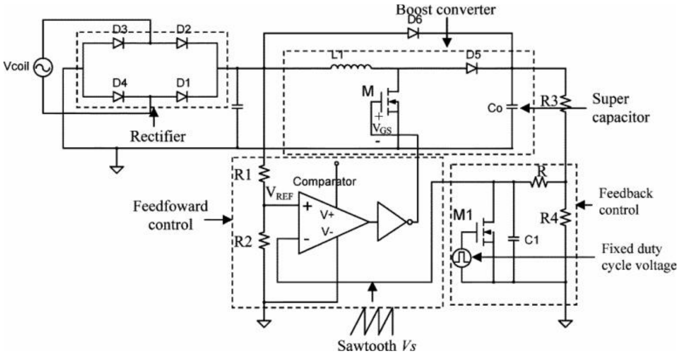

Figure 2-46. Energy harvester with feedforward and feedback control [82]

2.5.3.2 Piezoelectric energy harvester

Three conversion techniques for piezoelectric energy harvesting using switching conversion are reported in the literature: switched converter, synchronous charge extraction and synchronised switch harvesting on inductor (SSHI).

Switched converters for piezoelectric energy harvesting are based on standard DC-DC converters such as boost and buck converters. The advantage of this approach is the possibility to adjust dynamically their input impedance, hence optimize the energy generation by matching the harvester impedance. Ottman, et al. [83, 84] present a buck converter that has a three fold increase in the power generation compared to the simplest AC-DC conversion using a diode-bridge. Kong, et al. [85] selected a buck-boost converter, instead, to increase the flexibility of operation when the voltage from the harvester is lower than the output voltage of the system. Both designs include a closed-loop control that adjusts the duty cycle of the converter according to the average current transfer to the storage element. In both examples, the control system was powered externally.

Synchronous charge extraction is described by Xu, et al. [86], Richard, et al.[87] and Badel, et al. [88]. The principle of operation relies on the capacitive output impedance of the piezoelectric harvester. The charge accumulated on the output capacitor of the piezoelectric is removed each time the charge reaches a maximum. This occurs on the mechanical displacement maxima. It is at this point when the charge extraction is synchronized with the mechanical excitation. Figure 2-47a shows the extraction circuit. Transistor *T* is enabled only when the displacement reaches a maximum or a minimum; the energy stored on the piezoelectric capacitor is transferred to the coupled inductor *L*. The transistor *T* is disabled when the electrostatic energy is completely removed from the piezoelectric. Then, the energy is transferred from the secondary winding of the inductor into the storage element. The discharge cycle can be observed in figure 2-47b, where the discharge of the piezoelectric is accompanied by the drop in voltage.

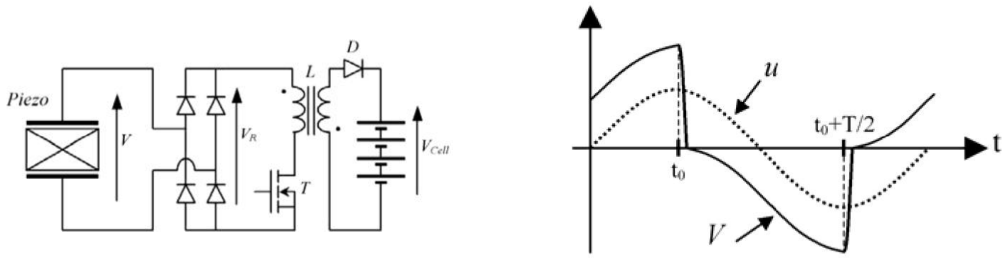

a) Circuit

b) Displacement and voltage at harvester waveforms

Figure 2-47. Synchronous charge extraction [88].

The SSHI (Synchronized Switch Harvesting on Inductor) technique is similar to the synchronous charge extraction in that in both cases the piezoelectric is connected to the converter when the displacement reaches a maximum. Each time a maximum displacement is reached, the switch closes transferring part of the electric charge from the piezoelectric blocking capacitor through the inductor into the storage element. The inductive switching leads to the inversion of the piezoelectric voltage [89].

The SSHI circuit is composed of an inductor *L* and an electronic switch *S* followed by a rectifier, as show in figure 2-48. Two interface circuits for the SSHI technique exist, “parallel” and “series”. The name refers to the position at which the inductor and switch are located in reference to the piezoelectric harvester, as show in figure 2-48.

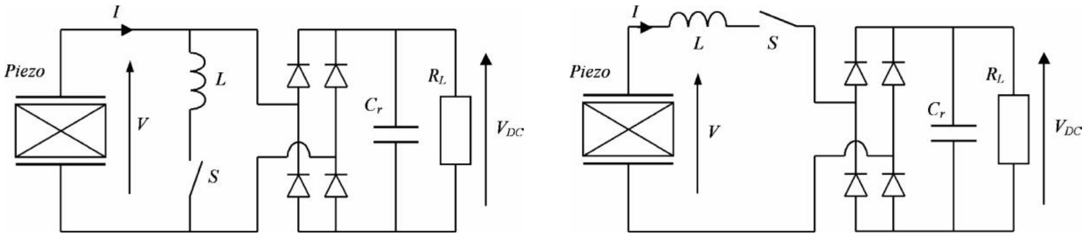

a. Parallel

b. Series

Figure 2-48. SSHI interface [90]

Guyomar, et al. [91] present the parallel SSHI technique. As described previously, the inductor *L* and the switch *S* are connected in parallel to the harvester. It is shown that the parallel SSHI has a superior performance for resonant structures with a weakly coupling, or for structures driven out of resonance. For structures driven at resonance, the maximum power harvested tends to a limit as the coupling factor increases, as show in figure 2-49. In the case of weakly coupled structures driven at resonance, parallel SSHI technique outperforms the standard techniques. Hence, less piezoelectric material is necessary to produce the same amount of power than in the standard technique. Conversely, more power can be generated from the same amount of piezoelectric material.

Series SSHI interface is similar to the parallel SSHI circuit, but the interface is connected in series to the piezoelectric. The switching control is the same as for the parallel circuit.

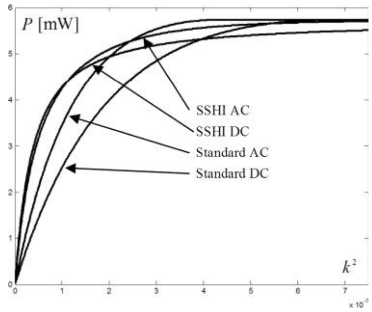

Figure 2-49. Power comparison between parallel SSHI and standard conversion[91].
AC corresponds to the case where the harvester is directly connected to the load, DC when the load is connected through a rectifier.

Mitcheson, et al. [92] points out that one disadvantage of the SSHI technique is that the charge extraction cannot be controlled independently of the voltage at the storage element, V_{dc} in figure 2-48. This implies that the optimal electrical damping cannot be set independently of the capacitor voltage. To overcome this dilemma Lallart, et al. [93] propose a double synchronized switch harvester, shown in figure 2-50. The circuit consists of a series SSHI attached to a buck-boost converter. This implementation ensures that the optimal electrical damping can be set independently.

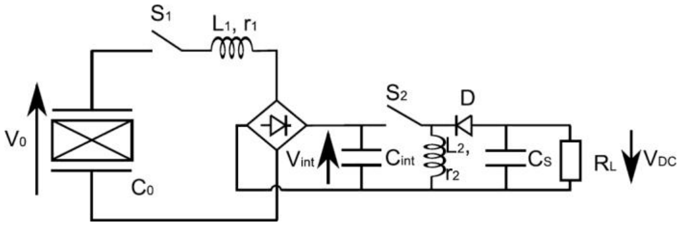

Figure 2-50. Double synchronized switch harvesting circuit [93]

2.5.4 Discussion

This section has presented different techniques for conditioning and conversion of the energy transduced by the harvester. The principal objective is to generate the maximum energy possible for the given conditions of operation. It was found that the active conversion schemes are more efficient than those using passive elements, due to their ability to adjust actively the impedance of the interface.

A significant point is the power consumed to control the active conversion, which for most of the cases presented was higher than the power generated by the harvester. As an example, simulations presented by Xu, et al. [86] suggest that their control would consume as low as 600 nW, but this was not verified , while the harvester produces 4.4 μW. Power consumption for the control was estimated at 5.74 mW by Ottman, et al. [84], while the harvester generates 30.66 mW. In the system presented by Lefeuvre, et al. [94] the overhead power is 160 μW, for a harvester producing 1.5 mW. It can be seen that for harvesters generating in the order of microwatts, the overhead power for active conditioning is still high enough to be considered for a fully autonomous sensor node.

2.6 Conclusions

This chapter has presented an overview of the potential techniques to extend the operation capability of vibration-based energy harvesters. First, considering those techniques that increase the frequency range of operation of a harvester. Second, presenting strategies towards achieving a tunable harvester that can adjust its mechanical properties to match the changing environmental conditions, e.g. base frequency.

Power management strategies to increase the power generated were also presented. Passive rectification and conversion were presented along with active techniques that utilize switches to maximize the power extraction.

The power overhead required to increase the bandwidth of operation and the power extraction from the harvester were discussed. This highlighted the fact that none of the designs presented operate under a fully autonomous mode; they require external power or manual user adjustment.

The present research aims to produce a fully autonomous energy harvester that will only operate from the energy harvested from the environment and that will independently adjust to operate under a wide range of frequencies. As stated on the report; Energy Autonomous Systems: Future Trends in Devices, Technology, and Systems [95]: “The research rarely covers (…) the complete functional chain to really address the autonomy”.

Chapter 3

Components of the tunable energy harvester

3.1 Introduction

This chapter presents the development of a tunable energy harvester, initially as a proof of principle to assess the challenges that such a system presents. Further operation and optimization of the system will be based on the findings presented here, and will be detailed in subsequent chapters.

In section 3.2 a description and performance of the electromagnetic energy harvester used in this research is presented. It is followed by the electrical components that form the tuning mechanism, control entity and energy extraction and rectification in section 3.3. Finally, in section 3.4, an alternative tuning mechanism is introduced as a point of comparison.

3.2 Harvester mechanical design

The vibration-based energy harvester selected for the present research was originally developed at the University of Southampton during the Framework 6 STREP project Vibration Energy Scavenging (‘VIBES’) [96] and subsequently optimized by Zhu, et al. [3, 66] by the integration of tuning capabilities.

The energy harvester transduces kinetic energy, in the form of vibration, into electrical energy using an electromagnetic transduction mechanism formed by a coil and permanent magnets. The design and integration of such a mechanism is discussed next.

3.2.1 Electromagnetic Harvester

The electromagnetic energy harvester design employs a cantilever beam with an inertial mass and four Neodymium Iron Boron (NdFeB) magnets attached to its free-end. The beam has an empty slot at its free end to accommodate the coil. The cross section of the harvester is presented in figure 3-1a. The NdFeB magnets are positioned in pairs on the top and bottom surfaces of the beam with the magnetic poles aligned to create a magnetic circuit, as shown in figure 3-1b. Two mild steel keepers are bounded to the magnet pairs to complete the magnetic circuit.

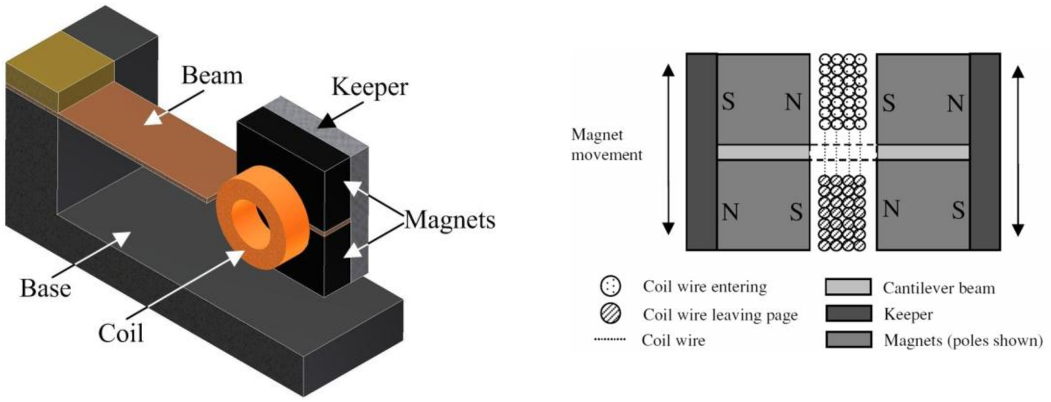

a. Longitudinal cross section view of electromagnetic energy harvester

b. Cross section view of four-magnet arrangement [20]

Figure 3-1. Schematic of electromagnetic energy harvester.

The stationary coil is attached to the base and centred between the four magnets to maximize the magnetic flux linkage. The beam moves when it is subject to base excitation, changing the magnetic flux within the coil, consequently generating a current, according to Faraday's law of induction as described by equation (3-1), where ε is the electromotive force in volts, and Φ_B is the magnetic flux and N is the number of turns of wire.

$$\varepsilon = -N\frac{d\Phi_{\mathrm{B}}}{dt} \tag{3-1}$$

The beam on the electromagnetic energy harvester has a thickness of 0.14 mm, an effective length of 13 mm and width of 5 mm. It has a 2 x 5.6 mm slot at the free end to accommodate the coil. Each of the NdFeB magnets has a geometry of 1.5 x 3 x 5 mm, grade 38H material. A tungsten mass is also attached to increase the total inertial mass. The coil is bonded to a support on the base, placing the coil at the centre of the beam's slot. An additional magnet is placed at the tip end of the beam, identified as the *1st tuning magnet* in figure 3-2. This magnet enables the tuning capability of the beam. Figure 3-2 presents the complete schematic of the electromagnetic energy harvester.

Table 3-1 summarizes the materials and characteristics of the different components used in the harvester. All magnets, mild steel keepers and additional tungsten mass are glued to the beam with cyanoacrylate, as well as the coil to its support.

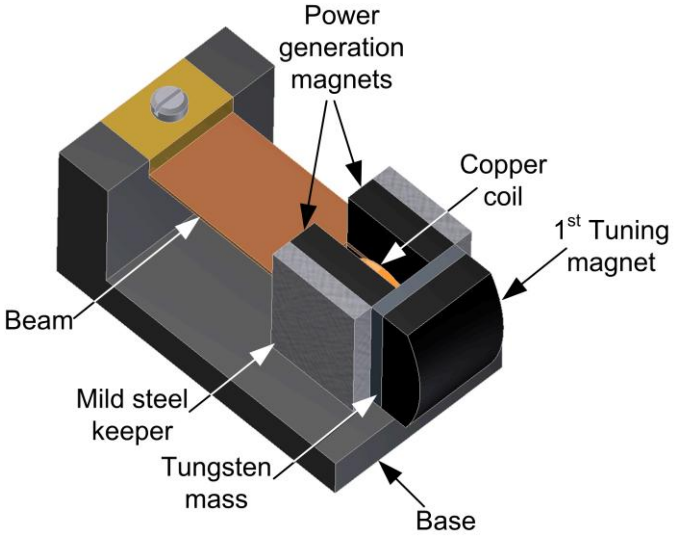

Figure 3-2. Tunable vibration-based electromagnetic energy harvester.

Table 3-1. Harvester materials

Component	Material
Magnet	NdFeB (Flux density = 1.22T)
Mass	Tungsten alloy
Keeper	Mild steel
Beam	BeCu
Base	Tecatron GF40
Coil	Copper

Three different coils were used during this research; their electrical characteristics are presented in table 3-2. They have similar dimensions with small variations due to the manufacturing process. Their outer and inner diameter, along with the coil's width are also presented in table 3-2, a graphical representation of the coil is illustrated in figure 3-3. Coil A was also used in a second harvester where the beam was replaced due to damage; in that case it will be identified as harvester A′.

Table 3-2. Coils characteristics

	Coil A	Coil B	Coil C
Wire diameter (μm)	16	16	25
Number of turns	6000	6000	2850
Resistance (kΩ)	4.50	4.80	0.606
Inductance (mH)	58	60	10
Outer diameter (mm)	4.85	5.02	4.50
Inner diameter (mm)	0.92	1.31	0.75
Width (mm)	1.31	1.47	1.28

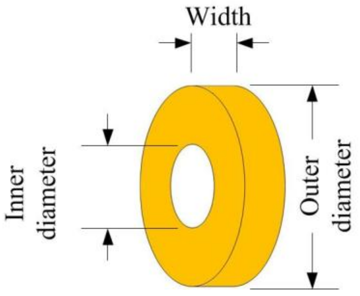

Figure 3-3. Coil dimensions

To evaluate the performance of the electromagnetic energy harvester a purpose built shaker test rig was used. It compromises a Labworks ET-126 Electrodynamic Transducer shaker connected to a signal generator HP 33120A through a Labworks PA-138 Linear Power Amplifier. The base acceleration at the shaker is measured using a PCB Piezotronics shear accelerometer model 355B04, with a sensivity of 1000 mV g^{-1}. The test rig is controlled using LabVIEW 8.0 and includes a Data Acquisition Card NI PCI-6281. A variable resistance and a vibrometer Keyence LC-2400W with a sensor head LC-2450 with a resolution of 0.5 μm are available and controlled by LabVIEW. The shaker rig is shown in figure 3-4.

The shaker test rig can be configured to generate a wide range of acceleration levels and frequencies. It is only limited by the maximum displacement that the base platform can extend to before contact with the shaker body occurs. The maximum displacement is 19.05 mm. The shaker can be driven up to a maximum frequency of 8500 Hz.

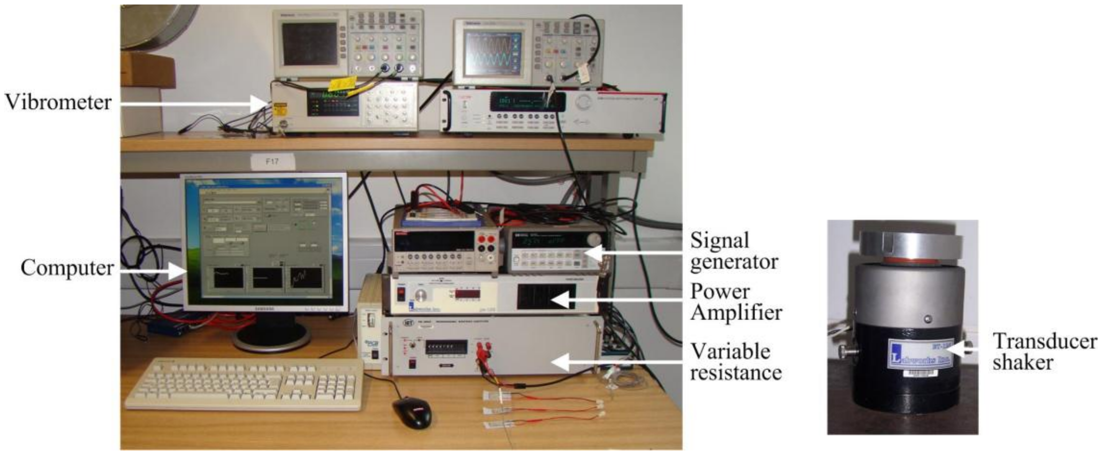

Figure 3-4. Shaker rig

The performance of the electromagnetic harvester, for each of the three coils, was evaluated using the shaker test rig to identify its frequency response and experimental maximum power generation when delivered into its optimum pure resistive load.

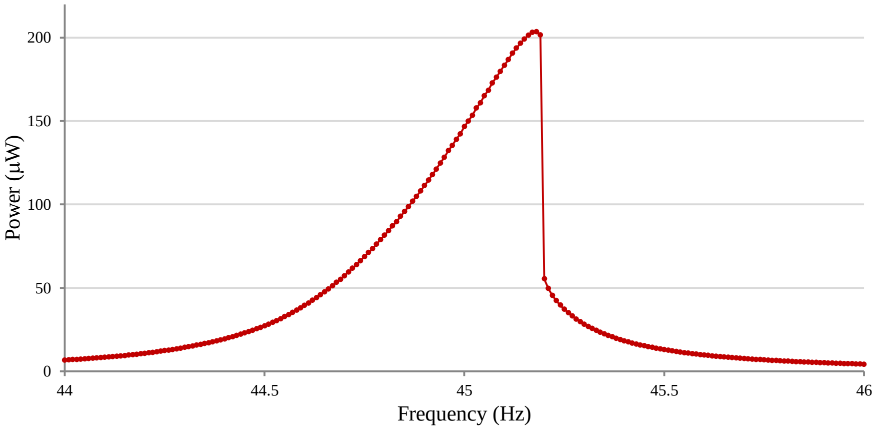

Figure 3-5. Frequency response of electromagnetic energy harvester

Figure 3-5 shows the response of the electromagnetic energy harvester, with coil A mounted, when the frequency increases. The excitation level was fixed at 0.588 ms^{-2} and the resistive load set at its optimum value for this harvester of 19750 Ω. The -3 dB bandwidth expands 0.33 Hz, from 44.87 to 45.2 Hz. The hard-spring non-linear response of the electromagnetic harvester is noticeable from the same figure. This harvester has a Q-factor of 136.

In figure 3-6 the non-linear response is further highlighted when the acceleration increases, i.e. beam's displacement increases, as described by Beeby, et al. [36]. It can be observed that the resonant frequency of the harvester changes with the variation of the acceleration, an effect of the non-linearity associated to the harvester. Figure 3-6b also shows the effect on the power when the displacement of the harvester increases beyond the maximum physically possible, resulting in the harvester impacting against its frame. The power generated reaches its maximum at this point and remains constant because the displacement cannot be increased any further. For harvester A′ this occurs from 45.25 to 45.55 Hz for an acceleration of 0.588 $ms^{-2}_{(rms)}$.

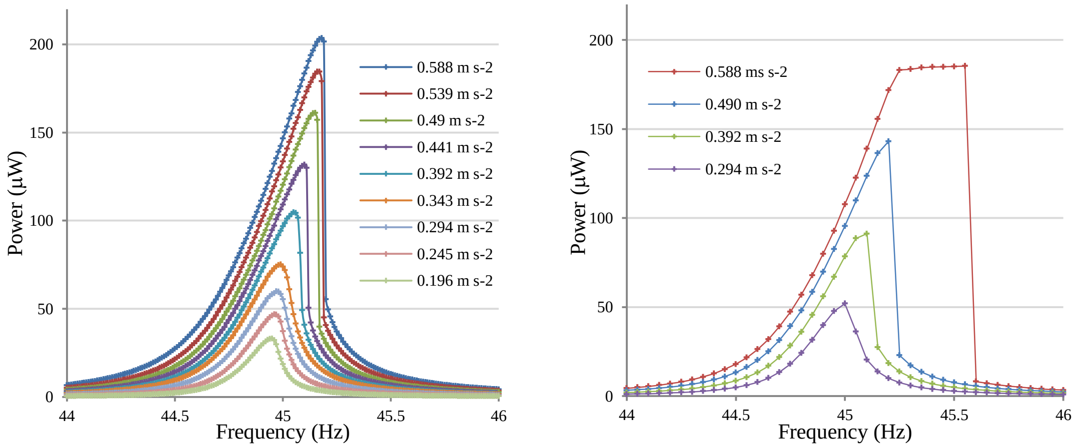

a. Harvester with coil A, load 19750 Ω   b. Harvester with coil A', load 26500Ω

Figure 3-6. Harvester response as base acceleration increases.

The resonant frequency is also affected by the load, as shown in figure 3-7 where coil B is loaded with different resistance values at selected frequencies and at a fixed acceleration of 0.588 $ms^{-2}_{(rms)}$. The maximum power is reached at a different load value for each frequency.

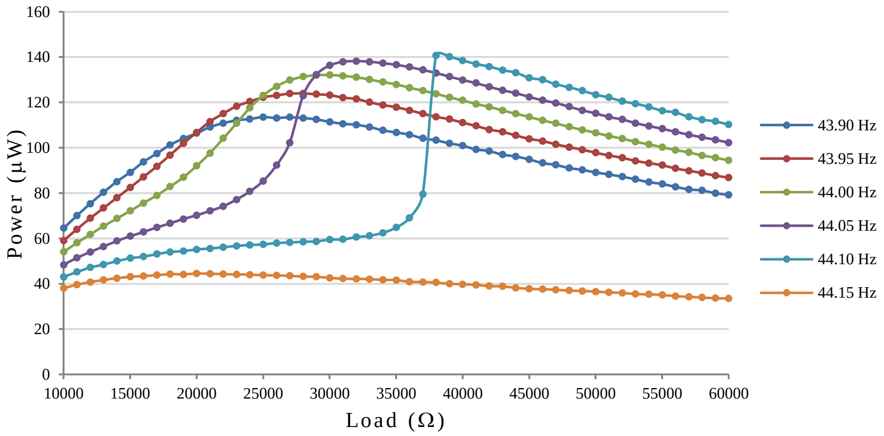

Figure 3-7. Power generation at different loads and frequencies for coil B

These results show two important points that must be taken into consideration for the design of the tunable energy harvester. First, the resonant frequency is a function of the acceleration and load, it is not a constant value; hence, the control system must be intelligent enough to compensate for this variation. Second, the harvester has a maximum physical displacement that is imposed by its physical frame; any contact between them must be avoided to protect the harvester from damage.

Table 3-3 summarize the results from the experimental tests carried out on the three coils. Even though harvester A and A′ use the same Coil A, their power generation differs by about 10%. This could be the result of small variations in the manufacturing process of the coils and the position of the coil in respect of the harvester beam. This latest effect can be observed in figure 3-8 which shows the response of the harvester when the position of the coil is adjusted towards the tip end of the beam. The power increases as consequence of the increase of the relative displacement of the beam at the tip end compared to the inner edge of the slot, also the resonant frequency increases.

Table 3-3. Harvester power.

	Harvester A	Harvester A′	Harvester B	Harvester C
Coil	A	A	B	C
Max. power @ 0.588 ms^{-2} (µW)	201	180	140	106
Optimal Load (kΩ)	26.50	36.00	33.00	1.00
Natural frequency (Hz) @ 0.294 ms^{-2}	45.25	46.3	44.05	46.70

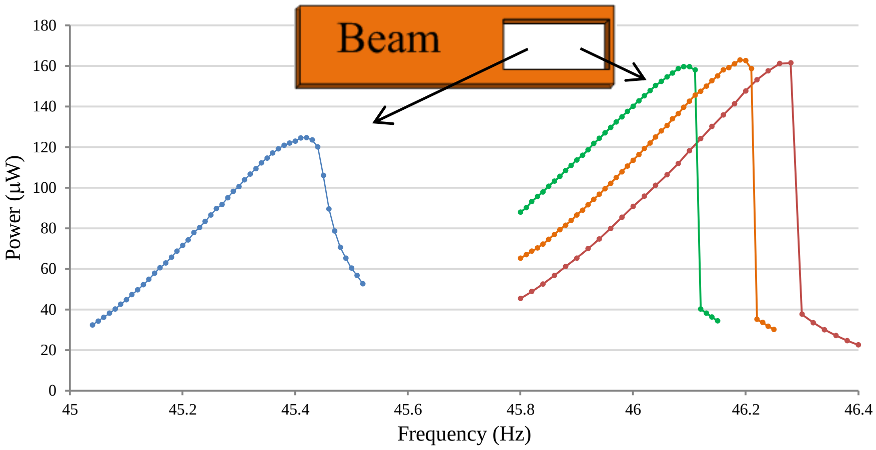

Figure 3-8. Resonant frequency and power variation as coil position changes.

3.2.2 Harvester frequency tuning principle

The tuning mechanism selected for this research was developed by Zhu, et al. [3]. The tuning principle of operation relies on the effect of the harvester resonant frequency when axial force is exerted on the beam. Axial compressive force reduces the resonant frequency of the beam, while tensile force increases it. Figure 3-9 presents a simulation of the harvester resonance frequency as function of the change in axial force applied to the beam, as expressed in equation (3-2) [66]. f_r is the resonant frequency without load, f_r*'* is the resonant frequency with axial load; F is the axial load and F_b is the compressive axial load required to buckle the beam.

$$f_r' = f_r\sqrt{1 + \frac{F}{F_b}} \tag{3-2}$$

Zhu, et al. [66] concluded that compressive force offers a larger bandwidth than tensile force, however compressive force also increases the parasitic damping. In contrast, the parasitic damping for axial tensile force remains almost constant. Hence, tensile force is preferred over compressive force.

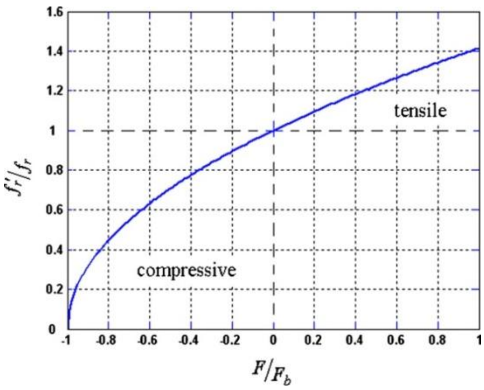

Figure 3-9. Change in resonant frequency with axial load [3].

The proposed tuning mechanism creates a non-contact axial tensile force by the use of two permanent magnets. The first tuning magnet is attached to the free end of the beam, as described in section 3.2.1., while a second tuning magnet is axially aligned to the beam. The assembly of both tuning magnets is presented in figure 3-10 with the beam bent up. The figure also shows the polarity arrangement of the tuning magnets to create a tensile force.

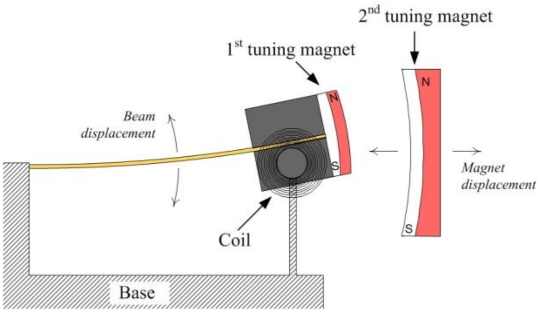

Figure 3-10. Tuning magnets ensemble
(not at scale).

The length and curvature of the tuning magnets were designed to maintain a constant distance between them when the beam moves as a consequence of the base excitation, therefore maintaining a constant force. Figure 3-11 shows the geometry and dimensions for the second tuning magnet.

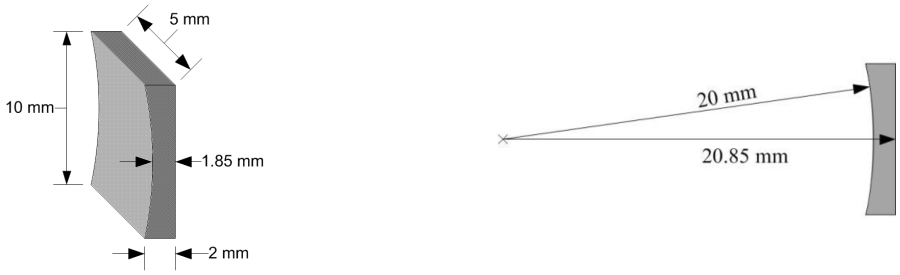

a. Magnet geometry b. radius of curvature

Figure 3-11. Second tuning magnet.

The second tuning magnet is mounted on a movable structure, allowing the adjustment of the distance between tuning magnets, i.e. the force exerted on the beam, and consequently the resonant frequency of the harvester.

The tensile force between tuning magnets was simulated and experimentally measured as show in figure 3-12, both results being in good agreement. The results are of great importance for the development of the autonomous harvester because they represent the maximum force required by the actuation mechanism to adjust the distance between magnets, as well as the force it must withstand to maintain the harvester at certain resonant frequencies. According to these results, the actuation mechanism must produce a maximum thrust of 4 N with a tuning distance (stroke) of at least 6 cm.

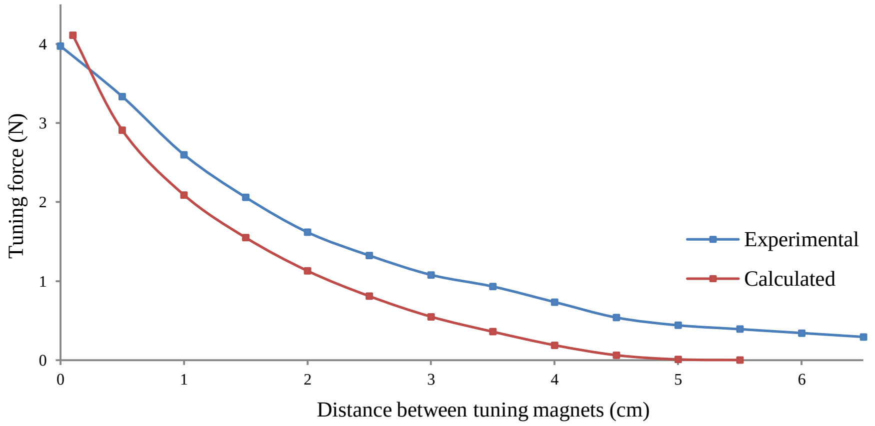

Figure 3-12. Tuning force as distance between tuning magnets varies.

3.3 Electrical components

The tuning capability of the energy harvester is based on its ability to adjust the tuning force exerted on the beam. This action requires not only an actuation mechanism, but also a method to control it. It is important to remember that the primary objective of the harvester is to generate the maximum amount of energy feasible; hence, the energy consumed during the tuning operation should be the lowest possible. Taking these considerations into account, the basic rule followed in the selection and integration of the components for the tunable energy harvester is their low energy consumption.

It is important to differentiate three energy concepts used throughout this document: energy generated, overhead energy and net energy. Energy generated is the energy transferred from the mechanical domain into the electrical domain by the electromagnetic harvester. Overhead energy is the energy used in the operation of the tunable energy harvester. Finally, net energy is the difference between the energy generated and the overhead energy, which is the energy available to the application electronics such as sensors and wireless transmitter. The aim is to reduce the overhead energy which increases the net energy available. In previous research by the author, et al. [74] an autonomous low power microsystem using an electromagnetic energy harvester was developed. From this research, a number of strategies were implemented to reduce the energy consumption of the system. The same strategies are applied here:

- Low power components.
- Power off all the electronics that are not in constant use, unless the start-up power is higher than the power saved by remaining active. Modify its duty cycle according to the needs of the system, as suggested by Arms, et al [97].
- Maintain in low power mode those components that cannot be switched off as recommended by Chandrakasan, et al [98].
- Reduce the computational processing in the microcontroller to reduce its duty cycle.
- Reduced voltage to reduce energy consumption.

3.3.1 Controller

One of the most significant potential applications of energy harvesting technologies is their use in environments where human activity is dangerous or prohibitive. It is expected that any adjustment required by the harvester must be made either by a remote command or autonomously by the harvester itself. Therefore, the harvester system must include an intelligent element to operate.

Already some examples of tuning strategies for energy harvesting have been presented in section 2.4. Nevertheless, most of them rely on the manual operation of the tuning mechanism contravening the principle of autonomous operation. In other cases, the overhead power is sourced from an external power supply and not from the power harvested.

An autonomous tunable energy harvester is proposed that relies exclusively on the energy harvested to sense the environment, control the operation of the system and adjust its tuning mechanism to maximize the net energy.

The three basic activities of sensing, supervision and adjustment are performed by a central entity in the form of a microcontroller. There are a large range of commercial microcontrollers with low power characteristics that make them suitable for energy harvesting purposes. A few examples are ATMEL ATmega series, Texas Instruments MSP430 and Microchip PIC16 family, all with similar performance. PIC16 family was selected for this research because the platforms required for it use were already available at the School of Electronics and Computer Science.

PIC16F884 was the microcontroller selected for the tunable energy harvester. It has 35 input/output ports and, significantly, an output port current of 25 mA. This characteristic allows to power devices directly from any of the ports. Table 3-4 summarize the most important characteristics of the microcontroller.

Table 3-4. PIC16F884 characteristics

Operating voltage	2.0 – 5.5 V
Standby current	50 nA @ 2.0 V
Analog/Digital converter	10-bit resolution, 14 channels
Timer/Counter	3
Program memory	4096 words
SRAM	256 bytes
EEPROM	256 bytes
I/O ports	35
Output port current	25 mA

3.3.2 Actuator

The design of the autonomous tunable energy harvester requires an actuation mechanism that can adjust the distance between the tuning magnets. The minimum mechanical specifications that such a device must fulfil are drawn from the results in figure 3-12:

- Stroke equal or higher than 6 cm.
- Minimum thrust of 4 N.

Additionally, the actuator must hold its position without further power consumption, e.g. when the power has been cut off.

The electrical considerations for the actuator follow the same as for the rest of the components in the system: low power consumption and low voltage. The actuator's travel resolution is not considered as important as the previous specification at this stage, where the proof of principle of the tunable energy harvester is assessed.

A survey on commercial actuators has identified two different technologies with potential use on the tunable system: piezoelectric and electromagnetic actuation.

Piezoelectric actuators convert electrical energy into motion. The moving part is fabricated using a piezoelectric material, which is in contact with the stator. The displacement of the piezoelectric material in the desired direction creates, by frictional force, displacement of the stator. The advantage of piezoelectric actuation is its low current consumption and high accuracy; this is overshadowed by the need of high driving voltages, typically tens of volts, requiring the voltage to be step-up with the associated power losses that this process would incur.

Electromagnetic actuators use an electric motor to create rotational motion, which can be mechanically transformed to linear displacement. Electromagnetic actuation is a technology well established and widely available commercially. In particular, actuators using stepper motors have the advantage that the shaft position can be controlled with precision by controlling the number of steps given. The drawback of this technology, in comparison to piezoelectric actuation, is its higher power consumption.

A variety of commercial linear actuators have been investigated, a selection of those with the most appropriate characteristics for use in the tunable energy harvesting are presented in table 3-5.

Table 3-5. Commercial linear actuators.

Type	Model	Manufacturer	Power (W)	Voltage (V)	Force (N)	Drawbacks
Piezoelectric	PiezoWave	PiezoMotor	0.28	4	0.5	Force
Electromagnetic	LPV2515	Nanotec	1.00	5	10	Voltage
Electromagnetic	PQ-12	Firgelli	1.25	5	6	
Electromagnetic	**LC1574W**	**Haydon**	**1.60**	**4**	**7**	
Electromagnetic	21H4AD	Haydon	2.45	2.5	10	Power
Electromagnetic	20541	Haydon	2.7	5	8	
Piezoelectric	Piezo Legs	PiezoMotor	10.5	42	6.4	
Piezoelectric	SQ-115	New Scale Technologies	1.50	Driver	5	External driver

It was identified that even when piezoelectric actuators consume less power than electromagnetic, their maximum thrust is relatively small, hence they are not suitable for the tuning system employed here.

The decision on the selection of the actuator was based on the voltage and power consumption required. The actuator LC1574W from Haydon was chosen due to its power consumption of 1.6 W at 4V. Even though it has higher power consumption than LPV2515 and PQ-12, its lower voltage makes it more appropriate for the tunable energy harvester. Table 3-6 presents the electrical characteristics of the LC1574W.

Table 3-6 Linear actuator characteristics

Model	Haydon LC1574W-V
Wiring	Bipolar
Power Consumption	1.6 W
Supply voltage	4 V
Current	200 mA/phase
Resistance	20 Ω/phase
Inductance	5.6 mH/phase
Stroke (mm)	12.7 mm
Thrust	7 N @ 100 steps/sec
Resolution	0.02 mm/step

The actuator selected has a two-phase stepper motor. The polarity and timing at which each phase is energized determines the direction of movement and speed of the shaft. The direction is selected according to the stepping sequence of the motor as suggested by the manufacturer in table 3-7, where Q_x-Q_y represents a switch pair that limits (OFF) or enables (ON) the current flow through the actuator according to the wiring diagram in figure 3-13. An additional condition, called “de-energized”, is proposed to restrict the current flow on the actuator. In this state, all the switches are disabled saving energy.

Table 3-7. Stepping sequence [99]

	Step	Q_2-Q_3	Q_1-Q_4	Q_6-Q_7	Q_5-Q_8	
Extend ⇩	1	ON	OFF	ON	OFF	Retract ⇧
	2	OFF	ON	ON	OFF	
	3	OFF	ON	OFF	ON	
	4	ON	OFF	OFF	ON	
	De- energized	OFF	OFF	OFF	OFF	

3.3.2.1 Switching control

The switching action is performed by a Metal-Oxide-Semiconductor Field-Effect Transistor (MOSFET) placed in a two H-bridge configuration, as show in figure 3-13. One H-bridge is connected to each of the actuator’s wiring, driving the polarity of the actuator from an ON to OFF state as required. Two different configurations for the H-Bridge were evaluated. The first configuration uses N-MOSFET exclusively, while a second uses a combination of N-MOSFET and P-MOSFET.

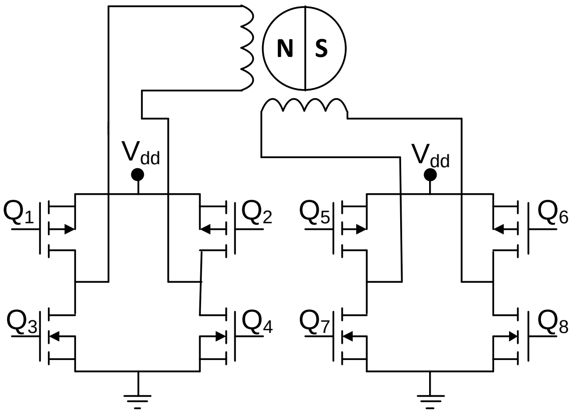

Figure 3-13. Wiring diagram, modified from [99]

- N-MOSFET

In this configuration all the transistors in the H-bridges are N-MOSFET. The advantage is that only four control lines are required to operate the H-Bridges, one line for each paired transistor. The transistor's control is achieved by varying the voltage at the gate between 0 V and the voltage at V_{dd}, limiting or allowing the current flow respectively.

Table 3-8 presents the results from Pspice simulations where a single H-Bridge was driven using a range of commercial N-MOSFETs models. The results indicate that the transistors in the path close to the positive voltage source V_{dd} (Q_1, Q_2, Q_5, Q_6 in figure 3-13) require a higher voltage at the gate than V_{dd} to operate in the saturation region, where the current flow through the MOSFET.

If the N-MOSFETs are driven at the same voltage level as V_{dd}, the current and voltage at the actuator do not reach the minimum requirement of 200 mA per phase and 4 V suggested by the manufacturer, the transistor operates in the linear region acting as a resistor. The voltage at the gate can be stepped-up to drive the N-MOSFET but this would incur in additional overhead power. To avoid this, an alternative configuration is proposed.

Table 3-8. N-MOSFET H-Bridge simulation

Model	(Q_1 -Q_2)		(Q_3 -Q_4)		Voltage at actuator terminals (V)	Current (mA)
	V_{gs}	V_{ds}	V_{gs}	V_{ds}		
ZVN3310A	2.64	2.64	4	0.347	1.007	45
MLP1N06CL	1.98	1.98	4	0.066	1.946	97.3
ZXMN2A14F	1.33	1.33	4	0.006	2.659	118
ZXMN2B14FH	0.94	0.94	4	0.006	3.038	152
ZXMN2B03E6	0.87	0.87	4	0.005	3.123	156
ZXMN2B01F	0.79	0.79	4	0.014	3.193	170

- N-MOSFET and P-MOSFET

In the second configuration, the N-MOSFETs at the top side of the H-Bridge are substituted by P-MOSFETs, as show in figure 3-13. Unlike the previous configuration, in this case each paired transistor is formed by one N-MOSFET and one P-MOSFET. This modification has as consequence that each paired transistor will need two control lines, instead of one as in the first configuration, for a total of eight lines for both H-Bridges. The voltage required to drive the MOSFET in the saturation region falls within the range of 0 V to V_{dd}, eliminating the need for a voltage step-up.

Simulations in Pspice using the second configuration show that current and voltage at the actuator reach values close to those specified by the manufacturer, 200 mA and 4 V, as show in table 3-9. The MOSFET selected were ZXM61P02F and its complementary ZXM61N02F.

Table 3-9. N-MOSFET and P-MOSFET H-Bridge simulation

Model	(Q_1 -Q_2)		(Q_3 -Q_4)		Voltage at actuator terminals (V)	Current (mA)
	V_{gs}	V_{ds}	V_{gs}	V_{ds}		
ZXM61P02F ZXM61N02F	-4	-0.06	4	0.023	3.91	195.5
ZXM61P02F ZXMN2B01F	-4	-0.06	4	0.016	3.91	195.86
FDV304P ZXMN2B01F	-4	-0.2	4	0.01	3.79	189.39

The second configuration was selected because the requirement of four extra control lines draw minimal energy compared to stepping-up the voltage as required for the first configuration.

3.3.2.2 Voltage reduction at actuator

The linear actuator is the element with the highest power consumption of all the components of the tunable energy harvester. To reduce this, the actuator was tested under different scenarios to characterize its performance. The main objective was to find an optimal operating setting, which required the minimum power possible, by means of increasing its actuation speed and reducing its operating voltage.

Increasing the speed reduces the time required to move the actuator, effectively reducing the energy used. However the actuator's thrust is inversely proportional to the speed, as shown in the actuator's manufacturer specification in figure 3-14. Furthermore, the thrust is also affected by the reduction in the voltage. Thus, speed, voltage and thrust are closely related in the operation of the actuator.

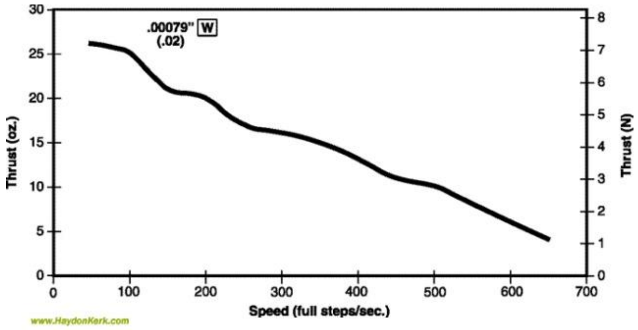

Figure 3-14. Step rate Vs. thrust. Haydon series 15000. [99]

The actuator was experimentally tested under different operating voltages. It was considered that the reduction in the voltage supply is the main factor in reducing the power consumption of the actuator because it also brings down the current consumption.

The actuator was driven with supply voltages ranging from 3 to 4 V, with a mechanical load of 6.4 N, at a speed of 100 steps s^{-1}. The power consumed by the actuator reduces as the supplied voltage reduces, as can be seen in figure 3-15. The actuator stopped moving and the power consumption increased to the nominal value of 1.6 W specified by the manufacturer for values below 3.4 V.

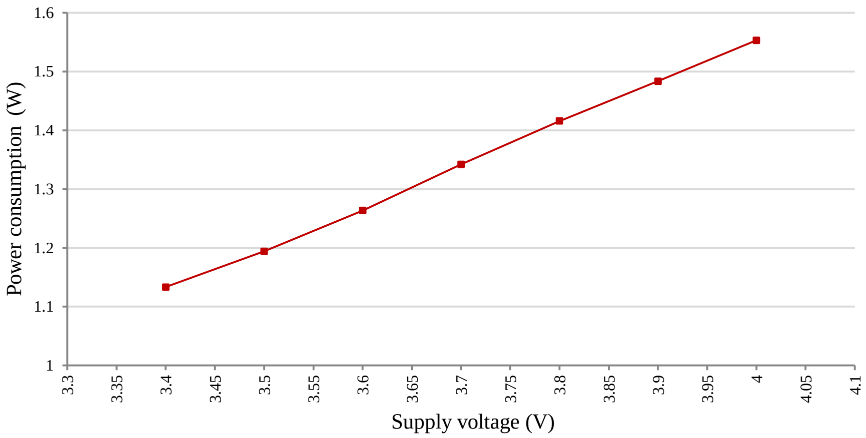

Figure 3-15. Actuator power consumption for different supply voltage**.**

Subsequent evaluation of tunable energy harvester, presented in section 4.2, will show that the optimal range of operation of the tuning mechanism is when the distance between tuning magnets is 5 to 3 mm apart. This has as a consequence that the maximal thrust needed reduces to 1 N.

The actuator was further evaluated at this new operating range while mounted on the shaker with the tuning mechanism and the harvester assembled. The tunable energy harvester was powered from an external power supply. The voltage and speed was varied to identify the combination with the lower voltage and maximum speed. It was found that the start-up voltage for the actuator was 2.6 V. Once moving, 2.4 V is sufficient to maintain actuation. The thrust generated at 200 steps s^{-1} was found to be sufficient to move the magnets against the maximum attractive force of 1 N that occurs when the tuning magnets are 1 mm apart. Increasing the actuator speed would prevent the actuator from moving.

Figure 3-16 shows the effect that the reduction in voltage supply has on the current and power consumed by the actuator. The power reduces from 216 $mA_{(rms)}$ and 0.86 W at 4.0 V to 130 $mA_{(rms)}$ and 0.34 W at 2.6 V. The current flow into the actuator when the voltage supply varies from 2.6 to 4 V for 4 consecutive steps at 200 steps s^{-1}, is presented in figure 3-17. It shows the drop in current from 251 to 159 mA_{peak}, when the voltage reduces from 4 to 2.6 V, respectively.

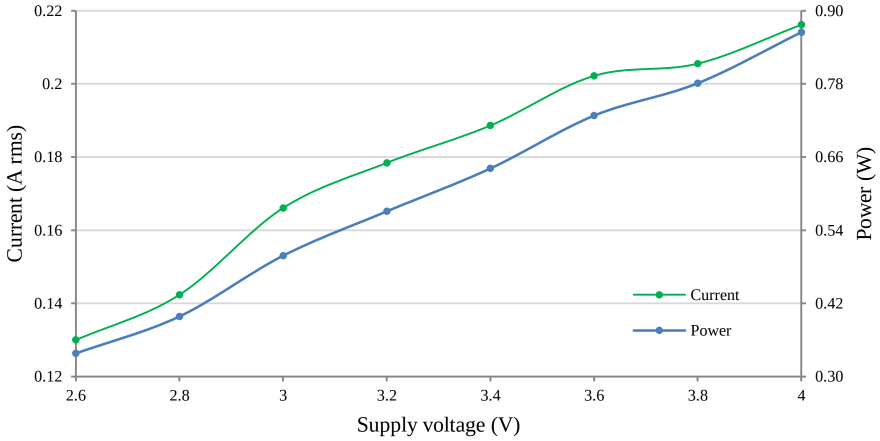

Figure 3-16. Actuator current at energy consumption at 200 steps s^{-1}

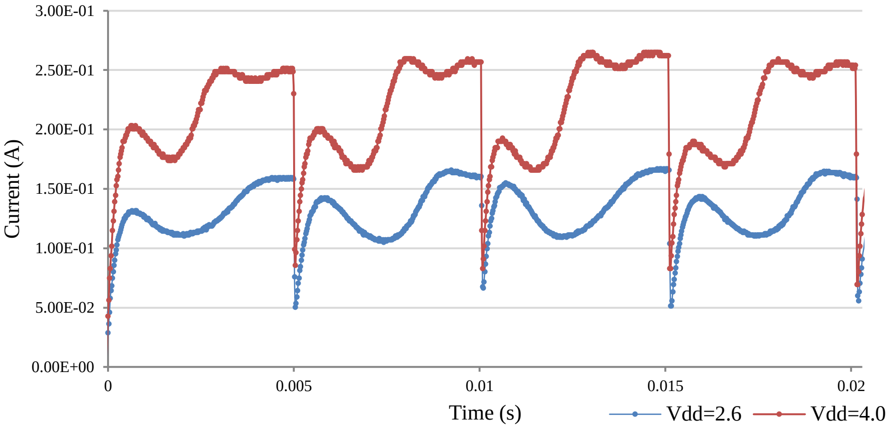

Figure 3-17. Current flowing into actuator at different supply voltages

The reduction in power consumption by the actuator of 60% when the supply voltage reduces from 4 to 2.6 V is the principal reason to select 2.6 V as the minimum operating voltage for the tunable energy harvester. Equally important is the time taken by the system to charge the storage capacitor, less time is necessary to charge the storage capacitor until its voltage reaches 2.6 V than 4 V.

3.3.3 Energy rectification and conversion

The electromagnetic energy harvester presented in section 3.2 generates low AC output voltages, from 350 mV$_{(rms)}$, when subject to base excitation. Consequently, it must be rectified and increased to a level greater than 2.0 V to be used by the electric load. From the different alternatives presented in section 2.5, a switched capacitor strategy was chosen in the form of a Dickson charge pump, or Voltage Multiplier

(VM), because it does not require an additional control to operate, saving overhead power. The VM operation is based on pumping charge from one stage to the next via a diode acting as a switch.

Schottky diodes have been selected because of their reduced voltage threshold, although affected by higher reverse current, compared to standard diodes. Three commercial Schottky diodes were identified with characteristic low forward voltage: BAT85, BAT760 and BAT754L. Their basic electrical characteristics are presented in table 3-10.

Table 3-10. Schottky diodes characteristics

Model	Threshold voltage	Reverse current	Forward current max.
BAT85	240 mV @ 0.1 mA	0.2 µA @ 5 V	200 mA
BAT754L	200 mV @ 0.1 mA	0.6 µA @ 5 V	200 mA
BAT760	100 mV @ 0.1 mA	5 µA @ 5 V	1000 mA

A 5 stage VM was built to evaluate the performance of each diode model. The VM was attached to the electromagnetic harvester, without the tuning mechanism, and a storage capacitor of 0.55 F was connected as the load. Figure 3-18 shows the electrical connection of the circuit. The purpose of this test was to identify the diode that charges the storage capacitor in the lowest time from 0 to 2.6 V. The electromagnetic harvester was excited at its resonant frequency with an acceleration of 0.588 $ms^{-2}{}_{(rms)}$.

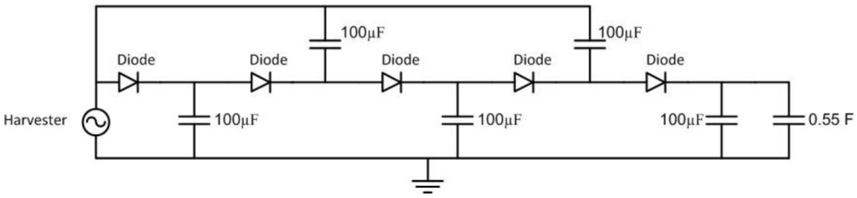

Figure 3-18. 5 stage VM

The experimental results presented in figure 3-19 show that model BAT760 and BAT754L reach 2.6 V in similar time, 37.8 and 38 hrs respectively, while BAT85 reaches the same voltage in 40.5 hrs. Based on these results and its low leakage current, diode model BAT754L was selected for the tunable energy harvester.

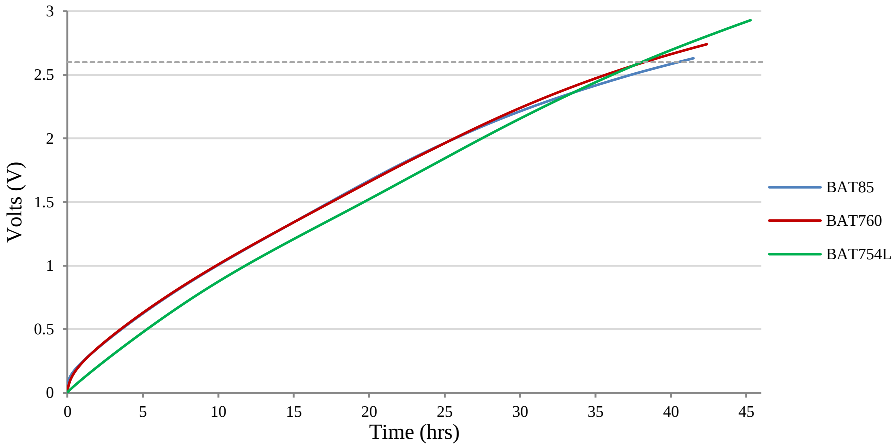

Figure 3-19. Charge of storage capacitor for different diodes

3.3.4 Energy storage

The energy can be employed by the application electronics once the energy has being rectified by the VM. Nevertheless, the energy available in the environment for transduction by the harvester may not be constant, or not enough to power the application electronics. Therefore the energy has to be saved and used when the system requires it, for example, when the base frequency changes and the resonant frequency of the harvester must be adjusted, or to sense and transmit information. An energy storage element in the form of a capacitor is chosen for the tunable energy harvester to fulfil this requirement. It has the advantage over batteries that it does not require extra circuitry to charge.

The storage capacitor size must be calculated to guarantee that sudden peaks in energy consumption, mainly due to the use of the actuator, can be accommodated. Otherwise, the adjustment of the resonant frequency cannot be accomplished, leaving the harvester inoperative due to disparities between its resonance frequency and the base frequency. As explained in section 3.3.2, the minimum start up voltage for the actuator is 2.6 V. Once moving, 2.4 V is sufficient to maintain actuation. The current consumed by the actuator at 2.6 V is 130 mA$_{(rms)}$ with peak current of 167 mA. The maximum time taken by the actuator to adjust the harvester's resonant frequency is 0.5 sec. This represents a 2 mm displacement at a speed of 200 steps per second. This range will be discussed in detail in section 4.4.1.

Simulations on Pspice show that the minimum capacitance required to operate the actuator is 0.5 F. In this case, the voltage drops 139 mV when the actuator is operated at an initial voltage of 2.6 V supplying 172 mA and reaching 2.45 V at 163 mA after 0.5 sec.

Different commercial capacitors were investigated in search for those models that fulfil the specifications of the tunable energy harvester: 0.5 F, peak current of 167 mA and operating voltage higher than or equal to 2.6 V. It was identified that supercapacitors, or electric double-layer capacitors, offer high capacitance values and low equivalent series resistance (ESR). They are relatively insensitive to charge and discharge cycles and do not require special circuitry to charge [100].

Commercial supercapacitors such as Panasonic Gold Capacitors [101] offer high capacitances, from 0.047to 50 F, however those models in the range of 0.5 F have low operating voltage or low discharging current in the range of microamperes to a maximum of 1 miliampere, as show in table 3-11. Alternatively, CAP-XX supercapacitors [102] have high peak current and operating voltage above 2.6 V which make them suitable for the tunable energy harvester, its characteristics are also presented in table 3-11. The capacitor selected was CAP-XX GS206F with a measured capacitance value of 0.55 F.

Table 3-11. Selection of commercial supercapacitors

Manufacturer	Model	Capacitance (F)	Max. Voltage (V)	Leakage Current (μA)	Peak Current (mA)	Drawbacks
CAP-XX	GS206F	0.6	4.5	2.09	30000	
CAP-XX	GS208F	0.9	4.5	2.27	30000	Capacitance
Panasonic	HW series	1	2.3	0.2	100	Capacitance & Current
Panasonic	SG series	0.47	5.5	0.2	1	Current

The charging time of the supercapacitor using the energy harvester was experimentally measured. The excitation level was fixed at 0.588 $ms^{-2}{}_{(rms)}$ and the harvester was driven at resonance frequency of 45 Hz, using coil A. The energy harvester and storage capacitor were connected to the VM, as shown in the insert of figure 3-20.

Figure 3-20 shows the increase in voltage at the storage capacitor as it charges. The output voltage from the harvester increases because of the increase in the impedance seen by the harvester. The voltage at the harvester starts at 144 mV$_{rms}$, reaching 589 mV$_{rms}$ after 63 hrs. The voltage at the storage capacitor reached 2.6 V in 38.09 hrs. The results collected are used as a benchmark for later tests of the tunable energy harvester.

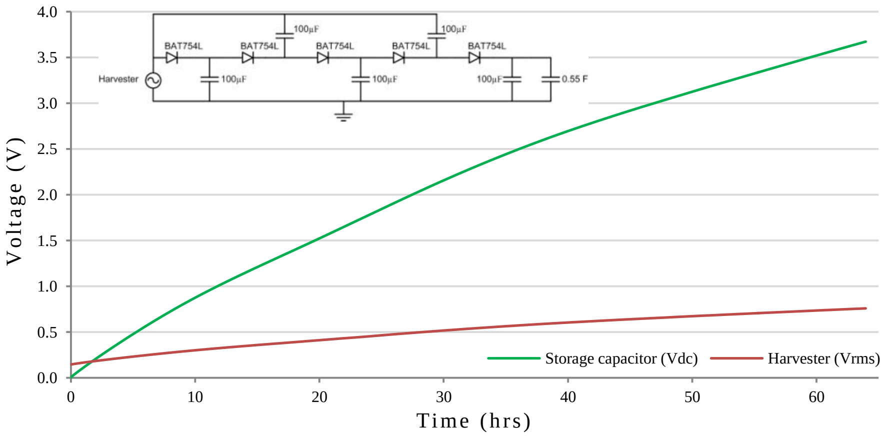

Figure 3-20. Storage capacitor charging time.

The power at the storage capacitor was indirectly measured to avoid the additional impedance that measuring the current using a current meter brings. The power is calculated based in two consecutive measurements of the voltage at the storage capacitor according to the equation (3-3).

$$\Delta P = \frac{C\left({V_2}^2 - {V_1}^2\right)}{2(t_2 - t_1)} \tag{3-3}$$

Figure 3-21 shows the calculated power for the previous test. It can be observed that after approximately 25 hrs the power reaches a level in the range of 20 µW, which is just 10% of the power that this coil generated when delivered into its optimal resistive load, as presented in table 3-3. The low level of power generation during the first 20 hrs of the test indicates that the harvester is operating below optimum. The power increases as the impedance seen by the harvester increases during the second half of the test.

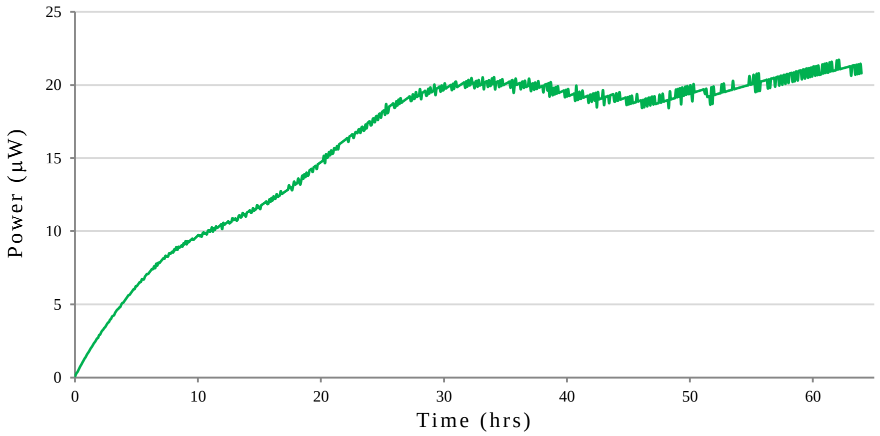

Figure 3-21. Power at storage capacitor.

3.4 Tuning upon a magnetic flux guide

A second tuning mechanism was also evaluated. This design relies on the disruption of the magnetic field created between the tuning magnets by inserting a material with high permeability acting as a flux guide. The flux guide alters the magnetic flux between the tuning magnets, which in turn modifies the force exerted on the cantilever, hence its resonant frequency.

This idea was originally proposed by Imperial College London as part of the Holistic Approach to Energy Harvesting Electronics project [103]. Here, it was evaluated with the aim of comparing the frequency range feasible and the force required to operate such a device.

The magnetic flux tuning mechanism utilises the same tuning structures as for the design previously proposed in this chapter, i.e. an electromagnetic harvester with an additional tuning magnet at its free-end, and a second tuning magnet positioned at close range of the harvester. Though, the second tuning magnet is fixed at a certain distance from the harvester and it does not move. Instead, an additional structure is included that holds the magnetic flux guide between the two tuning magnets, which also enables the adjustment of the overlap of the flux guide. Figure 3-22 presents a picture of the mechanism where the tuning magnets and flux guide can be observed.

Analysis of the tuning mechanism upon the magnetic flux guide, presented in Chapter 7, shows that this mechanism offers a lower resonant frequency range of adjustment for the same harvester than using the tuning mechanism presented in section 3.2. It requires a maximum thrust force of 1 N, if friction between the flux guide and the 2nd tuning magnet is avoided, which is similar to the maximum force required by the tuning mechanism based upon adjusting the distance between tuning magnets.

Further details about the tuning mechanism upon magnetic flux guide will be presented and discussed in Chapter 7.

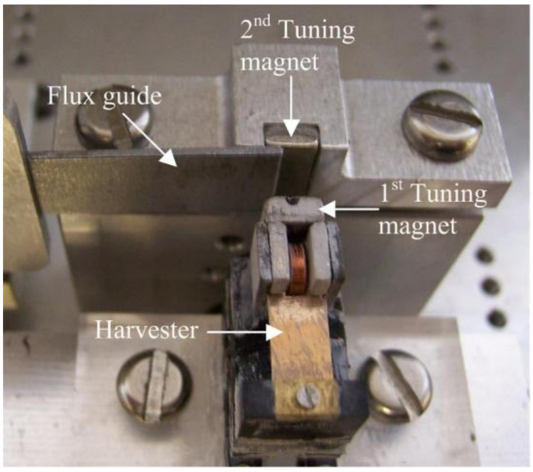

Figure 3-22. Magnetic flux tuning mechanism

3.5 Conclusion

This chapter detailed the different mechanical and electrical components of the tunable energy harvester. The electromagnetic energy harvester and the tuning mechanism that alters its resonant frequency were presented. Axial tensile load is applied to the cantilever structure of the harvester through a pair of tuning magnets. The distance between tuning magnets determines the force exerted on the cantilever, effectively changing its resonant frequency.

Experimental evaluation of four different harvesters has shown that they exhibit a hard spring non-linear behaviour. This effect increases as the base acceleration increases, resulting in a shift in the harvester resonant frequency; hence the control system must be able to compensate for the change in resonant frequency not only due to the tensile force exerted by the tuning magnets, but also due to the non-linear behaviour.

The selection of the electronic components for the tunable harvester was based on the need for low power consumption and low operating voltage. The element with the highest consumption is the actuator. Electromagnetic actuation was selected because it can generate the required level of thrust for the tuning mechanism proposed at the lowest power. To reduce its energy consumption, the operating voltage and speed of actuation were experimentally evaluated. The voltage was reduced from 4 to 2.6 V, reducing the power consumption by 60% of the manufacturer’s published value. The speed was set at 200 steps per second, to reduce the time taken by the actuator to adjust the harvester’s resonant frequency.

The charging of the storage capacitor was experimentally evaluated at a fixed base frequency and acceleration. The energy extraction and conversion is performed by a VM using Schottky diodes. It took 38.09 hrs to charge the storage capacitor to 2.6 V. This result was used as a benchmark for the optimization of the tunable harvester.

In conclusion, this chapter has presented the different mechanical and electrical components comprising the tunable energy harvester. The next chapter describes the development of a fully autonomous tunable energy harvester that is powered exclusively from the energy it harvests and that autonomously adjusts its resonant frequency to match the base frequency.

Chapter 4

Tunable energy harvester

4.1 Introduction

This chapter presents the characterization of the electromagnetic harvester including the tuning mechanism, denoted as tunable energy harvester. Section 4.2 describes an experimental investigation of the bandwidth of operation and the effect that the inclusion of the tuning mechanism has over the power generated. Two control strategies to operate the tunable energy harvester, open and closed loop, are discussed in section 4.3. Section 4.4 presents the three basic tasks required to control the tunable energy harvester: energy management, frequency measurement and phase difference measurement. The implementation of the control strategy in the microcontroller is presented in section 4.5. Finally, section 4.6 reports on the autonomous operation of the tunable energy harvester, where the system is powered exclusively by the energy it harvests to adjust its resonant frequency.

Throughout the present chapter the following terms will be used, they are related to the control mechanism of the tunable energy harvester:

- *Base acceleration and frequency*. Acceleration and frequency level measured at the shaker rig's transducer. This is considered the base excitation to which the tunable energy harvester must adapt.
- *Harvester voltage*. Output voltage generated by the harvester.
- *System voltage*. Voltage measured at the storage capacitor.

- *Base-Harvester period difference*. Period difference measured between the base acceleration and the harvester voltage.
- *Actuator position*. Position of the actuator measured in steps from a predefined origin.

4.2 Tuning Characterization

The bandwidth of operation of the tunable energy harvester was experimentally found by adjusting the distance between tuning magnets from 13 to 2 mm, in 1 mm decrements. The harvester A was connected to a resistance of 19.75 kΩ, which tests show was its optimal load, and the base acceleration remained at 0.588 $ms^{-2}_{(rms)}$ throughout the tests. This level of acceleration was set as the benchmark of operation of the tunable energy harvester because it is considered to be an indicative of the type of vibration levels found in industrial applications, as reported by Beeby, et al. [20]

For this test, the linear actuator and the microcontroller were externally powered. The actuator position was manually controlled through the microcontroller by the use of electrical switches that commands the extension or retraction of the actuator's shaft, increasing or decreasing the distance between tuning magnets

The resonant frequency and level of power generated was measured at each position. The resonant frequency of the harvester varies from 47.72 to 87.84 Hz, when the distance between tuning magnets reduces from 13 to 2 mm respectively, as shown in figure 4-1. Each line in figure 4-1 represents an adjustment of 1 mm, or 50 steps of adjustment on the actuator.

The variation in the resonant frequency per displacement increases as the distance between tuning magnets reduces, i.e. the resonant frequency changes by 0.73 Hz when the distance between tuning magnets decreases from 13 to 12 mm, while when the distance reduces from 3 to 2 mm, when the resonant frequency changes by 9.98 Hz. This non-linear behaviour is a consequence of the rapid increase in electromagnetic force between the tuning magnets as the distance reduces, as presented in figure 3-12.

The increasing electromagnetic force has a negative effect on the power generated by the harvester, which drops as the distance between magnets reduces. At 13 mm the power reaches 202 μW, reducing to 51 μW at 2 mm. Zhu, et al. [66] explains this effect as the result of the large restoring force caused by the tuning magnets, compared to the inertial force of the base acceleration, which increases the damping, and reduces the power. Furthermore, the harvester is subject to a sinusoidal base excitation, as shown in equation (4-1), where y displacement of the base, Y is the maximum amplitude and ω is the angular frequency. The base acceleration can be calculated by differentiation and it is written in equation (4-2).

$$y(t) = Y\, sin(\omega t) \tag{4-1}$$

$$\ddot{y}(t) = -\omega^2\, Y\, sin(\omega t + \pi) \tag{4-2}$$

Combining equations (4-1) and (4-2) show that, at a fixed acceleration, the maximum base displacement reduces as the angular frequency increases, as presented in equation (4-3). Therefore, the power generated by the harvester reduces taking into account that the power is proportional to the displacement, as presented in equation (2-3).

$$Y = \frac{\ddot{y}}{-\omega^2} \tag{4-3}$$

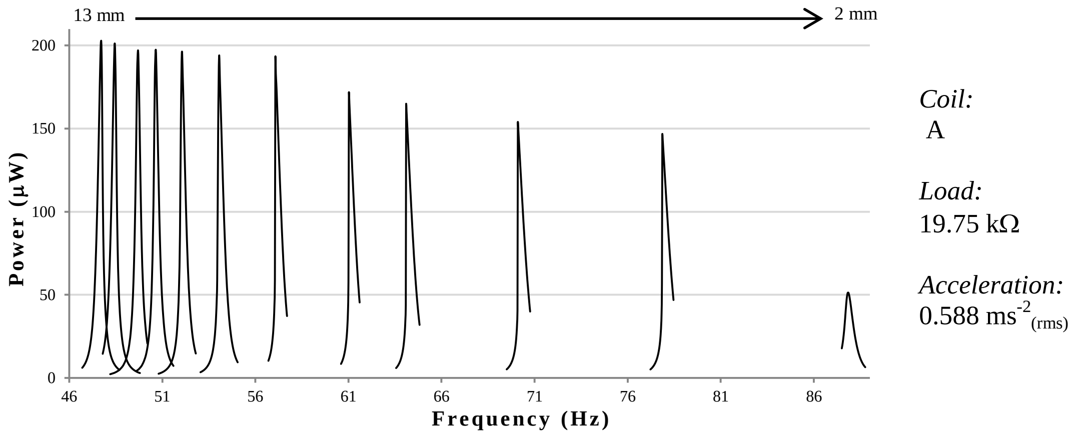

Figure 4-1. Resonance frequency variation as distance between tuning magnets decreases from 13 to 2 mm.

Two extreme cases can be observed from figure 4-1. At larger tuning distances, greater than 9 mm, the power generation is the higher; however, the frequency bandwidth between two consecutive lines is small. In contrast, at smaller tuning distances, the frequency bandwidth is larger but the decrease in the power generation is considerable.

The optimal range of operation for the tunable energy harvester considers the frequency bandwidth, the power generated and the displacement required to accomplish the proposed bandwidth. From these premises, the principal limiting factor is the linear actuator. It is the component with the highest energy consumption in the system. Considering these factors, the optimal distance between tuning magnets was constrained to 2 mm, from 5 to 3 mm apart. This represents 100 steps adjustment on the linear actuator. The range selected increases the bandwidth of operation of the harvester to 14.26 Hz, from 64.06 to 78.32 Hz, whilst the average power generated by the harvester reduces by 22%, compared to the case where the tuning mechanism is not present, as described below.

4.2.1 Resonance frequency at selected distance range

The variation in resonant frequency as function of the change in the distance between magnets was found experimentally. The distance was reduced in 20 μm decrements, or 1 actuator step, from 5 to 3 mm. The harvester was connected to a resistive load of 19.75 kΩ and the base acceleration was set to 0.588 $\text{ms}^{-2}{}_{(\text{rms})}$. The results are shown in figure 4-2, where the lines curves correspond to 60 μm adjustment for clarity in the graph.

It is shown that the resonant frequency can be tuned from 64.06 to 78.32 Hz, a range of 14.26 Hz, when the distance between magnets reduces from 5 to 3 mm. This range is measured from the frequency at which the power generation is maximum at 5 mm, to the frequency with the maximum power at 3 mm. This range represents a bandwidth increase of more than 21 times in respect to the harvester without tuning, where the -3 dB bandwidth is 0.65 Hz. On average, the resonance frequency changes by 0.142 Hz every time the distance between magnets is adjusted by 20 μm, or one step of the actuator.

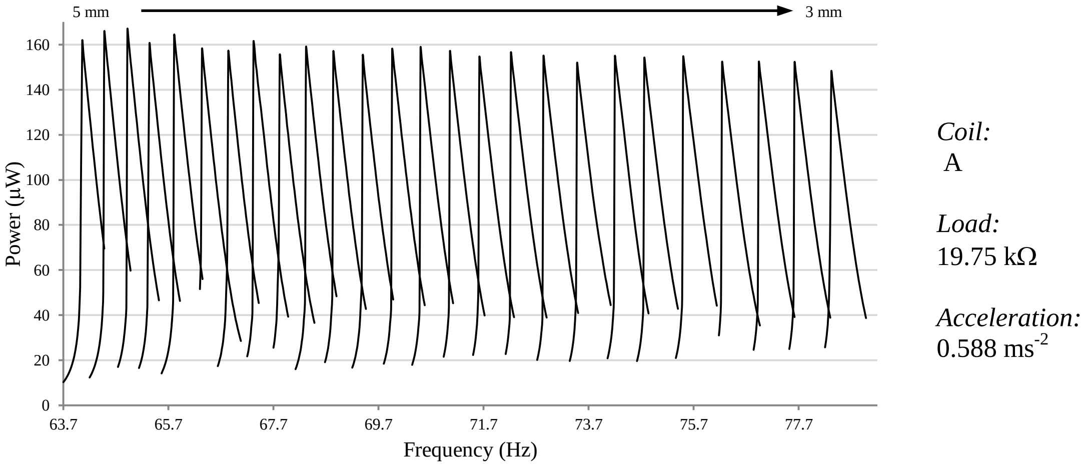

Figure 4-2. Resonant frequency range at 0.588 $\text{ms}^{-2}{}_{(\text{rms})}$

The observation of the variation of the resonant frequency as function of the distance between magnets was repeated at a lower base acceleration. This test was performed with the purpose of identifying the difference in the bandwidth as the base acceleration reduces.

The base acceleration was set at 0.294 $\text{ms}^{-2}{}_{(\text{rms})}$ with the harvester connected to a purely resistive load of 26.5 kΩ. The initial position of the actuator was set to coincide with a resonance frequency of 64.06 Hz, which corresponds to a distance between tuning magnets of 5 mm. Following the same procedure as previously; the acceleration remained constant and the actuator was adjusted by 1 step, 20 μm, on every occasion, reducing the distance between magnets. The results are presented in figure 4-3, where the curves correspond to 60 μm adjustment for clarity in the graph. The frequency bandwidth expands from 64.06 to 77.82 Hz, a total of 13.76 Hz. That is 0.5 Hz less than when the acceleration was set at 0.588 ms^{-2}, due to the slight non-linear behaviour of the harvester at higher acceleration.

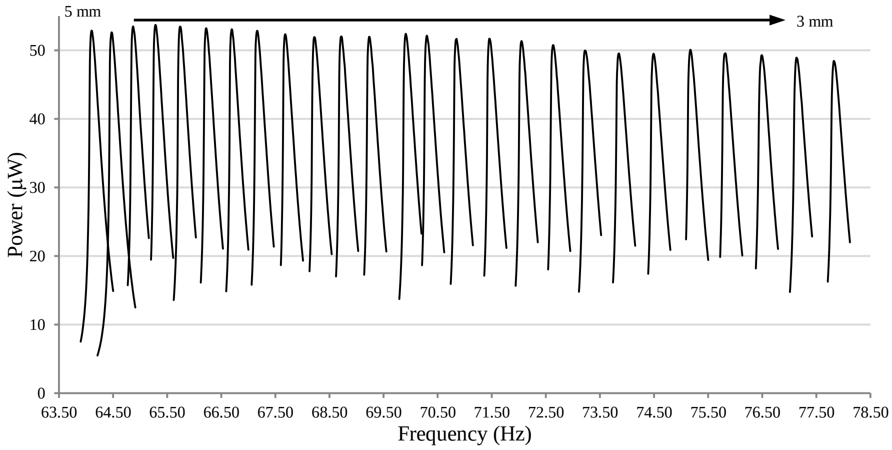

Coil:
A

Load:
26.5 kΩ

Acceleration:
0.294 ms^{-2}

Figure 4-3. Resonant frequency range at 0.294 ms^{-2}$_{(rms)}$

The results from the previous tests are presented in figure 4-4, where the relation between the tunable energy harvester's resonant frequency and the distance between tuning magnets is presented. The distance can also be measured in terms of the actuator position, as depicted in the same figure. The 100th step corresponds to a resonant frequency of 64.06 Hz, and the 200th step to the maximum resonance frequency in the range, either 78.32 or 77.82 Hz.

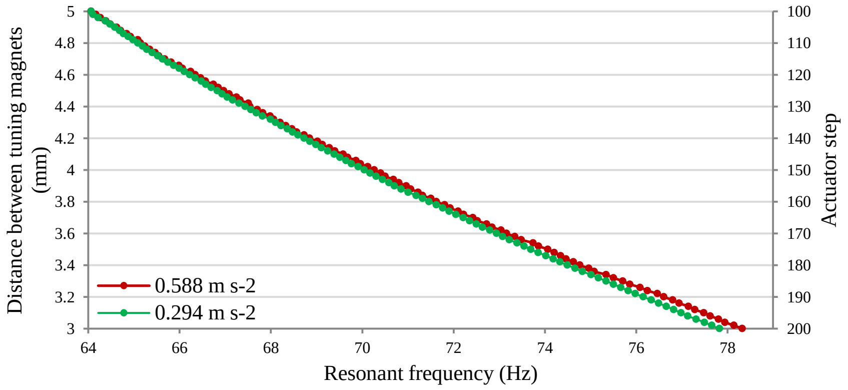

Figure 4-4. Resonant frequency as function of the distance between magnets, or actuator step.

The results from figure 4-4 are used to generate a mathematical expression relating the tunable energy harvester's resonant frequency to the actuator position, resulting in equations (4-4) and (4-5), for 0.588 $ms^{-2}{}_{(rms)}$ and 0.294 $ms^{-2}{}_{(rms)}$ respectively. The maximum error between the proposed mathematical expressions is 3.5 actuator's steps, occurring for a frequency of 78 Hz. These expressions will be used later in section 4.3 to control the position of the actuator.

$$Optimal\,position\ [step] = 6.99(frequency[Hz]) - 343.24 \tag{4-4}$$

$$Optimal\,position\ [step] = 7.21(frequency[Hz]) - 357.29 \tag{4-5}$$

4.3 Tuning control strategies

Previously Zhu, et al.[66] proposed a control strategy called "frequency transversal algorithm" for the same tunable energy harvester described in Chapter 3. This algorithm adjusts the actuator position by one step if the harvester voltage drops below certain voltage threshold. The actuator moves in one direction, one step at the time, looking for a position where the voltage reaches the threshold value. If that position is not found, the actuator returns to the previous position where the maximum voltage was registered and restarts the search in the opposite direction. If a maximum cannot be found, the actuator moves to the start position previously determined.

This approach did not take into consideration the effect that the input impedance of the electric load has over the harvester voltage, especially considering a supercapacitor as the energy storage element, or the effect that a higher acceleration has on the output voltage. Decreasing acceleration would result in a maximum output voltage that is below the threshold value even when harvester is at resonance. Furthermore, the power being generated drops significantly as the difference between base frequency and harvester's resonant frequency increases, while the voltage drops slightly. This can be observed in figure 4-5, where the base frequency and acceleration are 72 Hz and 0.588 $ms^{-2}{}_{(rms)}$, respectively. The tunable energy harvester was set at a resonant frequency of 72 Hz and connected to a 5 stage VM charging a storage capacitor of 0.55 F. As the distance between tuning magnets moves away from the optimal position altering the resonant frequency of the harvester, at a distance of 60 µm the power drops to a half while the voltage drops only 8%.

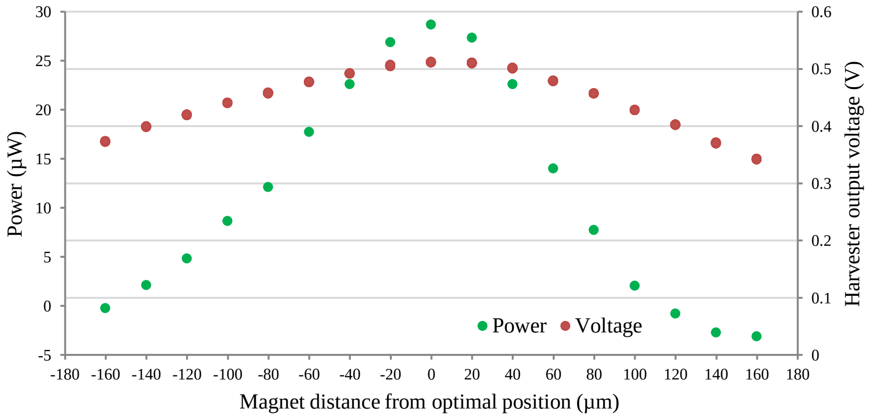

Figure 4-5 Variation of output voltage as harvester tuning magnets move from its optimal position.

Furthermore, the incremental adjustment of the actuator by one step at the time until the optimal position is found, consumes more energy compared to the adjustment of the actuator to its optimal position in a single movement. As will be discussed in section 4.6.2, more energy is consumed per step when the actuator moves one step than for larger adjustments in a single movement.

Building upon the results from the "frequency transversal algorithm", the control system devised for the tunable energy harvester must be able to determine the direction and distance by which the actuator has to be adjusted in order for the harvester's resonant frequency to match the base excitation. Furthermore, the control system cannot rely solely on the harvester voltage to identify if resonance has been reached; a more reliable approach is required.

4.3.1 Open loop control

The first control strategy proposed for the tunable energy harvester is based on the mathematical model of the tunable energy harvester using equation (4-4) or (4-5), where the position of the actuator is related to certain precise base frequency. This open loop control has only one input, the base frequency. It assumes that the harvester exhibits a linear behaviour, i.e. the resonant frequency remains the same for a given actuator position irrespective of the base acceleration level or electric load damping. However, this assumption is not valid because the harvester presents a non-linear behaviour, as can be seen in the change in resonant frequency for harvester A as the acceleration changes, as shown in in figure 4-6. The harvester was loaded with a pure resistance. The resonant frequency changes from 44.89 Hz at 0.196 ms^{-2}$_{(rms)}$ to 45.15 Hz at 0.637 ms^{-2}$_{(rms)}$, a variation of 0.32 Hz.

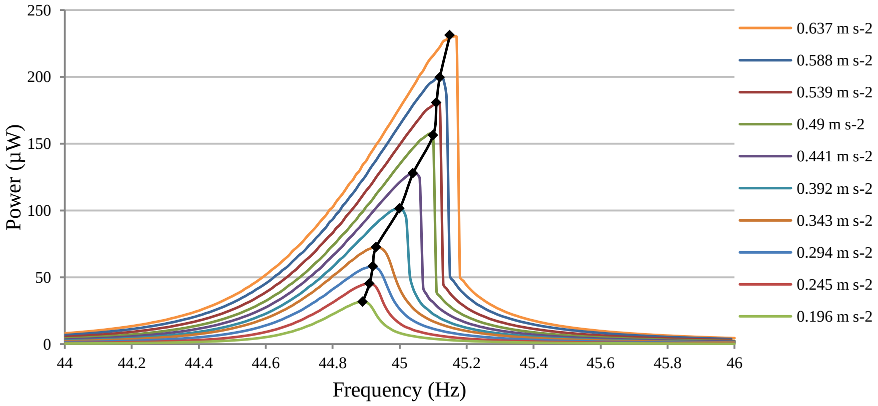

Figure 4-6. Resonant frequency variation as base acceleration changes

The resonant frequency is also affected by the load, as can be seen in figure 4-7. The optimal resistive load at 0.196 ms^{-2}$_{(rms)}$ is 49.5 kΩ, while at 0.637 ms^{-2}$_{(rms)}$ is 21 kΩ, a change of 28.5 kΩ.

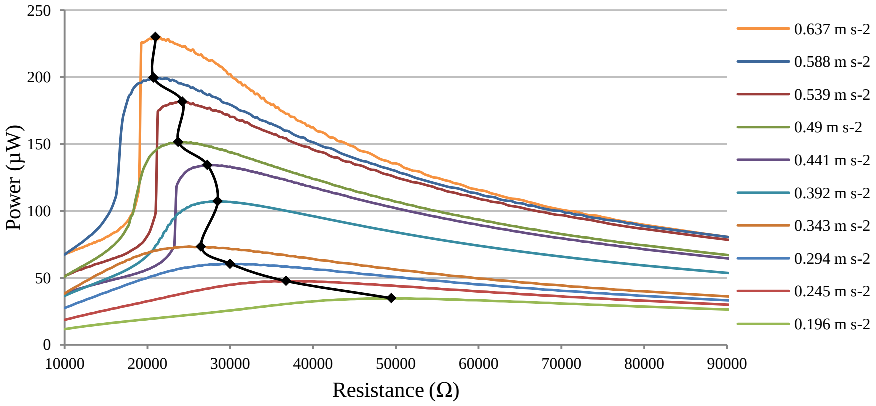

Figure 4-7. Resonant frequency variation as resistive load changes

The mathematical model of the tunable harvester could be improved to include the effect that acceleration and electric damping produces on the resonant frequency. Nevertheless, such a model would become increasingly complicated and the computational resources in the microcontroller may be insufficient or consume too much power to implement. An additional disadvantage of this strategy is its inability to identify the position of the actuator and compensate in case of error.

4.3.2 Closed loop control

To overcome the disadvantage that an open loop control imposes, a closed loop control strategy is proposed which includes the mathematical model relating the actuator position to the resonant frequency, and the capability to adjust the position of the actuator based on the phase difference, or period difference, between the harvester voltage signal and the base acceleration. The principle of operation of the control proposed is based on the phase difference between the harvester and the base excitation. The equation of motion for a single-DOF system with viscous damping excited by an harmonic force F_0, is given by equation (4-6) [39]. This is the same as equation (2-1), with the right hand-side replaced with the driving force.

$$m\ddot{z} + c_T\dot{z} + kz = F_o \sin \omega t \tag{4-6}$$

The vector relationship for the forced vibration is presented in figure 4-8. For harmonic motion, the phase of the velocity and the acceleration are ahead of the displacement by 90° and 180°, respectively. The damping force component ($c_T\omega$) is 90° ahead of the spring force (k), while the inertial force ($m\omega$) is 180°.

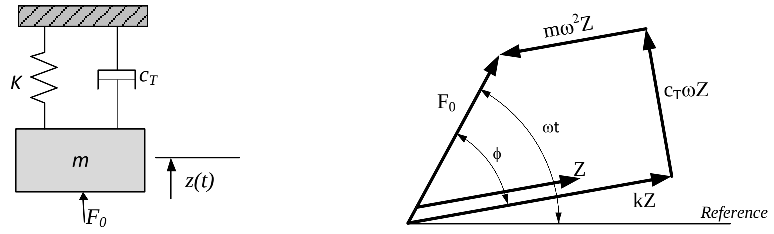

a. System representation b. Force vectors

Figure 4-8. Viscously damped system with harmonic excitation.

The amplitude and the phase (ϕ) between the mass and the force in equation (4-6) can be calculated from the force vector representation. For this purpose figure 4-8a is arranged as shown in figure 4-9. The mass amplitude (Z) can be found using the Pythagorean theorem, resulting in equation (4-7). The nondimensional expression for the amplitude is given by equation (4-8), where ω_n is the natural frequency of the system, ζ is the damping factor and ω is the excitation frequency.

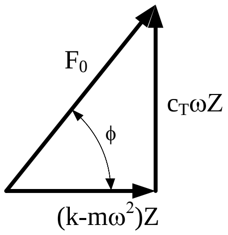

Figure 4-9. Viscously damped system vector force.

$$Z = \frac{F_o}{\sqrt{[k - m\omega^2]^2 + [c_T\omega]^2}} \tag{4-7}$$

$$\frac{Zk}{F_o} = \frac{1}{\sqrt{\left[1 - \left(\frac{\omega}{\omega_n}\right)^2\right]^2 + \left[2\zeta\left(\frac{\omega}{\omega_n}\right)\right]^2}} \tag{4-8}$$

Following the same method, the phase angle ϕ can be calculated from figure 4-9. The resulting expression is given by equation (4-9). The nondimensional representation of the phase angle is given in equation (4-10).

$$\tan\phi = \frac{c_T\omega}{k - m\omega^2} \tag{4-9}$$

$$\tan\phi = \frac{2\zeta\left(\frac{\omega}{\omega_n}\right)}{1 - \left(\frac{\omega}{\omega_n}\right)^2} \tag{4-10}$$

The nondimensional expressions show that the amplitude and phase angle are a function of the damping factor and the frequency ratio (ω/ω_n). The curves for equation (4-8) and (4-10) show that the damping factor has a major impact in the maximum displacement and phase angle near the resonance frequency of the system, as shown in figure 4-10 and figure 4-11, respectively. The system reaches its maximum displacement when the phase angle between the harvester and the base excitation is 90°. This effect is utilized in different control mechanisms to identify when the system is at resonance.

It is important to consider the effect of the damping factor in the phase angle. It can be observed in figure 4-11 that the bandwidth over which the phase angle changes from 0° to 180° is proportional to the damping. A large bandwidth would simplify the control system because it can calculate the error between the mass displacement and the base excitation based on the phase angle. However, the damping is inversely proportional to the displacement. The energy harvester was designed with a low damping, resulting in a rapid change in phase angle as the base frequency approaches the harvester resonant frequency.

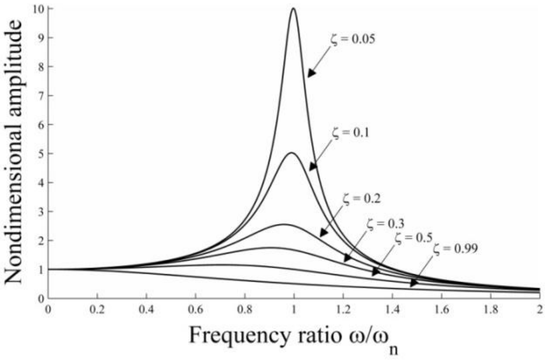

Figure 4-10. Amplitude of forced vibration for various degrees of damping

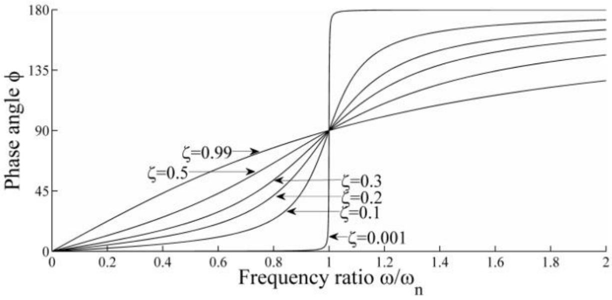

Figure 4-11. Phase angle between excitation force and mass displacement as function of the frequency.

An example of a control system that utilises the phase angle to operate is presented by Brennan [104]. He proposes an adaptive tuned vibration absorber (ATVA) where the stiffness of a mass absorber is adjusted to eliminate vibration. The natural frequency of the ATVA, pictured in figure 4-12a, is adjusted to coincide with that of the host structure. This condition occurs when the acceleration of the ATVA and the acceleration of the host is close to 90° as show in figure 4-12b and figure 4-12c.

The control system measures the phase of the acceleration between the host and the ATVA, then it adjusts the stiffness of the mass absorber until the phase is 90°. The vector analysis of figure 4-12c shows that when the phase angle of the system is considered, instead of the displacement, the system is at resonance when the phase angle between them is 90°.

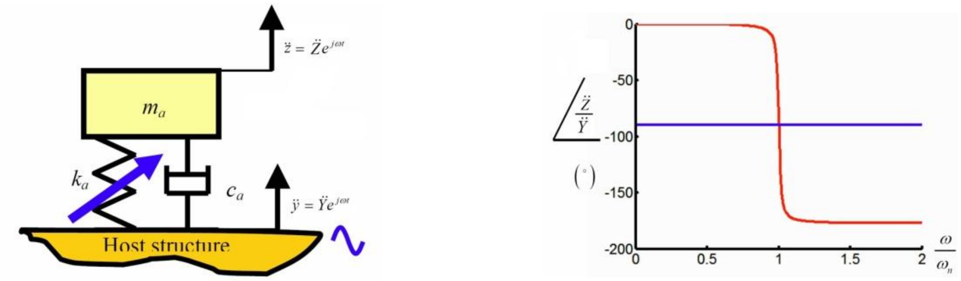

a. Schematic of ATVA

b. Phase relationship

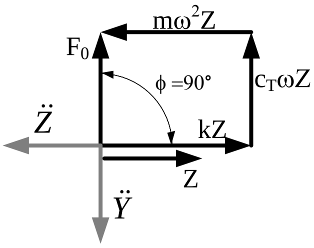

c. Force vector analysis when at resonance, ϕ=90°

Figure 4-12. Schematic of an ATVA and phase relation between the acceleration of the host structure and the ATVA mass, modified from [104].

Ramlan, et al. [33] investigate the effect on the power generation of a vibration-based energy harvester. The maximum input power occurs when the velocity of the displacement of the seismic mass ($\dot{Z}$) is in phase with the displacement of the base (Y). This occurs when the phase angle between them is 0°.

The closed loop control proposed in the present research aims to maintain the tunable energy harvester at this condition. The system measures the velocity of the harvester $(\dot{Z})$ through the harvester's output voltage, and the acceleration at the base $(\ddot{Y})$ using an accelerometer. The system is at resonance when the phase difference is 180°. However, the accelerometer was deliberately inverted to ease the calculation process in the microcontroller. This resulted in a measurement of the acceleration shifted by 180° or $(-\ddot{Y})$. Under this condition, the system is at resonance when the phase angle between the harvester velocity and the inverted base acceleration is 0°, or the period difference is 0 sec, as presented in figure 4-13.

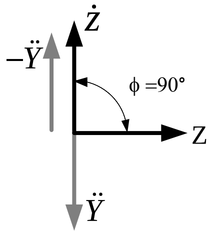

Figure 4-13. Phase difference between harvester velocity and base acceleration when system is at resonance

The limitation of this approach is the narrow band at which the phase difference can be used to recognize when the harvester is at resonance. For harvester A with a Q-factor of 136, or a damping ration of 0.003, the phase shifts rapidly from -90° to 90°. Therefore, the closed loop control must be able to identify that the system is at resonance on that range. In this case, the -3dB band expands from 44.95 to 45.40 Hz, which represents a phase difference variation from -60° to 60° phase angle.

The close loop control proposed here combines the mathematical model of the harvester from equation (4-4) and the measurement of the period difference to adjust the harvester resonant frequency, through the tuning mechanism, to coincide with the base frequency. The mathematical model brings the actuator close to its optimal position, and then the period difference is used to fine-tune the harvester mechanism. With this approach, the non-linear behaviour, not included in the mathematical model, can be compensated by the use of the period difference. Once the actuator has been brought within a short distance of its optimal, the period difference can provide information regarding the direction at which the actuator has to be further adjusted, i.e. extend when the phase difference is below 0° or retract when it is above 0°. It is important to mention that the system measures the period difference and not the phase. Nevertheless, the same principle applies, instead of aiming for a 0° angle, the system aims for a time difference in the period of the signal of 0 sec.

4.4 Control system components

The control strategy proposed has as input references: the base frequency, the period difference between base acceleration and the harvester output voltage, and the voltage at the storage capacitor. The output is the adjustment of the actuator position to alter the resonant frequency of the tunable energy harvester to match the base frequency. Figure 4-14 presents the diagram of the closed loop control proposed.

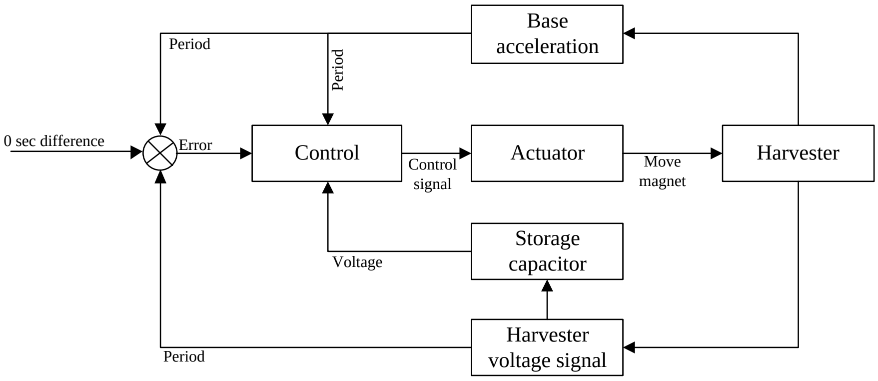

Figure 4-14. Control loop block diagram

There are three basic activities that the system must accomplish:

- *Energy management*. Sensing of the voltage at the storage capacitor and activities related to the reduction of the power consumption in the system.
- *Frequency measurement*. Measurement of the base frequency.
- *Period difference*. Measurement of the period difference between the base acceleration and the harvester voltage.

4.4.1 Energy management

One of the energy management activities is to ensure that a certain minimum level of energy is available to enable the adjustment of the tuning mechanism. This is performed by measuring the voltage at the storage capacitor. If the voltage is equal or higher than 2.6 V, then the actuator can be operated to adjust the harvester resonant frequency. This is the minimal operating voltage for the actuator, as described in section 3.3.2. If this requirement is not fulfilled, the control system cannot operate and the system goes to sleep mode. In this low energy consumption mode, all the peripherals are de-energized and the microcontroller is put on low power mode. The control system periodically returns from this low energy mode to measures if the voltage has reached the threshold value of 2.6 V. When the voltage at the storage capacitor is in the range between 2.0 to 2.6 V, the control system is operative, but it is unable to perform any tuning on the harvester.

It is important to consider the behaviour of the microcontroller when the voltage at the storage capacitor is below the 2.0 V, which is the minimum required by the microcontroller. In particular, how the microcontroller reacts to the slow rising voltage at the storage capacitor. The manufacturer does not guarantee the operation of the microcontroller below 2.0 V; hence, the exact behaviour of the microcontroller is uncertain.

Cold start-up

In a previous research by the author, et al. [74], a similar microcontroller was powered by an energy harvester. The harvester was deployed with the storage capacitor depleted. As the voltage on the capacitor increased, the power consumed by the microcontroller during start up increased beyond the values publicised by the manufacturer when the voltage surpassed 0.9 V. The same effect was observed when the voltage reduced below 1.3 V. The increase in power consumption could be related to the start-up process of the microcontroller. The microcontroller was designed to have a rapid power up and stabilization period in the power signal. According to the manufacturer [105], the supply voltage should rise at least at 0.05 V per millisecond, rise from 0 to 2 V in 100 μsec, to ensure internal reset. However, the nature of the energy harvesting application presented here limits the charging rate to hours, instead of milliseconds. This slow voltage rise appears to have the effect of constantly resetting the microcontroller, increasing its power consumption. The result was that the system was kept in a continuous loop never passing the 0.9 V level.

A cold start-up circuit is included to avoid the resetting condition of the microcontroller. A voltage level detector switch drives an N-MOSFET placed between ground and a "virtual ground". All the circuitry is connected to the cold start-up system through the virtual ground (V_GND). Only the voltage multiplier and the cold start-up circuitry are directly connected to ground, as show in figure 4-15. A voltage detector Torex XC61C was included with a switching voltage of 2.0 V. This value is lower than the minimum voltage required to operate the tuning mechanism, but was selected to evaluate the performance of the system at "low voltage", between 2.0 to 2.6 V. When the voltage at the storage capacitors reaches 2.0 V, the voltage detector turns the MOSFET on enabling the flow of current from the virtual ground to ground, effectively powering the rest of the electronics.

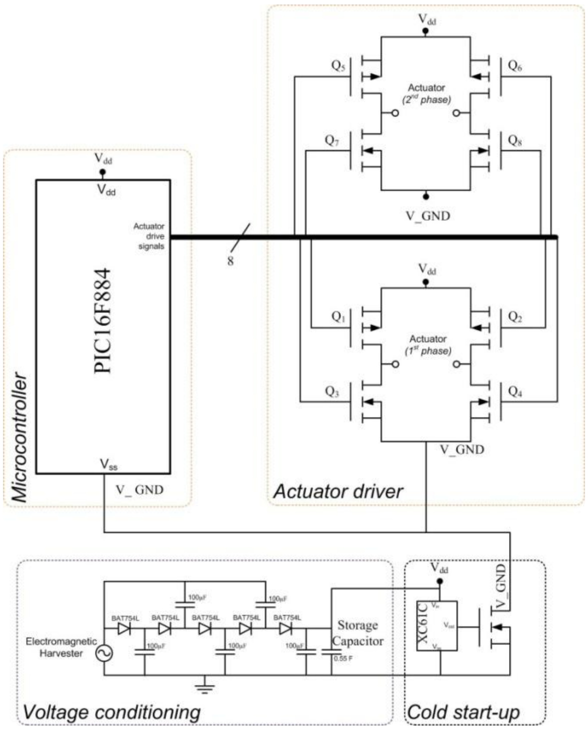

Figure 4-15. Virtual ground connection.

Voltage at storage capacitor.

The microcontroller is disconnected from ground, and not operative, until the voltage at the storage capacitor reaches 2.0 V. From this voltage onwards, the control system has to identify when the voltage at the storage capacitor has reached the minimum threshold of 2.6 V to operate the actuator. The method used to accomplish this task involves the use of the analogue-to-digital converter (ADC) and the internal fixed voltage reference feature in the microcontroller.

The internal reference voltage is fixed at 0.6 V and is independent of the voltage supply. The ADC uses the voltage supply, in this case the voltage at the storage capacitor, as its reference voltage. A simple algorithm is proposed that relates the result from the ADC to the voltage at the storage capacitor, presented in equation (4-11). The ADC has a resolution of 10-bit, where the maximum count corresponds to a voltage equal or higher than the voltage supply. Increasing the voltage at the storage capacitor results in a decrement on the conversion result from the ADC, as show in figure 4-16. A threshold bit count of 236 bits is selected that corresponds to a voltage at the storage capacitor of 2.6 V. Whenever the ADC result is lower than this value, then the voltage is higher than 2.6 V.

$$Conversion\ (bits) = \frac{0.6\ (V) * 1024\ (bits)}{voltage\ supply\ (V)} \quad \textbf{(4-11)}$$

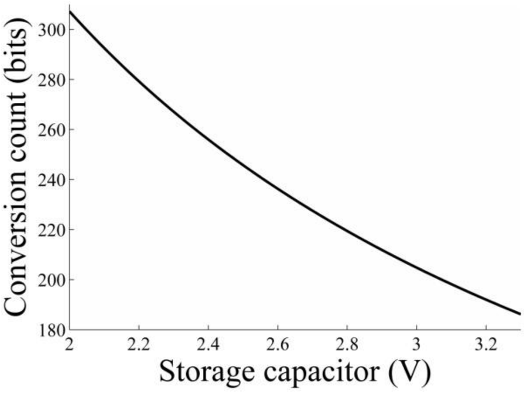

Figure 4-16. Analogue-to-digital conversion of fixed voltage reference

Revised actuator speed

The optimal tuning distance has been identified as the gap of 3 to 5 mm between tuning magnets. This reduces the force that the tuning mechanism must be able to generate to adjust the tuning, which in turn can be translated to a lower voltage to drive the actuator.

The tuning mechanism was experimentally tested operating in the reduced gap range at different voltages and speeds. The tests showed that the actuator could move at voltages as low as 2.3 V. However, the actuation starts only after missing some steps at the beginning of the actuation. This creates a particular challenge for the tuning mechanism; where the system needs to adjust 1 step, but the actuator cannot move and wastes energy in the process. The optimal relation between voltage and speed was found to be 2.6 V at 200 steps per second. This setting guarantees that the actuator is able to move one step at the point of maximum strain, i.e. 3 mm between magnets. This result sets the maximum voltage required by the entire system at 2.6 V.

4.4.2 Frequency meter

Frequency meter is one of the reference values to be used by the control. The control system must be capable of identifying any change in the base frequency to adjust the tunable harvester to this new frequency. For the frequency range proposed from 64.06 to 78.32 Hz, one step of the actuator represents on average an adjustment of 0.14 Hz on the harvester resonant frequency. Therefore, the maximum permissible error for the frequency meter system must be equal or lower to this value.

Even though this activity is referred to as the frequency meter, the system calculates the period of the signal not its frequency. For simplicity, however, the term frequency meter will continue to be used when referring to the measurement of the period. In those cases where further detail is required, the appropriate distinction between frequency and period will be made.

- *Accelerometer*

The base acceleration can be measured using an accelerometer attached to the base, where the acceleration output signal can be analysed to calculate the frequency. Three commercial accelerometers were evaluated to compare their sensitivity and output noise. All have an analogue output, which interfaces with the microcontroller through the ADC converter. Their principal characteristics are presented in table 4-1.

Table 4-1. Accelerometers

Model	Supply voltage (V)	Supply current (μA)	Maximum acceleration (ms^{-2})	Sensitivity (V / ms^{-2})	Noise density ($\mu m\ s^{-2} / \sqrt{Hz}$)
LIS3L06AL	2.4 - 3.6	950	2.0	0.053	490.5
MMA7360L	2.2 – 3.6	400	1.5	0.081	3433.5
ADXL330	1.8 – 3.6	320	3.0	0.033	3433.5 (z-axis)

The importance of the noise and sensitivity characteristics of the accelerometers lies in the low level of acceleration at which the harvester operates (0.588 $ms^{-2}{}_{(rms)}$). It is necessary for the accelerometer to measure this acceleration, i.e. possess high sensitivity, but also have low output noise. From the three commercial accelerometers identified, LIS3L06AL has the lowest noise density, but a sensitivity 35% lower than the MMA7360L. Most importantly, it was observed that LIS3L06AL has lower high frequency noise than the other accelerometers hence it was selected for the system. The frequency meter routine relies on sampling the fewest number of cycles possible to save energy; the error can be reduced by increasing the number of samples or using of a filter at the accelerometer output signal to ameliorate the noise. In either case, more energy would be required.

To calculate the period of the base excitation, the system samples the analogue signal from the accelerometer, using the ADC, looking for the maximum voltage value. Then it uses this maximum value to calculate the time taken between two consecutive maxima.

Experimental tests of this approach showed an error of more than 4 Hz for frequencies ranging from 63 to 78 Hz. The tests were performed using the shaker rig, with the base acceleration fixed at 0.588 $ms^{-2}{}_{(rms)}$. The principal cause of the error was due to quantization errors while converting the analogue signal from the accelerometer. The low level of acceleration resulted in an output signal from the accelerometer varying ± 0.044 V around the zero-g level, which corresponds to half the voltage supply. This small variation was converted by the ADC to a count varying ± 17 bits, which generated the quantization errors. This resulted in a difficulty to identify with precision the exact point in time at which the accelerometer reaches its maximum acceleration.

A second strategy was to calculate the time between inflection points of the signal, where the derivative of the signal becomes zero. The error was reduced to less than 0.5 Hz; however, it did not meet the minimum criteria of 0.14 Hz. In an effort to reduce the error, the average of eight consecutive measurements was calculated. This resulted in a maximum error of 0.3 Hz, which is still above the target value. Figure 4-17 shows the maximum and minimum error found for the frequency meter for a selected set of base frequencies.

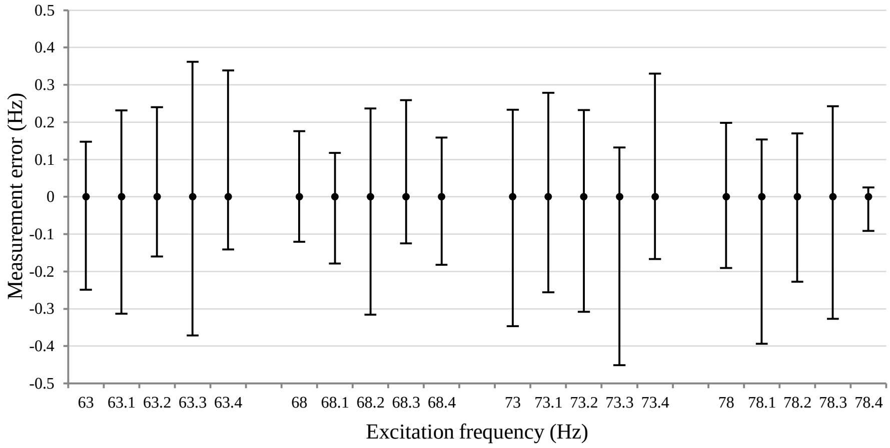

Figure 4-17. Frequency meter error, minimum and maximum error from central frequency.

- Frequency meter using the harvester output voltage

An alternative method to calculate the frequency included the use of the harvester voltage signal rather than the accelerometer. The harvester voltage also contains information regarding the base frequency; however, its amplitude varies depending on the electric load and level of mistuning. The worst-case scenario occurs when the difference between harvester resonant frequency and base frequency is maximum, which corresponds to a difference of 14.26 Hz for the proposed bandwidth of operation of the tunable energy harvester. Under this condition, the harvester output signal has a peak voltage of 30 mV at 0.588 $ms^{-2}{}_{(rms)}$, when the storage capacitor is at 2.6 V. This corresponds to ± 12 bits at the ADC.

The harvester output signal can be smaller than the accelerometer output signal, for example, when it is off resonance. However, the harvester voltage changes polarity every half cycle irrespective of the degree of mistuning, while the accelerometer signal is centred at half the supplied voltage. The advantage of changing polarity for the present design resides on the facility to connect a zero-crossing detector in conjunction with the capture mode feature in the microcontroller. The microcontroller starts an internal timer every time it senses either the rising or the falling edge of the signal. Using this technique the base period is measured between two consecutives signal rise of the zero-crossing detector.

The harvester output signal cannot be directly connected to the microcontroller because its negative polarity could damage it. In addition, the minimum threshold voltage required by the capture mode feature is higher than the harvester's voltage. According to the manufacturer [105] the threshold for a voltage supply of 2.6 V is around 1.5 V for rising edge, and 0.9 V for falling edge. Therefore, the signal from the harvester was squared, where every positive cycle of the harvester output voltage coincides with a high state value of the square signal and every negative cycle with a low state value. This is achieved by eliminating the negative cycle using a Schottky diode. Then the signal is squared using a non-inverting amplifier to detect the zero-crossing of the signal irrespective of its amplitude. The Schottky diode has the additional function of reducing the current leakage from the amplifier into the harvester, which was observed during experimental tests. Figure 4-18 shows the different stages of the process.

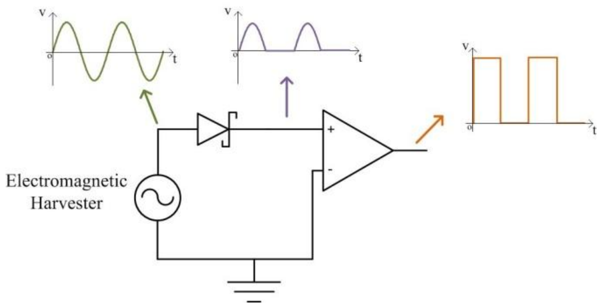

Figure 4-18. Signal conditioning for frequency meter.

The worst-case scenario was simulated to verify the performance of the frequency meter. A signal generator with a sinusoidal signal at 60 $mV_{peak\text{-}peak}$ was connected to the signal conditioning circuitry in figure 4-18. The frequency was adjusted from 63 to 79 Hz, increased by 0.1 Hz between measurements. The system was powered from an external power supply. In the same manner as the case where the accelerometer was used, the microcontroller measured eight samples and calculated the arithmetic mean to reduce the error. This process was done 32 times to evaluate the minimum and maximum error. The results show that the error varies from -0.06 to +0.09 Hz, as presented in figure 4-19. This is within the maximum permissible error of 0.14 Hz. Therefore this approach was selected to measure the period of the base excitation.

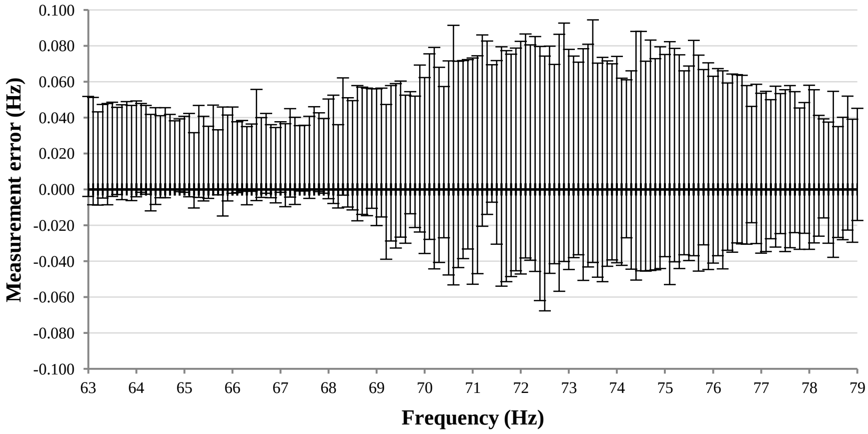

Figure 4-19. Frequency meter error, minimum and maximum error from central frequency, using capture mode feature.

- Optimal position according to excitation period

As previously mentioned, the period of the base excitation is the value measured by the system and not the frequency, hence the mathematical expression relating the position of the actuator to the resonant frequency of the tunable energy harvester presented in equation (4-4) is modified to use the period instead of the frequency. Figure 4-20 presents the updated version of figure 4-4 including an additional axis with the resonant period.

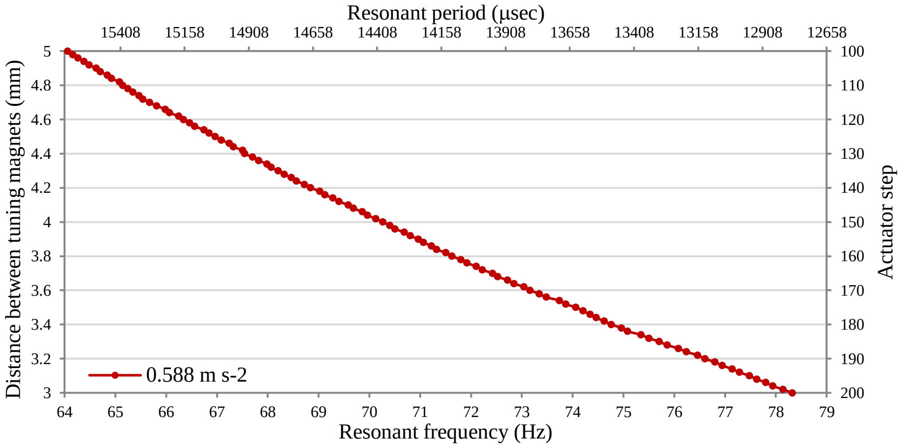

Figure 4-20. Resonant period as function of the distance between magnets, or actuator step.

From the results in figure 4-20 a mathematical expression relating the optimal position of the actuator as function of the base frequency period is proposed using the polynomial curve fitting function in Matlab. The resulting polynomial, equation (4-12), was restricted to 1st degree to ease the calculation load that solving a higher degree polynomial incurs.

$$Optimal\ position\ [step] = 648 - \frac{7}{200}(period\ [\mu sec]) \tag{4-12}$$

The mathematical expression was compared against experimental values. This was found to result in a maximum error of 2 actuator steps, or 40 μm, higher than the experimental result, but in most of the range the error was within 1 step, or 20 μm, as shown in figure 4-21.

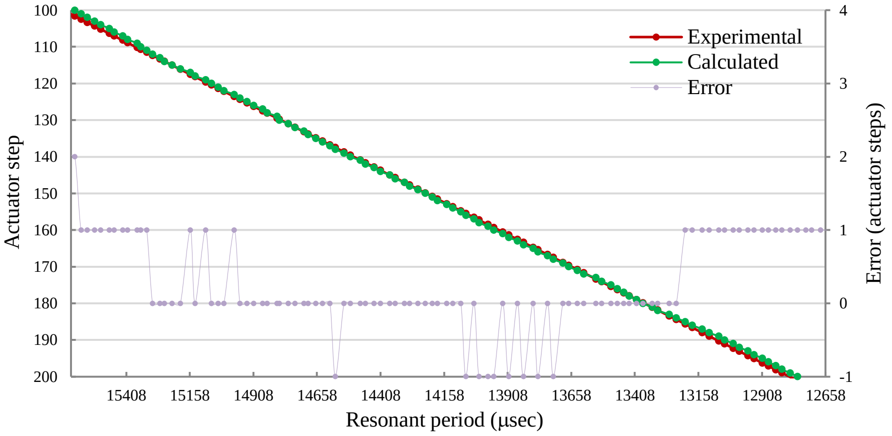

Figure 4-21. Comparison between experimental and calculate optimal position

4.4.3 Period difference

The period difference (or the phase difference, in terms of degrees) between the harvester output voltage and the base excitation provides information to evaluate the degree of mistuning of the harvester, as explained in section 4.3.2. The velocity of the harvester is measured in the same manner as for the frequency meter. The base excitation is measured using an accelerometer. The placement of the accelerometer on the shaker is shown in figure 4-22. As discussed previously, the system measures the period of the base excitation and the harvester voltage. In the same mode, the system measures the period difference between the harvester and the base, and not the phase.

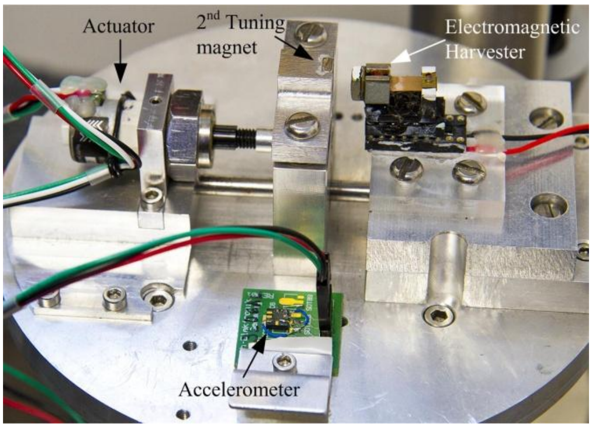

Figure 4-22. Accelerometer mounted on shaker.

The period difference algorithm proposed here measures the time between the falling edge of the harvester signal to the instant when the accelerometer signal crosses its mean value, or inflection point. This time is defined as “crossing time” in figure 4-23. The period difference is calculated as the difference between the base period, measured using the harvester, minus the crossing time. The period difference can be either positive or negative depending if the harvester signal leads or lags the accelerometer.

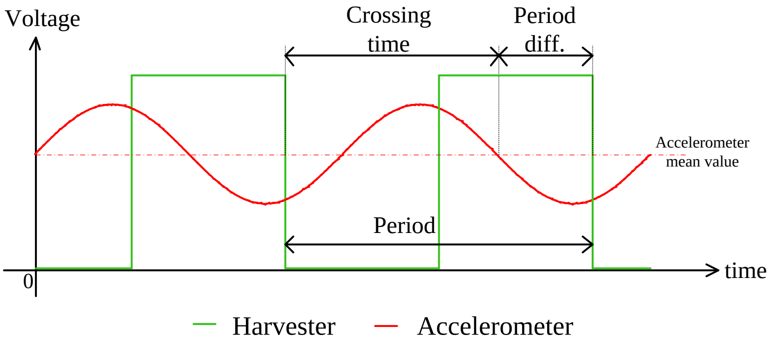

Figure 4-23. Period difference calculation

The period difference algorithm was implemented in the microcontroller and experimentally evaluated for three different excitation frequencies: 64, 72 and 78 Hz. The acceleration was maintained at 0.588 $ms^{-2}{}_{(rms)}$. The harvested was connected to a 5 stage VM with a 0.55 F storage capacitor with a resistance in series to maintain 2.6 V. The microcontroller and additional electronics were powered from an external supply. The harvester resonant frequency was adjusted on each occasion, using the movable tuning magnet, to match the three different frequencies. Then the period difference was measured every 20 µm, 1 actuator step, from -180 µm to 180 µm from the initial resonant position, taking 32 measurements each position. The results are presented in figure 4-24.

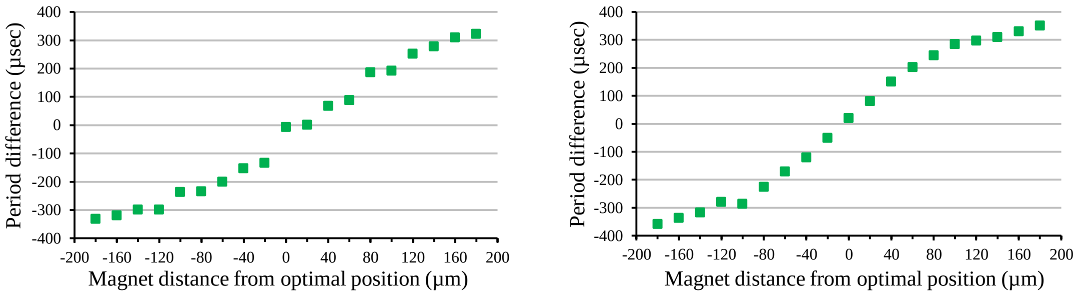

a. 64 Hz.

b. 72 Hz

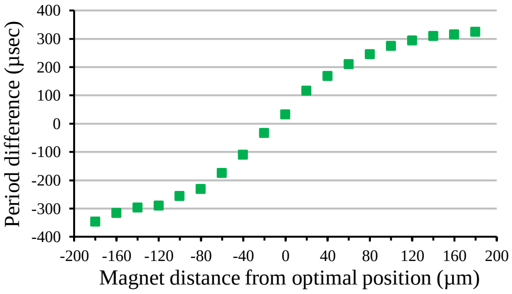

c. 78 Hz

Figure 4-24. Period difference for selected excitation frequencies, average values.

The period difference provides two important parameters for the control system. First, the sign indicates if the position of the tuning magnet is below, negative, or above, positive, the optimal position. Secondly, the period difference magnitude provides an indication of the error between the actuator position and the optimal position, where the harvester is at resonance. At resonance, the period difference is 0 µsec, or 0° degrees. Unlike the equation (4-8) and (4-10), where the phase angle is a function of the displacement of the harvester in relation the displacement at the base, here the period difference is measured between the velocity of the harvester and the base acceleration. Hence, the harvester is at resonance when the angle is 0° degrees, or the period difference is 0 sec.

The phase difference has a positive and negative limit which corresponds to a phase shift of ± 90º, or a period difference of approximately ± 350 µsec for the range of frequencies where the harvester operates. This limit is reached as the error between the harvester resonant frequency and the base frequency increases, as can be seen in figure 4-24. The bandwidth of the intermediate region is a function of the damping, as presented in section 4.3.2. For the harvester studied here, this region is restricted from –120 to 120 µm, in terms of tuning magnet distance. Beyond this region, the result of measuring the period difference will be the maximum or minimum values regardless of the mismatch between the harvester resonant frequency and the base frequency. Hence, the period difference is only suitable when the distance between tuning magnets is less than ±120 µm, or ±6 actuator steps, from its optimal position.

To validate the period-difference control strategy, the rate of energy transferred into the storage capacitor was measured through the power at the storage capacitor when the actuator moves around its optimal position. The base frequency was 72 Hz at an acceleration of 0.588 ms$^{-2}{}_{(rms)}$, figure 4-25 presents the results. The maximum power is reached when the period difference is 0 µsec. The –3dB power bandwidth is located in the region between -60 to 60 µm, or -3 to 3 actuator steps respectively.

It is also important to notice that when the tunable magnet is further away from the optimal position, the power collected into the capacitor becomes negative. This shows that the storage capacitor is losing energy rather than collecting it.

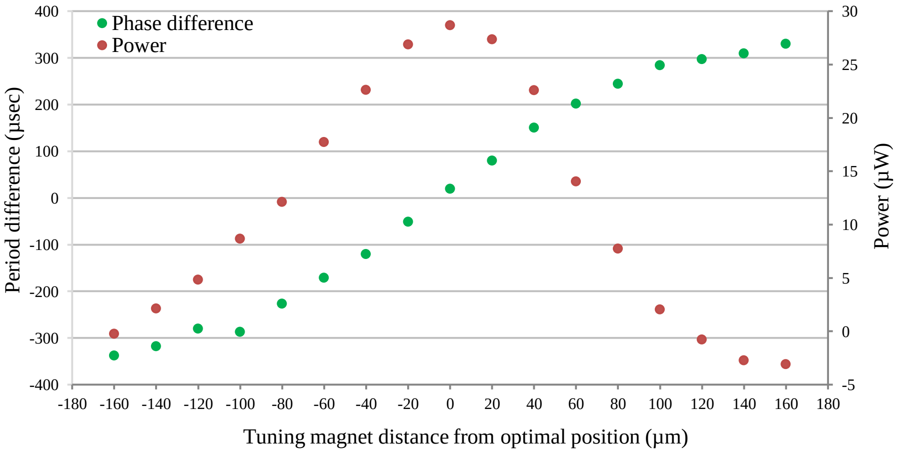

Figure 4-25. Comparison between period difference and power at the storage capacitor as the actuator moves away from its optimal position.

4.5 Closed loop control implementation

The components and strategies presented in sections 4.4 were implemented to create a fully tunable energy harvester. In first instance, the system was assessed as a proof of principle to identify those areas that can be further optimized. This section describes and presents the experimental tests performed.

4.5.1 Control sequence

As described in section 4.4.1, the microcontroller is enabled after the voltage in the storage capacitor reaches 2.0 V. Below this value, the harvester operates as a fixed frequency energy harvester with the voltage multiplier and storage capacitor connected. The system lacks of any control or intelligence to adapt itself and to increase its performance.

The microcontroller enters in operation when the voltage reaches 2.0 V. The control sequences initiate as presented in figure 4-26; first by sampling the voltage available at the storage capacitor. If this is lower than 2.6 V, the microcontroller enters a low power mode where the power consumption is the minimum possible while still operating. The microcontroller is kept in this state for around 320 secs, which is the time taken by the internal watchdog timer to overflow, and returns to normal mode to sample the voltage available.

If the voltage is equal or higher than 2.6 V, then the base frequency is measured using the harvester output signal as described in section 4.4.2. Next, the optimal position of the actuator is calculated according to equation (4-12), at such position the harvester’s resonant frequency matches the excitation frequency according to the model based on data from figure 4-20. If the difference between the current position of the actuator and the optimal position is higher than 3 actuator steps, the actuator moves to the optimal position. When the difference is less than 3 actuator steps, a fine tuning control using the period difference between the harvester output voltage and the base excitation is initialized.

The fine tuning is performed by calculating the period difference between the accelerometer attached to the base and the harvester voltage signal, as described in section 4.4.3. If the difference is higher than 100 μsec, the control commands the adjustment of the movable magnet in the direction required, as per the sign of the period difference. The actuator position is adjusted proportionally to the amount of error. When the period difference has reached an error lower than 100 µsec, then the harvester is considered to be at resonance. The microcontroller is placed on low power mode for another 320 secs then the voltage at the storage capacitor is measured, continuing with the control sequence described previously.

On every occasion that the adjustment of the actuator is needed, 5 seconds in low power mode are added to allow the tunable energy harvester to settle. This reduces the error when calculating the base frequency, and the period difference.

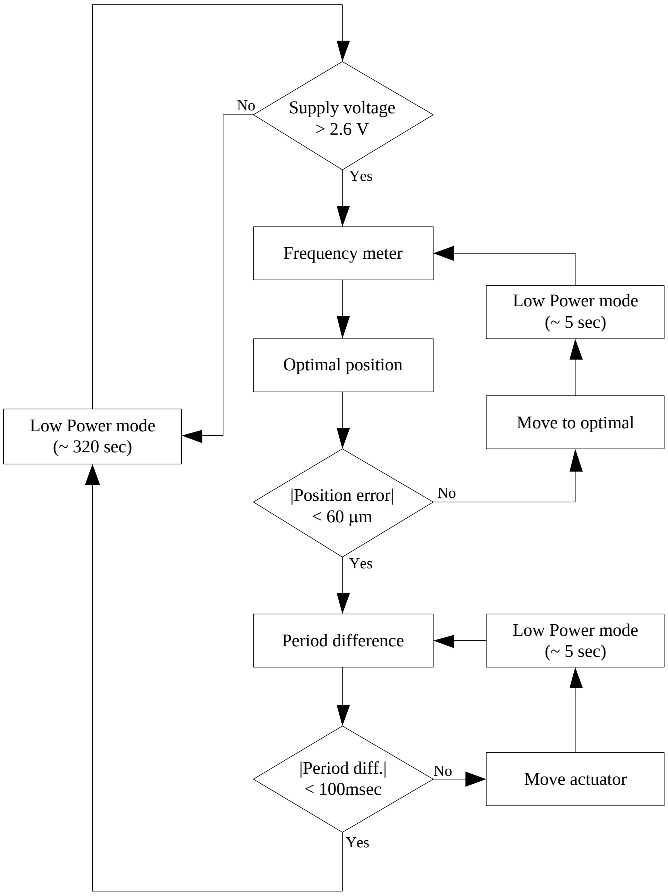

Figure 4-26. Control flow chart

4.5.2 Programming

The control strategies and routines were programmed on the microcontroller with MPLAB IDE software version 8.0 from Microchip Technology Inc. Assembler language was used to program the microcontroller because the execution of every instruction and routine can be accurately controlled and measured facilitating its debugging, and mostly reducing the number of instructions and execution time. This compared to programming the microcontroller using, for example, C, where conditional structures, iterations, among others features, are not supported directly by the microcontroller; hence they have to use a compiler to convert them into machine code [106], where the user doesn’t have control over the final sequence of instructions programmed into the microcontroller.

A serial connection between the microcontroller and a personal computer was enabled for debugging purposes. This connection was utilized to transmit information related to the different states of the control at each stage. However, due to its high power consumption, this connection was disabled when the tunable energy harvester was powered solely by the energy harvested. A manual override feature was also included in the microcontroller to operate the actuator independently. The complete program listing is presented in appendix A.

4.5.3 Control verification

The performance of the tuning control was evaluated on first instance with the microcontroller and actuator powered from an external supply. The harvester was connected to the storage capacitor through a 5 stage VM. The tunable energy harvester was initially tuned at a resonance frequency of 64 Hz with acceleration of 0.588 $ms^{-2}{}_{(rms)}$.

As shown in figure 4-27, at the time zero the base frequency changed to 77.5 Hz, maintaining the same acceleration. At approximately 22 seconds, the microcontroller returns from its low power mode and starts the control routine by measuring the excitation period. It then commands the adjustment of the actuator to its new optimal position. This can be observed by the increase of the output voltage from the harvester. Next, the period difference is measured once the movable magnet has been adjusted to its optimal position according to the model described in section 4.4.3. The actuator is further adjusted until the period difference is lower than 100 µsec, which occurs from around 26 to 28 seconds, finalizing the tuning adjustment. The harvester output voltage returns to a similar level than before the frequency change, showing the correct operation of the tuning control.

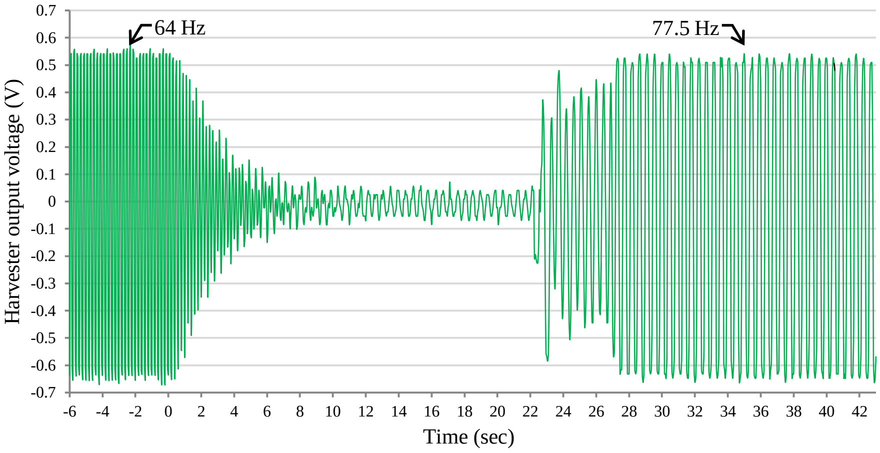

Figure 4-27. Resonance tuning.
Harvester output voltage as frequency changes from 64 to 77.5 Hz at 0 sec.

4.6 Autonomous operation

After verifying the correct operation of the tuning control, the autonomous operation of the system was evaluated. The objective was to power the entire tunable energy harvester solely from the energy harvested. The electrical connections between the different electronic components are presented in figure 4-28. The electromagnetic harvester was connected to the storage capacitor through a 5 stage VM, while the rest of the components where powered from the energy stored at the storage capacitor.

The tests were performed at a fixed acceleration of 0.588 $ms^{-2}{}_{(rms)}$ at an initial frequency of 64 Hz. The harvester resonant frequency was also initially set to 64.06 Hz. The first stage of the test evaluates the response of the system when the voltage available at the storage capacitor is lower than 2.0 V. Figure 4-29 presents the results of this test.

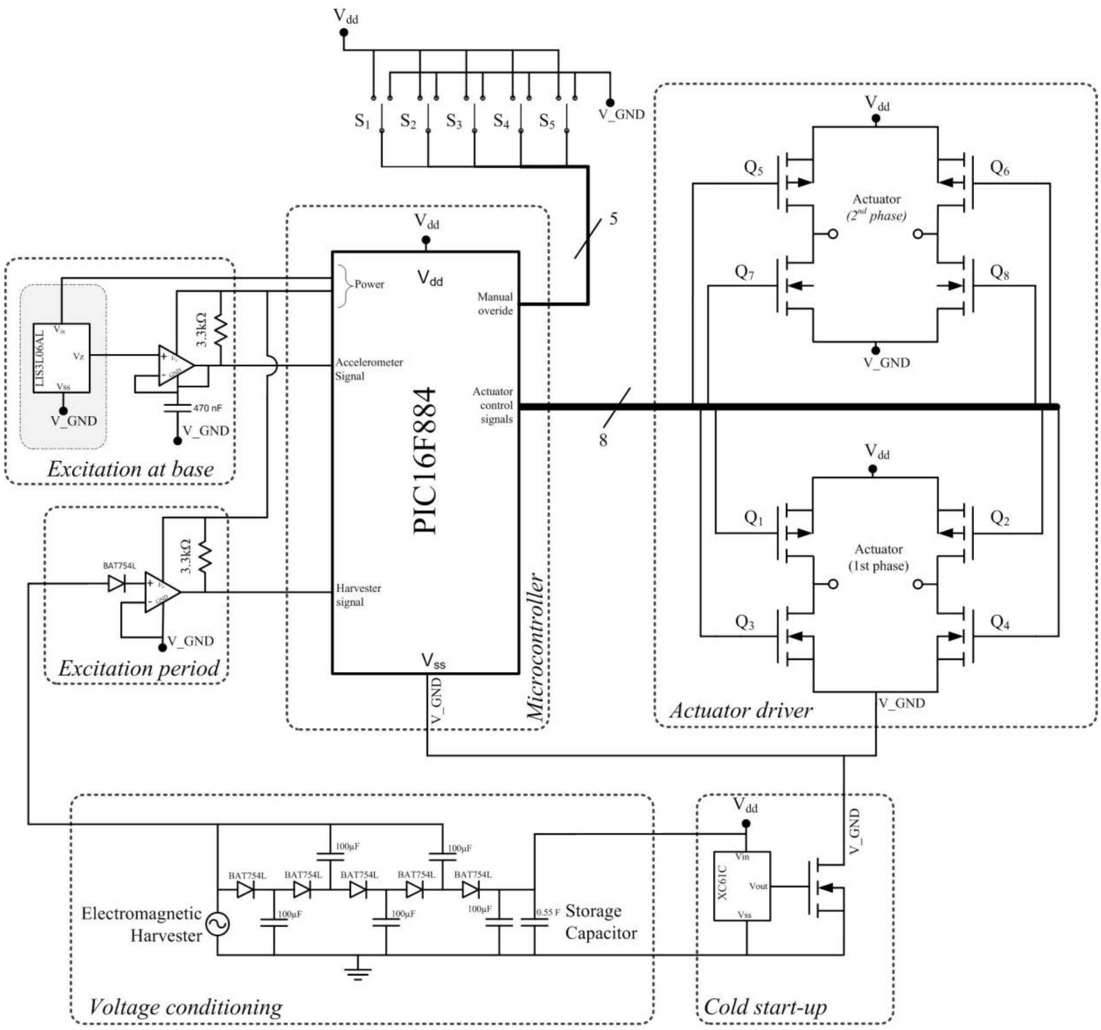

Figure 4-28. Tunable energy harvester electronic components schematic

4.6.1 Cold start-up

The experimental results show that the tunable energy harvester requires 22.65 hrs to charge the storage capacitor from 0 to 2.0 V; and 35.15 hrs to reach 2.6 V, as shown in figure 4-29.

The energy saved into the storage capacitor is also as shown in figure 4-29. After an initial high power level, the power drops to approximately 10 μW. It then increases steadily until the voltage at the storage capacitor reaches 2.0 V. At this point, the cold start-up circuit enables the microcontroller, and few periods of power loss are observed, which corresponds to the tunable energy harvester using more power from the storage capacitor. The power level stays at a constant value of around 20 μW without any further increase until the voltage reaches 2.6 V. This is the value at which the control is fully operational, where the actuator can be operated if there is a mismatch between the harvester's resonant frequency and the base frequency.

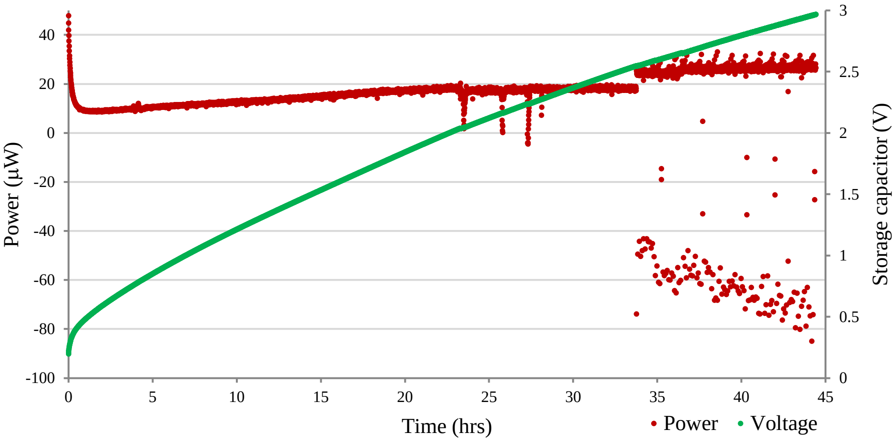

Figure 4-29. Charge of storage capacitor

After reaching 2.6 V at the storage capacitor, the tasks performed by the microcontroller increase considerably increasing the power overhead, as described in the control flow chart in figure 4-26. This increase in activity can be observed in figure 4-30, which is a detailed view from Figure 4-29, where the power in the storage capacitor drops approximately every 5 min (or 320 sec) as consequence of this increase of power overhead.

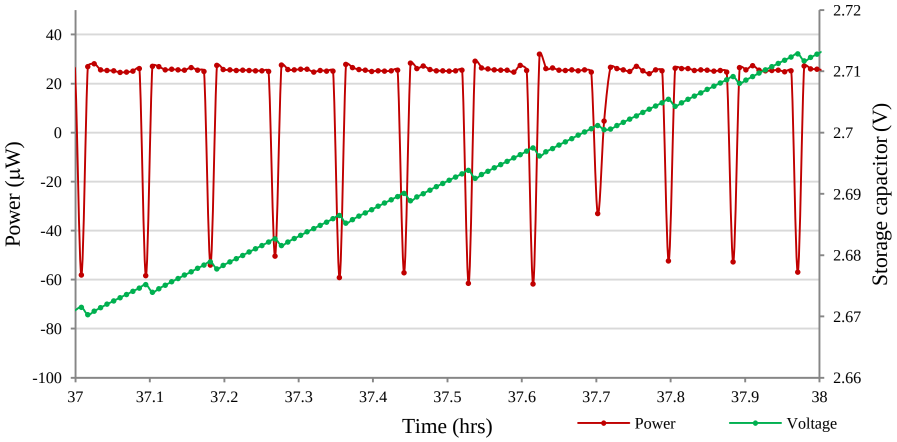

Figure 4-30. Charge of storage capacitor when voltage is higher than 2.6 V.

4.6.2 Resonant frequency tuning

Further tests were carried out to verify the tuning capability of the system. Similarly to the previous test, the acceleration was maintained at 0.588 $ms^{-2}{}_{(rms)}$ and the frequency was changed only when the time since the last frequency change was more than 360 seconds and the voltage at the storage capacitor was higher than 2.6 V. This guaranteed that the tunable harvester had returned at least once from the low power model; that it had sensed the frequency; and, that it had the minimum energy required to move the actuator. The tunable energy harvester was powered by the harvester with the same electrical connections as in figure 4-28.

The initial sets of frequencies were chosen to force an adjustment of 1 actuator step on every occasion. Figure 4-31 depicts the voltage at the storage capacitor and the voltage at the harvester output. It can be observed that when the frequency changes, the voltage at the harvester drops, as a direct consequence of the mismatch between its resonance frequency and the base frequency. The adjustment of the resonance frequency can be observed when the harvester voltage returns to the level it had before the frequency was changed. The drop in voltage at the storage capacitor corresponds to the power drawn by the electronics, including the actuator, to measure and adjust the harvester resonant frequency.

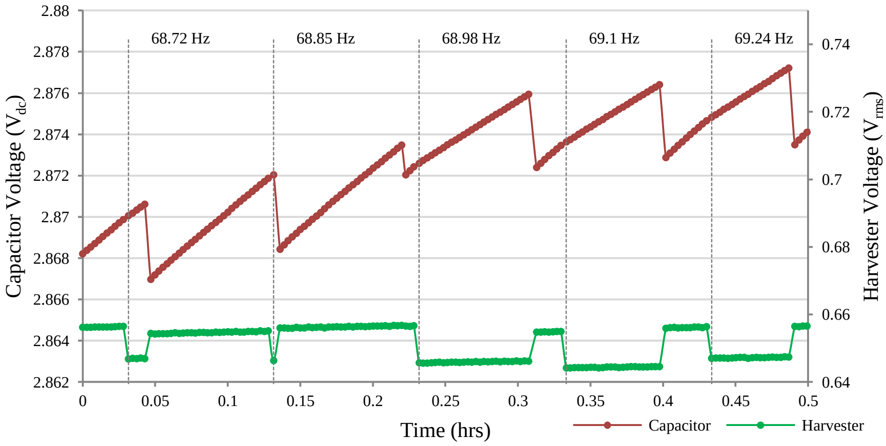

Figure 4-31. Harvester tuning when frequency varies by 0.13 Hz, approx.

The tunable energy harvester was also tested for a frequency adjustment of 1.04 Hz, which is achieved by an adjustment of 8 actuator steps, and is presented in figure

4-32. In this figure, it can be observed as a slight drop in voltage between frequency changes. This drop is the result of the microcontroller returning from low power mode and sensing the base frequency, which in that case has not changed since last adjustment. Hence, the microcontroller returns to low power mode without any further action taken.

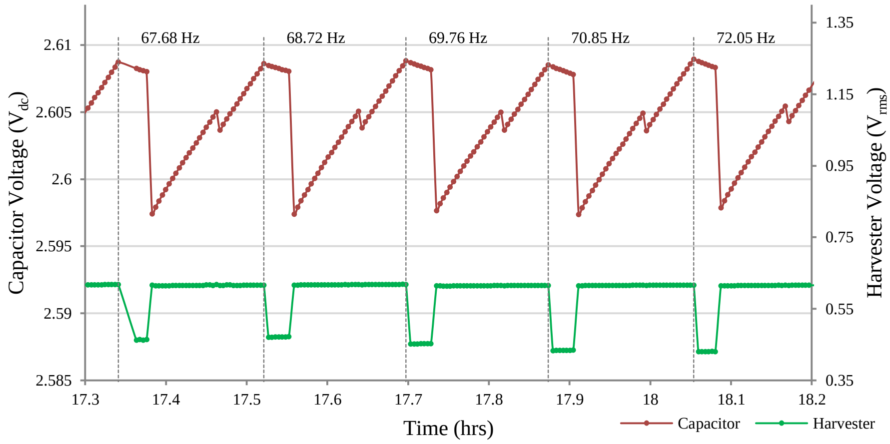

Figure 4-32. Harvester tuning when frequency varies by 1.04 Hz, approx.

The worst-case scenario was also studied. In this situation, the base frequency changes by 14 Hz on each occasion. Figure 4-33 presents the results. It is evident the drop in voltage at the harvester when the frequency changes. It reduces from approximately 0.6 to 0.03 V_{rms}.

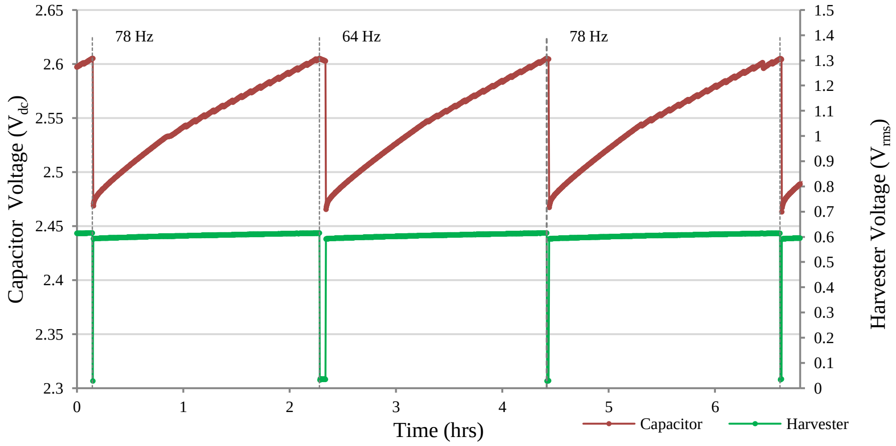

Figure 4-33. Harvester tuning when frequency varies by 14 Hz.

In addition to validate the operation of the tunable energy harvester for a range of frequencies, of the utmost importance was to collect information regarding the time taken by the harvester to harvest the energy used during tuning. The recovery time is defined as the time taken by the tunable energy harvester to reach the same voltage level at the storage capacitor as was present before any sensing or adjustment was performed, which is related to the amount of energy required to charge the capacitor to its initial voltage value. Tests were performed with different frequencies steps in order to evaluate the recovery time for each case; the results are presented in table 4-2.

Table 4-2. Tunable energy harvester tuning results

Frequency step (Hz)	Actuator adjustment (steps)	Voltage drop (mV)	Recovery time (sec)
0.00	0	1.28	75
0.14	1	3.84	250
0.27	2	3.91	256
0.54	4	6.12	267
0.68	5	7.56	332
0.82	6	9.19	453
1.09	8	12.04	604
1.36	10	13.57	643
2.04	15	17.82	859
2.72	20	24.00	1076
3.40	25	26.28	1287
4.08	30	36.28	1815
5.44	40	44.66	2144
6.80	50	59.99	2841
14.00	100	137.08	7542

There is a clear relationship between the distance the actuator has to be adjusted and the recovery time, as shown in figure 4-34. In the worst-case scenario, when the actuator has to move 100 steps, the tunable energy harvester required 2.09 hrs, on average, to reach the initial voltage before adjustment. Alternatively, only 250 sec are necessary when the actuator moves by just 1 step. These results indicate the maximum frequency change at which the tunable energy harvester can operate. It is capable of performing its tuning operation only when the base frequency changes at a rate that is lower than the time it takes to harvest the energy used during tuning, i. e. 0.14 Hz in 250 sec, or 14 Hz in 7542 sec. This frequency change rate can be extrapolated for lower frequency-time variations.

If the tunable energy harvester does not require any adjustment, because its resonant frequency coincides with the base frequency, then the system requires 75 sec to collect the amount of energy that was used in the process of making this decision.

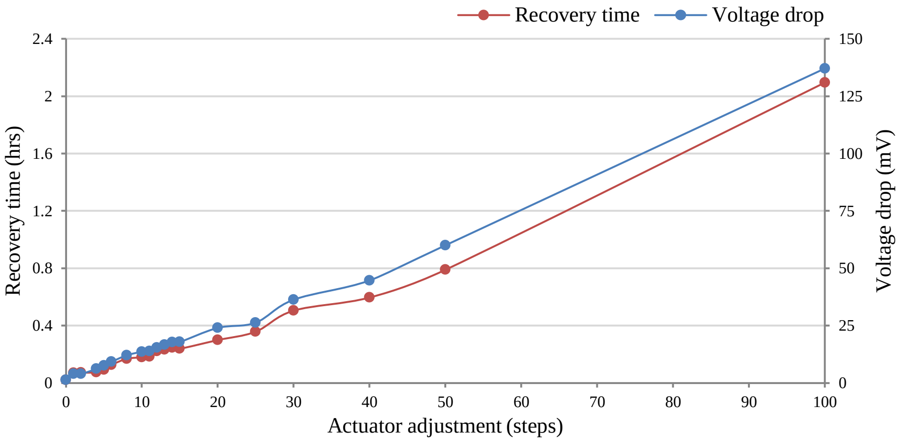

Figure 4-34. Recovery time and voltage drop at storage capacitor as function of actuator adjustment.

The ratio between the recovery time and voltage drop to the actuator adjustment is presented in figure 4-35. It is important to mention that figure 4-35 has a logarithmic x-axes, this with the purpose of presenting in greater detail the performance of the tunable harvester when the actuator moves few steps, compared to when it moves in greater lengths. The same figure also includes the case where no adjustment is required by the actuator as point of comparison.

The drop in voltage per step is higher for small adjustments. It appears that more energy is required in this case than for large adjustments. The apparent increase in energy consumption arises from the portion of the energy required by the actuator to initiate its movement. This portion of energy gradually reduces as the actuator continues its movement and it is inherent to any displacement of the actuator, regardless the length and the number of steps taken.

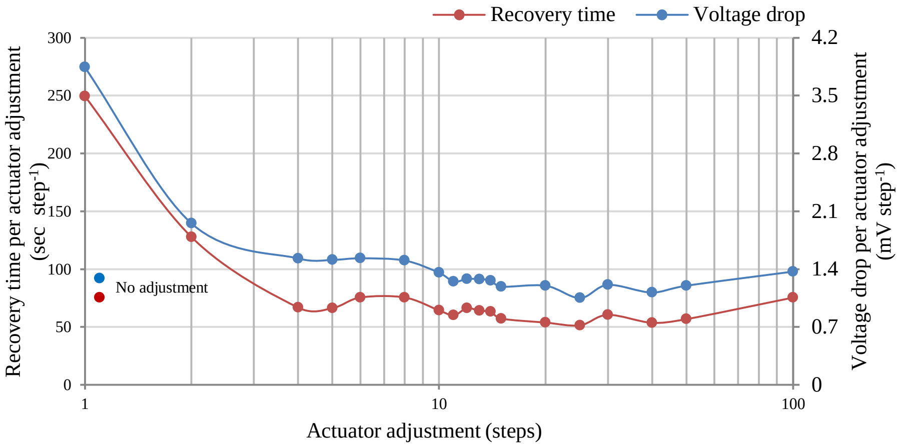

Figure 4-35. Recovery time and voltage drop per actuator step adjustment

4.6.3 Energy consumption

The energy consumption of every electronic component in the system was measured. These included the energy consumed by the microcontroller during specific routines, e.g. frequency meter, period difference, etc. In addition, the energy consumed by those electronic components connected directly to the microcontroller, were also measured, such was the case of the operational amplifier and accelerometer. Likewise, the energy consumed by the actuator when it moves 1 and 100 steps was also measured. The results are presented in table 4-3. The values reported represent the average time and current measurements taken to perform every routine or action, in all cases the voltage has been considered constant at 2.6 V. The current consumed by the actuator when it moves by 1 step has been adjusted to compensate for the power used to initiate actuation.

The power at the storage capacitor was considered to be 40 μW, which corresponds to the root mean square value of the power calculated using equation (3-3) for the tests presented in table 4-2.

Table 4-3. Energy consumed and harvested by the tunable energy harvester when different actions are performed.

Action or subroutine	Time (ms)	Current (µA)	Power (µW)	Energy (µJ)
Voltage detection	320000	1	2.6	832.00
Low power mode (5sec)	5000	3.77	9.8	49.01
Low power mode (320sec)	320000	3.77	9.8	3136.64
Reference voltage	0.075	495	1287.0	0.10
Frequency meter	149	1936	5033.6	750.01
Calculate optimum position	0.3	456	1185.6	0.36
Difference current position Vs optimum	0.052	415	1079.0	0.06
Measure accelerometer	15.84	2461	6398.6	101.35
Measure period difference	175.5	2390	6214.0	1090.56
Calculate period difference	0.092	440	1144.0	0.11
Control using period difference	149.32	2836	7373.6	1101.03
Actuator (1 step given)	5	312000	811200.0	4056.00
Actuator (100 steps given)	500	156000	405600.0	202800.00
Energy harvested	320000		40.0	12800.00

Figure 4-36 presents a comparative of the energy consumed by the tunable energy harvester when the actuator is not adjusted and when it is moved 1, 8, 10 and 100 steps. In the same figure, "voltage detector" corresponds to the power consumed by the cold start-up circuitry; "Actuator" encircles the energy used by the actuator, not considering the energy used by the microcontroller to drive it; "Microcontroller" includes the energy used or sourced from the microcontroller to operate the tunable energy harvester. The times considered to calculate the energy consumption are the same as those presented in table 4-2.

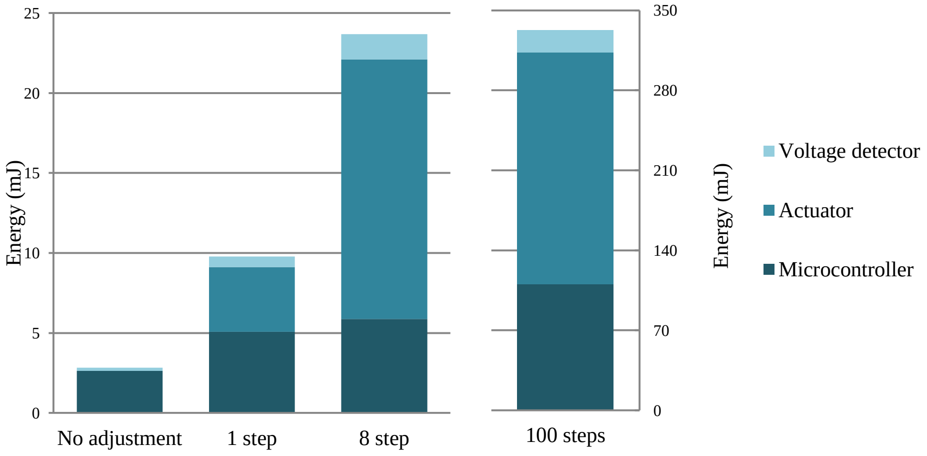

Figure 4-36. Energy consumption

Figure 4-37 presents the energy consumed by each routine in the microcontroller when the actuator has been adjusted by 100 steps and the voltage at the storage capacitor reaches the same value as before the adjustment, which represents a period of 7542 sec. Analysis of the energy consumed by the microcontroller shows that those routines that include the operation of the operational amplifier or the ADC, or both, consume the highest levels of energy: “frequency meter”, “measure accelerometer” and “calculate period shift”. Additionally, the energy consumed while the system is in low power mode is the highest, however it must be put in perspective by considering that the system remains in this mode, around 7360 sec out of 7542 sec, 97% of the time.

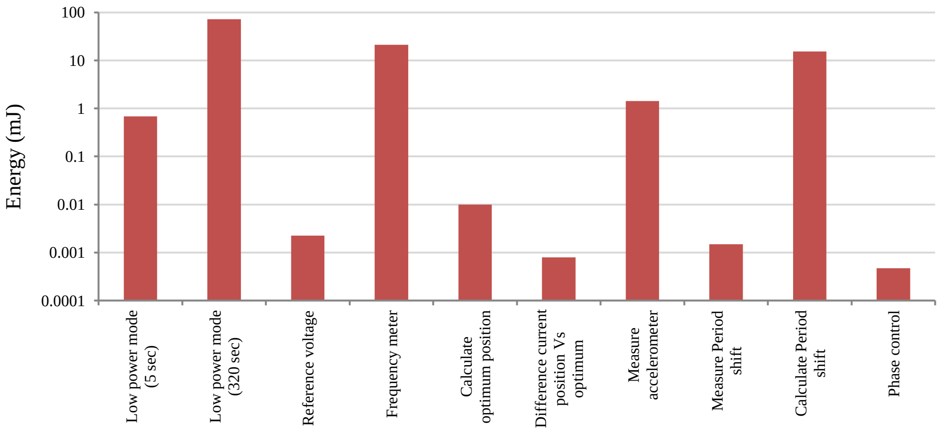

Figure 4-37. Energy consumption for each routine in the microcontroller after the actuator is adjusted 100 steps and the storage capacitor reaches the initial voltage prior adjustments, 7542 sec.

4.7 Conclusion

In this chapter, the autonomous operation of the tunable energy harvester has been presented. The maximum bandwidth of operation of the harvester extends from 47.72 to 87.84 Hz. This corresponds to an adjustment of 11 mm in the distance between the tuning magnets. The optimal bandwidth of operation was considered the frequency range that requires the minimal tuning displacement and maximal bandwidth, while maintaining a power generation level of at least 75% of that generated when the harvester operates at resonance without the tuning mechanism. This range was found to be between 64.06 to 78.32 Hz, for a displacement of 5 to 3 mm between tuning magnets. A mathematical algorithm relating the position of the actuator to the resonant frequency of the harvester was identified based on experimental results from the harvester. This algorithm is utilized to control the optimal position of the actuator when in operation.

Two control systems were proposed; open and closed loop. Both cases utilize the same mathematical algorithm for the harvester. In the case of the closed loop system, a fine tuning control is added that adjusts the position of the actuator based on the period difference between the base acceleration and the harvester output voltage signal. This fine tuning control compensates for the non-linear behaviour of the harvester, resulting in a more accurate control compared to the open loop system.

In conclusion, the operation of a tunable energy harvester powered exclusively by the energy it harvests has been demonstrated. It was shown that there is an optimal range of operation, which maximizes the tuning range whilst reducing the use of the actuator. It was also found that the control must have feedback to compensate for the non-linear behaviour of the harvester; otherwise, the control cannot guarantee that the harvester is at resonance.

The next chapter describes the optimization of the tunable energy harvester by improving its power extraction and its operation as an energy source for a wireless sensor node.

Chapter 5

Optimization

5.1 Introduction

This chapter describes the optimization of the tunable energy harvester by increasing the performance of the energy extraction and conversion. Section 5.2 presents an experimental study on passive and active methods to improve the impedance load seen by the harvester, consequently increasing the energy transferred to the storage capacitor. The effects that the improved energy conversion has on the control of the system and the harvester are presented in section 5.3. The operation of the tunable harvester with the improvements proposed is reported in section 5.4. Finally, section 5.5 presents the operation of the tunable energy harvester as a wireless sensor node.

5.2 Power extraction

The initial design of the tunable energy harvester, presented in chapter 4, included a 5 stage VM that rectifies and increases the voltage generated by the harvester. The intention of that initial design was to establish the challenges and the feasibility of an autonomous tunable energy harvester. The optimization of the impedance load was not considered. This section describes the strategies followed to increase the power generated by improving the impedance load seen by the harvester. By harvesting more energy, the tuning mechanism can be operated more frequently providing a more flexible system.

The harvester generates an alternate voltage signal, whilst, the electric load requires direct voltage. This difference creates the need for rectification. Additionally, the voltage generated by the harvester may not be enough to operate the electric load. It can also vary according to the level of base acceleration and the degree of mistuning of the harvester's resonant frequency. Therefore, the power extraction circuit should tackle two tasks: optimized the electric load to maintain the power generation at a maximum and secondly condition the harvester output voltage signal to be usable by the electric load, as defined by Mitcheson, et al. [68].

Two main strategies for power rectification and adjustment can be identified for the energy harvester: passive rectification and synchronous rectification. This chapter presents the designs evaluated for both types of power extraction: voltage multiplier and active conversion and regulation.

5.2.1 Optimal resistive load

The performance of the tunable energy harvester is not only increased by tuning its resonance frequency to match the base frequency, but also the optimization of the electric load can increase it. Stephen [107] concluded that maximum power is transferred to the electric load when its resistance is equal to the coil resistance and the mechanical damping. Hence, there is an optimal load that results in the maximum power transfer. This can be seen by the effect that varying the load has on the power generation as described below.

5.2.1.1 Resistive load

To analyse the effect that the load has on the power generation, the tunable energy harvester was connected to a pure resistive load, as shown in the diagram of figure 5-1. The base acceleration remained at 0.588 $ms^{-2}{}_{(rms)}$ while the frequency was set at different values along the range of operation of the tunable energy harvester.

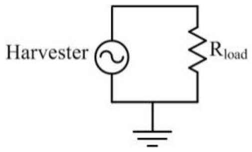

Figure 5-1. Harvester connected to resistive load

- Harvester A

Harvester A was connected to a pure resistive load as in figure 5-1. The harvester resonant frequency and base frequency was set at three different values: 64, 70 and 78 Hz. Then the resistive load was varied and the power measured. The results are presented in figure 5-2. The base acceleration remained fixed at 0.588 $ms^{-2}{}_{(rms)}$.

The maximum power of 160 μW is generated when the base frequency is 64 Hz. The power reduces for the other two frequencies due to the increase in damping generated by the tuning mechanism and reduction in the base amplitude as the frequency increases, for a fixed acceleration. The maximum power is generated when the voltage at the generator is 1.65 V_{rms} and the load resistance equals 17 kΩ, as shown in figure 5-2. This voltage is also similar for the maximum power generated with the other two frequencies.

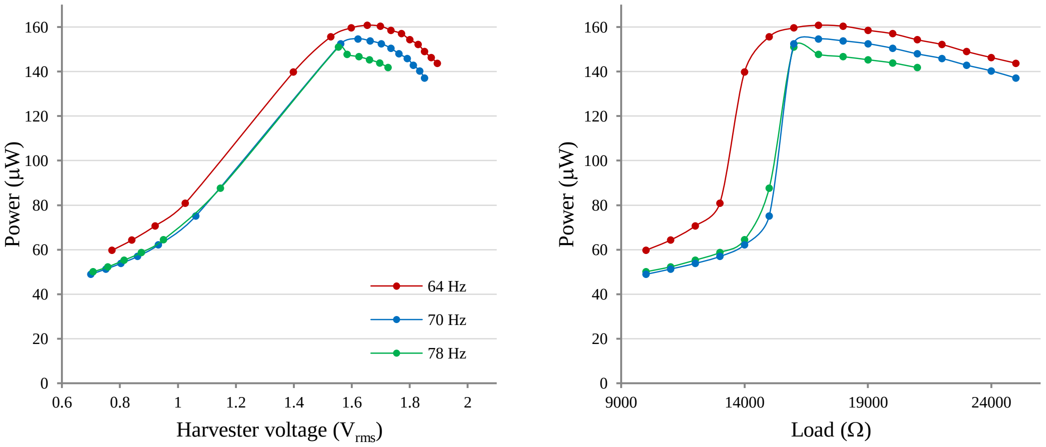

a. Power generated as function of the voltage b. Power generated as function of the resistive load

Figure 5-2. Power generation as base frequency changes for harvester A

The -3dB power range is reached for the three frequencies when the harvester output voltage is higher than 1.1 V_{rms}, although it corresponds to a slightly different resistive load on each case: 13 kΩ for 64 Hz, 15 kΩ for 70 and 78 Hz.

The performance of harvester A was also evaluated when there is a divergence between its resonant frequency and the base frequency. For this purpose, the tuning mechanism was adjusted from 20 μm below its optimum to 40 μm above optimum position. The power generated was measured at different resistive load and the base frequency remained at 64 Hz. The results are presented in figure 5-3.

The maximum power is generated at different loads depending on the level of mistuning. At resonance, the maximum power of 160 μW, occurs at 1.65 V_{rms} or 17 kΩ. Off-resonance, i.e. the position of the tuning magnets is 20 μm away from its optimum, it reaches a maximum power of 144 μW at 1.4 V_{rms}, or 15 kΩ. For higher levels of mistuning, the power reduces even further to 32 μW at 0.6 V_{rms}, or 11 kΩ.

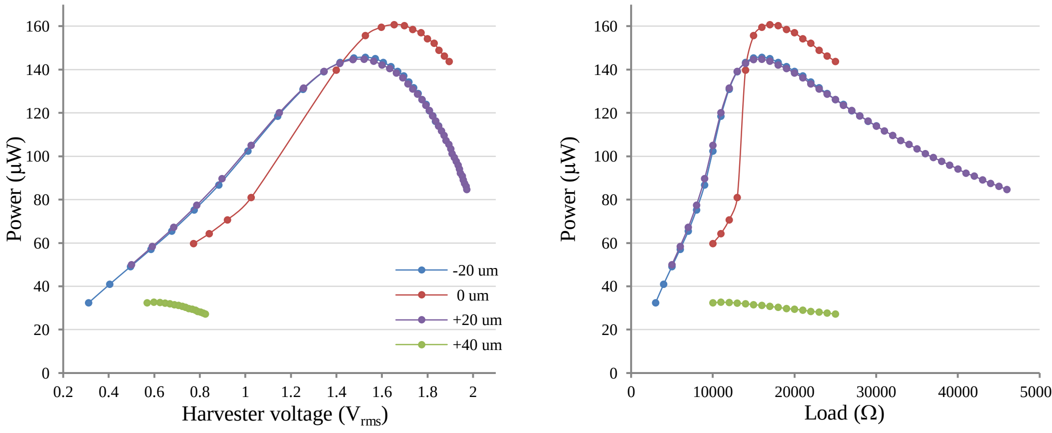

a. Power generated as function of the voltage b. Power generated as function of the resistive load

Figure 5-3. Power generation as tuning mechanism changes position for harvester A

- Harvester B

The physical and electrical differences in the coils used in harvester A and B, as presented in table 3-2 and table 3-3, result in different power generation levels. Harvester A produced up to 201 μW, whilst harvester B produced 140 μW when delivered into an optimal resistive load.

The performance of harvester B was also evaluated when only a resistive load is connected. The frequency was varied from 43.90 to 44.15 Hz, and the tuning mechanism was removed. The results are presented in figure 5-4. The maximum power of 140 μW is reached when the harvester voltage reaches 3.1 V_{rms} at 44.10 Hz, for a resistive load of 38 kΩ. The -3dB power range of the maximum power is reached at 1.57 V_{rms}, or 36 kΩ.

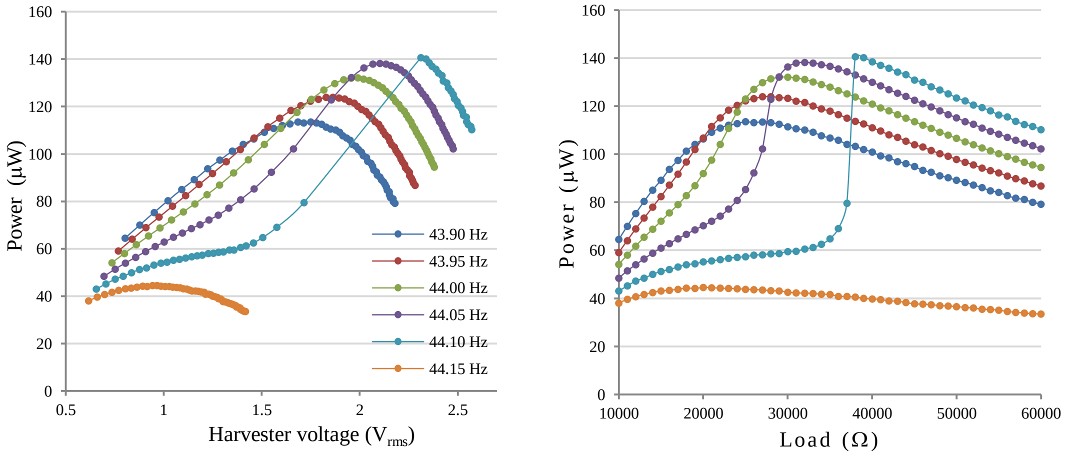

a. Power generated as function of the voltage b. Power generated as function of the resistive load

Figure 5-4 Power generation as base frequency changes for harvester B

- Harvester C

Harvester C was evaluated without the tuning mechanism. The maximum power is generated when the resistive load is 1 kΩ, which corresponds to a harvester output voltage of 0.313 V_{rms}. as presented in Figure 5-5. The -3dB range, in terms of harvester voltage, starts when it reaches a value of 0.113 V_{rms} or 250 Ω.

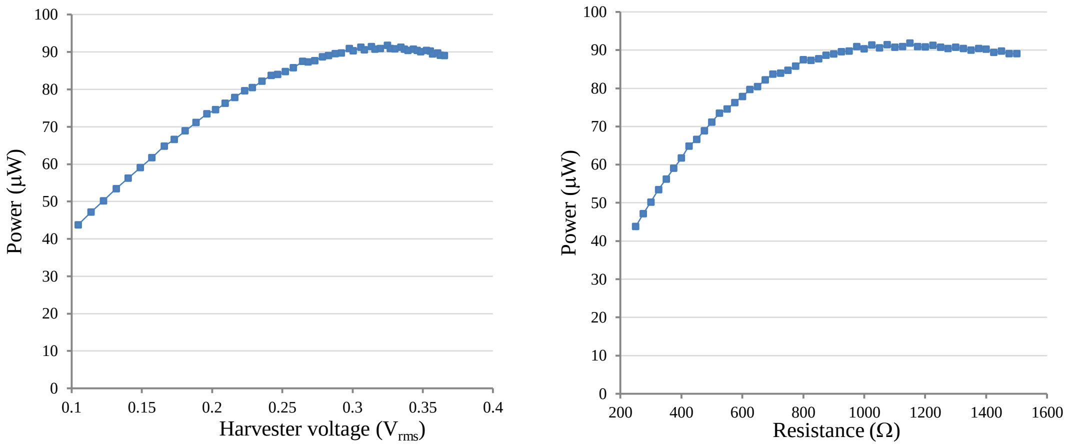

a. Power generated as function of the voltage b. Power generated as function of the resistive load

Figure 5-5. Power generation for harvester C

5.2.1.2 Summary of results

Table 5-1 shows a summary of the results for the three harvesters when connected to a purely resistive load. The optimal load differs between harvesters as consequence of the difference in their physical and electrical characteristics, e.g. coil resistance. The harvester voltage at which they generate the maximum power is used as an indirect indication to identify if the harvester is optimally loaded.

Table 5-1. Optimal load and harvester output voltage

Harvester		Maximum power (µW)	Optimal Load (kΩ)	Harvester voltage (V_{rms})	
				Optimal	-3dB
A	(at 64 Hz)	160	17.0	1.65	> 1.10
	(at 45.25 Hz)	201	26.5	2.20	>1.42
B		140	33.0	2.31	>1.17
C		90	1.0	0.31	>0.11

5.2.2 Voltage multiplier

The performance of the different harvesters when connected to a voltage multiplier was analysed. The objective was to identify and compare their performance against that of the pure resistance, by measuring the time taken on each case to reach 2.6 V at the storage capacitor.

For this analysis, the harvesters were connected to a VM and the energy was saved in a 0.55 F storage capacitor. Additionally, harvester A was evaluated when the energy is delivered to a resistive load, instead of the storage capacitor. Figure 5-6 shows the circuit connection for the 5 stage VM, where the load element corresponds to either a storage capacitor or a resistance. The insertion of the VM has the effect of reducing the impedance seen by the harvester by a factor λ^{-2}, as explained by Saha, et al. [75], where λ is the number of stages in the VM. If the load is a resistance, the optimal load is higher compared to the case where the harvester is loaded only with a resistance.

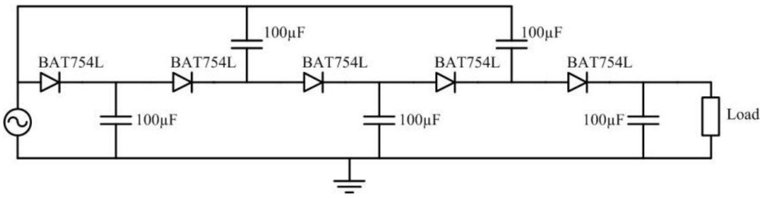

Figure 5-6. Harvester connected to a 5 stage VM load

- Harvester A

Harvester A was connected to a 5 stage VM, while the power was delivered into a resistive load. The base frequency was set at 44.97 Hz at 0.588 $\text{ms}^{-2}_{(\text{rms})}$. The maximum power in the resistance was 108 µW. This occurs when the load is 690 kΩ, with a harvester voltage of 1.462 V_{rms}. The power reduces to a half when the load is 177.5 kΩ and the harvester voltage 0.688 V_{rms}, as shown in figure 5-7.

This test revealed that the original design was not operating at the optimal load because when the voltage at the resistive load reached 2.6 V, the power was 46 µW, and the harvester voltage was 0.606 V_{rms}. This is a reduction of 57% compared to the maximum feasible power.

The presence of the VM reduces the resistance load by a factor of λ^{-2}, in this case by 1/25. Hence, a resistance of 690 kΩ is reflected in the harvester as a 27.6 kΩ resistance. This value is close to the optimal resistive load of 26.5 kΩ as presented in table 5-1.

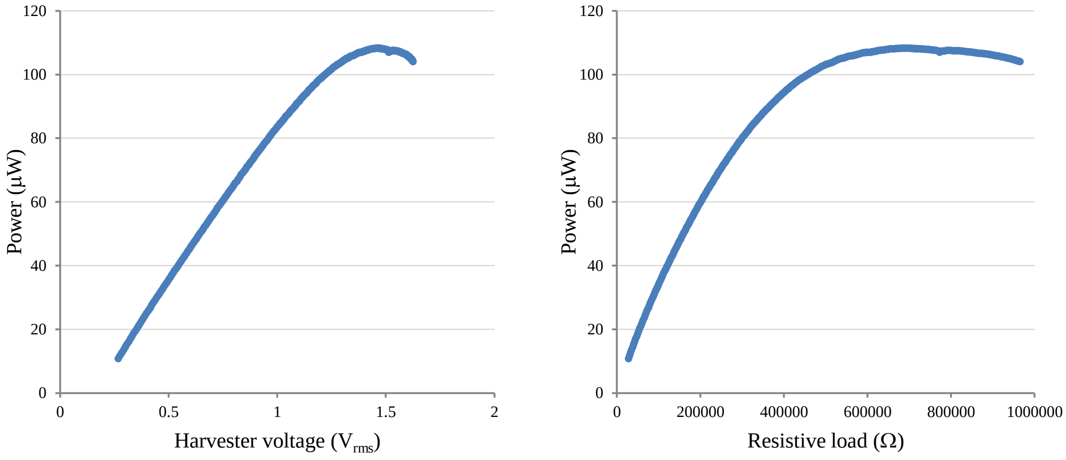

a. Power generated as function of the voltage. b. power generated as function of the resistive load.

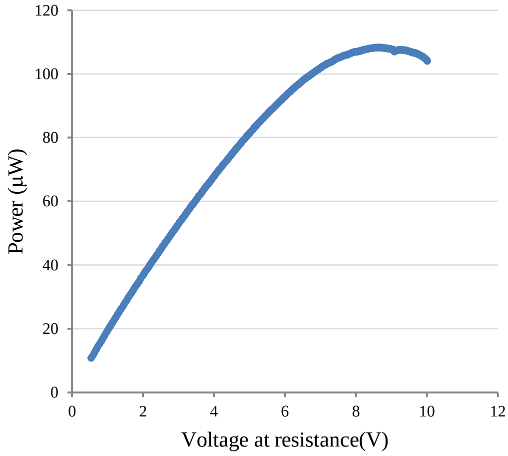

c. Power as function of the voltage at the harvester

Figure 5-7. Power saved into storage capacitor for a 5 stage VM using harvester A

Considering that the maximum power is generated when the voltage at the harvester is 1.65 V$_{rms}$, and the requirement of the tunable energy harvester to operate at 2.6 V. The harvester voltage needs to be doubled. Hence, instead of using 5 stages for the VM, 2 stages were considered to be more suitable for this harvester.

Harvester A was evaluated with 5 and 2 stage VM using the same connection as in figure 5-6 and figure 5-8, respectively. In both cases a 0.55 F storage capacitor was used.

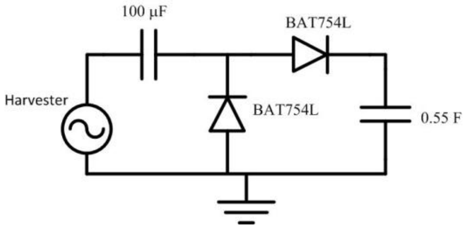

Figure 5-8. 2 stage VM

The results show that the time taken to reach 2.6 V at the storage capacitor reduces from 43.19 hrs, for the 5 stage VM, to 17.9 hrs , in the case of the 2 stage VM, as presented in figure 5-9a. This is a reduction in time of more than 58%. It can be observed that for the 2 stage VM the voltage at the harvester increases at a higher rate than in the case of the 5 stage VM, as shown in figure 5-9b. The power at the storage capacitor reaches a higher rate for the 2 stage VM, at 37 µW, than for the 5 stage VM, which only reaches 18µW, as presented in figure 5-10.

None of the two configurations, the voltage at the harvester reaches the optimal voltage of 1.6 V_{rms}. Although the 2 stage VM brings the voltage closer to this value. It can be concluded that because the 2 stage VM presents an impedance closer to the optimal for the harvester, it can extract more energy than using the 5 stage VM.

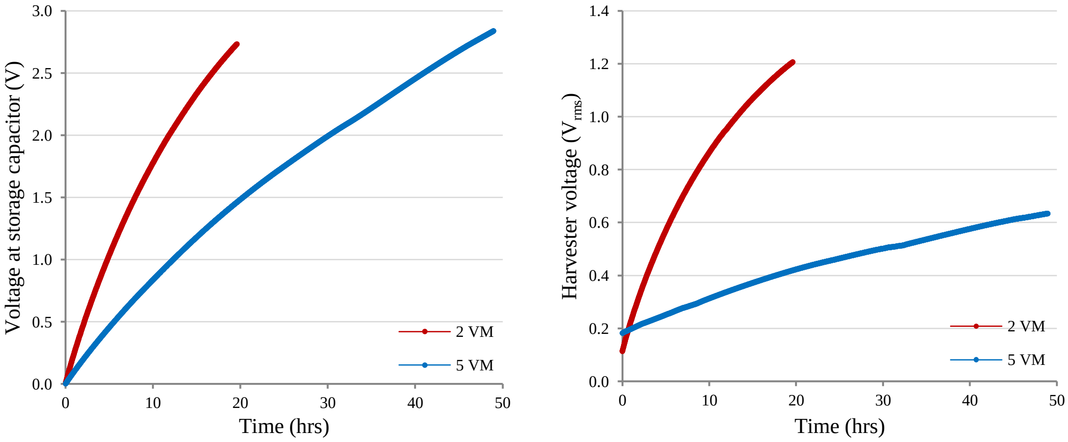

a. Voltage at storage capacitor b. Harvester output voltage

Figure 5-9. Charge time comparison of 2 and 5 stage VM for harvester A.

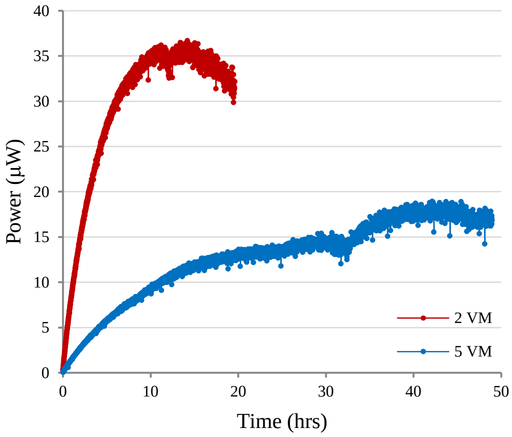

Figure 5-10. Comparison of power at the storage capacitor for 2 and 5 stage VM for harvester A.

- Harvester B

Harvester B has an optimal output voltage of 2.31 V_{rms}. Following the same logic than for Harvester A, a voltage doubler would bring the voltage at the load to 2.6 V but it will result in a lower than optimal voltage at the harvester. A second option was to rectify the signal using a diode bridge and use the storage capacitor to smooth the voltage ripple. This second option requires the harvester to generate a higher output voltage than optimal. To determine which technique was better, both strategies were evaluated.

The diode bridge was implemented using the same type of Schottky diode as those used for the 2 stage VM, due to its lower voltage threshold than standard diodes. The circuit schematic of the diode bridge is shown in figure 5-11.

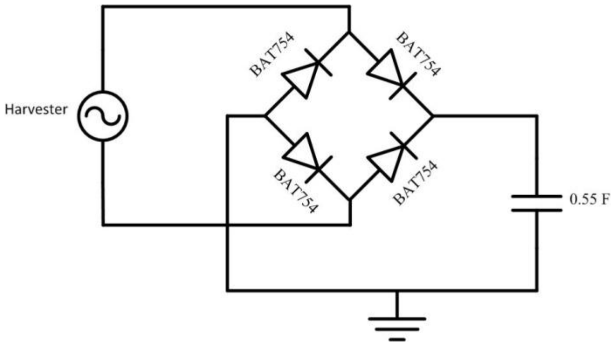

Figure 5-11. Diode bridge

During these tests, the base frequency was set at 60 Hz and the base acceleration remained at 0.588 $ms^{-2}_{(rms)}$.The experimental results show that the diode bridge charges the capacitor in the lowest time. The voltage at the storage capacitor reaches 2.6 V in 9.49 hrs for the diode bridge, while it takes 19.92 hrs for the 2 stage VM. This represents an improvement of more than 50%. The results are presented in figure 5-12a, where also the results from Harvester A are included.

The power at the storage capacitor reaches up to 69 μW when the diode bridge is used. This compares to 40 μW for the 2 stage VM, as presented in figure 5-12b. The voltage at the harvester was not included for the diode bridge case because the attachment of the probes at the output of the harvester affected the performance of the harvester, reducing its energy generation.

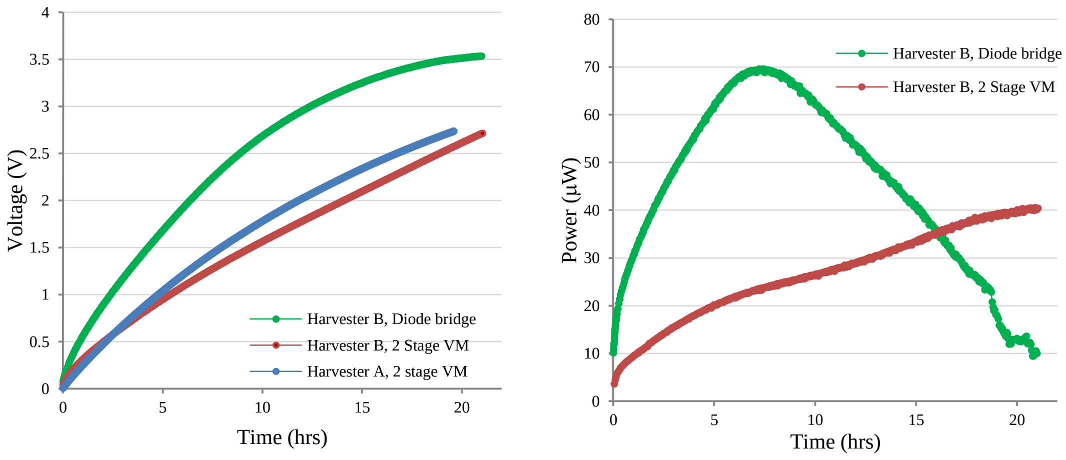

a. Voltage at storage capacitor b. Power at the storage capacitor

Figure 5-12. Charging time for harvester B

- Harvester C

Harvester C was built with 25 μm wire; this reduces its overall resistance resulting in lower optimal load, consequently lower optimal output voltage: optimal load of 1000 Ω with an output voltage of 0.31 V_{rms}.

Harvester C was connected to a 5 stage VM and the base frequency was set at 46.8 Hz. It reaches 2.6 V in 18.81 hrs. The time is comparable to the time taken by harvester A when the energy is rectified with a 2 stage VM. Harvester C reaches its optimal voltage of 0.31 V after 5.2 hrs from the start of the test, resulting in an increase in power being saved into the storage capacitor, as shown in figure 5-13c.

The maximum power saved in the storage capacitor occurs at different voltage on each harvester, as show in figure 5-13d, as a consequence of the difference in the coil characteristics. For Harvester C this occurs at 0.42 V_{rms} and at 1 V_{rms} for Harvester A.

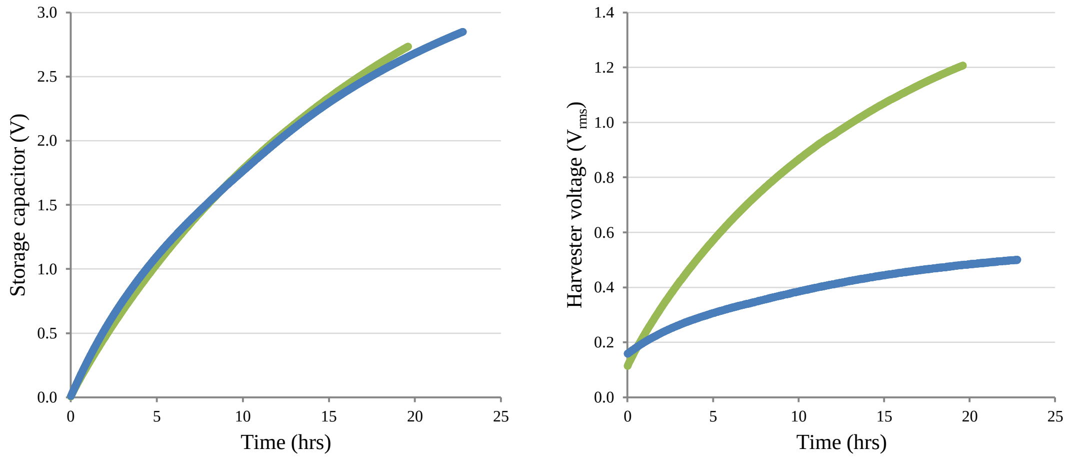

a. Storage capacitor charging time

b. Harvester output voltage

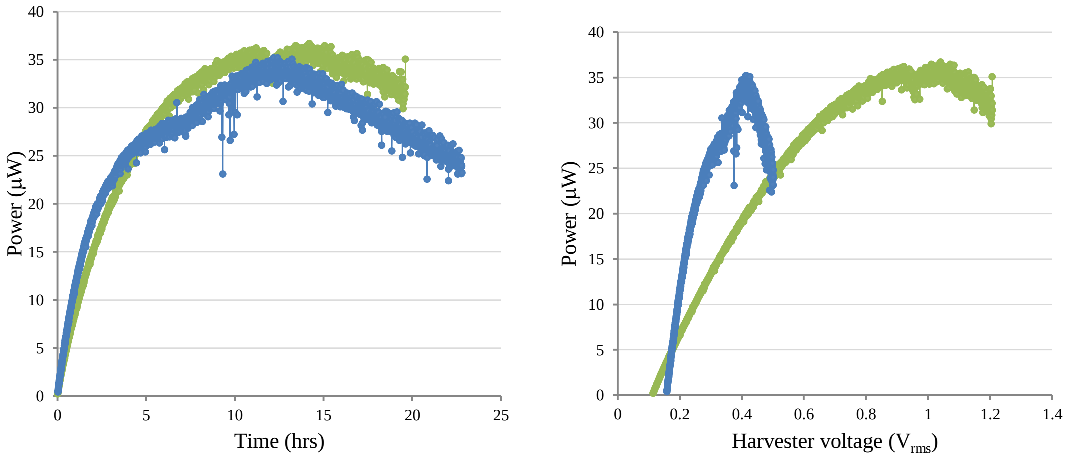

c. Power at the storage capacitor

d. Power at the storage capacitor as function of harvester voltage

Harvester A, 2 stage VM — Harvester C, 5 stage VM

Figure 5-13. Comparison of Harvester A and C.

5.2.3 Comparison to initial design of tunable energy harvester

The results presented in the previous section were compared against those collected from the initial design of the tunable energy harvester presented in section 3.3.4. In that case, the harvester A was connected to a 5 stage VM. It required 38 hrs to reach 2.6 V at the storage capacitor. The power at the storage capacitor reached a maximum of 23 μW, as shown in figure 5-14. The voltage steadily increased from 144 mV_{rms} at the beginning of the test, to 759 mV_{rms} after 64 hrs. In contrast, when harvester B was used to charge the storage capacitor trough a diode bridge, the time needed to reach 2.6 V was 9.49 hrs, as shown in figure 5-14. This is a reduction of 75% in the charging time.

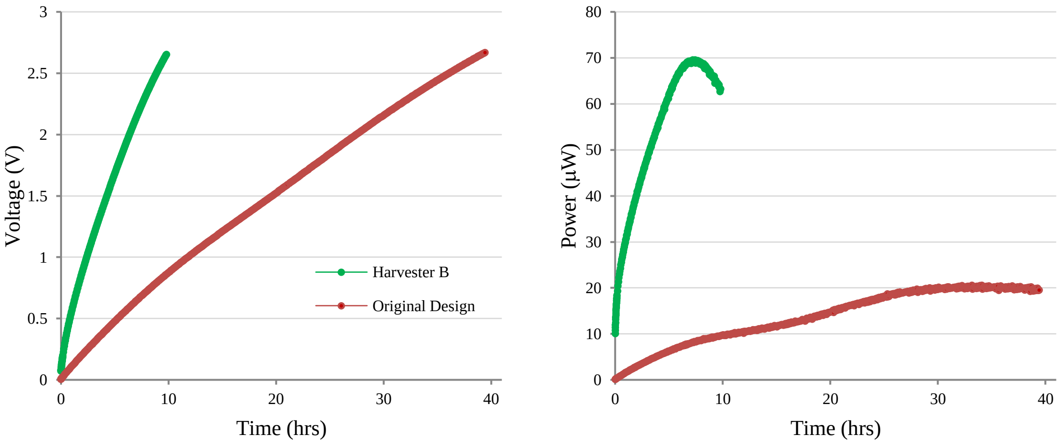

a. Voltage at storage capacitor b. Power at the storage capacitor

Figure 5-14. Power and harvester output voltage when charging the storage capacitor.

5.2.4 Discussion

The main limitation on the use of the VM or diode bridge to rectify the energy generated by the harvester is their inability to adapt the impedance seen by the harvester. As the storage capacitor charges, the current reduces, resulting in a change in its impedance, which cannot be compensated to maintain a maximum power generation. The VM can be optimized to increase the power generation, but this will only occur for certain range of impedances in the storage capacitor.

The next section presents an alternative approach that actively adjusts the impedance seen by the harvester that could result in more power at the storage capacitor and consequently a faster charging time.

5.2.5 Active conversion and regulation

An optimal load for the energy harvester results in the maximum power at the electric load. This optimal load is also related to an optimal output voltage level from the harvester, as it was presented in the previous sections in this chapter. Here it is proposed to maintain the harvester at this optimum voltage by adjusting the impedance seen by the harvester by means of controlling the charge and discharge of an intermediate storage capacitor.

The impedance matching design compromises a 2 stage VM that rectifies and increases the energy from the harvester. The rectified energy is stored in an intermediate capacitor. Next, a boost converter periodically transfers energy from the intermediate storage element into a larger storage capacitor. The energy extracted from the intermediate storage is sufficient to maintain the voltage at the harvester close to its optimal. The resulting impedance matching circuit is presented in figure 5-15.

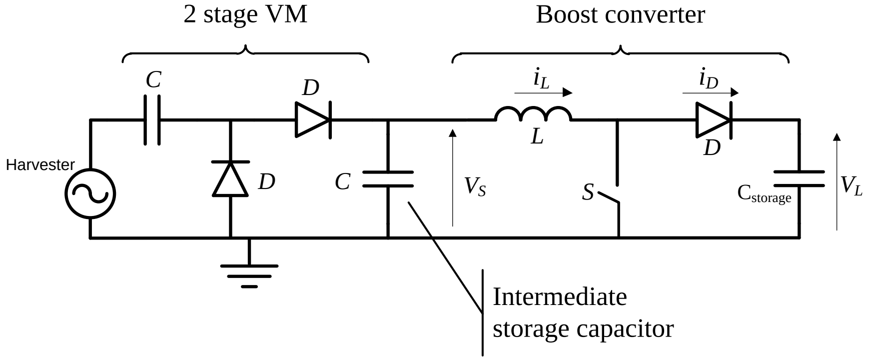

Figure 5-15. Impedance matching circuit

The boost converter operates in discontinuous conduction mode. The current through the inductor reaches a maximum while the switch is enabled. It then reduces linearly to zero when the switch is disabled [108]. The voltage ration between the input (V_S)

and the output (V_L) voltage is given by equation (5-1); where D is the duty ratio, T is the switching period and I_0 is the average diode current (i_D).

$$\frac{V_L}{V_S} = 1 + \frac{V_s D^2 T}{2 L I_0} \tag{5-1}$$

The peak current flowing into the inductor is given by equation (5-2). Increasing the duty cycle would result in a larger inductor current that will flow from the intermediate storage capacitor into the inductor. The voltage at the storage capacitor must be maintained within certain limits to guarantee that the harvester operates at its optimal load. Hence, the inductor current, i.e. duty cycle, must be selected to keep the voltage close to the optimal.

$$I_m = \frac{V_S D T}{L} \tag{5-2}$$

A CMOS low voltage switch, model ADG701 from Analog Devices was implemented as the switching element in the boost converter. It was controlled through the microcontroller, which allows the adjustment of the switching period and duty cycle. The objective was to identify the combination of switching period and duty cycle that charges the storage capacitor in the lowest time.

For the evaluation of the impedance matching circuit Harvester C was used. The storage capacitor in this test was 2.2 mF to reduce the time taken during each test. The tuning mechanism was removed and the base frequency was adjusted at the beginning of each test to coincide with the resonant frequency of the harvester. The microcontroller and switch were powered from an external supply.

5.2.5.1 Switching time

The optimal switching period was first evaluated. The duty cycle, or “ON” states of the switch, remained constant at 10 μs. The switching period was varied from 1 to 150 ms. The purpose was to extract energy form the intermediate storage capacitor once or twice each cycle of the harvester, while maintaining the voltage at the harvester higher than 0.3 V_{rms}. The results are presented in figure 5-16, where also the case where the capacitor is charged using the 5 stage VM is presented.

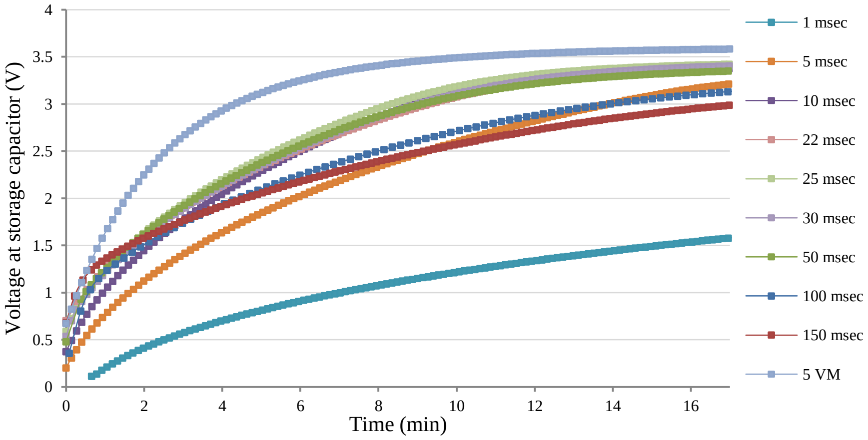

Figure 5-16. Storage capacitor charging time as switching period increases

The time required to charge the capacitor reduces when the switching period is between 10 to 50 msec, with the minimum time when the switching is 25 msec. However, the capacitor is charged at a faster rate when the 5 stage VM is used. In that case, the voltage at the storage capacitor reaches 2.6 V in 2.9 min, whilst it takes 5.9 min when the switching period is 25 msec. Analysis of the power delivered by the harvester into the impedance matching circuit shows that the efficiency of the circuit is low. The power generated is around 100 µW for the switching period of 25 msec during the entire test. However, the maximum powered at the storage capacitor is 25 µW, falling to 20 µW after 17 s, as shown in figure 5-17b and figure 5-17c where only the switching time cases with the maximum charging rate are presented.

Figure 5-17a shows that the harvester generates more power when the voltage at the harvester is between 0.3 to 0.5 V_{rms}. This can also be compared to the power generated when the 5 stage VM is connected, where the maximum power corresponds to this range of voltages.

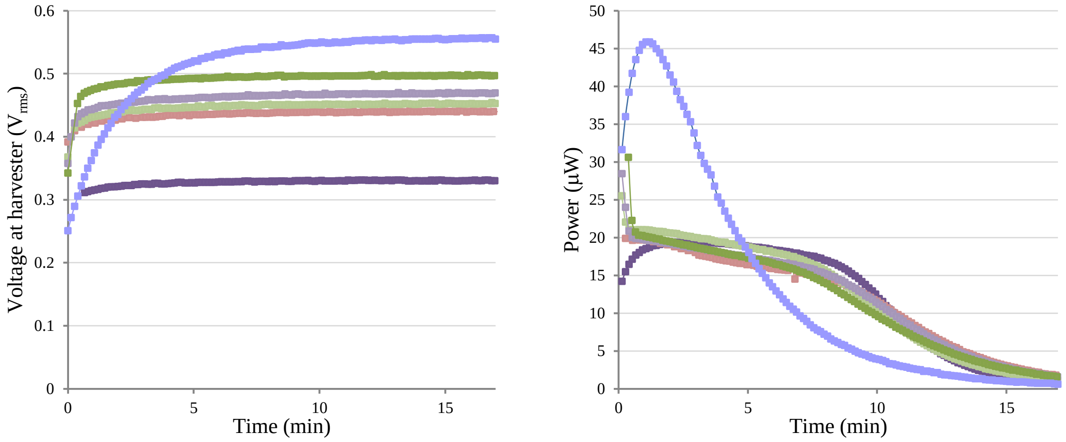

a. Harvester voltage

b. Power at the storage capacitor

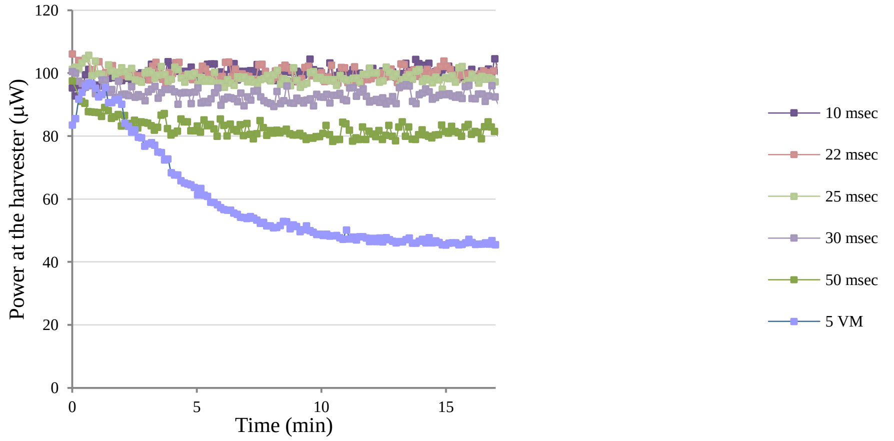

c. Power generated by harvester

Figure 5-17. Harvester performance as switching period of boost converter varies

5.2.5.2 Duty cycle

The optimum duty cycle of the converter, i.e. the time the switch is enabled, was investigated next. The switching period was fixed at 20 ms, this was experimentally found to be the one with the highest charging rate during the previous test. The duty cycle was adjusted from 1 to 10 µsec, the results are presented in figure 5-18 and figure 5-19

The capacitor reaches 2.6 V in 5.12 min when the switch is enabled during 5 µsec every switching period, as presented in figure 5-18a. This corresponds to a duty cycle of 0.025%. The power generated by the harvester in this case reduces from 100 µW, at the beginning of the test, to 71 µW towards the end for the test. The power at the storage capacitor reduced from an initial value of 50 to 17 μW, as presented in figure 5-18b and figure 5-19b. It can be seen in figure 5-18a that the voltage at the harvester increases from 0.3 to 0.5 V_{rms} during the test.

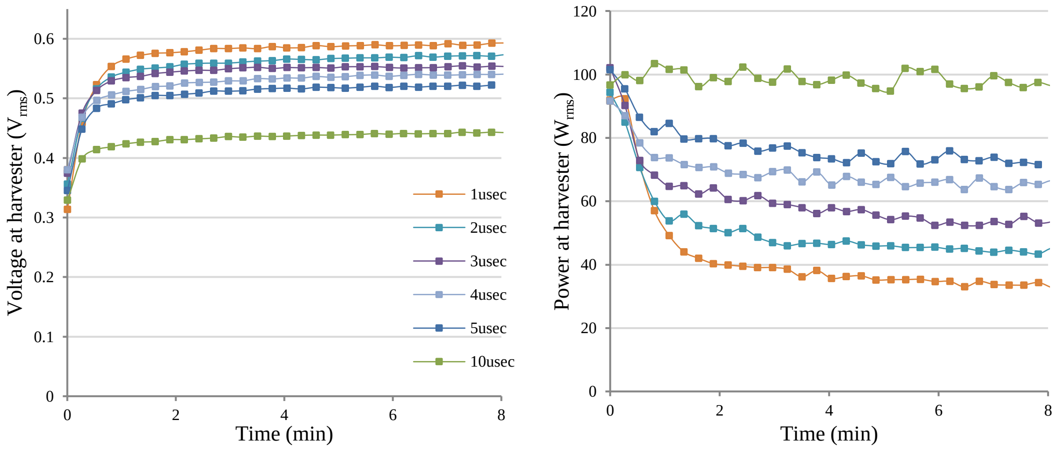

a. Harvester voltage

b. Power generated by harvester

Figure 5-18. Harvester performance as duty cycle of impedance matching circuit varies

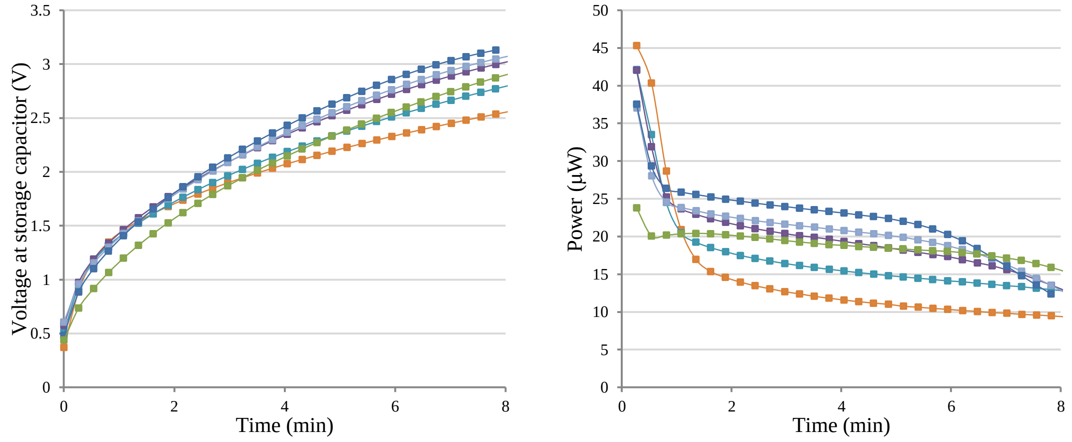

c. Voltage at storage capacitor

d. Power at storage capacitor

Figure 5-19. Storage capacitor performance as duty cycle of impedance matching circuit varies

In subsequent tests the 2.2 mF storage capacitor was replaced by a capacitor of 0.55 F to compare the performance of the impedance matching circuit against the 5 stage VM, the results are presented in figure 5-20 and figure 5-21.

Figure 5-21c shows that 90% of the maximum power at the storage capacitor is reached when the harvester voltage is between 0.3 to 0.4 V_{rms}. In the case of the test with the impedance matching circuit, this occurs between 0.53 to 1.50 hrs, which represented 0.97 hrs that the harvester operates within the 90% of the maximum power generation. Afterwards, the harvester voltage increases, reducing the power.

In the case of the 5 stage VM, the harvester voltage remains in the 90% maximum power range for a total of 5.62 hrs. This is longer than for the impedance matching circuit. This explains the higher charging rate for the 5 stage VM compared to the proposed impedance matching circuit.

The time taken by the 5 stage VM to reach 2.6 V is 17.7 hrs. In the case of the impedance matching circuit, the test was carried out for 22 hrs reaching 1.64 V. Considering the trend on the voltage for matching circuit, it was calculated that it will take 30 hrs to reach 2.6 V. The 5 stage VM charges a 41% faster than the impedance matching circuit. It is expected that the charging time would be lower than for the 5 stage VM if the impedance matching circuit was adjusted actively during charge to maintain the optimal voltage at the harvester.

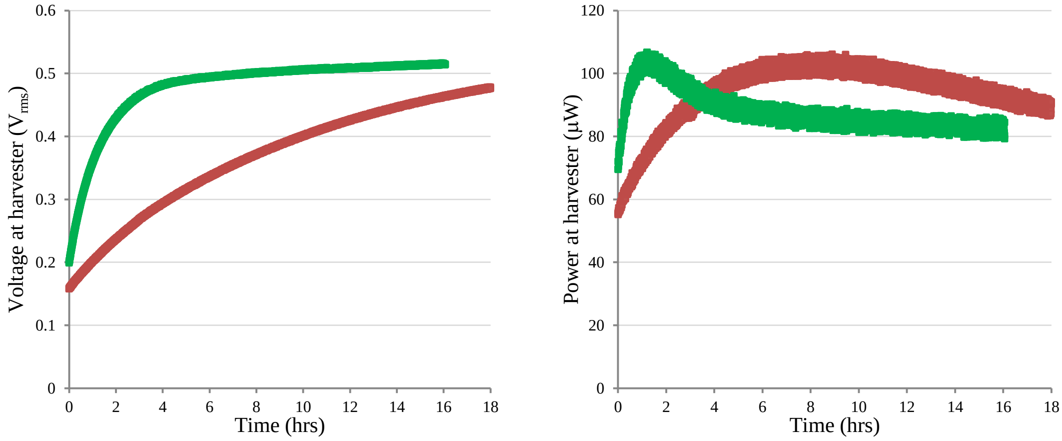

a. Voltage at the harvester

b. Power generated by harvester

Figure 5-20. Harvester performance as duty cycle of impedance matching circuit varies for a 0.55 F storage capacitor

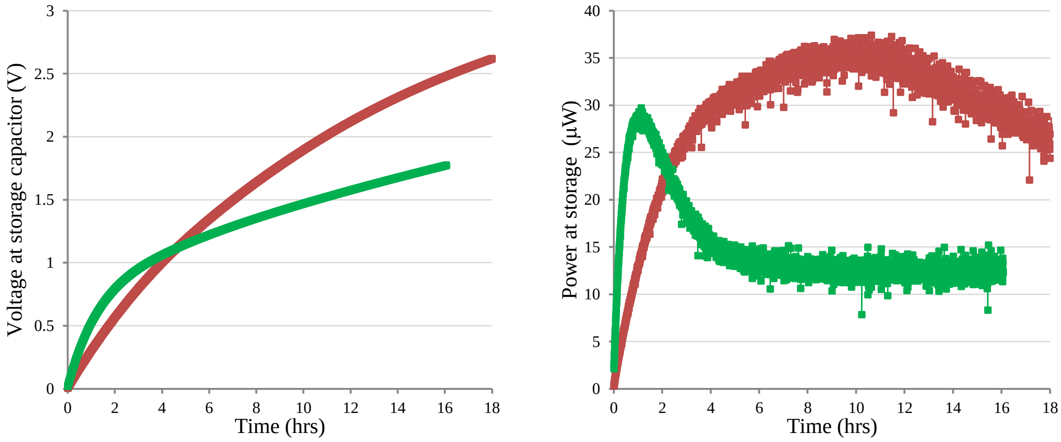

a. Voltage at storage capacitor

b. Power at the storage capacitor

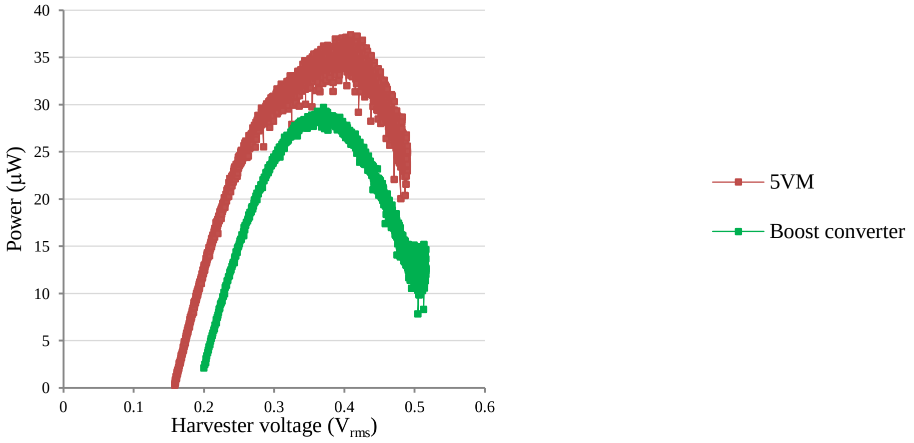

c. Power at storage capacitor as function of harvester voltage

Figure 5-21. Harvester performance comparison for a 0.55 F capacitor

5.2.5.3 Discussion

The power consumed by the boost converter to operate, and by the microcontroller to drive it, were not considered during the test. Therefore, the power at the storage would reduce if this were included. On the contrary, the VM does not require any overhead power to operate, but its low efficiency and inability to adjust to the changing impedance limits its range of use.

The design of low power solutions for energy rectification and conditioning are beyond the scope of the present work. The literature presented in section 2.5.3 gave some examples of purpose-built switching techniques, but most of them are aimed at harvesters that generate power in the order of milliwatts, because their overhead power is in the region of hundreds of microwatts. Hence, they are incompatible for any of the harvesters presented in this work, which generate between 100 to 200 μW.

5.3 Optimized operation of tunable energy harvester

The evaluations of the different harvesters built during this project have shown that harvester B has the lowest charging time when the energy generated is processed by a diode-bridge. Hence, harvester B was selected to evaluate the optimized performance of the tunable harvester. However, the inclusion of the diode-bridge, instead of the 5 stage VM from the original design, forced the redesign of the method used to collect information regarding the base frequency.

5.3.1 Period meter

The original design of the tunable energy harvester collected information regarding the base frequency by sampling the signal at one of the terminals of the harvester, while the second terminal was grounded. In the case of the diode-bridge, none of the terminals were grounded. The lack of a permanent ground reference resulted in erroneous ADC conversion when the base frequency was measured using the signal from one terminal.

An alternative approach was to momentarily connect one of the harvester terminals to ground while the ADC conversion occurred. However, this was unsuccessful because the impedance seen by the harvester changes when the terminal is grounded, which combined with the non-linear response of the harvester, resulted in the change of the harvester resonant frequency. The harvester has a different resonance frequency when the diode bridge is connected than when one of its terminals is grounded. The result was that the resonance frequency was being adjusted only for the second case, rather than for the diode-bridge case, which is the one required.

The solution selected was the use of an operational amplifier as a comparator where each of the harvester terminals is connected to comparator inputs. The variation of the voltage in the harvester produces a square wave whose frequency is the same as the harvester output voltage. A low pass filter was installed at the output of the operational amplifier to reduce the false triggering of the timer in the MCU when the difference in voltage of the terminals reduces.

The comparator circuit diagram is presented in figure 5-22. A 10 MΩ resistance was connected between each of the terminals of the harvester and ground to share the same ground reference as the operational amplifier.

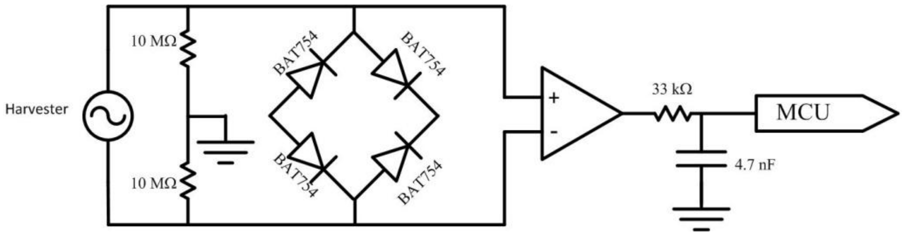

Figure 5-22. Comparator circuit diagram

5.3.2 Bandwidth of operation

The variation of the resonant frequency of the harvester B when the distance between magnets changes was experimentally evaluated, in the same manner as for harvester A in section 4.2. First, the frequency response over a large range of tuning distance was performed to identify the optimal range, where the minimum displacement gives a maximum variation in resonant frequency, with the minimum energy consumption.

The tuning was performed with harvester B connected to a resistance of 35 kΩ. The base acceleration remained at 0.588 $ms^{-2}{}_{(rms)}$. The experimental results are presented in figure 5-23. The magnet tuning distance was reduced in 1 mm step, from 7 to 1 mm. The change in resonant frequency has a similar pattern as for harvester A, as shown previously in figure 4-1. The effect of the distance between tuning magnets on the resonance frequency and power generation has a great influence at small tuning distances, resulting in a larger change in resonance frequency and reduction in power generated as the distance between magnets reduces.

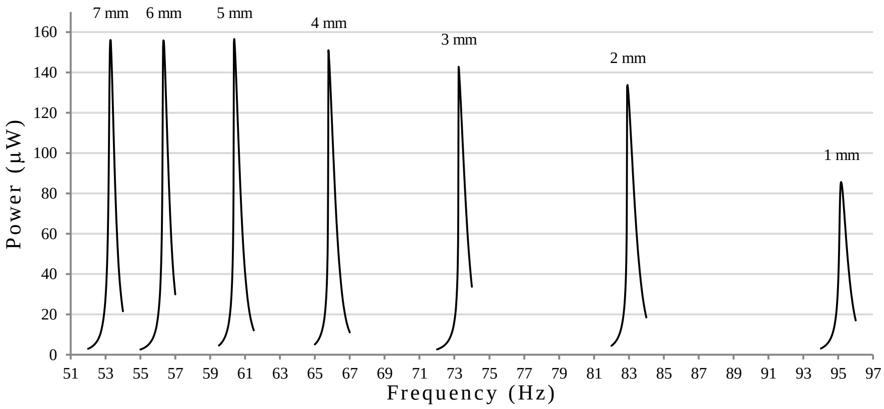

Figure 5-23. Resonance frequency change as magnet tuning distance reduces from 7 to 1 mm

The optimal range of operation for the tunable energy harvester was selected between 5 to 3 mm, which corresponds to 100 steps given by the actuator. The frequency of operation expands from 60.62 to 74.26 Hz, while the power generated reduces from 156 to 143 μW in this range, respectively. This is purely due to the increased frequency at a fixed acceleration resulting in a lower amplitude, i.e. no additional damping occurs.

The resonance frequency every 200 μm, or 10 actuator steps, was measured along the range proposed. The starting point was at a distance of 5 mm between tuning magnets, which was considered to be at the 100th step of the actuator, reducing to 3 mm, the 200th step on the actuator. The results, presented in figure 5-24, are used to create a mathematical equation relating the harvester resonance frequency to a position of the actuator.

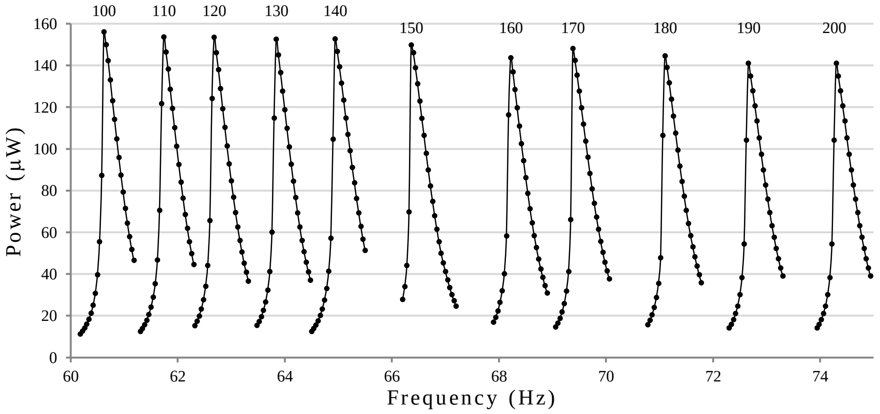

Figure 5-24. Resonance frequency variation as actuator moves 10 steps, starting at step 100th.

The resulting equation (5-3) is used by the system control to adjust the position of the actuator to match the base frequency. It is important to mention that the system measures the period of the excitation instead of its frequency.

$$Optimal\ position\ [step] = 200 - \frac{(period\ [\mu sec]) - 13480}{30} \tag{5-3}$$

The maximum error between the experimental optimal position of the actuator to that calculated using equation (5-3) is 5 actuator steps. This error is compensated by the use of the fine tuning control, as previously described in section 4.5. The comparison between the harvester resonant frequency as function of the actuator position is shown in figure 5-25, where the experimental and calculated cases are presented.

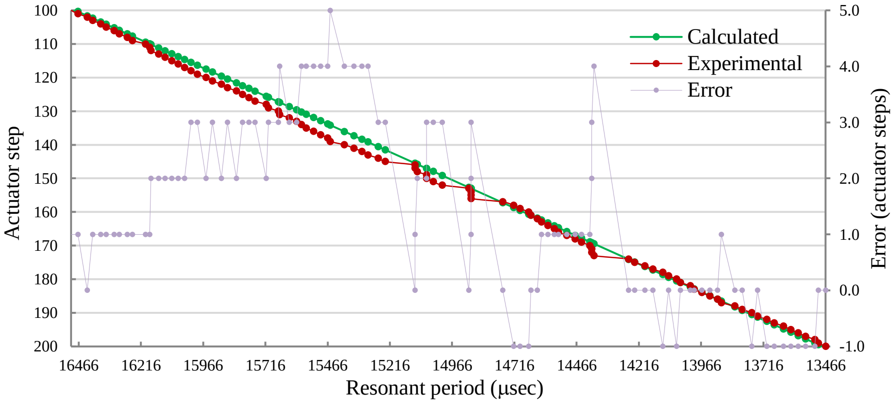

Figure 5-25. Comparison between experimental and calculate optimal position

5.3.3 Non-linear response

The replacement of the VM by a diode-bridge resulted in more power at the storage capacitor and the increase of the harvester displacement. As the displacement increases, the non-linear behaviour becomes more evident as described by Beeby, et.al. [36]. This can be observed in figure 5-26. The harvester resonant frequency was set at 67.11 Hz, which corresponds to the actuator step position 153th. The harvester was connected to the diode bridge; the storage capacitor was connected to an external power supply to maintain 2.6 V throughout the test. The actuator was adjusted from step 100th increasing until step 200th, measuring the displacement at each step; then, decreasing from step 200th to 100th.

The displacement of the harvester increases as the actuator moves closer to the optimal position. The response of the harvester is different according to the direction of adjustment. When the actuator position increases, the displacement of the harvester is in stages and it does not reach the maximum level seen when the adjustment is in the opposite direction, as shown in figure 5-26. When the actuator’s step position reduces, the displacement has a more gradual increase and reaches a higher value. This is due to the soft non-linear behaviour of the harvester.

To avoid the low level of displacement, i.e. low energy generation, the control strategy was modified to add 5 step every time it calculates the optimal position of the actuator. The intention of this modification was to force the fine adjustment of the resonant frequency to be made by decreasing the actuator step position.

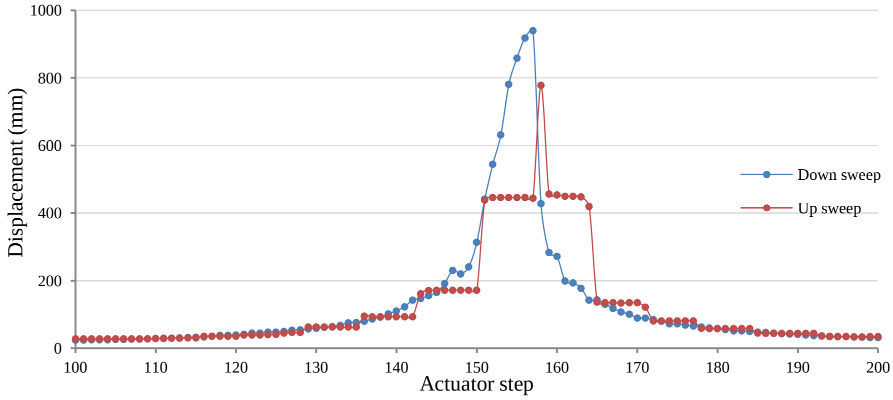

Figure 5-26. Displacement of harvester B as the actuator position is adjusted. First increasing its position, then decreasing.

5.4 Autonomous operation of tunable energy harvester

The autonomous operation of the tunable energy harvester with the optimized power extraction and control system was evaluated. The system was powered exclusively from the energy harvested and saved into the storage capacitor. The base frequency was varied along the range of operation proposed for Harvester B, 60.62 to 74.26 Hz, at different intervals to measure the voltage drop at the storage capacitor due to the adjustment of the resonance frequency, and the time taken to harvest the power used in this process. The base acceleration remained at 0.588 $\mathrm{ms^{-2}}_{\mathrm{(rms)}}$.

Figure 5-27 shows the circuit diagram of the optimized tunable energy harvester, including the diode bridge for voltage conditioning and the comparator used to sample the base frequency.

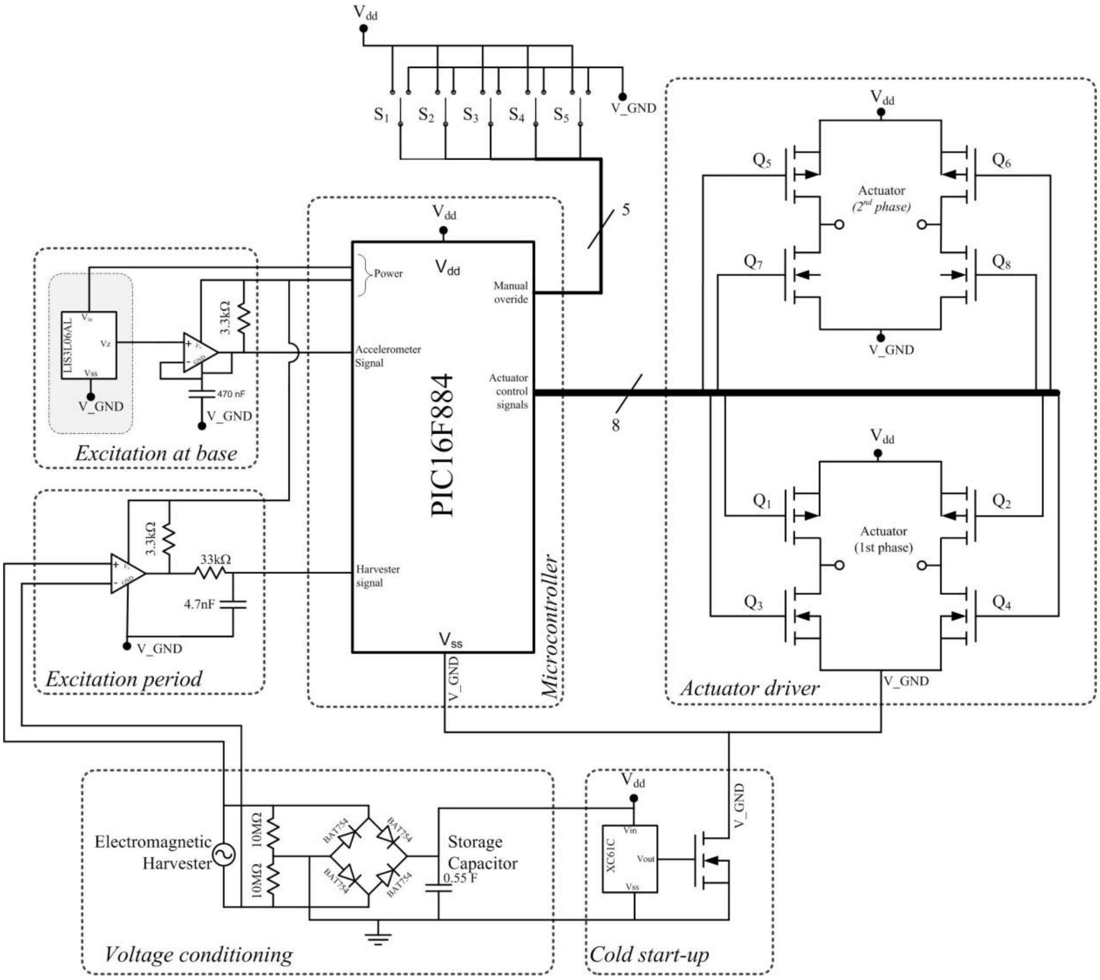

Figure 5-27. Circuit diagram of tunable energy harvester

5.4.1 Tuning of harvester resonant frequency

The tuning capabilities of the tunable energy harvester were assessed by changing the base frequency at regular intervals, which corresponds to the actuator being adjusted by 1, 5, 10, 20, 30, 40, 50 and 100 steps per frequency change.

During this evaluation, the base frequency was adjusted to a new frequency only if the voltage at the storage capacitor was higher than 2.6 V and the time elapsed since the last frequency change was more than 400 s. This guarantees that the harvester has returned from its low power mode at least on one occasion during this period, and if deemed necessary, adjusted the actuator position.

5.4.1.1 1 step adjustment

Figure 5-28 presents the experimental results when the base frequency changes by 0.14 Hz, which corresponds approximately to 1 step adjustment on the actuator position. The power at the storage capacitor drops as the base frequency changes as a consequence of the divergence between the harvester resonant frequency and the base frequency. When the system recognises the change in frequency, it commands the adjustment of the actuator, resulting in a larger power loss from the storage capacitor due to the use of the actuator.

The power at the storage capacitor increases beyond 100 μW once the harvester resonant frequency was adjusted. It can also be seen that the voltage at the storage capacitor increases during the test despite power being used to operate and adjust the tunable energy harvester, i.e. more power is generated than the power is consumed to operate the tunable energy harvester.

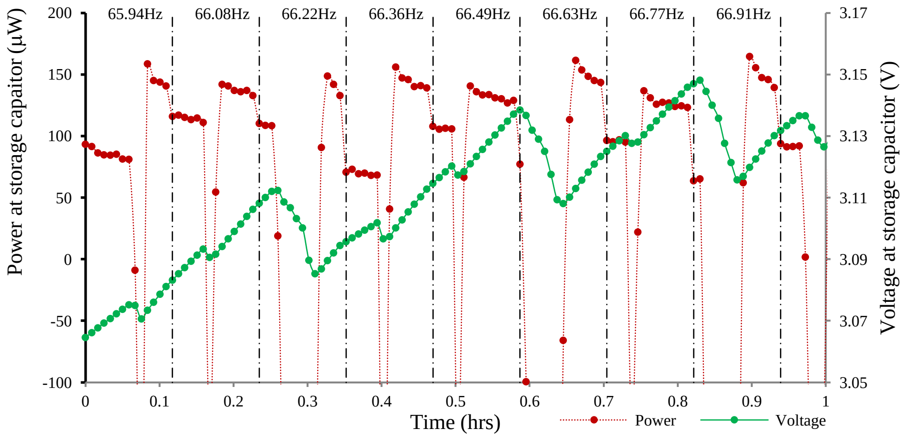

Figure 5-28. Power and voltage at the storage capacitor as harvester resonant frequency is adjusted as the base frequency changes by 0.14 Hz, 1 actuator step

The adjustment in the harvester resonant frequency is evident in figure 5-29 where the harvester displacement is shown. The displacement was measured using a vibrometer. This measurement was used to confirm that the adjustment of the harvester has been performed. The reduction in the displacement can be observed when the base frequency changes, which later recovers when the actuator position is adjusted.

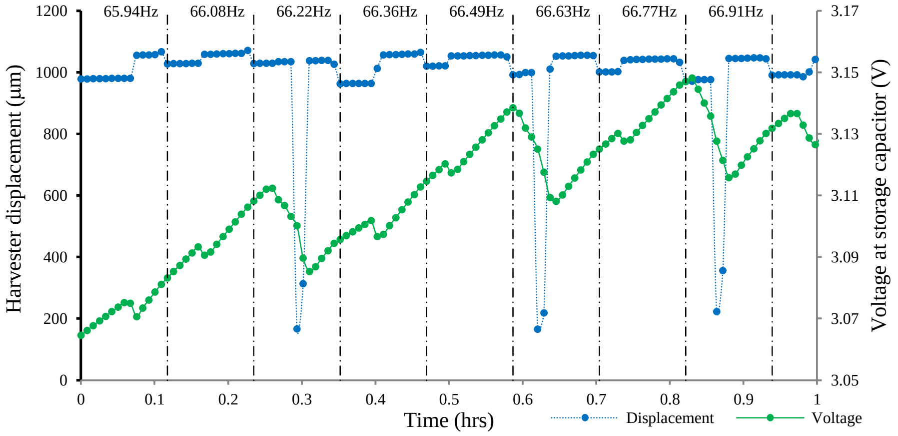

Figure 5-29. Harvester displacement as resonant frequency is adjusted to that at the base frequency

5.4.1.2 Multistep adjustment

The tunable energy harvester was also evaluated when the base frequency changes by 0.65, 1.30, 2.77, 4.17, 5.56, 6.95 and 13.89 Hz on each occasion. These resulted in the adjustment of the actuator by 5, 10, 20, 30, 40, 50 and 100 steps respectively.

Figure 5-30a presents the case when the base frequency is adjusted by 1.30 Hz, 10 actuator steps. The power has a higher drop compared to the previous case because there is a larger disparity between the harvester resonant frequency and the base frequency. On this occasion the power drops to negative values when the base frequency changes; i.e. more power is used to operate the tunable energy harvester, than the power it generates. The amplitude of the harvester during operation is shown in figure 5-30b.

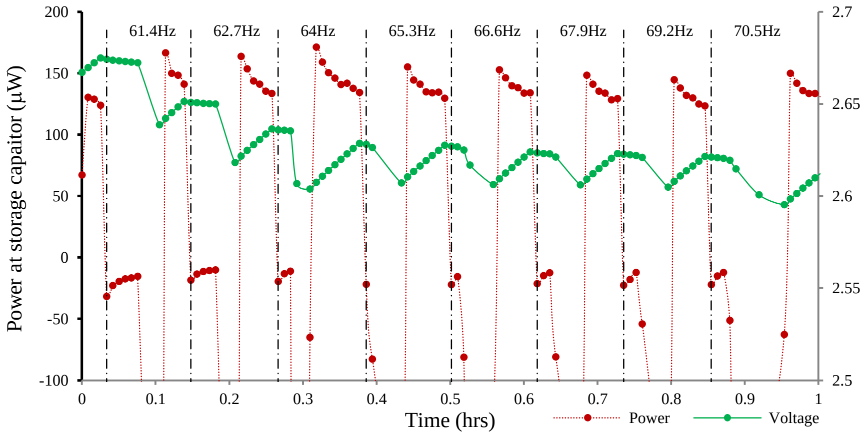

a. Power and voltage at storage capacitor

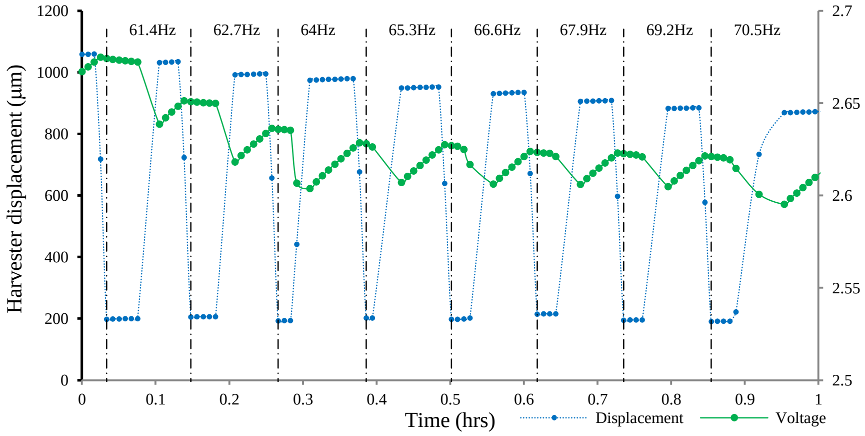

b. Harvester displacement as harvester resonant frequency is adjusted

Figure 5-30. Harvester resonant frequency adjustment as base frequency increases by 1.30 Hz, 10 actuator steps approximately

The base frequency was then adjusted by 6.95 Hz, which corresponds to 50 steps adjustment of the actuator. The results are presented in figure 5-31. On average, the voltage at the storage capacitor drops 80 mV every time the actuator was used to adjust the harvester resonant frequency. On every occasion, the voltage at the storage capacitor reduced below the 2.6 V threshold, forcing the system to remain in low power mode and not measuring the base frequency until the voltage rises above the threshold.

Figure 5-31b shows the displacement of the harvester as the resonant frequency is adjusted. It should be also noted that the maximum displacement reduces as the frequency increases.

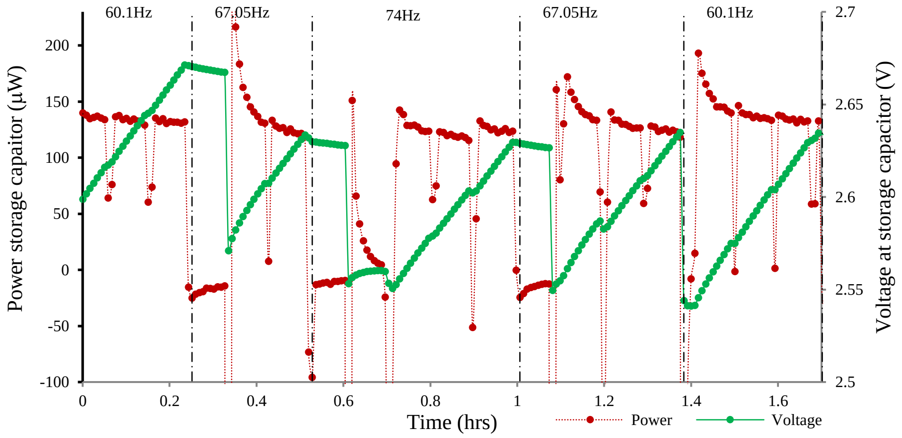

a. Power and voltage at storage capacitor

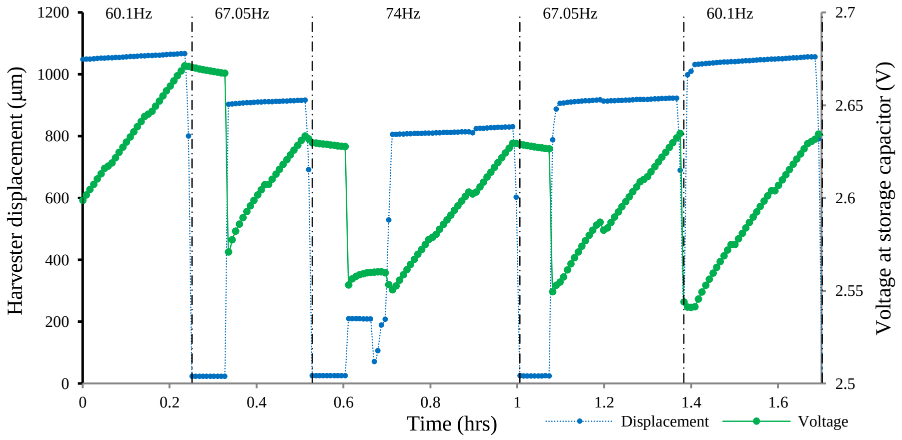

b. Harvester displacement as harvester resonant frequency is adjusted

Figure 5-31. Harvester resonant frequency adjustment as base frequency increases by 6.95 Hz, 50 actuator steps approximately

The worst-case scenario for the tunable energy harvester is when the base frequency changes by 13.89 Hz. This supposes an adjustment of 100 actuator steps. Similarly, to the previous tests, the power drops when the base frequency changes, as well as when the system returns from low power mode. Nevertheless, the major drop occurs when the actuator is adjusted by 100 steps to its new optimal position. This can be observed in figure 5-32.

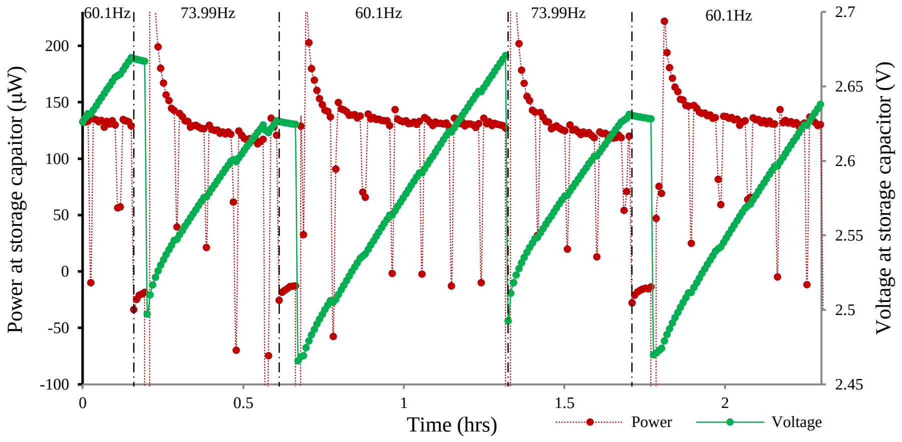

a. Power and voltage at storage capacitor

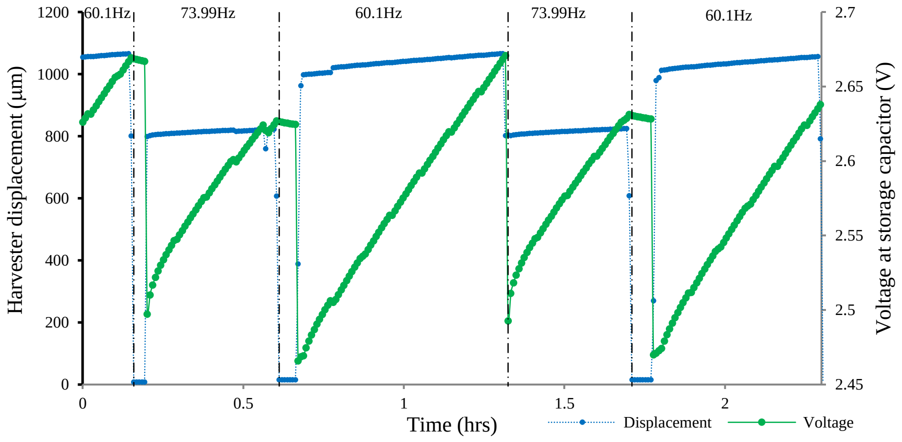

b. Harvester displacement as harvester resonant frequency is adjusted

Figure 5-32. Harvester resonant frequency adjustment as base frequency increases by 13.89 Hz, 100 actuator steps approximately

5.4.2 Voltage drop and recovery time

Table 5-2 summarizes the results from the previous tests. The voltage drop and recovery time are presented for each case. The values reported are average values calculated over a range of tuning cycles.

The voltage drop and recovery time per step of adjustment is higher when the actuator position moves few steps, as can be seen in figure 5-33. It then reduces as the length of adjustment increases. The reason for the relative increase in power consumption for small adjustments resides in the higher proportion of energy required to initiate movement. Once in movement, this proportion diminishes and more energy is used to maintain movement.

Table 5-2. Voltage drop and recovery time

Frequency step (Hz)	Actuator adjustment (steps)	Voltage drop (mV)	Recovery time (sec)
0.00	0	1	< 30
0.14	1	12	246
0.65	5	13	236
1.30	10	21	333
2.77	20	43	603
4.17	30	58	694
5.56	40	76	938
6.95	50	86	1153
13.89	100	166	1810

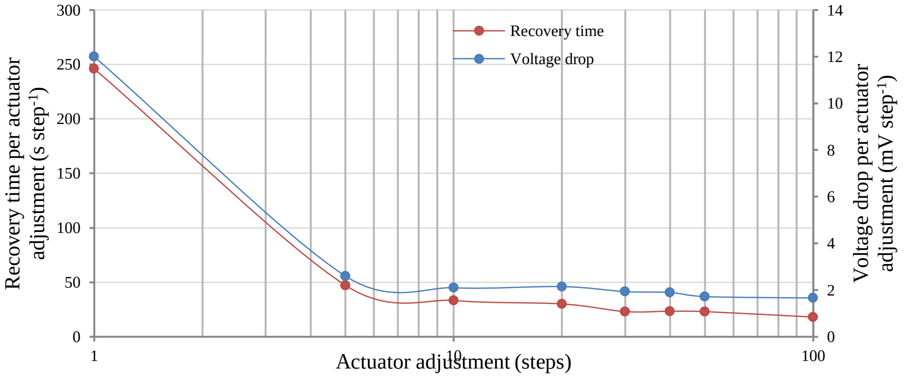

Figure 5-33. Recovery time and voltage drop per actuator step adjustment

The increase in the performance of the optimized tunable energy harvester can be appreciated from the comparison with the results from the original design given in table 4-2. The comparison is shown in figure 5-34. Even though the voltage drop per adjustment is higher for the optimized design, the recovery time is up to 76% faster than the original design. Therefore, the optimized tunable energy harvester has a better performance than the original presented in chapter 4.

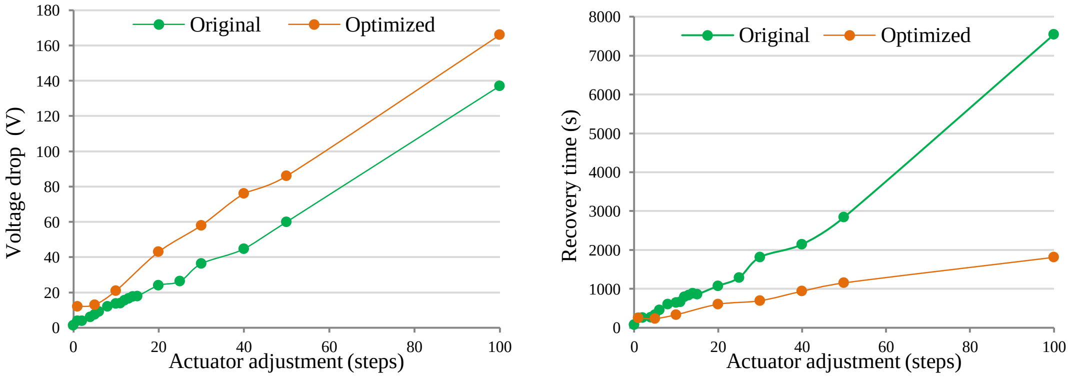

a. Voltage drop

b. Recovery time

Figure 5-34 Comparison between original and optimized tunable energy harvester

5.5 Autonomous tunable wireless sensor node

The ultimate purpose of the tunable energy harvester is to operate as the power source for a wireless sensor node. To evaluate the performance of the tunable energy harvester in this capacity, a wireless sensor node was installed. A wireless node eZ430-RF2500 from Texas Instruments [109] was connected to the tunable harvester providing the capability of sensing and data transmission. The eZ430-RF2500 includes a microcontroller MSP430 and a transceiver CC2500. It has an integrated voltage and temperature sensor.

The wireless node was connected directly to the storage capacitor. It was programmed to transmit 3 bytes of information split into 2 bytes for temperature and 1 byte for voltage measured at the storage capacitor. A reception node was also designed to receive the data transmitted, it was connected and powered by a computer. The wireless node devices were provided by the Holistic Approach to Energy Harvesting Electronics project [103].

The test was designed to evaluate the performance of the autonomous tunable energy harvester as data is collected and transmitted. The data transmission occurred at three different duty cycles depending on the voltage at the storage capacitor. The base frequency was altered to force the adjustment of the harvester resonant frequency.

The data duty cycle were set as follow:

- 1 transmission every minute if the voltage at storage capacitor is lower than 2.8 V.
- 1 transmission every 5 seconds if the voltage is between 2.8 to 2.9 V.
- 1 transmission every second if the voltage is higher than 2.9 V.

The harvester’s resonant frequency was adjusted at the beginning of the test to coincide with a base frequency of 59.5 Hz. The base acceleration remained at 0.588 $ms^{-2}{}_{(rms)}$ during the entire test.

The wireless node has a current consumption while transmitting of 17.4 mA at 2.9 V. Every transmission lasts for 4.5 msec. The total energy consumed per transmission is 211 μJ. The wireless node is put on low power mode when not transmitting, consuming around 1 μA.

The test was divided into 3 sections, as shown in figure 5-35. During sections A and C the base frequency remained constant at 59.5 and 64.5 Hz, respectively. In section B the base frequency was adjusted by 5 Hz, which corresponds to an adjustment of approximately 40 actuator steps. The wireless node was programmed to swap the state of an output port every time a transmission has occurred. This was used as a flag to validate the correct operation of the system. This is also visible in figure 5-35.

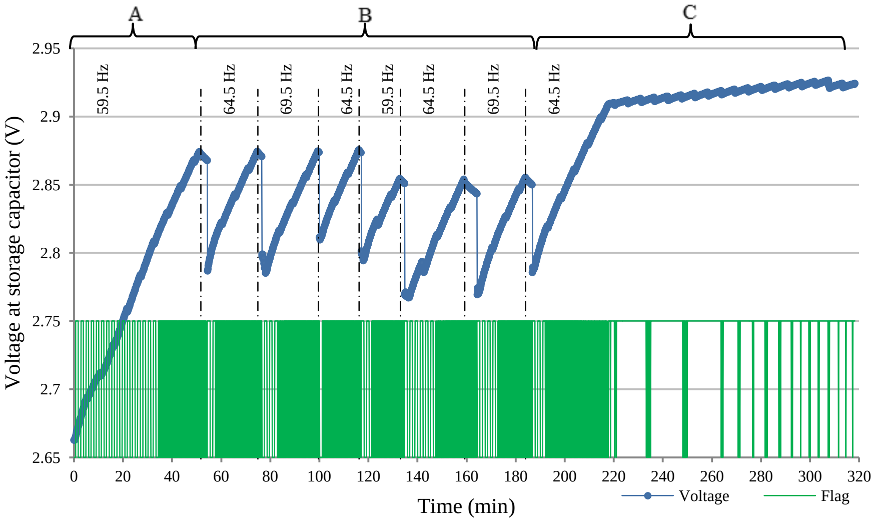

Figure 5-35. Operation of autonomous tunable energy harvester

The test started with the storage capacitor at 2.66 V. The data is transmitted every minute until the voltage reaches 2.8 V. A detailed examination of the power at the storage capacitor shows a reduction in the power saved because a portion of the energy is being used by the wireless node for transmission. This represents a drop in power of around 19 μW from the average power at the supercapacitor of 130 μW, as shown in figure 5-36.

The tunable energy harvester returns from its low power mode every 320 s, approximately, and measures the voltage and base frequency. The voltage drops on average 2 mV during this process, and more power is used than the power that is generated, draining the storage capacitor. The average power at the storage capacitor when the tunable harvester is in low power mode and no transmission occurs is 130 µW.

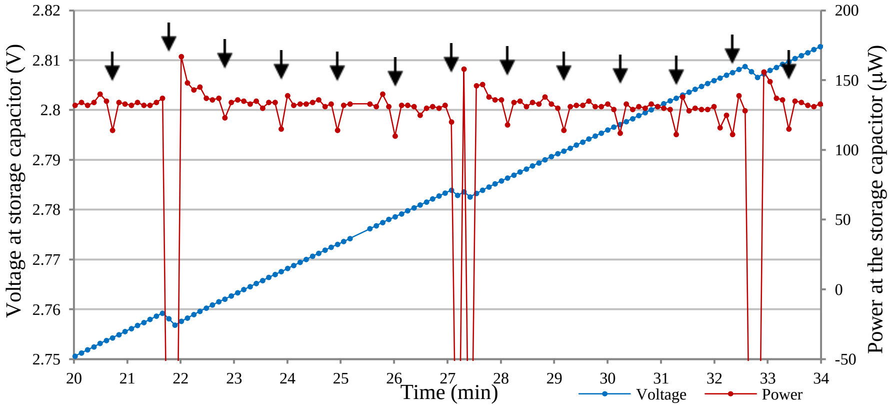

Figure 5-36. Voltage and power at storage capacitor when wireless node transmit one every minute. Arrows mark a transmission event.

During the section B of the test, the base frequency changes and the wireless node continue transmitting according the voltage available. The results show that the power generated is enough to perform the tuning of the harvester and transmit data at regular intervals.

In the last section of the test, section C, the base frequency was kept constant. This allowed the storage capacitor to save energy and reach the 2.9 V threshold. At this voltage, the data transmission occurs once every second. At this rate of transmission, the tunable energy harvester generates more energy than it consumes, as can be seen in the small rise in the voltage in figure 5-37. The average net power at the capacitor was 15 µW.

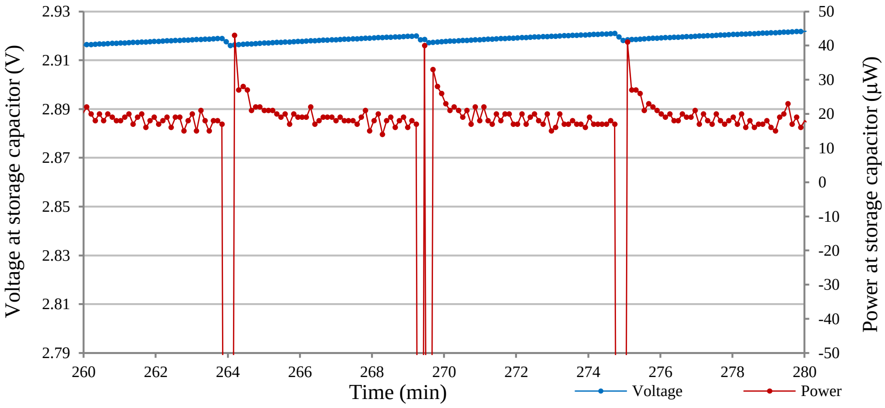

Figure 5-37. Voltage and power at storage capacitor as data is transmitted once every second

5.6 Conclusion

This chapter has presented the optimization of the power extraction and conversion from the harvester. The optimal load for each harvester differs due to their different mechanical and electrical characteristics. In some cases, for example Harvester A, a 2 stage VM charges the storage capacitor at a faster rate than the original 5 stage VM used for the initial tests. This change reduced the charging time from 0 to 2.6 V from 43.19 hrs to 17.9 hrs; a 58% reduction. The optimized energy extraction and conversion using harvester B reduced the recovery time by up to 76% compared to the initial tests using harvester A (with the original 5 stage voltage multiplier); this equates to a recovery time reduction from 2.1 hours to 0.5 hrs when the harvester resonant frequency has been adjusted by 14 Hz, or 2 mm.

The disadvantage of a passive power extraction and conversion is the inability to adapt the impedance seen by the harvester to extract the maximum power. Active conversion was evaluated as a solution. However, the power overhead required for such systems surpass the additional power generated by the harvester at the acceleration set for these tests of 0.588 $ms^{-2}{}_{(rms)}$.

The last section of this chapter presented the autonomous operation of the optimized tunable energy harvester with a wireless sensor node connected. The harvester generated enough energy to adjust its resonant frequency and to power the wireless node while transmission occurred at various duty cycles. This exemplifies the use of the energy harvester to power a wireless sensor node in an environment where the base frequency changes over time.

In conclusion, the power transduced to electrical energy can be increased if the harvester load is optimized. However, the energy generated by the harvester presented here is not enough to power active impedance matching circuitry; hence, the only solution is to improve the passive extraction and conversion circuit.

The next chapter explores the operation of the tunable energy harvester under high and real base acceleration. The implications on the control system and operation of the tunable harvester are presented.

Chapter 6

Harvester performance at high and real environmental acceleration

6.1 Introduction

The first section of this chapter presents the use of the tuning mechanism as a protection mechanism that prevents the physical contact between the harvester and the base when the base acceleration increases beyond a maximum threshold, effectively reducing the risk of physical damage.

The second section analyses the operation of the tunable energy harvester when the base excitation replicates the excitation from the engine of a ferry. The harvester performance and the consequent modifications required on the system to operate the tunable energy harvester in such a real application scenario are presented.

6.2 Over range protection

This section presents two over range protection algorithms that prevent the excessive displacement of the harvester by adjusting its spring stiffness, by changing its resonant frequency away from the base frequency. This, effectively maintain the harvester displacement within a finite range.

The importance of preventing excessive displacement of the harvester arises from the mechanical characteristics of the device, as well as the geometry of the package containing it. An excessive displacement could produce a constant physical impact between the harvester and the base, or excessive stress in the spring element of the harvester that can lead to fatigue failure.

For a high-Q harvester, such as the one presented here, it has a maximum displacement when its resonant frequency is close to the base frequency. The amplitude of the harvester displacement drops significantly as the resonant frequency moves away from the base frequency, as shown in figure 6-1 for a low damping single degree of freedom system. The protection mechanism adjusts the harvester resonant frequency away from the base frequency to reduce its displacement.

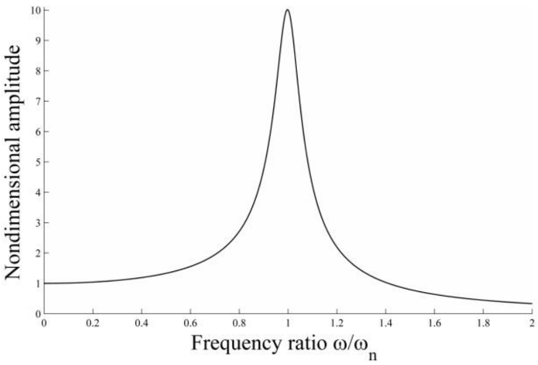

Figure 6-1. Amplitude of forced vibration for a damping factor of 0.05

The physical structure of the tunable energy harvester allows a maximum vertical displacement at the free end of the cantilever of approximately 2.1 mm, as shown in figure 6-2. This distance is measured from lower edge of the mild steel keeper to the base. Finite element simulations using static analysis in ANSYS predicts that a displacement of 18 mm is necessary to produce a stress in the cantilever equivalent to the yield strength of the material, and a displacement of 4.5 mm produces a stress equivalent to the maximum fatigue stress. Hence, in this case the maximum displacement for the harvester is limited by its physical geometry and not by the material employed in its construction.

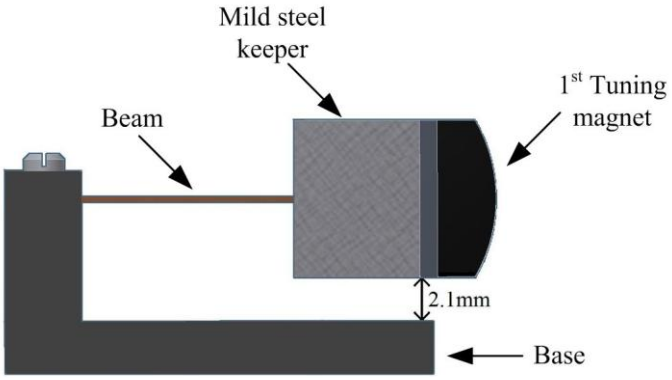

Figure 6-2. Harvester lateral view showing the maximum possible physical displacement

The power generation is proportional to the displacement of the mass; hence, the maximum displacement is desirable. However, the physical contact with the base must be prevented due to potential risk of damage to the harvester.

The displacement of the cantilever can be expressed as function of the base excitation frequency ω and acceleration a, the cantilever spring stiffness k and mass m, and finally the damping coefficient c, as described in equation (6-1) [107]. Hence, the displacement of the cantilever can be adjusted by modifying the spring stiffness in the same manner as when the harvester resonant frequency is tuned to the base frequency. In this instance, the tuning mechanism changes the harvester spring stiffness to detune the harvester, reducing its displacement amplitude.

$$Z = \frac{m\,a}{\sqrt{(k-\omega^2 m)^2 + c^2\omega^2}} \tag{6-1}$$

6.2.1 Maximum acceleration

To identify the maximum acceleration that produces a displacement of 2 mm, Harvester A was connected to a 5 stage VM and a 0.55 F storage capacitor. A variable resistive load was connected in parallel to the storage capacitor to draw energy from it to maintain a constant voltage. The base acceleration was gradually increased while the displacement at the tip end of the cantilever was measured using a laser vibrometer.

The voltage at the storage capacitor was varied from 2.6 to 3.2 V while maintaining the same base acceleration. The acceleration was gradually increased until the maximum displacement of 2 mm was measured on the cantilever. The test was performed at 64, 70 and 78 Hz. In every case, the harvester's resonant frequency was adjusted at the beginning of the test using the tuning mechanism to match the base frequency.

The experimental results showed that the displacement increases as the voltage at the storage capacitor rises for a fixed acceleration, as shown in figure 6-3 where the linear trend line is presented. The maximum acceleration permissible was selected based on the maximum displacement when the voltage reaches 3.2 V. The maximum acceleration for each frequency is presented in table 6-1. The increase in displacement is a consequence of the reduction in the electric damping as the voltage as the storage capacitor increases.

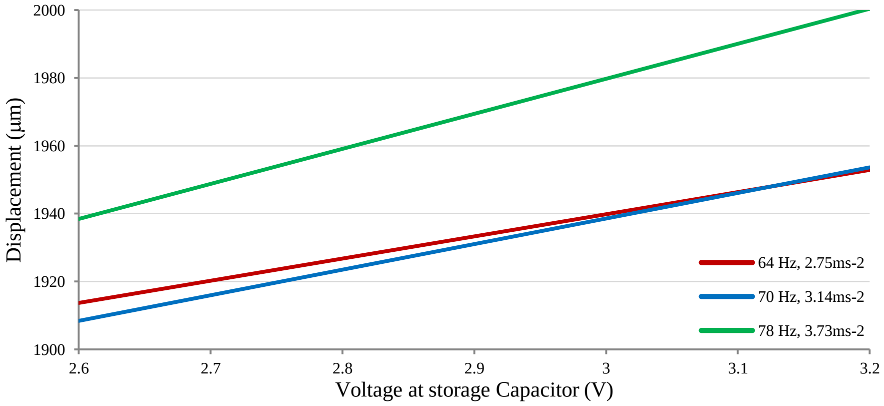

Figure 6-3. Displacement variation trend lines as voltage at storage capacitor increases

The maximum acceleration increases with the frequency because the displacement at the base is the inverse of the frequency, i.e. the base amplitude reduces as shown in equation (4-3).

Table 6-1. Maximum tolerable acceleration

Frequency (Hz)	Acceleration ($ms^{-2}{}_{(rms)}$)
64	2.75
70	3.14
78	3.73

A mathematical expression describing the maximum base acceleration tolerable as a function of its period was developed based on the experimental results from table 6-1. The equation (6-2) has been constrained to a first order polynomial to reduce the processing time in the microcontroller. The period is measured using the input voltage signal from the harvester.

$$Max.Accel.[bit\ count] = 420 - \frac{Period\ [\mu sec]}{64} \tag{6-2}$$

The maximum tolerable acceleration is calculated by the control system and compared against the peak acceleration measured from the accelerometer. If the acceleration is higher than the maximum calculated, the resonant frequency of the harvester is adjusted to reduce its displacement.

6.2.2 Displacement control

Two over range protection algorithms were evaluated. The first algorithm uses the period difference between the harvester voltage and the base acceleration to adjust the level of mistuning. The second algorithm modifies the position of the movable tuning magnet away from its optimal position in proportion to the difference between the maximum acceleration tolerable and the current base acceleration.

6.2.2.1 Period difference

If the maximum acceleration has been reached, this mechanism increases the period difference between the harvester and the base excitation by moving the tuning magnet. This action detunes the harvester, reducing its displacement.

The practical implementation of this algorithm is by adding an error of 30 µsec to the period difference measurement for every 0.135 ms^{-2} of over acceleration. The maximum base acceleration can be increased up to 32% more than when no protection control is utilized, e.g. from 2.75 to 3.63 $ms^{-2}_{(rms)}$ at 64 Hz.

The operation of the period difference algorithm is presented in figure 6-4. The increase in acceleration shifts the resonant frequency of the harvester due to its non-linearity. In consequence, the tuning control adjusts the position of the magnets to reduce the period difference. This adjustment of the actuator is shown as arrow marks in figure 6-4. As the acceleration increases beyond the maximum allowed for this frequency, the error added to the period difference measurement inhibits any further adjustment of the tuning magnets, effectively limiting the displacement of the harvester.

This algorithm is constrained by the rapid change in period difference from a negative to a positive maximum, or vice versa, as the harvester resonant frequency moves away from the base frequency. Hence, it can operate only in the proximity of the resonant frequency.

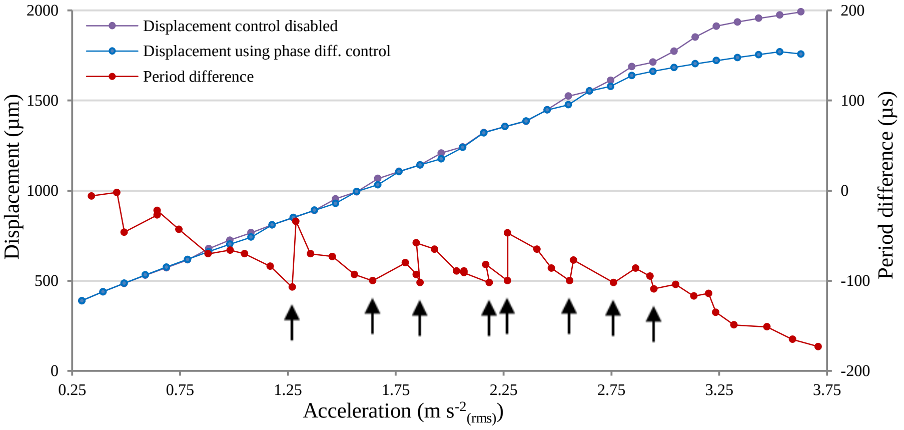

Figure 6-4. Harvester displacement as base acceleration increases for the case where no over range protection is used, and when the period difference over range protection is enabled. Arrow marks correspond to the adjustment of the tuning magnets.

6.2.2.2 Magnet position

A second protection algorithm was developed to increase the range of acceleration at which the tunable energy harvester can operate. This scheme was based upon the known position of the movable magnet and its distance from the optimal position, at which the harvester is at resonance. If the base acceleration exceeds the maximum tolerable, the tuning magnet is moved away from its optimal position. The amount of adjustment required is proportional to the level of over acceleration.

The over range protection algorithm was implemented using a single and double slope rate of adjustment. In the first case, the actuator is adjusted by 20 μm, or one actuator step, every time the difference between the maximum permissible acceleration and the base acceleration increases by 0.265 $ms^{-2}{}_{(rms)}$; starting from the maximum tolerable acceleration of 2.97 $ms^{-2}{}_{(rms)}$. In the second case, the magnet is adjusted at a different rate depending on the acceleration level. After the maximum permissible base acceleration has been reached, the magnet is adjusted 20 μm every 0.265 $ms^{-2}{}_{(rms)}$ until the acceleration level reaches 5.12 $ms^{-2}{}_{(rms)}$. Then the magnet position is adjusted 20 μm every 0.765 $ms^{-2}{}_{(rms)}$. These tests were performed maintaining a constant base frequency of 64 Hz. Both cases are presented in figure 6-5 where the over range protection using the magnet position has been implemented.

It can be observed that the second solution has a better performance. It allows the harvester to maintain a larger displacement, hence a larger energy generation, than using the single slope option. The maximum acceleration that the protection system can control is limited by the acceleration range of the accelerometer used in the system, which is 9.81 ms^{-2}. This limit can be observed in figure 6-5 where around 9.81 ms^{-2} the displacement increases in both cases. Beyond 9.81 ms^{-2} the system is unable to differentiate any further increase in acceleration.

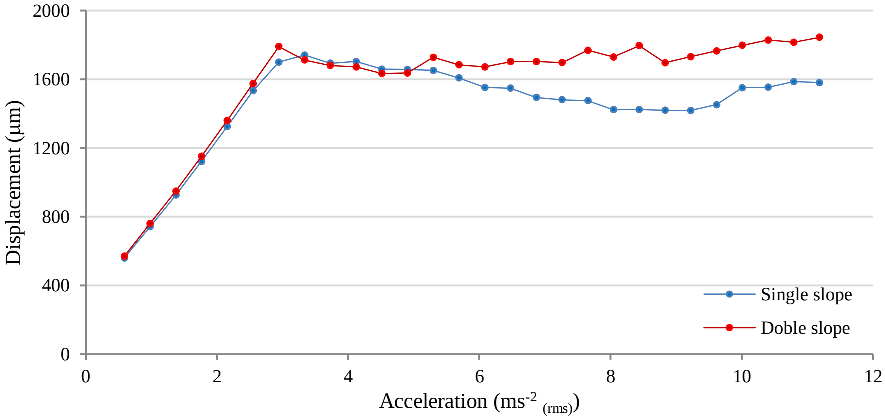

Figure 6-5. Over range protection using magnet position for single and double slop of adjustment

Figure 6-6 shows the effect of the over range protection based on the magnet position algorithm at different base frequencies and acceleration. The over range protection does not intervene in the adjustment of the tuning mechanism until the acceleration reaches the maximum tolerable for each frequency. Below the maximum acceleration, the displacement of the harvester increases as the acceleration increases. Once the maximum acceleration is reached, the over range protection starts adjusting the position of the magnet, effectively reducing the harvester displacement.

The maximum over range protection range occurs when the harvester resonant frequency and base frequency are set at 64 Hz. In that case, the maximum acceleration tolerable increases from 2.75 to 9.81 $ms^{-2}{}_{(rms)}$, or 257% compared to the non-protected case.

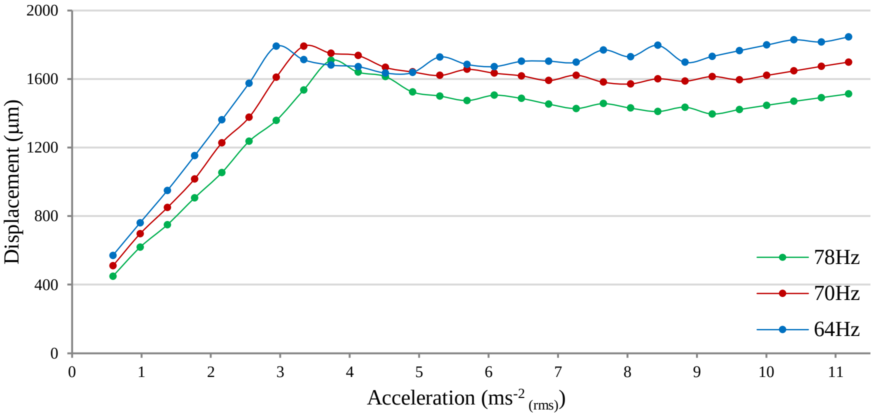

Figure 6-6. Over range protection using magnet position for three different base accelerations

6.2.3 Comparison of over range protection algorithms

Table 6-2 presents a comparison between the two algorithms proposed here. The protection algorithm using the magnets position has a larger operating range than using the period difference, up to 256% more than when no protection is used. The main limiting factor is the acceleration range of the accelerometer. However, this can be replaced if needed.

The period difference algorithm is less appropriate due to the high-Q performance of the harvester that results in a rapid change of period as the harvester resonant frequency approaches the base frequency.

Table 6-2. Performance comparison of maximum acceleration reached for each protection algorithm

Frequency	No protection	Period difference		Magnet position	
(Hz)	($ms^{-2}{}_{(rms)}$)	($ms^{-2}{}_{(rms)}$)	Increase	($ms^{-2}{}_{(rms)}$)	Increase
64	2.75	3.63	32%	9.81	256%
70	3.14	3.92	24%	9.81	212%
78	3.73	4.32	15%	9.81	163%

6.3 Operation in real environments

Until now the operation of the tunable energy harvester was only evaluated when the base excitation had a single frequency component. This section explores the operation of the tunable harvester when the base excitation resembles the frequency spectrum taken from a real environment.

The vibration data from a ferry engine (8-cylinder 4-stroke diesel engine) was collected. The pick-up accelerometer was fixed to the frame of the engine, as shown in figure 6-7a. The acceleration was sampled at 1000 samples per seconds. Only 16 seconds were used to replicate the excitation on the shaker rig because of memory restrictions in the signal generator driving the transducer shaker. However, this period is representative of the ferry moving at a constant speed. The ferry engine has an acceleration peak at 47.24 Hz at 4.53 ms^{-2}, as show in the frequency spectrum presented in figure 6-7b.

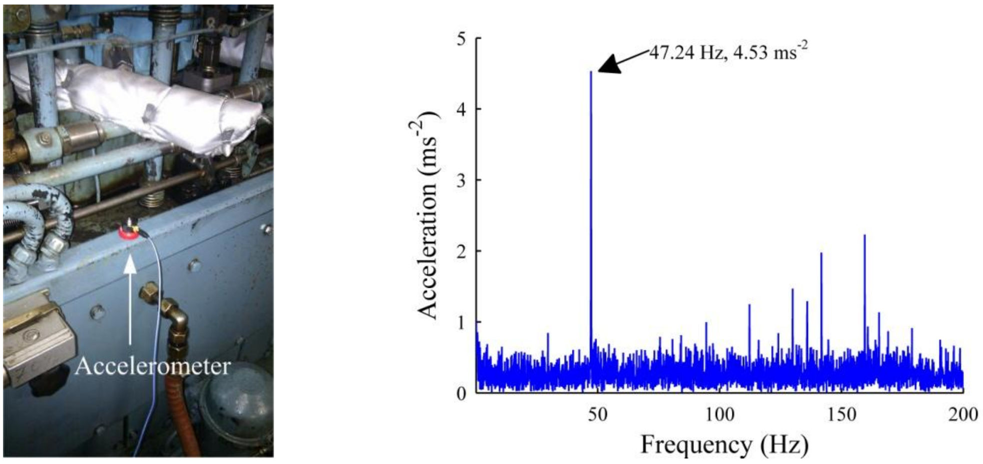

a. Accelerometer attachment b. Acceleration spectrum

Figure 6-7. Ferry engine acceleration data

6.3.1 Harvester response to ferry acceleration

The ferry frequency spectrum was shifted by 18.85 Hz using Matlab thus the peak acceleration frequency falls within the tuning range of the tunable energy harvester. The acceleration peak, originally at 47.27 Hz, was shifted to 66.12 Hz. The frequency spectrum was then loaded into the shaker test rig. The peak acceleration was reduced to 0.588 $ms^{-2}{}_{(rms)}$ to coincide with the level used in previous analysis in this work.

Initially, the behaviour of the harvester was analysed when its resonant frequency does not coincide with the frequency peak from the ferry data. The harvester operates as a band pass filter, it amplifies the displacement of those frequency components at the same frequency as its resonant frequency. Therefore, the frequency of the harvester output voltage is the same as its resonance frequency and not the base frequency, as was the case for the pure sinusoidal base excitation.

6.3.2 Implications for the tuning control

The time-varying base excitation resulted in number of alterations to the sensing and control of the tunable harvester. The frequency meter routine had to be modified to compensate for the increase in noise in the base excitation. In addition, the control was altered to compensate for the increasing non-linear behaviour observed in the harvester, along with other changes described next.

6.3.2.1 Frequency meter

In previous chapters, the base excitation was a harmonic vibration with a single tone. Under this condition, the harvester output voltage had the same frequency as the base. When the single tone excitation is replaced by a multiple frequency vibration, like the ferry spectrum, the harvester output voltage has the same frequency as its resonant frequency. In this case, the harvester amplifies the amplitude of the frequency component that coincides with its resonance frequency. This effect resulted in the inability to use the harvester to measure the dominant frequency at the base. Instead, the harvester output voltage was utilised to measure the resonant frequency of the harvester. An external accelerometer was necessary to measure the base frequency, instead.

Measuring the dominant frequency became more complex due to the broad range of frequencies measured at the ferry engine. The base frequency, more precisely its period, was measured by calculating the point of maximum inflection of the acceleration signal, and then measuring the time taken to complete a cycle. Eight consecutives cycles were measured and the average calculated. If the difference between the minimum and maximum period measured was higher than 200 μs, the measurement was considered erroneous and the measurement re-started. If the resulting frequency was within the predetermined range of 60 to 78 Hz, then the result was considered as valid. If the frequency was beyond the range, the frequency measurement was re-started. Finally, two consecutive measurements were taken to calculate the dominant frequency. The measurement of the harvester resonant frequency was performed in the same way, in this case using the signal from the harvester output voltage.

The dominant base frequency and harvester resonant frequency were measured using the previous technique. The harvester resonant frequency was adjusted at six different frequencies: 60.12, 61.91, 64.6, 66.12, 70.43 and 73.1 Hz. 32 consecutive measurements were performed for each frequency. The results show a maximum error of 2 Hz when measuring the resonant frequency, and 3.2 Hz when measuring the dominant base frequency, as shown in figure 6-8a and figure 6-8b.

The principal source of error rises from the reduced number of cycles taken to calculate the frequency. More cycles and computational resources are needed to increase the accuracy of the measurement. However, this has a penalty on the power consumption. The measurement of the period difference has an even greater error than the frequency meter. It would require more samples to produce an accurate measurement. Therefore, it was discarded for these reasons.

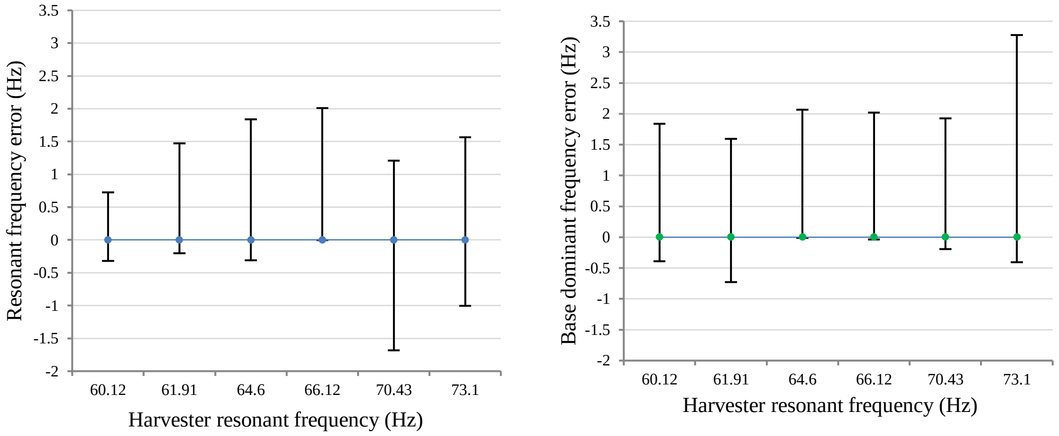

a. Error measuring harvester resonant frequency

b. Error measuring dominant base frequency as the harvester resonant frequency changes

Figure 6-8. Error measuring harvester resonant frequency and dominant base frequency

6.3.2.2 Harvester tuning

The non-linear behaviour of the harvester is more evident when the base excitation is the ferry spectrum. The maximum power can only be reached when the resonant frequency of the harvester is adjusted from a higher to lower frequency. Considering this effect and the inability to fine-tune using the period difference, the tuning control was modified to track the position of the actuator at which harvester resonant frequency and dominant base frequency are equal. In first instance, the optimal position of the actuator according to equation (5-3) is calculated. If the difference between optimal and current position is higher than 200 μm, or 10 actuator steps, the actuator moves to such a position. If the difference is lower, the control starts a tracking routine as described below. The tracking starts by reducing the distance between tuning magnets by 20 μm (one step) at the time. This action has the effect of increasing the resonant frequency of the harvester. The reduction continues for 200 μm (10 steps). Then the distance between tuning magnets is increased by 20 μm, for up to 200 μm, reducing the harvester resonant frequency.

The power at the storage capacitor is measured each time the actuator is adjusted by 20 μm. This is realized by measuring the voltage variation at the storage capacitor for a period of 160 s and calculating the average power at the storage capacitor using equation (3-3). If the power is higher than is 90 μW, then that position is considered suitable for the tunable energy harvester and the tracking routing stops. If the 90 μW threshold is measured while reducing the distance between tuning magnets, the control increases the distance by 20 μm in an attempt to validate that the high energy level on the harvester had been reached.

6.3.3 Experimental results

Experimental tests were performed using Harvester B loaded with a storage capacitor of 0.55 F through a diode-bridge. The microcontroller, actuator and electronic components were powered from an external power supply to allow the communication between the microcontroller and a computer for debugging purposes. The dominant base frequency remained at 66.12 Hz with a peak acceleration of 0.588 $\mathrm{ms}^{-2}{}_{(\mathrm{rms})}$.

Initial tests evaluated the tuning of the harvester when its resonance frequency is below the dominant base frequency. The harvester resonant frequency was adjusted at 65.6 Hz at the beginning of the test. The magnet tuning distance reduces one step at the time and the power at the storage capacitor measured, as shown in figure 6-9. After 10 consecutive steps are given reducing the tuning distance, the power at the storage capacitor did not reach the 90 μW threshold. Therefore, the actuator is adjusted in the opposite direction. After five steps, the power reaches the threshold value and the tuning is finished. In total, the actuator adjusted the position of the actuator initially by 10 steps in one direction, later the actuator was adjusted 5 steps in the opposite direction and finally finding the position at which the power reached the threshold. It can be observed that the final position of the actuator corresponds to a position that was previously occupied by the actuator, but on that occasion, the power was small. The high energy level only occurred when the actuator was adjusted in the opposite direction. This shows the practical consequence of the soft non-linearity of the harvester.

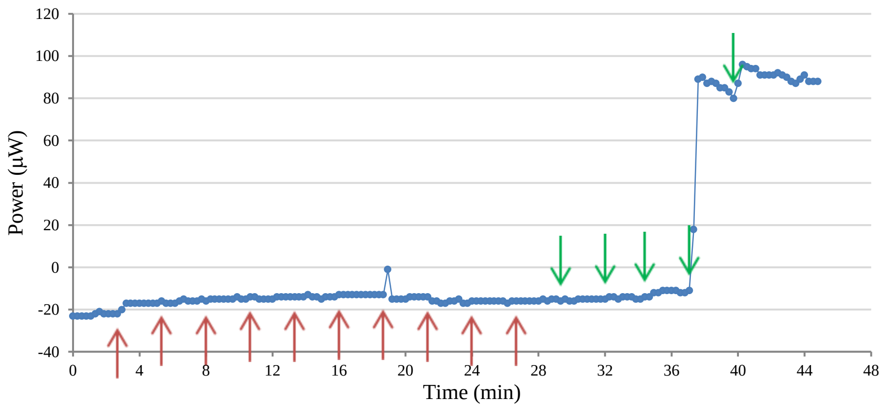

Figure 6-9. Harvester tuned from a lower to a higher frequency.
Magnets tuning distance reduces one step (up arrow mark), increases one step(down arrow mark).

A second test presents the performance of the control system when initial resonant frequency of the harvester is higher than the dominant base frequency, 72.68 and 66.12 Hz, respectively. The control system calculates the optimal position of the tuning mechanism based on the base frequency. At around the 2nd minute of the test, the actuator moves 44 steps (increasing the tuning distance by 0.88 mm) to the optimal position calculated. This brings the power at the storage capacitor to a level of 80 µW, still not reaching the 90 µW threshold. Next, the control system starts tracking the optimal position by moving the actuator one step at the time, beginning by reducing the tuning distance. After just one adjustment, the threshold is reached. The tuning distance is increased by one actuator step resulting in the reduction of the power, confirming the harvester is at its high energy level, as shown in figure 6-10.

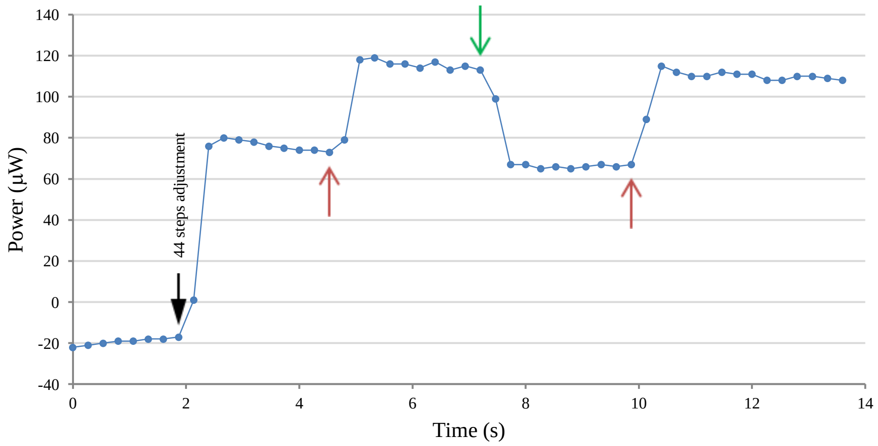

Figure 6-10. Harvester is tuned from a higher to a lower frequency.
Magnets tuning distance (up arrow) reduces one step, (down arrow) increases one step.

Similar tests with the initial harvester resonant frequency at a higher value than the dominant base frequency show a similar behaviour. It appears that the soft non-linear behaviour is not present. However, this was not observed when the initial resonant frequency was lower than the base frequency. In this case, the resonant frequency has to surpass the base frequency, and then reduce it to reach the high energy level.

6.3.4 Discussion

A number of challenges were identified when the tunable energy harvester is exposed to a base excitation with multiple frequency components, like the ferry spectrum. First, it requires more computational resources to identify the dominant base frequency. These include increasing the number of samples taken from the accelerometer to increase the accuracy of the measurement. Secondly, the non-linear behaviour of the harvester resulted in more energy used to adjust the harvester resonant frequency from a lower to a higher frequency. Finally, the method to identify when the harvester is generating the maximum power is slow, losing time adjusting the harvester. The method proposed here requires minutes to measure the power saved into the storage capacitor to determine if the harvester resonant frequency matches the dominant base frequency, instead of seconds as when the base frequency was a single tone signal.

6.4 Conclusion

This chapter has presented the operation of the tunable energy harvester when an increase in base acceleration results in the physical contact between the harvester and its frame. The over range protection mechanism adjusted the resonant frequency of the harvester when an over acceleration is measured. This results in a reduced displacement of the harvester, effectively protecting it from physical contact and potential damage. The protection mechanism proposed here adjusts the position of the actuator proportionally to the level of over acceleration. This mechanism increased the maximum acceleration that the tunable harvester can withstand from 2.75 to 9.84 $ms^{-2}_{(rms)}$, at 64 Hz, and increase of 256%. It was only limited by the acceleration range of the accelerometer selected.

This chapter also presented the experimental evaluation of the tunable energy harvester when the base excitation resembles the frequency spectrum from a real application. In this case, the spectrum replicates the vibration of a diesel engine. The first observation is that the harvester acts as a band pass filter, i.e. the output voltage signal has the same frequency as the harvester's resonant frequency. Therefore, the harvester cannot be used to measure the dominant base frequency, but can instead measure the resonant frequency of the harvester. The dominant base frequency is measured using an external accelerometer. The maximum error measuring, either the harvester's resonant frequency or the dominant base frequency, were 2 and 3 Hz respectively. The main source of error was the limited number of samples used to calculate either frequency. A more accurate measurement would require not only more samples but also more computational work, adding power overhead.

The harvester's non-linear behaviour increases when it is exposed to the real frequency spectrum. The harvester only reaches its higher energy status when its resonant frequency is adjusted from a higher to a lower value.

In conclusion, the exposure of the harvester to real environments requires modification of the control strategy to compensate for its non-linear behaviour and a more accurate method to sense the base excitation, which results in an additional power overhead compared to the case where the harvester is exposed to a pure tone sinusoidal excitation.

Chapter 7

Energy harvester tuned upon a magnetic flux guide

7.1 Introduction

This chapter presents an alternative method to adjust the resonant frequency of a kinetic energy harvester. This method is based on the variation of the magnetic flux between the tuning magnets by inserting a material with high permeability as a flux guide between them.

This idea was originally proposed by Imperial College London as part of the Holistic Approach to Energy Harvesting Electronics project [103]. It is evaluated as part of this thesis to investigate if frequency tuning can be achieved at a lower energy budget.

7.2 Magnetic tuning using a flux guide

This thesis has presented the tuning of the energy harvester using the variation of attractive force between two tuning magnets. One tuning magnet was placed at the end of the cantilever and a second tuning magnet was attached to an actuator, thereby enabling the distance between the magnets to be adjusted. The harvester resonant frequency varies as a consequence of the varying strain forces exerted in the cantilever by the magnets.

A second method to tune the harvester has been proposed that relies on the variation of the magnetic flux between the tuning magnets. The magnetic flux is altered by inserting a movable flux guide between the two tuning magnets. This modifies the magnetic forces on the cantilever and consequently its resonant frequency. The distance between tuning magnets is kept constant, i.e. the second tuning magnet does not move.

The same cantilevered shape energy harvester as described in section 3.2 was used to evaluate the magnetic flux guide tuning mechanism. Three different harvesters were used during practical tests, their characteristics are presented in table 3-2 and table 3-3.

7.2.1 Operation

The principle of operation of the magnetic flux guide tuning approach is to vary the magnetic tuning force exerted on the harvester by varying the position of a moveable flux guide placed between the two tuning magnets. The tuning magnets are stationary and the magnetic flux path between the two magnets will depend upon the position of the flux guide. The tuning mechanism from Chapter 3 was modified so that both magnets remain at a constant separation and a piece of ferrite with dimensions 30x15x1.5 mm, slides between the tuning magnets as shown in figure 7-1. The fixed tuning magnet is 10x5x2 mm and has a magnetic flux density of 1.22 T. The ferrite was mounted on a single axis translation stage attached to a manual micrometer to allow it to slide in and out between the two tuning magnets.

The resonant frequency and power generated where measured at fixed intervals as the ferrite was removed. The harvester was connected to an optimal resistive load and the power was calculated from the developed voltage.

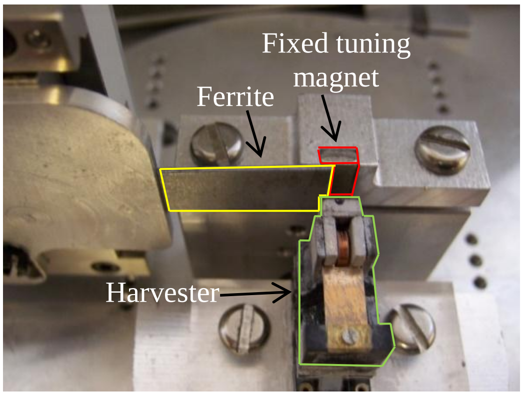

Figure 7-1. First design of magnetic tuning using flux guide

The ferrite's initial position corresponds to a 0 mm tuning gap. In this position the fixed tuning magnet is fully covered by the ferrite as shown in figure 7-2a. The tuning gap can be adjusted from 0 to 9 mm by increasing the gap, as shown in figure 7-2b. In figure 7-2, the direction of movement of the harvester when excited is normal to the X-Y plane, while the ferrite orientation and gap adjustment are in the Y direction.

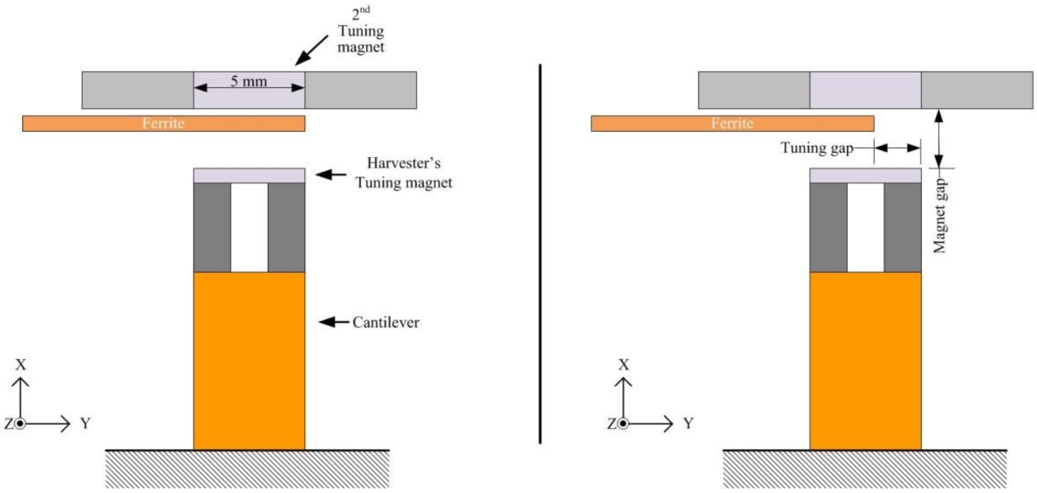

a. Initial position, gap = 0 mm. b. Gap increase.

Figure 7-2. Diagram of magnetic tuning flux guide, top view.

7.2.2 Resonant frequency and power generation

The magnet's gap (distance between tuning magnets) was set at three different values: 4, 3 and 2 mm. The resonant frequency for the three cases, without the ferrite present, was found to be 63.6, 69.6 and 78.1 Hz, respectively and the acceleration was fixed at 0.588 $ms^{-2}_{(rms)}$.

The ferrite was inserted and the tuning gap adjusted from 0 to 9 mm. The resonant frequency changes as a consequence. The power generated by the harvester as the gap increased is shown in figure 7-3. There is a small change in resonant frequency of 1.6 Hz when the tuning gap varies between 0 to 4 mm. However, with the tuning gap varying from 4 to 9 mm the resonant frequency changes by 13 Hz, from 62.1 to 75.1 Hz respectively, when the gap between tuning magnets is 2 mm. The power generated also increases with increasing tuning gap, finally reaching a value similar to the case where the ferrite has being completely removed, as shown in figure 7-3b.

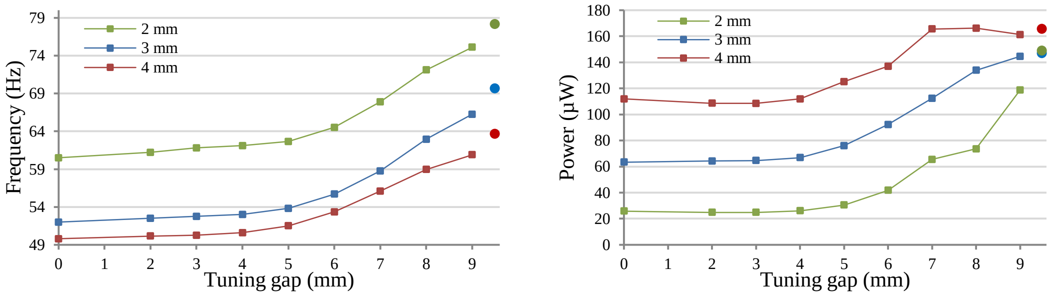

a. Resonant frequency b. Power generation

Figure 7-3. Resonant frequency and power generation as gap varies, at three different tuning distances. (Circular marks correspond to the case were the ferrite has been completely removed)

The magnet gap is a larger influence on power output. As the gap reduces, the power generated falls from 165 µW, for a 4 mm magnet gap, to 65 µW for a 2 mm magnet gap. This is due to an increase in damping as described by Zhu et.al. [3]. This is shown clearly in figure 7-4 where the average Q-factor falls from 304 at 4 mm to 185 at 2 mm. Table 7-1 summarizes the results for various magnet gaps. Even though, the variation of the tuning distance is not the base for this tuning mechanism, its influence must be considered due to its influence on the power generated and the resonant frequency range.

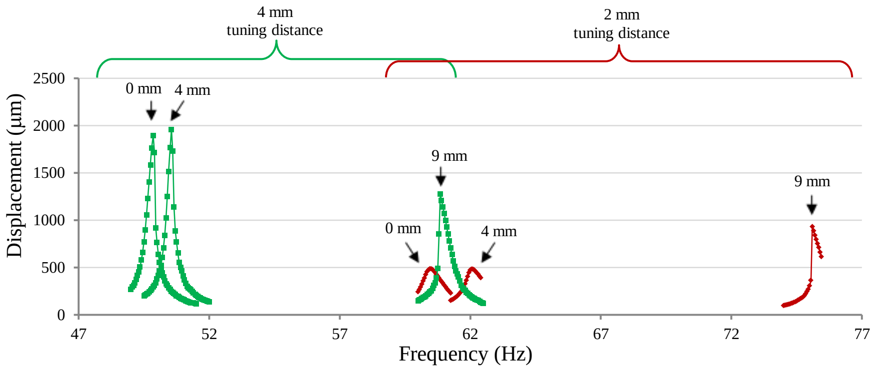

Figure 7-4. Cantilever tip-end displacement for different tuning distances and tuning gaps

Table 7-1. Resonant frequency and power generation

Distance between tuning magnets (mm)	Resonant frequency without ferrite (Hz)	Resonant frequency range using ferrite (Hz)	Maximum power (μW)
4	63.60	49.80 – 60.90	166.20
3	69.60	52.00 – 66.25	144.55
2	78.10	60.50 – 75.10	118.78

The most significant result from this arrangement, however, is the uneven distribution of the flux across the gap between the tuning magnets. This produces an asymmetrical force on the cantilever causing it to displace laterally during each vibration cycle. This had the effect of bringing the harvester magnets into contact with the coil and the repeated physical contact caused the coil to break.

7.3 Design 2: Improved magnetic flux design

A second design was investigated in order to provide a more even distribution of the magnetic flux to produce a symmetrical tuning force and prevent damage to the coil. This design incorporates a mild steel block situated 1 mm from the fixed tuning magnet that allows the insertion of a mild steel flux guide as shown in figure 7-5. The sliding flux guide was mounted on a single axis translation stage and attached to a manual micrometer that enabled its position to be adjusted to increase or decrease the gap. As part of this experiment, the influence of the fixed tuning magnet’s thickness was also investigated.

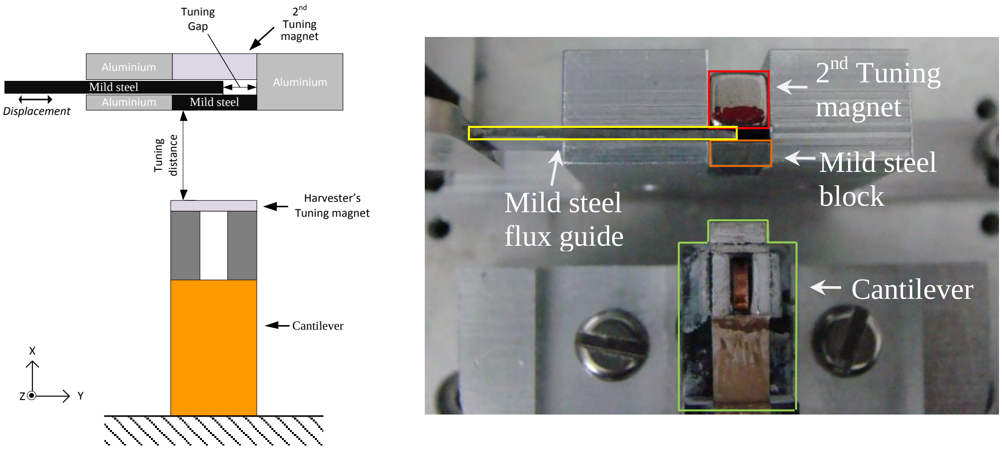

a. Schematic b. Picture

Figure 7-5. Magnetic flux interrupter second design, top view.

7.3.1 Resonant frequency and power generation

Results were obtained for distances between the cantilever tuning magnet and the mild steel block (hereafter referred to as the tuning distance) of 2.5, 4.5 and 6.5 mm. Three fixed tuning magnets of 1, 3 and 5 mm thickness were tested on each position. The harvester B was connected to an optimum resistive load of 33 kΩ. Figure 7-6 presents the variation in resonant frequency as the tuning gap increases. There is a non-linear response of the resonant frequency with tuning gap. For the 5 mm thickness magnet at a tuning distance of 6.5 mm, the frequency initially falls from 53.6 to 52.3 Hz as the tuning gap increases from 0 to 4 mm, and then increasing from 52.3 to 55 Hz as the tuning gap widens beyond 4 mm.

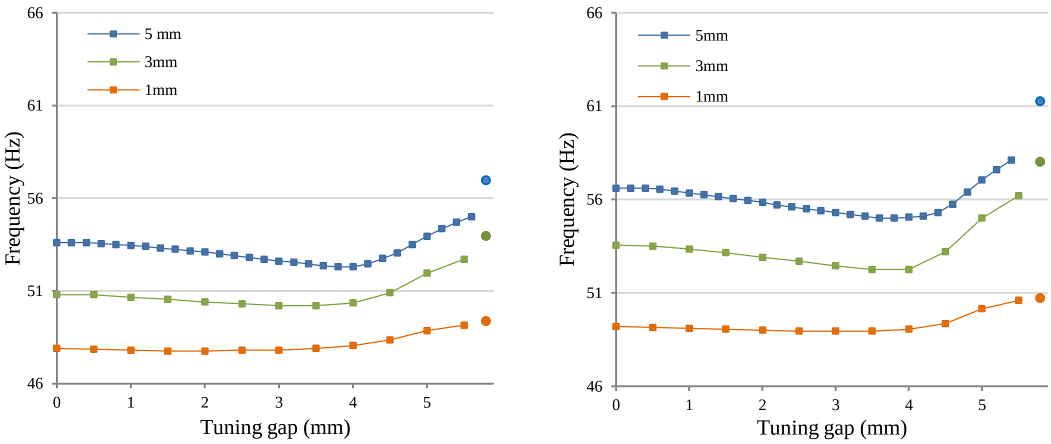

a. Tuning distance: 6.5 mm b. Tuning distance: 4.5 mm

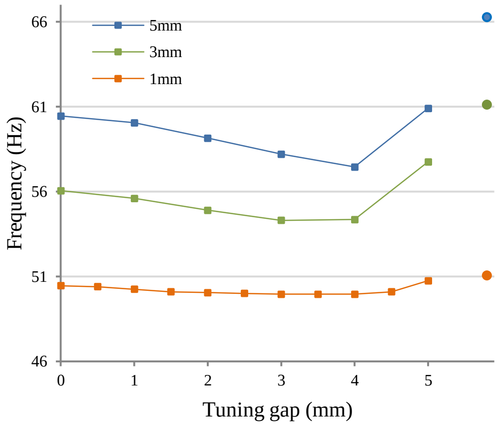

c. Tuning distance: 2.5 cm

Figure 7-6. Resonant frequency variation as flux guide is removed.
Blue line corresponds to a fixed tuning magnet thickness of 5mm, green line for 3 mm thickness and orange line to 1 mm thickness. (Circular marks correspond to the case where the flux guide has been completely removed.)

The thickness of the tuning magnet affects the initial resonant frequency and the tuning range but has negligible effect on the power output. The maximum tuning range occurs for tuning gaps from around 4 to 5.5 mm, which produces a maximum frequency change of 3.45 Hz (5 mm thick tuning magnet, 2.5 mm tuning distance). This would be the optimum tuning gap range since it requires the flux guide to move the shortest distance. However, the tuning distance also increases the level of damping, which in consequence reduces the power generated, as shown in figure 7-7 and figure 7-8. It is important to notice that the power generated at a fixed tuning distance remains almost constant regardless of the tuning gap. Figure 7-8 shows the frequency response of the generator for tuning gaps of 6.5 and 2.5 mm. The increased damping at a tuning distance of 2.5 mm reduces the power from 156 to 31 μW for a tuning gap of 0 mm, while the frequency range increases from 2.95 to 6.5 Hz. The average Q-factor reduces from 191 at 6.5 cm to 90 at 2.5 mm.

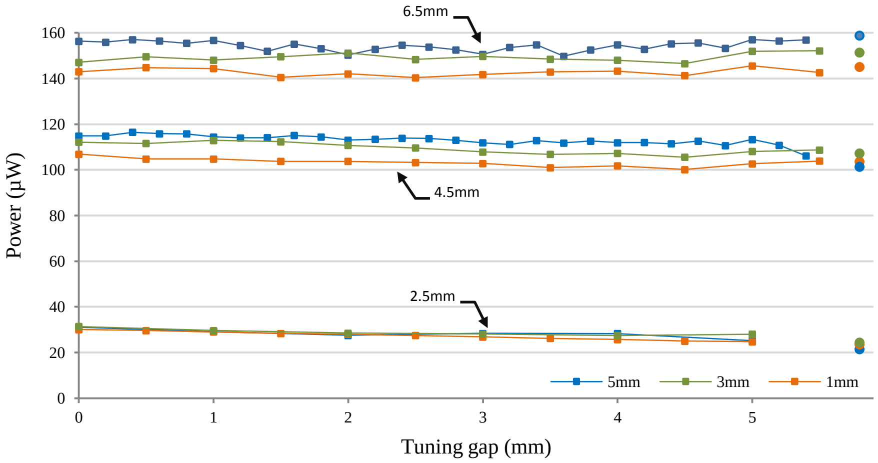

Figure 7-7. Power generation as flux guide is removed.
Blue line corresponds to a 5mm thickness magnet, green line for 3 mm thickness and orange line to 1 mm thickness. (Circular marks correspond to the case when the flux guide has been removed completely.)

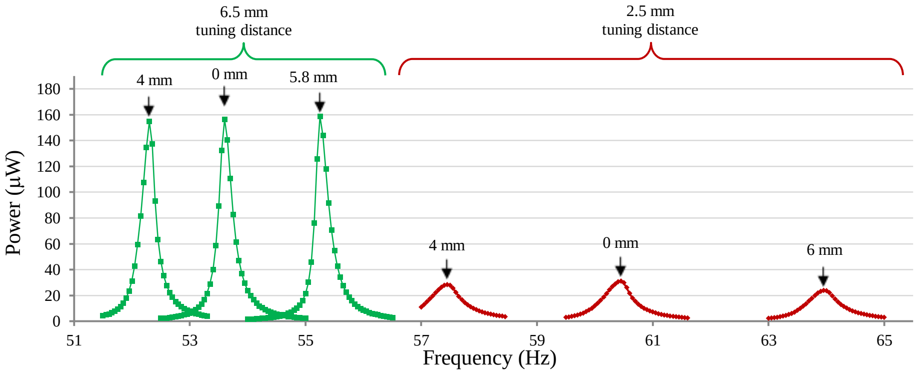

Figure 7-8. Frequency response for different tuning distances and tuning gaps. Magnet thickness of 5 mm.

Table 7-2 presents a summary of the resonant frequency and power generation using the second flux guide arrangement. The achievable frequency range is less than that obtained with the first arrangement but the tuning gap range is reduced from 4 to 1.5 mm whilst power output is comparable apart from the 2.5 mm tuning distance, which produces a power output of around 30 μW.

Table 7-2. Resonant tuning range and power generation for 2nd design.

Distance between harvester and tuning mechanism (mm)	Magnet thickness (mm)	Resonant frequency without flux guide (Hz)	Resonance frequency range (Hz)	Maximum power (µW)
6.5	5	56.95	52.3 – 55.25	157
	3	53.95	50.2 – 52.7	152
	1	49.35	47.75 – 49.15	145
4.5	5	61.25	55.0 – 58.1	116
	3	58	52.25 – 56.2	112
	1	50.7	48.95 -50.6	106
2.5	5	66.25	57.45 – 60.9	31
	3	61.1	54.3 – 57.75	31
	1	51.05	49.95 – 50.75	30

7.3.2 Magnetic flux density

In order to investigate the non-linear change in frequency, the magnetic flux density was measured experimentally at the middle point of the tuning distance when this was set to 6.5 mm, see figure 7-9a. The change in magnetic flux density matches the change in resonant frequency, i.e. it decreases until the tuning gap reaches 4 mm, then it increases at a higher rate as shown in figure 7-9b.

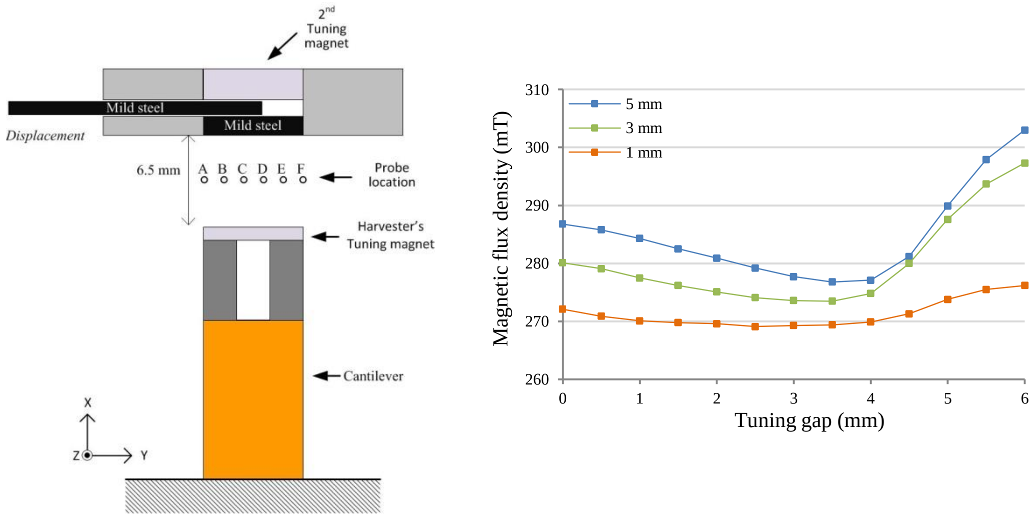

a. Probes position

b. Magnetic flux variation

Figure 7-9. Magnetic flux density variation as tuning gap increases for each of the magnet's thickness.

Finite element analysis (FEA) in Comsol shows that the magnetic flux density at the midpoint along the tuning distance is not uniform. The magnetic flux density was calculated at six different points along the mid line and the results are given in figure 7-10. The non-symmetry between probes *A* and *F* shows that the force exerted on the cantilever is not uniform, resulting in a lateral motion during each cycle. This asymmetric force is lower than in the first magnetic flux tuning mechanism in section 7.2 and the magnets did not contact the coil with this experimental arrangement.

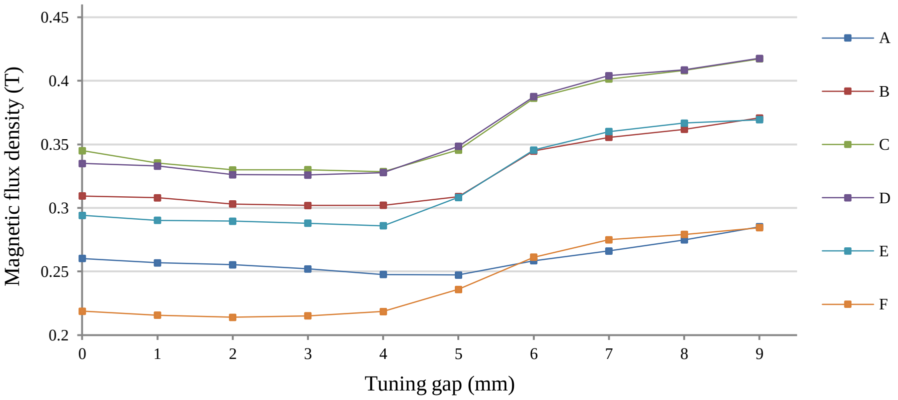

Figure 7-10. Finite element analysis of magnetic flux density as tuning gap increases

FEA shows the magnetic flux lines are flowing through the flux guide back to the second tuning magnet producing a non-symmetrical flux density as shown in figure 7-11. This asymmetry is stronger when the tuning gap is 4 mm. The magnetic flux density is symmetrical when the flux guide is removed, as shown in figure 7-11d.

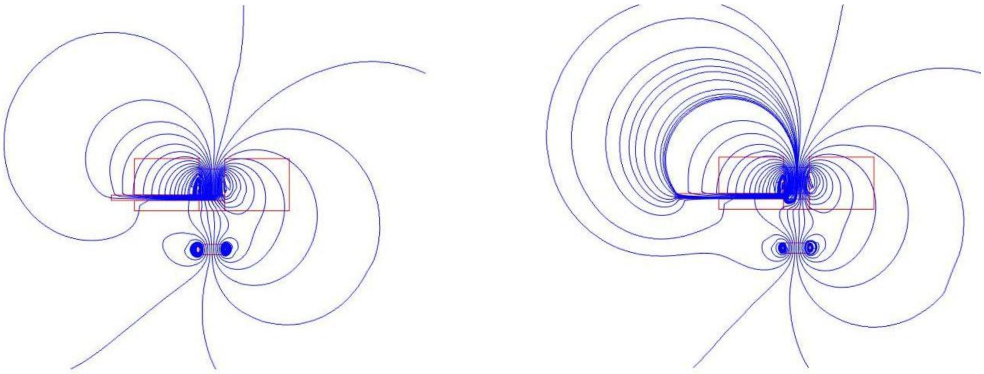

a. Gap: 0 mm b. Gap: 4 mm

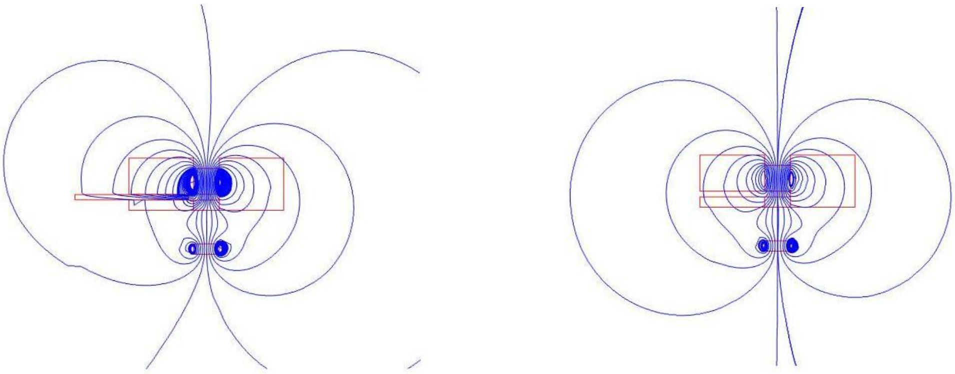

c. Gap: 6 mm d. Flux guide removed

Figure 7-11. Graphical FEA of magnetic flux density (top view).

7.3.3 Force on flux guide

An important point that must be considered is the force required to move the flux guide. The force should be reduced to minimize the power consumption of the actuator used in any future automated tuning mechanism. The force was measured using a digital force gauge when the tuning distance was 6.5 mm, the results are shown in figure 7-12.

The force on the flux guide varies with the magnet size and, to a lesser extent, the tuning distance. This force is dominated by the contact friction between the magnet surface and the flux guide. The larger tuning magnet increases the attraction between the magnet and the guide increasing the friction in the assembly. The maximum tuning force experienced by the moving magnet tuning arrangement described in previous chapters was less than 1 N. Therefore, the tuning mechanism proposed in this chapter would consume more energy due to a larger thrust required by the actuator.

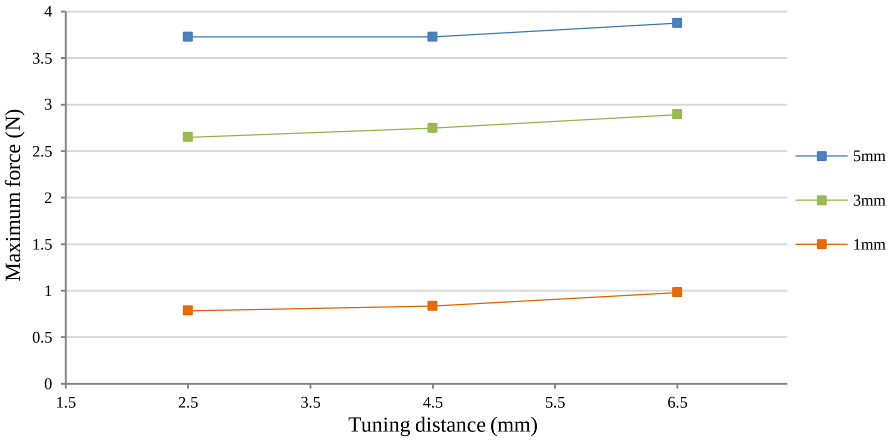

Figure 7-12. Maximum force required to move flux guide for three different magnet thicknesses: 5, 3 and 1 mm.

7.4 Design 3: Flux guide with vertical displacement.

A third magnetic flux guide design was proposed to address the non-uniform magnetic flux and to reduce the frictional force on the flux guide. The first modification was to reduce the size of the flux guide to reduce the effect on the flux density around the harvester, the geometry of the flux guide was 5x13x1 mm. Secondly, the tuning arrangement was modified to move the flux guide in the vertical direction. This resulted in the non-uniform distribution of the magnetic flux which was now aligned in the vertical direction, which will cause no lateral displacement of the cantilever. The flux guide is positioned directly in front of the fixed tuning magnet without any guiding slot. This reduced the friction forces to only those exerted between the magnet and the guide. The sliding mild steel has been mounted on a single axis translation stage with a manual micrometer, as shown in figure 7-13.

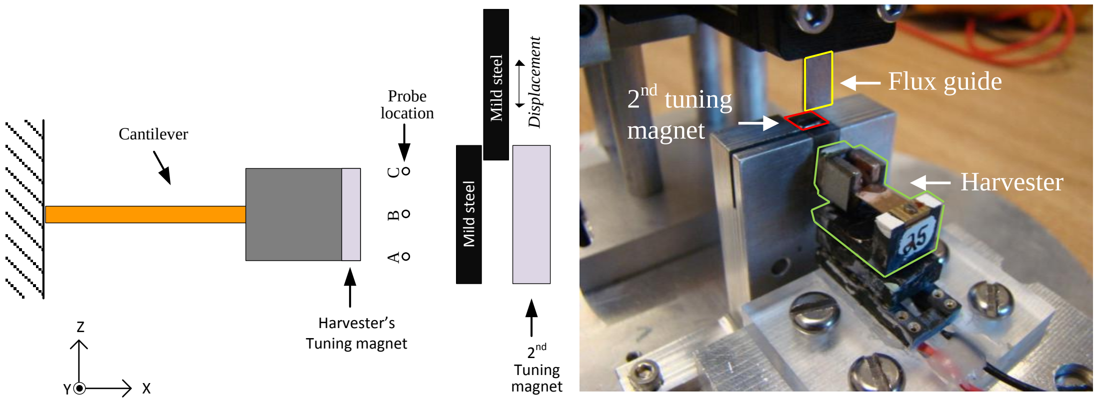

a. Schematic b. Picture

Figure 7-13. Vertical magnetic flux guide

A 5 mm thickness magnet was used as the fixed tuning magnet for all the tests. The tuning distance was varied from 3, 5, 7 and 10 mm. The results show a similar change in the resonant frequency as with the horizontal flux guide. First, there is a slow drop in the resonant frequency as the tuning gap increases, then a rapid increase towards the non-tuned resonant frequency, as show in figure 7-14a. Furthermore, the frequency range increases as the tuning distance reduces. As with the previous designs, the decrease of the tuning distance increases the damping in the harvester, reducing its power generation, as depicted in figure 7-14b and figure 7-15. Table 7-3 summarizes the results of the test with the 3rd design.

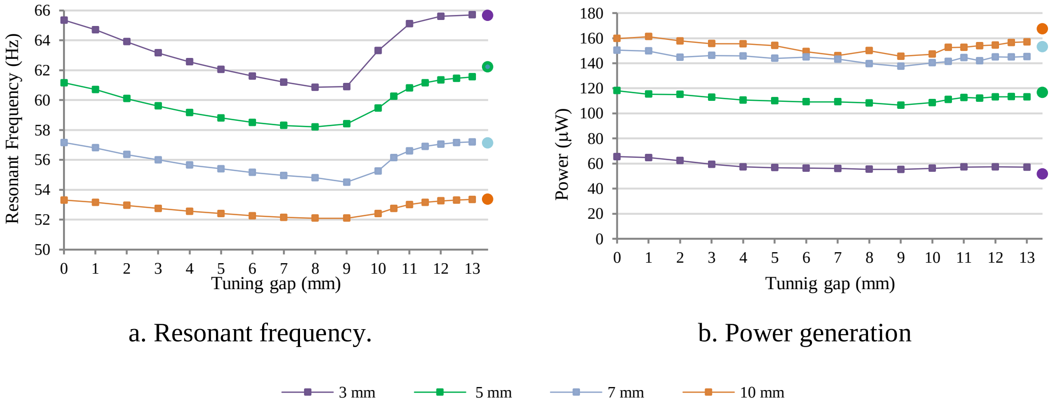

a. Resonant frequency. b. Power generation

Figure 7-14. Resonant frequency and power generation at different tuning distance.

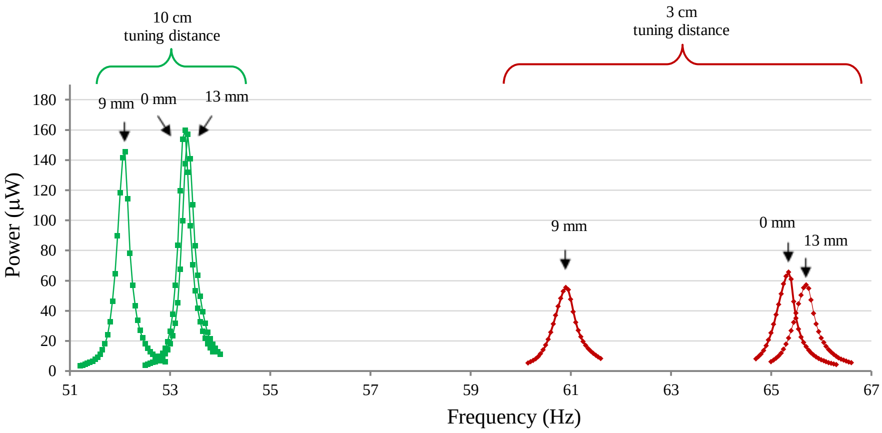

Figure 7-15. Frequency response for different tuning distances and tuning gap

Table 7-3. Resonant tuning range and power generation for 3rd design.

Tuning distance (mm)	Resonant frequency without guide (Hz)	Resonant frequency range using guide (Hz)	Maximum power (µW)
3	65.65	60.85 – 65.70	65.48
5	62.20	58.20 – 61.60	118.18
7	57.10	54.50 – 57.25	150.41
10	53.35	52.10 – 53.35	161.17

7.4.1 Magnetic flux density

The magnetic flux density is not uniform, as in the previous design. It creates an additional force on the cantilever that pulls it down. However, the coil is not damaged because this force is in the same direction as the movement of the cantilever, Z-direction, in figure 7-13a. Figure 7-16 presents the FEA of the magnetic flux density when the tuning distance is 5 mm. The effect of the flux guide on the magnetic flux is shown in Figure 7-17. The magnetic flux density follows the path of the flux guide due to its lower reluctance than that of the air surrounding the harvester.

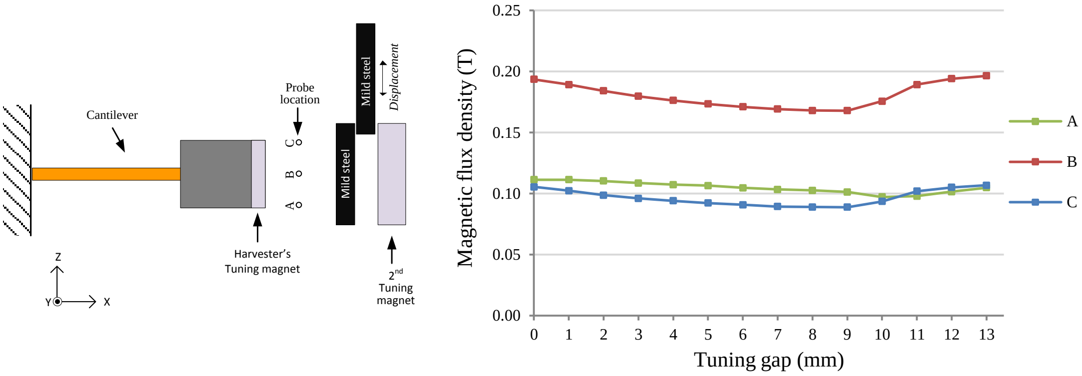

a. Test points location b. Magnetic flux

Figure 7-16. FEA of magnetic flux density as function of the gap

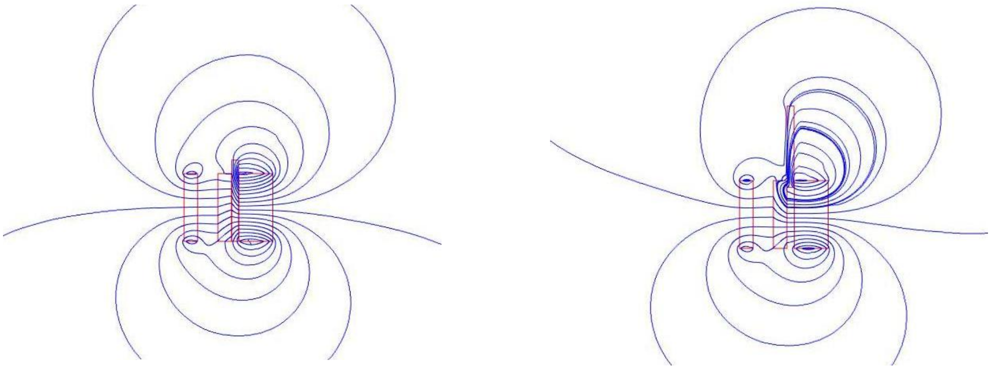

a. Tuning gap: 0 mm b. Tuning gap: 9 mm

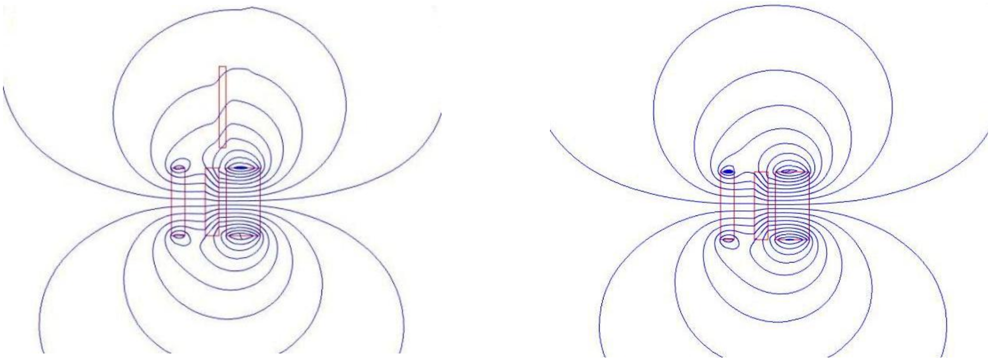

c. Tuning gap: 13 mm d. Flux guide removed

Figure 7-17. FEA of magnetic flux density (lateral view).

7.4.2 Force on flux guide

Due to the experimental arrangement, it was not possible to measure the force required to move the flux guide. The electromagnetic force on the flux guide was calculated using FEA. The force has been divided into its X and Z components to identify the main contributor and calculate the maximum force that an actuator has to withstand to operate this mechanism. The force on the Y-direction is negligible due to the orientation of the tuning magnets.

The results from FEA analysis show that the maximum force on the flux guide, in the X-direction, occurs when the gap is approximately 3 mm, as shown in figure 7-18. Meanwhile the force in the Z-direction peaks when the gap reaches 10 mm, as presented in figure 7-19. A positive force on the Y-axis, translates in the flux guide being pulled towards the 2nd tuning magnet. Once the tuning distance increases beyond 10 mm, the flux guide is not in contact with the magnet and the force on the Z-direction becomes dominant, pulling the flux guide downwards.

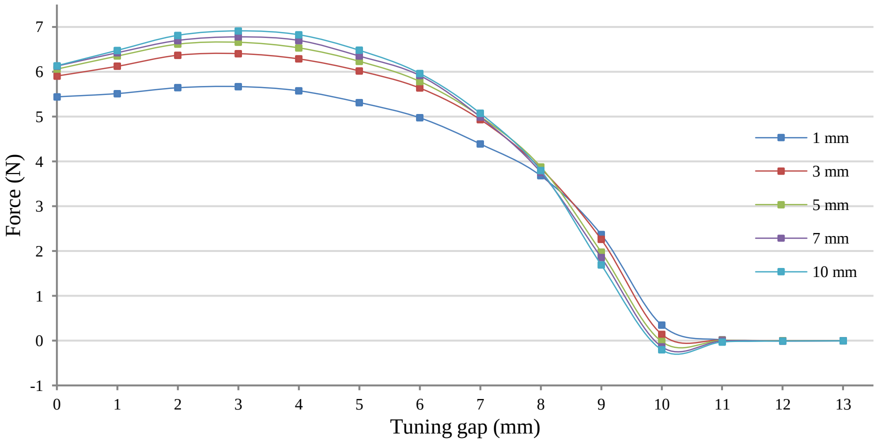

Figure 7-18. Electromagnetic force exerted on flux guide on X-direction, at difference tuning gap and tuning distances.

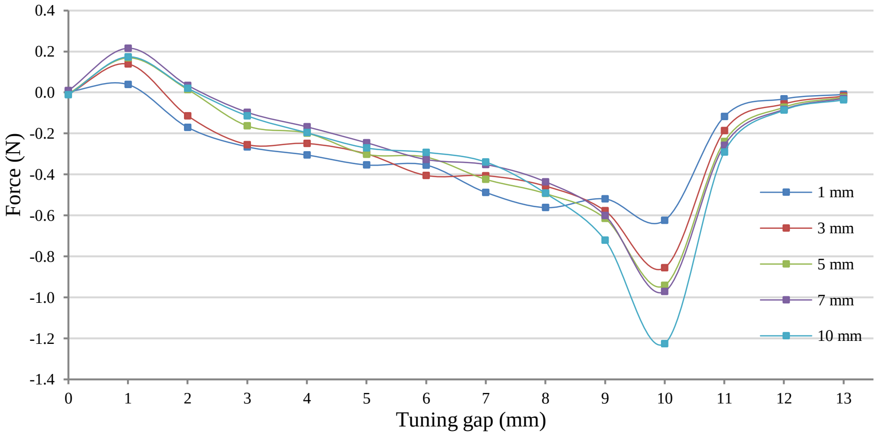

Figure 7-19. Electromagnetic force exerted on flux guide on Z-direction (at different tuning distances).

The force required by the any future actuation mechanism to move the flux guide can be calculated based on the friction between flux guide and magnet. The 2nd tuning magnet has a zinc coating and the flux guide is considered to be steel. The static friction coefficient for zinc-steel is 0.5. Therefore, the maximum force on the actuator is 3.32 N at a tuning distance of 5 mm. Experimental tests using a spring force gauge found a maximum force of 3.77 N for the same the tuning distance.

7.5 Discussion

The main challenge encountered during these practical applications has been the effect of the non-uniform forces on the harvester. This creates a lateral displacement of the cantilever, which subsequently resulted in damage to the coils.

The influence of the magnetic flux on the harvester resonant frequency has a maximum effect when the overlap between the fixed tuning magnet and the flux guide is minimum. For the designs presented here, this corresponds to a gap of 4 and 9 mm for the horizontal and vertical designs respectively. Operating in this range gives the greatest change in frequency for the shortest distance move of the flux guide, which is an important consideration when using an automated actuator to control the guide position. The results also show a clear trade-off between the achievable bandwidth and the power output from the generator. In particular, reducing the tuning distance (the gap between tuning magnets in design 1 or the gap between the fixed mild steel flux guide and the magnet on the cantilever in designs 2 and 3) to increasing the magnetic tuning forces reduces the power generated due to the increased damping on the cantilever. The length of the flux guide could be reduced to cover partially the fixed tuning magnet and still achieve optimal bandwidth of operation. The power required by the future actuation mechanism could be minimized if the friction between flux guide and magnet is reduced. A possible option is to avoid the contact of these two elements by increasing the distance between them.

7.6 Conclusion

This chapter has presented the tuning of the energy harvester using a magnetic flux guide. Three different configurations were evaluated. In the first two designs, the flux guide is oriented perpendicular to the motion of the cantilever. This geometry introduces asymmetrical forces on the cantilever resulting in lateral displacement of the harvester, and caused damage to the harvester due to physical contact between the cantilever and the coil.

The effect of the flux guide on the resonant frequency of the harvester has maximum effect when the geometric overlap between the fixed tuning magnet and the flux guide is a minimum. For the designs presented here, the resonant frequency has a larger variation as the overlap reduces from 1 mm. This range offers a larger frequency bandwidth with a reduced displacement than when the tuning gap increases from 0 mm, reducing the energy required by an actuation mechanism in an automated system.

Analysis of the forces exerted on the flux guide have shown that, if the friction between the guide and the fixed tuning magnet can be avoided by either leaving a gap between them or by reducing the friction coefficient, the maximum force required to move the guide can reduce to 1.2 N. This is similar to the force required in the case of the tuning mechanism based on varying the distance between magnets, presented previously, but in that case the bandwidth of operation is larger.

It is concluded, that the magnetic flux guide tuning mechanism is less effective than the tuning mechanism based on distance between tuning magnets, presented in previous chapters, because it requires the same force by the actuator to adjust the flux guide but with a smaller frequency bandwidth. Although the asymmetry in the force exerted on the harvester will not affect its physical structure, it can augment its non-linear behaviour increasing the complexity of the control system thus adding power overhead.

Chapter 8

Conclusions and Future Work

8.1 Summary of work

Vibration-based energy harvesting has emerged as an alternative source of energy for low power wireless sensor systems due to the potential availability of kinetic energy in modern life. In the literature, the most common mechanical design that couples environmental vibrations into the transduction mechanism is the inertial-based generator. They are designed with a high Q-factor to maximize its displacement, which maximises their power generation. However, resonant generators have a limited bandwidth of operation, which is inversely proportional to the Q-factor. Maximum generation occurs when the resonant frequency matches that of the environment.

A solution to this trade-off is to tune the resonant frequency of the harvester. Different research groups have proposed mechanisms to achieve this goal. However, none of them has presented a fully functional example where the tunable energy harvester system operates autonomously without relying on external energy or manual adjustment, which ultimately defeats the purpose of an energy harvester.

This research detailed the development of an autonomous tunable energy harvester that adjusts its resonant frequency to match the base frequency relying only on the energy harvested, whilst operating automatically. It further presented the optimization of the power extraction and conversion from an electromagnetic transduction mechanism attached to the tunable harvester, in particular, methods to optimize the impedance load seen by the harvester.

Chapter 2 presented a literature review of the vibration-based energy harvesters. First, the inertial-based linear model used to represent the behaviour of the vibration-based energy harvester was reviewed. Next, strategies to increase the frequency range of the vibration-based harvester were presented. These can be divided into those that widen the bandwidth of the harvester and those that tune the harvester's resonant frequency. Power extraction and conversion techniques were also reviewed.

Chapter 3 detailed the elements comprising the tunable energy harvester, the tuning mechanism and the electronic components. It presented the experimental performance of the harvester outlining its non-linear behaviour, i.e. the harvester resonant frequency shifts as the acceleration increases.

A set of strategies were introduced to reduce the energy consumption of the system:

- Use of low power electronic components.
- Reduce the voltage of operation.
- Power off those components that are not in constant use.
- Maintain in low power mode those components that cannot be powered off.
- Reduce the computational charge on the microcontroller to keep it in low power mode.

The actuator is the component with the highest power consumption in the system. The power it consumes was reduced by reducing the voltage of operation. This resulted in a reduction in power consumption of 60% compared to the values published by the manufacturer. The driving electronics associated with the actuator were developed offering a solution that can operate the actuator using the same voltage as the supply, although at a cost of increasing the number of control lines.

Passive power extraction and conversion was evaluated using switching capacitors configured as a voltage multiplier and a boost converter. The energy harvested was delivered to a storage capacitor from which the rest of the system is powered.

Chapter 4 detailed the characterisation of the tunable energy harvester. The harvester resonant frequency can be adjusted using the tuning mechanism to achieve a range of more than 40 Hz. However, the use of the actuator is costly in terms of power consumption if the entire 40 Hz range was used, especially at low frequencies, where a large displacement of the tuning mechanism changes the resonant frequency by a small amount. For the higher frequencies in the range, the increasing damping created by the tuning magnets and the lower displacement of the harvester as the frequency increases, result in a reduction of the power harvested. Therefore, an optimal bandwidth of operation was proposed from 64.06 to 78.32 Hz, which required an adjustment of the tuning magnets of 2 mm, from 5 to 3 mm apart, and the power generated reduces by 25% in comparison to the power generated when the harvester operates at its untuned resonant frequency of 46.3 Hz.

Two control strategies were evaluated: open and closed loop. Open loop control relied on a mathematical model of the harvester’s resonant frequency as a function of the distance between tuning magnets. This approach is simple but lacks robustness because it does not consider the non-linear behaviour of the harvester. A closed loop control system was then proposed that also used the mathematical model of the harvester, but it added a fine tuning mechanism that adjusts the resonant frequency based on the period difference between the base acceleration and the harvester output voltage signal.

The control system adjusts the harvester resonant frequency to match the base frequency. The time required to harvest the energy used during adjustment and operation of the system varies according to the level of mistuning. The power extraction and conversion were not optimized, but the results collected during these tests were used as a benchmark for the subsequent evaluation of the system. It was concluded that there is an optimal range of operation for the tunable energy harvester and that the control mechanism requires a closed loop to achieve a fully functional autonomous control of the tunable energy harvested.

Chapter 5 investigated the optimization of the power extraction and conversion. In the initial design of the tunable energy harvester, presented in chapter 3 and chapter 4, the power extraction and conversion was performed by a 5 stage VM. In chapter 5, the number of stages was adjusted or replaced by a diode bridge, to improve the load seen by the harvester. This achieved a reduction of 75% in the charging time for Harvester B connected to a diode bridge, i.e. a reduction in the system recovery time after frequency adjustment. However, the passive extraction and conversion of the energy cannot adapt the impedance of the load to maximize the power generation. To achieve this, an active conversion mechanism was proposed, whereby an intermediate storage capacitor is charged through a 2 stage VM, then the energy is extracted via a boost converter. The experimental results show a lower efficiency when using this design in comparison to a diode bridge, due to the power losses associated with the commercial components used. Therefore, it was concluded that passive processing of the energy is preferable for the harvester presented here since its low power generation cannot sustain an active energy processing system. The potential of the system as a power source for a wireless sensor system was also demonstrated in this chapter.

Chapter 6 presented the operation of the tunable energy harvester when it is exposed to high levels of acceleration. Even though high displacements are desired to produce more energy, increasing levels of displacement can result in physical contact between the harvester and its frame. To avoid this, a protection mechanism was implemented that automatically detunes the harvester, reducing its displacement. The protection algorithm adjusts the resonant frequency of the harvester proportionally to the level of over acceleration, providing a level of protection of up to 256% above the non-protected acceleration level.

Chapter 6 also analysed the operation of a tunable harvester when the base excitation resembles the frequency spectrum from a real application. The harvester amplifies the amplitude of those components in the spectrum that share the same frequency as its resonant frequency. This characteristic was used to measure its resonant frequency, leaving the accelerometer as the only method to sense the base frequency. The limited number of samples taken to measure the dominant frequency at the base, as well as for the harvester resonant frequency, resulted in a large error in these measurements. In consequence, the control system was modified to first adjust the distance between magnets using the mathematical model, and then track the power at the storage capacitor to find the optimal position. It was also observed that the non-linear behaviour of the harvester was intensified when the spectrum of a real application was used, which forced the control system to adjust the harvester resonant frequency from a higher to a lower frequency to reach its high energy level.

It was concluded that the use of the tunable energy harvester in a real application requires additional signal processing to distinguish the frequency component with the highest energy. It was also required to adjust the control mechanism to force the harvester to take the high energy level, by adjusting its resonant frequency from a high to low frequency.

Chapter 7 investigated an alternative mechanical tuning method that modifies the magnetic flux between the tuning magnets by inserting a magnetic flux guide. Simulations and experimental analysis show that the flux guide has a larger effect on the resonant frequency when the overlap between the guide and the fixed tuning magnet decreases from 1 mm. The non-symmetrical distribution of the magnetic flux, due to the presence of the flux guide, resulted in displacement of the cantilever in the same direction as the flux guide, and subsequent contact between the beam and fixed coil, damaging the coil in designs 1 and 2. Therefore, the position of the guide was set in the same direction as the displacement of the harvester, as presented in design 3. There is a trade-off between the frequency bandwidth and power generation. More power can be harvested when the tuning distance is large, but the tuning range reduces. If compared to the tuning mechanism previously employed in this research, less force is necessary to move the flux guide, but it requires a similar or larger displacement to reach the same bandwidth of operation. Therefore, the tuning design that uses the variable distance between tuning magnets is preferred because it require less energy to operate.

In conclusion, this thesis has presented the development of an autonomous tunable energy harvester, its characterization and the design of the electronic system and algorithms to control it. It utilizes the harvester not only as a transduction mechanism, but also as a sensor. The reduction in the power consumed by the system was one of the objectives in this research using commercial components. The increase in the power harvested through the optimization of the load was considered of paramount importance to increase the efficiency and flexibility of the tunable energy harvester. The system has demonstrated its functionality as a power source for a wireless sensor node.

8.2 Future work

The results presented have highlighted areas that would benefit from further investigation. This section will discuss those areas considered to have a higher impact on the future development of an autonomous energy harvester.

8.2.1 Active load matching

Active load matching is an important area of development for future energy harvesting. This research analysed the operation of active power extraction and conversion, but the adjustment of the duty cycles was not investigated. A first challenge in this area is the reduction of the power consumed by the control system operating the matching circuit. The literature reports some examples of active matching circuits for piezoelectric transduction harvesters, but the power consumed is measured in hundreds of microwatts, which is above the power level generated by the harvester presented in this thesis. More research is needed to develop a circuit matching design for low power energy harvesters with power consumption in the range of microwatts that can adapt the load seen by the harvester and effectively increase the power generation.

8.2.2 Simulation of energy harvesting systems

The joint simulation of the energy harvester and the extraction and conversion electronics was performed using Pspice using the ICES tool kit [110]. The base excitation was simulated using a sinusoidal voltage source at the desired frequency. However, the simulation time-step must be small to calculate accurately the displacement of the harvester. This resulted in vast memory use and large processing time, and eventually in the incapacity to simulate the system for long periods. Other options like Simulink were investigated, but the difficulty to model electronic components on this platform also inhibited its use in this research.

The main challenge in this area is to incorporate the mechanical and electrical components of the harvester system into a single simulation toolkit. Such toolkits must be able to simulate the operation of the harvester for long periods while offering the flexibility to add electrical and mechanical component, and at the same time model its behaviour, e.g. the non-linearity of the harvester.

8.2.3 Low power electronics for energy harvesting

In this research, only commercial components were employed. In most cases, they were designed for applications where the power consumption is not a major limitation, e.g. the microcontroller. Energy harvesting applications do not require many of the resources available on today’s microcontroller to operate. Hence, a low speed microcontroller would be able to operate the energy harvester and reduce the power consumed in the process.

8.2.4 Operation in real applications

The analysis of the operation of the tunable energy harvester in a real application contributed to identify areas that required further investigation. The main challenge in this case is to identify the dominant frequency component from the base excitation. This would require additional sampling and processing time, which in turn consume power. A possible solution is a digital signal process system to compute the frequency and provide the profile of the spectrum to the control system.

A novel method to identify when the harvester resonant frequency matches the dominant frequency at the base is also necessary. The current method of measuring the power at the storage capacitor is slow and power consuming. A possibility is to measure the frequency spectrum of the harvester to identify if it is at resonance.

Appendix A

Program listing

```
;*************************************************************
;               Filename:       01Jun11.asm                                   *
;               Author: Ivo Ayala                                             *
;                                                                             *
;               Clock:          Internal Oscillator @ 4MHz                    *
;*************************************************************
                list            p=16f884        ; list directive to define processor
                #include        <p16f884.inc>; processor specific variable definitions

__CONFIG      _CONFIG1, _DEBUG_OFF & _LVP_OFF & _FCMEN_OFF & _IESO_OFF & _BOR_OFF & _CPD_OFF & _CP_OFF & _MCLRE_OFF &
_PWRTE_ON & _WDT_OFF & _INTRC_OSC_NOCLKOUT
                __CONFIG    _CONFIG2, _WRT_OFF & _BOR21V

;See page 195 on Datasheet
;(_DEBUG_OFF)                   In-circuit Debugger mode        OFF
;(_LVP)         Low Voltage programming:                        OFF
;(_FCMEN)       Fail-safe clock monitor:                        OFF             (Allows ;the device to continue operating should external osc fail.)
;(_IESO)        Internal External Switchover:  OFF              (Internal/external swtich ;over. Used for two-speed star-up seq.)
;(_BOR)         Brown-out Reset Selection:                      OFF             (Disabled)
;(_CPD)         Data code protection:                           OFF
;(_CP)          Code protection:                                OFF
;(_MCLRE)       RE3/MCLR:                                                       OFF
;(_PWRTE)       Power-up Timer Enable                                           ON
;(_WDT)         Watch dog timer                                 OFF
;(_INTRC_OSC_NOCLKOUT)          Internal Oscillator                             No clock ;out
;(_WRT)         Flash program memory self write                 OFF (No prog memmory ;write protection)
;(_BOR21V)      Brown-out Reset to:                                                                     2.1V

                cblock          H'20'                           ;Allocated in Bank 0
                ADCch                           ;ADC channel to be sampled
                ResultLow                       ;Lower 8 bits conversion
                ResultHigh                      ;Higher 8 bits conversion
                PotenH                          ;Potentiometer
                PotenL
                Cycles                          ;Register number of half-cycles
                ASampH
                ASampL
                BSampH
                BSampL
                FirstSampH                      ;First sampling High
                FirstSampL                      ;First sampling Low
                SecondSampH                     ;Second sampling High
                SecondSampL                     ;Second sampling Low
                SamplingH
                SamplingL
                MaxH
                MaxL
                MinH
                MinL
                MeanH
                MeanL
                GeneH                           ;Maximum value at the Generator
                GeneL
                Clock1H                         ;Time of 1 sampling
                Clock1L
                Clock2H                         ;Time of 2 sampling
                Clock2L
                FreqH           ;Register containing difference between 1 and final time ;sampling
                FreqL
                Cycle_1H                        ;1 cycle measure
                Cycle_1L
                ShiftH                          ;Phase shift
                ShiftL
                Value1L                         ;Higher value register LSB
                Value1H                         ;Lower value register LSB
                Value2L                         ;Higher value register MSB
                Value2H                         ;Lower value register MSB
                AbsoluteH                       ;Absolute value MSB
                AbsoluteL                       ;Absolute value LSB
                AccelppL                        ;Accelerometer Peak-peak value
                AccelppH                        ;Accelerometer Peak-peak value
                Detuning_Reg1H                  ;Internal register Detuning function
                Detuning_Reg1L                  ;Internal register Detuning function
                Detuning_Reg2H                  ;Internal register Detuning function
                Detuning_Reg2L                  ;Internal register Detuning function
                OverAccelH                      ;Over acceleration value
                OverAccelL                      ;Over acceleration value
                Waveside                        ;1st Flags Register
                Waveside2                       ;2nd Flags Register
                BinaryToLCD                     ;Stores the binary number to be send to ;the LCD
                BinaryCount                     ;Stores the counter when :sending Binary number to LCD
                TenK                            ;B4
                Thou                            ;B3
                Hund                            ;B2
                Tens                            ;B1
```

```
        Ones                  ;B0
        NumH                  ;A3*16+A2
        NumL
        PhaseH                ;Phase shift count
        PhaseL                ;Phase shift count
        TravelStep            ;Current step sequence
        StepH                 ;Step High
        StepL                 ;Step Low
        OptStepH              ;optimal postion
        OptStepL
        FixedRefH             ;Result form Fixed Reference = 0.6V ADC conversion
        FixedRefL
        R_DEL1                ; Delay register
        R_DEL2                ; Delay register
        R_WDATA_TMP1
        R_WDATA_TMP2
        R_SEND_W_TMP
        R_WTMP                ; W storage
        R_STMP                ; STATUS storage
        R_STMP1               ; Send temp register
        R_PSEC
        X_IntH                ;Dividend
        X_IntL                ;Dividend
        Y                     ;Divisor
        Counter               ;Counter used on Division routine
        Counter_1             ;Counter :used for multiple freq. ;measurements
        Counter_2             ;Extra counter
        d1                    ;used on delay routine
        d2                    ;used on delay routine
        d3                    ;used on delay routine
                              ;Phase shift routine variables(Start)
        highs

        endc

        cblock    H'A0'                 ;Allocated in Bank 0
                  WatchDog              ;Save WDTCON value
        endc

        org        0x000                ; processor reset vector
        goto       main                 ; go to beginning of program

        org       0x04
        goto      inter                 ;Go to interrup

main
;BBBBBBBBBank 000000000000000
        bcf       STATUS,RP1            ;Bank0
        bcf       STATUS,RP0            ;
        clrf      PORTA                 ;Init/clear PORTA
        clrf      PORTB                 ;Init/clear PORTB
        clrf      PORTC                 ;Init/clear PORTC
        clrf      PORTD                 ;Init/clear PORTD
        clrf      PORTE
        clrf      INTCON                ;Disable Interrupts and clear some flags
        movlw     b'00110000'           ;Set :Timer1 Control: :Prescaler 1:8, ;Internal CLock, Stops Timer1
        movwf     T1CON
        movlw     b'01000100'           ;ADCS=Fosc/8;Channel:AN1,Disable ADC
        movwf     ADCON0

;BBBBBBBBBank 11111111111111111
        bcf       STATUS,RP1            ;Bank1
        bsf       STATUS,RP0            ;
        movlw     b'01100000'           ;IRCF(Internal Oscillator Freq= 4MHz)
        movwf     OSCCON                          ;Oscillator control configuration
        movlw     b'00000000'           ;TUN<4:0> Factory-calibrated freq.
        movwf     OSCTUNE
        movlw     b'00001011'           ;Set RA<7:4,2> as outputs, RA<3,1:0> as inputs
        movwf     TRISA
        movlw     b'00000000'           ;Set RB<7:0> as outputs, RB<?:?> as inputs
        movwf     TRISB
        movlw     b'00010100'           ;Set RC<7:5,3,1,0> as outputs, RC<4,2> as inputs
        movwf     TRISC
        movlw     b'00001111'           ;Set RD<7:4> as outputs, RD<3:0> as inputs
        movwf     TRISD
        movlw     b'00000000'           ;Set RE<3:0> as outputs, RE<?:?> as inputs
        movwf     TRISE
        movlw     b'10000000'           ;Set Conversion Result Right justified, Vdd and Vss as Vref
        movwf     ADCON1

;BBBBBBBBBank 22222222222222222
        bsf       STATUS,RP1            ;Bank2
        bcf       STATUS,RP0            ;
        movlw     b'00010110'           ;Watch Dog timer control. scale 1:65535, WDT turned off (320sec)
        movwf     WatchDog              ;Save WDTCON value
        movwf     WDTCON

        bcf       CM1CON0,7             ;Disable comparator C1
        bcf       CM2CON0,7             ;Disable comparator C2

;BBBBBBBBBank 33333333333333333
        bsf       STATUS,RP1            ;Bank3
        bsf       STATUS,RP0            ;
        movlw     b'00001011'           ;Set ANS<7:4,2> as Digital I/O, ANS<3,1:0> as Analog Input.
        movwf     ANSEL                 ;Analog select register ANS<7:0>
        movlw     b'00000000'           ;Set ANS<13:8> as Digital I/O, ANS<?:?> as Analog Input.
        movwf     ANSELH                ;Analog select high register ANS<13:8>
```

```
          bcf       STATUS,RP1            ;Bank0
          bcf       STATUS,RP0            ;

;Initialize variables and routines
          call      MotorOFF
          movlw     d'100'
          movwf     StepL
          clrf      StepH
          clrf      Waveside
          clrf      Waveside2

WaitForConver_0

;********************************Select the desired routine to be performed.***********************
WaitForConver_1
          btfsc     PORTD,0               ;Is the Normal Operation switch pressed?
          goto      Normal_Operation;1,   Goto to Normal Operation
          btfss     PORTD,3               ;Is the Extend Switch pressed?
          goto      $+3                   ;0,         No pressed Extend Switch
          call      Extension             ;1,         Goto Extend routine
          goto      WaitForConver_0       ;           Extend routine FINISHED
          btfss     PORTD,2               ;Is the Retract switch pressed?
          goto      $+3                   ;0,         No pressed Retract Switch
          call      Retraction            ;1,         Goto Retract routine
          goto      WaitForConver_0       ;           Retract routine FINISHED
          btfss     PORTC,4               ;Is the Phase measure switch pressed?
          goto      $+3                   ;0,         No pressed Phase measure switch
          goto      Phase_Meas            ;           Goto Phase measure routine
          goto      WaitForConver_0       ;           Phase measure routine FINISHED
          goto      WaitForConver_1       ;           RETURN to query switches

Normal_Operation
          call      Voltage_Main          ;Compare Vdd agins Vref(internal),
                                          ;input= <NONE>
                                          ;output= Waveside<5>      1, Vdd > 2.6V
                                          ;                         0, Vdd < 2.6V

          btfss     Waveside,5            ;1, Vdd > 2.6V
          goto      low_power             ;0, Vdd < 2.6V

Normal_Operation_0
          call      Freqmeter             ;USING LM2903
                                          ;Measure frequency from signal at CCP1
                                          ;input= <NONE>
                                          ;output= FreqH/L

          call      Wave                  ;Calculate accelerometer (AN0) Max,Min, Mean
                                          ;input= <none>
                                          ;output= MaxH/L, MinH/L, MeanH/L, AccelppH/L

          call      Detuning              ;Calculate the over acceleration and set the detuning value
                                          ;Input= FreqH/L, AccelppH/L,
                                          ;Output= OverAccelH/l, Waveside2<1> 1->accel>max, 0->accel<max

          call      Optimum               ;Calculate the optimal position
                                          ;Input= FreqH/L
                                          ;Output= OptStepL
                                          ;Waveside<4>= 1 -> Ok, 0 -> Calculation error (measure not valid)

          btfss     Waveside,4            ;1,Frequency IN range
          goto      low_power             ;Frequency out of range

          call      Steps_to_Optimum      ;Calculate number of step to optimal position and move to that location
                                          ;Input= OptStepl, OverAccelH/L, Waveside2<1>
                                          ;Output= Waveside<7>, 0 -> more than 10 steps, 1 -> less or equal to 10 steps.

          btfsc     Waveside2,1           ;0-> accel < maximum
          goto      low_power             ;1-> accel > maximum, control using step count only

Normal_Operation_1_A
          btfsc     Waveside,7            ;0, optimal position > 10 steps.
          goto      Normal_Operation_1

;         call      low_routine           ;Sleep Routine
          goto      Normal_Operation_0

Normal_Operation_1                        ;Move acuator using frequencye as input signal.
          call      Freqmeter             ;USING LM2903
                                          ;Measure frequency from signal at CCP1
                                          ;input= <NONE>
                                          ;output= FreqH/L

          call      Wave                  ;Calculate accelerometer (AN0) Max,Min, Mean
                                          ;input= <none>
                                          ;output= MaxH/L, MinH/L, MeanH/L, AccelppH/L

          call      Detuning              ;Calculate the over acceleration and set the detuning value
                                          ;Input= FreqH/L, AccelppH/L,
                                          ;Output= OverAccelH/l

          call      low_routine           ;Sleep Routine

          call      Phase                 ;Calculate phase shift between Generator (CCP1) and Accelerometer (AN0)
                                          ;Input= MeanH/L
                                          ;output= PhaseH/L
```

```
                call        Phase_Shift             ;Calculate Phase Shift (difference) between [Generator - Accelerometer]
                                                    ;Input: Phase, Freq, OverAccelH/l
                                                    ;Output: Shift, Waveside<6>: 0-> Negative shift, 1-> Positive Shift.

                call        Ctrl_Phase              ;Control using Phase shift. Move acordenly and update current Step.
                                                    ;Needed= Shift, Waveside<6>
                                                    ;Output= Possible update StepH/L, Waveside2<0>, 0-> Not finished, 1->Finished

                btfss       Waveside2,0             ;1, Ctrl_Phase FINISHED
                goto        Normal_Operation_1      ;Continue control using phase shift
                goto        low_power

Phase_Meas                                          ;Multiple measurment (NO control)

                clrf        Counter_2               ;Used for multiple measurements

Phase_Meas_0

                call        Freqmeter               ;USING LM2903
                                                    ;Measure frequency from signal at CCP1
                                                    ;input= <NONE>
                                                    ;output= FreqH/L

                call        Optimum                 ;Calculate the optimal position
                                                    ;Input= FreqH/L
                                                    ;Output= OptStepL
                                                    ;Waveside<4>= 1 -> Ok, 0 -> Calculation error (measure not valid)

;               call        Detuning                ;Calculate the over acceleration and set the detuning value
                                                    ;Input= FreqH/L, AccelppH/L,
                                                    ;Output= PhaseShiftAdjH/L.

                call        Wave                    ;Calculate accelerometer (AN0) Max,Min, Mean
                                                    ;input= <none>
                                                    ;output= MaxH/L, MinH/L, MeanH/L


                call        Phase                   ;Calculate phase shift between Generator (CCP1) and Accelerometer (AN0)
                                                    ;Input= MeanH/L
                                                    ;output= PhaseH/L

                call        Phase_Shift             ;Calculate Phase Shift between Generator Vs Accelerometer
                                                    ;Input: Phase, Freq, OverAccelH/l
                                                    ;Output: Shift, Waveside<6>: 0-> Negative shift, 1-> Positive Shift.

                goto        WaitForConver_1

;               goto        low_power

;//////////////////////////////////////////////////////////////////////////////////////////////////////////////////////////////////////////
;----------******Programm********-----------------------------------------------------------------------------------------------
;//////////////////////////////////////////////////////////////////////////////////////////////////////////////////////////////////////////

;**************Low Power routine (start)**********************************************
low_power                   ;WDT Slepp
                            ;input= <none>
                            ;output= <none>

                bsf         STATUS,RP1              ;Bank2
                bcf         STATUS,RP0              ;
                bsf         WDTCON,SWDTEN           ;Enable WDT

                bcf         STATUS,RP1              ;Bank0
                bcf         STATUS,RP0              ;

                sleep

                bsf         STATUS,RP1              ;Bank2
                bcf         STATUS,RP0              ;
                bcf         WDTCON,SWDTEN           ;Disable WDT

                bcf         STATUS,RP1              ;Bank0
                bcf         STATUS,RP0              ;

                goto        WaitForConver_1
;**************Low Power routine (End)***********************************************

;------------------------------------------------------------------------------------------------------------------------
;----------******Routines********-----------------------------------------------------------------------------------------
;------------------------------------------------------------------------------------------------------------------------

;**************Low Power routine (start)**********************************************
low_routine                 ;WDT Sleep SHORT sleep routine
                            ;input= <none>
                            ;output= <none>

                bsf         STATUS,RP1              ;Bank2
                bcf         STATUS,RP0              ;

                movlw       b'00001100'             ;Watch Dog timer control. scale 1:2048, WDT turned off    (10sec)
                movwf       WDTCON
                bsf         WDTCON,SWDTEN           ;Enable WDT

                bcf         STATUS,RP1              ;Bank0
                bcf         STATUS,RP0              ;
                sleep
```

```
            bsf         STATUS,RP1              ;Bank2
            bcf         STATUS,RP0              ;
            bcf         WDTCON,SWDTEN           ;Disable WDT

            movfw       WatchDog                ;Restore original WDTCON
            movwf       WDTCON

            bcf         STATUS,RP1              ;Bank0
            bcf         STATUS,RP0              ;

            return
;**************Low Power routine (End)************************************************

;********************Verified voltage at main (START)*******************************
Voltage_Main            ;Compare Vdd agins Vref(internal),
                        ;input= <NONE>
                        ;output= Waveside<5>    1, Vdd > 2.6V
                        ;                       0, Vdd < 2.6V

            bsf         Waveside,3              ;Select flag for Vref
            call        ADCconversion           ;Input: flag Waveside<3,2>
                                                ;Output: ResultHigh, ResultLow
            movfw       ResultHigh
            movwf       FixedRefH
            movfw       ResultLow
            movwf       FixedRefL

;For voltage lower than 2.6V (START)
            movf        FixedRefH,0             ;Renew Z flag
            btfss       STATUS,Z                ;1, Vdd > 2.41V
            goto        Under_Voltage           ; Vdd < 2.41V

            movlw       d'241'                  ;For 2.6V (adjusted)
            subwf       FixedRefL,0             ;Subtract FixerRefL - 240'd, store in W
            btfsc       STATUS,C                ;0, FixedRefL < 240'd (voltage higher than 2.6V)
            goto        Under_Voltage           ;Voltage lower than 2.6V

            bsf         Waveside,5              ;Vdd > 2.6V

            return
;For voltage lower than 2.6V (END)

Under_Voltage
            bcf         Waveside,5              ;Vdd < 2.6V

            return
;************************Verified voltage at main (END)***************************
;*************Capture mode in CCP1 Frequencymeter(START)**********************
Freqmeter               ;USING LM2903
                        ;Measure frequency from signal at CCP1
                        ;input= <NONE>
                        ;output= FreqH/L

            bsf         PORTE,1                 ;Power-on Op-Amp

            clrf        CCP1CON                 ;Suggested by DS31014A
            movlw       b'00000100'             ;Capture mode, every falling edge, start capture mode
            movwf       CCP1CON                 ;
            bcf         PIR1,CCP1IF             ;clear flag (sugested by AN594)

            movlw       b'00000000'             ;ADJUST TIMER1 increased by d'32' counter
            movwf       TMR1H
            movlw       b'00100000'
            movwf       TMR1L
            clrf        Cycles

            ;Do not take into account the first cycle to avoid error due to opamp turning-on when the generator is
            ;in positive part of its cycle
            btfss       PIR1,CCP1IF             ;1,Capture occurred.
            goto        $-1                     ;Capture NOT occurred

            call        Delay_10msec_4MHz
            bcf         PIR1,CCP1IF             ;clear flag

            ;First cycle to be considered.
            btfss       PIR1,CCP1IF             ;1,Capture occurred.
            goto        $-1                     ;Capture NOT occurred

            bsf         T1CON,TMR1ON            ;Enable timer1

            call        Delay_10msec_4MHz
            bcf         PIR1,CCP1IF             ;clear flag

Freqmeter_1
            btfss       PIR1,CCP1IF             ;1,Capture occurred.
            goto        $-1                     ;Capture NOT occurred

            incf        Cycles
            btfsc       Cycles,3                ;0, 8 Cycles NOT completed
            goto        Freqmeter_2             ;8 cylces completed

            call        Delay_10msec_4MHz
            bcf         PIR1,CCP1IF             ;clear flag
            goto        Freqmeter_1

Freqmeter_2
```

```
            clrf        CCP1CON                 ;Disable comparator
            bcf         PIR1,CCP1IF             ;clear flag

            bcf         PORTE,1                 ;Power-off Op-Amp
            bcf         T1CON,TMR1ON            ;Disable TMR1

            movfw       TMR1H                   ;Move Timer1 to "Freq" register (Frequency measure)
            movwf       FreqH
            movfw       TMR1L
            movwf       FreqL

            return
;*******Capture mode in CCP1, Frequencymeter(END)********************
;************Calculate optimum step position based on frequency (Start)*********************************************
Optimum                 ;;Model for 16.C generator
                        ;Calculate the optimal position
                        ;[200-(Period-13480)/30]
                        ;Input= FreqH/L
                        ;Output= OptStepL
                        ;Waveside<4>= 1 -> Ok, 0 -> Calculation error (measure not valid)
            bcf         Waveside,4              ;bit low until no error in calculation
            movfw       FreqH                   ;Move FreqH to ASamp
            movwf       ASampH
            movfw       FreqL
            movwf       ASampL
            movlw       d'52'                   ;Move d'13480 to BSamp
            movwf       BSampH
            movlw       d'168'
            movwf       BSampL
            call        Order                   ;16-bits substraction (|ASamp - BSamp| = Absolute)
            btfsc       Waveside,0              ;0, (ASampH > BSampH) OR (ASampL => BSampL)
            goto        ErrorValue              ;(ASamp < BSamp), Clock < d'13600. Freq. > 74.62 Hz

;Verified Absolute < d'3841 ([3841=17241-13480] new value to allow low freq at 58Hz)
            movfw       AbsoluteH
            sublw       d'14'                   ;(k-W)(d'14 - AbsoluteH), store W
            btfss       STATUS,C                ;1,(d'14 => AbsoluteH)
            goto        ErrorValue              ;(d'14 < AbsoluteH). Freq. < 58Hz

LSB
            btfss       STATUS,Z                ;1,(d'14 = AbsoluteH)
            goto        DivByX                              ;0,(d'14 > AbsoluteH)
            movfw       AbsoluteL
            sublw       d'177'                              ;(k-W)(d'86 - AbsoluteL), store W
            btfss       STATUS,C                ;1,(d'86 => AbsoluteL)
            goto        ErrorValue              ;0,(d'86 < AbsoluteL). Freq. < 58Hz

;Divide by d'X
DivByX
            movfw       AbsoluteH
            movwf       X_IntH
            movfw       AbsoluteL
            movwf       X_IntL
            movlw       d'30'
            movwf       Y
            call        Div16by8                ;X_Int / Y = X_Int
            movfw       X_IntL

            sublw       d'200'                  ;Substract 200
            movwf       OptStepL                ;Optimum position in OptStepL.
            bsf         Waveside,4              ;bit Set  for "OK"
            return                              ;Don't sent serial

;************Calculate optimum step position based on frequency (End)******************
;******Calculate number from the "current step position" to the optimal position and move there (Start)***
Steps_to_Optimum        ;Calculate number of step to optimal position and move to that location
                        ;Input= OptStepl, OverAccelH/L, Waveside2<1>
                        ;Output= Waveside<7>, 0 -> more than 10 steps, 1 -> less or equal to 10 steps.

            bsf         Waveside,7              ;Default value. (<= 5 steps)

            ;substract the steps if accel is above maximum
            btfss       Waveside2,1             ;1,accel > maxim
            goto        move_to_optimal_A       ;0, accel < maxim. Cotinue normal operation

            movfw       OverAccelL
            btfsc       STATUS,C
            goto        move_to_optimal_A       ;OverAccelL = 0

move_to_optimal_B
            decf        OptStepL,1              ;Decrement optimal step
            decfsz      OverAccelL,1            ;Decrement optimal step
            goto        move_to_optimal_B

move_to_optimal_A
            clrf        ASampH
            movfw       OptStepL
            movwf       ASampL
            clrf        BSampH
            movfw       StepL
            movwf       BSampL
            call        Order                   ;(|ASamp - BSamp| = Absolute), Waveside<0> =1 if (ASamp < BSamp) Increasing
                                                ;Waveside<0> =0 if               (ASampH > BSampH) OR (ASampL => BSampL) Decreasing

move_to_optimal
            movf        AbsoluteL,1             ;Refresh Z flag. If currently in optimal position, do not move.
```

```
            btfsc       STATUS,Z                ;0,Absolute not= 0.
            return

            btfsc       Waveside2,1             ;0, accel < maximum, follow normal control using phase shift
            goto        move_to_optimal_2       ;1, accel > maximum, control using step count

move_to_optimal_1
;[TEST]Test for detuning using step count{
            movlw       d'11'                   ;Is optimal position equal or less than 10 steps?
            subwf       AbsoluteL,0             ;AbsoluteL - 11, store in W.
            btfss       STATUS,C                ;1, AbsoluteL >= 11 steps.
            return                              ;AbsoluteL < 11 steps. Don't move, optimal < 11steps}

move_to_optimal_2
            bcf         Waveside,7              ;Flag, more than 10 steps

            btfsc       Waveside,0              ;0, Optimal position is greater than current position.
            goto        RetrAct

ExtendAct                                       ;Extend actuator till reach optimal position.

ExtendAct_0
            movlw       d'5'                    ;(TEST, overstep) to overstep due to nonlinearity
            addwf       AbsoluteL,1             ;(TEST, overstep) Add overstep to AbsoluteL

ExtendAct_1
            call        extend
            decf        AbsoluteL
            btfss       STATUS,Z                ;1, Absolute = 0
            goto        ExtendAct_1
            call        MotorOFF
            return
RetrAct

RetrAct_0
            call        retract                 ;Rectract actuator till reach optimal position.

            decf        AbsoluteL
            btfss       STATUS,Z                ;1, Absolute = 0
            goto        RetrAct_0
            call        MotorOFF
            return
;******Calculate number from the "current step position" to the optimal position and move there (End)***
;***********Calculate accelerometer Max, Min and Mean value (Start)********************************
Wave                                ;Calculate accelerometer (AN0) Max,Min, Mean
                                    ;input= <none>
                                    ;output= MaxH/L, MinH/L, MeanH/L
            bsf         PORTE,2                 ;Power-on Accelerometer
            bsf         PORTE,1                 ;Power-on Op-Amp
            call        delay_1ms_4MHz          ;To allow settling time on Op-AMP
            call        delay_1ms_4MHz          ;To allow settling time on Op-AMP

            clrf        highs
            clrf        MaxH
            clrf        MaxL
            movlw       d'255'
            movwf       MinH
            movwf       MinL

            bcf         Waveside,2              ;Select AN0 (accelerometer)
            call        ADCconversion           ;Result in "ResultHigh<1:0>" and "ResultLow<7:0>" (Bank 0)

            movfw       ResultHigh              ;Move ResultHigh to FirstSampH
            movwf       FirstSampH              ;
            movfw       ResultLow               ;Move ResultLow to FirstSampL
            movwf       FirstSampL
Wave_0                                          ;Found the second point in the signal to establish if is increasing or decreasing
            call        delay_1ms_4MHz

            bcf         Waveside,2              ;Select AN0 (accelerometer)
            call        ADCconversion           ;Result in "ResultHigh<1:0>" and "ResultLow<7:0>" (Bank 0)


            movfw       ResultHigh              ;
            movwf       SecondSampH             ;
            movfw       ResultLow               ;
            movwf       SecondSampL

            movfw       SecondSampH
            subwf       FirstSampH,0            ;(FirstSampH - SecondSampH), store in W
            btfss       STATUS,C                ;1, (FirstSampH => SecondSampH)
            goto        Maximum_1               ;(FirstSampH < SecondSampH)
            btfss       STATUS,Z                ;1,(FirstSampH = SecondSampH)
            goto        Minimum_1               ;(FirstSampH > SecondSampH)

            movfw       SecondSampL
            subwf       FirstSampL,0            ;(FirstSampL - SecondSampL), store in W
            btfss       STATUS,C                ;0,(FirstSampL => SecondSampL)
            goto        Maximum_1               ;(FirstSampL < SecondSampL)
            btfsc       STATUS,Z                ;0(FirstSampL NOT= SecondSampL)
            goto        Wave_0                  ;(FirstSampL = SecondSampL)
            goto        Minimum_1               ;(FirstSampL > SecondSampL)

;Found Minimum and Maximum values
Minimum
            call        Delay_2.5msec_4MHz
            call        Delay_2.5msec_4MHz
```

```
Minimum_1
                movlw           b'11110000'
                andwf           highs,1

Minimum_0
                bcf             Waveside,2                      ;Select AN0 (accelerometer)
                call            ADCconversion                   ;Result in "ResultHigh<1:0>" and "ResultLow<7:0>" (Bank 0)
                movfw           ResultHigh                      ;
                movwf           SamplingH                       ;
                movfw           ResultLow                       ;
                movwf           SamplingL

                movfw           MinH
                subwf           SamplingH,0                     ;(SamplingH - MinH), store W
                btfss           STATUS,C                        ;1, (SamplingH =>MinH)
                goto            renew_min                       ;(SamplingH < MinH)
                btfss           STATUS,Z                        ;1, (SamplingH = MinH)
                goto            count_min                       ;(SamplingH > MinH)

                movfw           MinL
                subwf           SamplingL,0                     ;(SamplingL - MinL), store W
                btfss           STATUS,C                        ;1,(SamplingL => MinL)
                goto            renew_min                       ;(SamplingL < MinL)
                btfsc           STATUS,Z                        ;0,(SamplingL > MinL)
                goto            Minimum_0                       ;(SamplingL = MinL)

count_min
                incf            highs
                btfss           highs,3                         ;wait for 8 samples Higher to MinH/MinL
                goto            Minimum_0
                bsf             highs,7                         ;Set highs<7> = Minimum Found [FLAG]
                btfss           highs,6                         ;1,Maximum already found
                goto            Maximum
                bsf             highs,4                         ;Set highs<4> = Max and then Min found[FLAG]Increasing
                goto            stay

renew_min
                movfw           SamplingH
                movwf           MinH
                movfw           SamplingL
                movwf           MinL
                movlw           b'11110000'
                andwf           highs,1
                goto            Minimum_0

Maximum
                call            Delay_2.5msec_4MHz
                call            Delay_2.5msec_4MHz

Maximum_1
                movlw           b'11110000'                     ;Restart counter without affecting Min and Max Flag
                andwf           highs,1

Maximum_0
                bcf             Waveside,2                      ;Select AN0 (accelerometer)
                call            ADCconversion                   ;Result in "ResultHigh<1:0>" and "ResultLow<7:0>" (Bank 0)
                movfw           ResultHigh                      ;
                movwf           SamplingH                       ;
                movfw           ResultLow                       ;
                movwf           SamplingL


                movfw           SamplingH
                subwf           MaxH,0                          ;(MaxH - SamplingH), store W
                btfss           STATUS,C                        ;1, (MaxH => SamplingH)
                goto            renew_max                       ;(MaxH < SamplingH)
                btfss           STATUS,Z                        ;1, (MaxH = SamplingH)
                goto            count_max                       ;(MaxH > SamplingH)

                movfw           SamplingL
                subwf           MaxL,0                          ;(MaxL - SamplingL), store W
                btfss           STATUS,C                        ;1,(MaxL => SamplingL)
                goto            renew_max                       ;(MaxL < SamplingL)
                btfsc           STATUS,Z                        ;0,(MaxL > SamplingL)
                goto            Maximum_0                       ;(MaxL = SamplingL)

count_max
                incf            highs
                btfss           highs,3                         ;wait for 8 samples Higher to MinH/MinL
                goto            Maximum_0

                bsf             highs,6                         ;Set highs<6> = Maximum Found. [FLAG]
                btfss           highs,7                         ;1,Minimum already found
                goto            Minimum
                bcf             highs,4                         ;Clear highs<4> = Min and then Max found[FLAG] Decreasing
                goto            stay

renew_max
                movfw           SamplingH
                movwf           MaxH
                movfw           SamplingL
                movwf           MaxL
                movlw           b'11110000'
                andwf           highs,1
                goto            Maximum_0
```

```
;Calculate mean value from Minimum and maximum values calculated previously
stay
            movfw       MaxH                    ;Verified (Min < Max)
            subwf       MinH,0                  ;(MinH - MaxH), store W
            btfss       STATUS,C                ;1,(MinH => MaxH)
            goto        stay_0                  ;(MinH < MaxH)
            btfss       STATUS,Z                ;1,(MinH = MaxH)
            goto        Wave                    ;(MinH > MaxH)

            movfw       MaxL
            subwf       MinL,0                  ;(MinL - MaxL), store W
            btfss       STATUS,C                ;1,(MinL => MaxL)
            goto        stay_0                  ;(MinL < MaxL)
            goto        Wave                    ;(MinL => MaxL)


stay_0

            bcf         PORTE,2                 ;Turn-off Accelerometer
            bcf         PORTE,1                 ;Power-off Op-Amp

            movfw       MaxH
            movwf       ASampH
            movfw       MaxL
            movwf       ASampL
            movfw       MinH
            movwf       BSampH
            movfw       MinL
            movwf       BSampL
            call        Order                   ;Calculate absolute difference
            movfw       AbsoluteH
            movwf       AccelppH
            movwf       MeanH
            movfw       AbsoluteL
            movwf       AccelppL
            movwf       MeanL

            bcf         STATUS,C
            rrf         MeanH,1
            rrf         MeanL,1                 ;Rotate Left, store F [Divide by 2]

            movfw       MinL
            addwf       MeanL,1                 ;Add MinL + MeanL, store in MeanL
            btfsc       STATUS,C                ;0, no Overflow when (MinL + MeanL)
            incf        MeanH                   ;Overflow when (MinL + MeanL)
            movfw       MinH
            addwf       MeanH,1                 ;;Add MinH + MeanH, store in MeanH

            return                              ;Do not display anything
;***********Calculate accelerometer Max, Min and Mean value (End)***************************************************
;***********Calculate Zero crossing shift (Start)*******************************
Phase                   ;Zero crossing time between Generator(CCP1) and Accelerometer(AN0)
                        ;Input= MeanH/L
                        ;output= PhaseH/L


            bsf         PORTE,2                 ;Power-on Accelerometer
            bsf         PORTE,1                 ;Power-on Op-Amp
            call        delay_1ms_4MHz          ;To allow settling time on Op-AMP
            clrf        Counter_1
            clrf        PhaseH
            clrf        PhaseL

Phase_0
            clrf        CCP1CON                 ;Suggested by DS31014A
            movlw       b'00000100'             ;Capture mode, every falling edge, start capture mode
            movwf       CCP1CON                         ;
            bcf         PIR1,CCP1IF             ;clear flag (sugested by AN594)

            clrf        TMR1H
            clrf        TMR1L

            ;Do not take into account the first cycle to avoid error due to opamp turning-on when the generator is
            ;in positive part of its cycle
            btfss       PIR1,CCP1IF             ;1,Capture occurred.
            goto        $-1                     ;Capture NOT occurred

            call        Delay_3msec_4MHz
            bcf         PIR1,CCP1IF             ;clear flag

            btfss       PIR1,CCP1IF             ;1,Capture occurred.
            goto        $-1                     ;Capture NOT occurred

            bsf         T1CON,TMR1ON            ;Enable timer1

Phase_1                 ;Wait here till mean > current
            bcf         Waveside,2              ;Select AN0 (accelerometer)
            call        ADCconversion           ;Result in "ResultHigh<1:0>" and "ResultLow<7:0>" (Bank 0)

            movfw       ResultHigh              ;
            movwf       SecondSampH             ;
            movfw       ResultLow               ;
            movwf       SecondSampL

            movfw       SecondSampH
            subwf       MeanH,0                 ;(MeanH - SecondSampH), store in W
```

```
            btfss       STATUS,C                ;1, (MeanH => SecondSampH)
            goto        Phase_1                 ;(MeanH < SecondSampH)
            btfss       STATUS,Z                ;1,(MeanH = SecondSampH)
            goto        Phase_2_1               ;(MeanH > SecondSampH)

            movfw       SecondSampL
            subwf       MeanL,0                 ;(MeanL - SecondSampL), store in W
            btfss       STATUS,C                ;0,(MeanL => SecondSampL)
            goto        Phase_1                 ;(MeanL < SecondSampL)

Phase_2_1
            call        Delay_3msec_4MHz

            btfss       PORTC,2                 ;If port is UP is a wrong measurement
            goto        Phase_2_2               ;Correct measurement
            bcf         T1CON,TMR1ON            ;Disable timer1
            bcf         PIR1,CCP1IF             ;clear flag


            goto        Phase_0

Phase_2_2
            call        Delay_3msec_4MHz

Phase_2                 ;Wait here till mean < current

            bcf         Waveside,2              ;Select AN0 (accelerometer)
            call        ADCconversion           ;Result in "ResultHigh<1:0>" and "ResultLow<7:0>" (Bank 0)

            movfw       ResultHigh              ;
            movwf       SecondSampH             ;
            movfw       ResultLow               ;
            movwf       SecondSampL

            movfw       SecondSampH
            subwf       MeanH,0                 ;(MeanH - SecondSampH), store in W
            btfss       STATUS,C                ;1, (MeanH => SecondSampH)
            goto        Phase_3_1               ;(MeanH < SecondSampH)
            btfss       STATUS,Z                ;1,(MeanH = SecondSampH)
            goto        Phase_2                 ;(MeanH > SecondSampH)

            movfw       SecondSampL
            subwf       MeanL,0                 ;(MeanL - SecondSampL), store in W
            btfss       STATUS,C                ;0,(MeanL => SecondSampL)
            goto        Phase_3_1               ;(MeanL < SecondSampL)
            goto        Phase_2

Phase_3_1
            call        Delay_3msec_4MHz
            call        Delay_3msec_4MHz

Phase_3                 ;Wait here till mean > current
            bcf         Waveside,2              ;Select AN0 (accelerometer)
            call        ADCconversion           ;Result in "ResultHigh<1:0>" and "ResultLow<7:0>" (Bank 0)

            movfw       ResultHigh              ;
            movwf       SecondSampH             ;
            movfw       ResultLow               ;
            movwf       SecondSampL

            movfw       SecondSampH
            subwf       MeanH,0                 ;(MeanH - SecondSampH), store in W
            btfss       STATUS,C                ;1, (MeanH => SecondSampH)
            goto        Phase_3                 ;(MeanH < SecondSampH)
            btfss       STATUS,Z                ;1,(MeanH = SecondSampH)
            goto        Phase_4                 ;(MeanH > SecondSampH)

            movfw       SecondSampL
            subwf       MeanL,0                 ;(MeanL - SecondSampL), store in W
            btfss       STATUS,C                ;0,(MeanL => SecondSampL)
            goto        Phase_3                 ;(MeanL < SecondSampL)

Phase_4                                         ;Average 4 measurements?

            bcf         T1CON,TMR1ON            ;Disable timer1
            clrf        CCP1CON                 ;Disable comparator
            bcf         PIR1,CCP1IF             ;clear flag

;verify that the last reading is within the range expected <2800usec
            movfw       TMR1H                   ;
            sublw       d'10'                   ;Verify if TMR1H/L > 2800
            btfsc       STATUS,C                ;0,(TMR1H/L  > 2800), therefore bad reading
            goto        Phase_4_1               ;restart last measurement
            goto        Phase_0

Phase_4_1
            movfw       TMR1L                   ;ADD TIMER1 + Phase (Add phase measure of each cycle)
            addwf       PhaseL,1                ;ADD TMR1L + PhaseL, store f
            btfsc       STATUS,C                ;Carry?
            incf        TMR1H,1                 ;Add 1, store f
            movfw       TMR1H
            addwf       PhaseH,1                ;ADD TMR1H + PhaseH, store f

            incf        Counter_1,1

            btfsc       Counter_1,2             ;0, 4 Measures done?.
            goto        Phase_5                 ;Yes, 4 measures DONE
```

```
                goto        Phase_0

Phase_5
                clrf        CCP1CON                 ;Disable comparator
                bcf         PIR1,CCP1IF             ;clear flag
                bcf         PORTE,2                 ;Turn-off Accelerometer
                bcf         PORTE,1                 ;Power-off Op-Amp
                clrf        Counter_1

Phase_5_0
                bcf         STATUS,C
                rrf         PhaseH,1
                rrf         PhaseL,1                ;Rotate Left, store F [Divide by 2]

                incf        Counter_1,1
                btfss       Counter_1,1             ;1, 4 division done.
                goto        Phase_5_0

                return
;***********Calculate Zero crossing shift (End)********************************
;***********Calculate phase shift (Start)********************************
Phase_Shift                 ;Calculate Phase Shift between Generator Vs Accelerometer
                            ;Input: Phase, Freq, OverAccelH/l
                            ;Output: Shift, Waveside<6>: 0-> Negative shift, 1-> Positive Shift.


                btfss       Waveside,4              ;1,No error in frequency calculation
                return


                movfw       FreqH                   ;Move "Freq" to "Cycle_1" register to calculate time for 1 cycle
                movwf       Cycle_1H                ;
                movfw       FreqL
                movwf       Cycle_1L


                clrf        Counter_1

Phase_Shift_1                                       ;Divide "Freq" by 8 to obtain 1 cycle count
                incf        Counter_1               ;Increment Counter_1 resgister
                btfsc       Counter_1,2             ;0,8 division done?
                goto        Phase_Shift_2           ;1 cycle count DONE
                bcf         STATUS,C
                rrf         Cycle_1H,1
                rrf         Cycle_1L,1              ;Rotate Left, store F [Divide by 2]
                goto        Phase_Shift_1

Phase_Shift_2                                       ;Calculate Phase shift count (Value and If positive or negative)


                movfw       Cycle_1H                ;Move 1 cycle count to ASamp
                movwf       ASampH
                movfw       Cycle_1L
                movwf       ASampL
                movfw       PhaseH                  ;Move Phase register to BSamp
                movwf       BSampH
                movfw       PhaseL
                movwf       BSampL
                call        Order                   ;Input: ASampH, ASampL, BSampH, BSampL
                                                    ;Output: AbsoluteH, AbsoluteL, Waveside<0>
                                                    ;Waveside<0> =1 if          (ASamp < BSamp) Increasing
                                                    ;Waveside<0> =0 if          (ASampH > BSampH) OR (ASampL => BSampL) Decreasing
                movfw       AbsoluteH               ;Move to "Shift" register
                movwf       ShiftH
                movfw       AbsoluteL
                movwf       ShiftL

Positive2

                btfsc       Waveside,0              ;0,Negative value
                goto        Phase_Shift_3
                bcf         Waveside,6              ;0, Negative shift
                goto        Phase_Shift_4

Phase_Shift_3                                       ;Positive value
                bsf         Waveside,6              ;1, Positive shift

Phase_Shift_4                           ;Adjustment due to OVER ACCELERATION-------------------------**************-------------*********--
;
;               btfss       Waveside,6              ;1,Positive
;               goto        Phase_Shift_5 ;Negative
;
;               movfw       OverAccelL
;               addwf       ShiftL,1                ;add
;               btfsc       STATUS,C
;               incf        ShiftH,1
;               movfw       OverAccelH
;               addwf       ShiftH,1
;
;               return

                return
;Phase_Shift_5                                      ;Shift is positive
;               movfw       OverAccelH              ;Move over acceleration to ASamp
;               movwf       ASampH
;               movfw       OverAccelL
```

```
;           movwf       ASampL
;           movfw       ShiftH                  ;Move Phase register to BSamp
;           movwf       BSampH
;           movfw       ShiftL
;           movwf       BSampL
;           call        Order                   ;Input: ASampH, ASampL, BSampH, BSampL
;                                               ;Output: AbsoluteH, AbsoluteL, Waveside<0>
;                                               ;Waveside<0> =1 if      (ASamp < BSamp) Increasing
;                                               ;Waveside<0> =0 if      (ASampH > BSampH) OR (ASampL => BSampL) Decreasing
;           movfw       AbsoluteH               ;Move to "Shift" register
;           movwf       ShiftH
;           movfw       AbsoluteL
;           movwf       ShiftL
;

;;WHEN Adding the error
;           btfss       Waveside,0              ;1, OverAccel < Shift -> Positive number (no need to change flag)
;           bsf         Waveside,6              ;0, OverAccel >= Shift -> Negative number
;
;           return

;***********Calculate phase shift (Start)********************************
;***********Calculate Detuning adjustment (Start)********************************
Detuning                ;Calculate the over acceleration and set the detuning adjustment value
                        ;Input= FreqH/L, AccelppH/L,
                        ;Output= OverAccelH/L.Waveside2<1> 0-> acceleration < maximum, 1-> acceleration above maximum
                        ;Maximum accel formula= 420-(Period/64)

            clrf        OverAccelH
            clrf        OverAccelL
            clrf        Counter_1

            bsf         Counter_1,0             ;add 1 to Counter_1
            movfw       FreqH
            movwf       Detuning_Reg1H
            movfw       FreqL
            movwf       Detuning_Reg1L

            movlw       d'1'                    ;Mov d'420 to Reg2
            movwf       Detuning_Reg2H
            movlw       d'164'
            movwf       Detuning_Reg2L

Detuning_1                                      ;Divide "FreqH/L" by 64 to obtain
            incf        Counter_1               ;Increment Counter_1 resgister
            btfsc       Counter_1,3             ;0,64 division done?
            goto        Detuning_2              ;1 cycle count DONE
            bcf         STATUS,C
            rrf         Detuning_Reg1H,1
            rrf         Detuning_Reg1L,1        ;Rotate Left, store F [Divide by 2]
            goto        Detuning_1

Detuning_2                                      ;Substract Reg2-Reg1
            bcf         STATUS,C
            movfw       Detuning_Reg1L
            subwf       Detuning_Reg2L,1        ;subtract (f-w) (Reg2L - Reg1L), store in Reg1
            btfss       STATUS,C
            decf        Detuning_Reg2H

            movfw       Detuning_Reg1H
            subwf       Detuning_Reg2H,1        ;subtract (f-w) (Reg2H - Reg1H), store in Reg1

Detuning_3                                      ;calculate over acceleration

            movfw       Detuning_Reg2H          ;Move maximum accel allowed to ASamp
            movwf       ASampH
            movfw       Detuning_Reg2L
            movwf       ASampL
            movfw       AccelppH                ;Move current accel to BSamp
            movwf       BSampH
            movfw       AccelppL
            movwf       BSampL
            call        Order                   ;Input: ASampH, ASampL, BSampH, BSampL
                                                ;Output: AbsoluteH, AbsoluteL, Waveside<0>
                                                ;Waveside<0> =1 if      (ASamp < BSamp) Increasing
                                                ;Waveside<0> =0 if      (ASampH > BSampH) OR (ASampL => BSampL) Decreasing

            btfss       Waveside,0              ;1, current acceleration > maximum permissible
            goto        Detuning_7              ;0, current acceleration < maximum

;Over acceleration value and set error
            bsf         Waveside2,1             ;1-> acceleration > maximum

            movfw       AbsoluteH               ;Move to OverAccel register
            movwf       OverAccelH              ;Over acceleration error
            movfw       AbsoluteL
            movwf       OverAccelL

;Test if acceleration is higher than 255'b = 442mg. for a variable error adjustment

            movf        OverAccelH,1            ;update Z flag
            btfss       STATUS,Z                ;1, OverAccel < 255
            goto        Detuning_5_B            ;0, over acceleration > 255'b, divide by 32

;{Try division by 32 after 255'b
            btfsc       OverAccelL,7            ;0, over acceleration < 127'b, divide by 16
            goto        Detuning_5_B            ;1, over acceleration > 127'b, divide by 32
```

```
            clrf        Counter_1               ;Division by 16
            bcf         STATUS,C

Detuning_4                                      ;Divide the error by 16
            btfsc       Counter_1,2             ;0,16 division done?/ Or division by 8
            goto        Detuning_5              ;1 cycle count DONE
            bcf         STATUS,C
            incf        Counter_1               ;Increment Counter_1 resgister
            rrf         OverAccelH,1
            rrf         OverAccelL,1            ;Rotate Left, store F [Divide by 2]
            goto        Detuning_4

Detuning_5_B
            movlw       d'3'                    ;Division by 32
            movwf       Counter_1               ;Division by 32
            movlw       d'96'                   ;add 96'd to compensate for division. (125/16=7, 128/32=4)(3*32=96)
            addwf       OverAccelL,1
            btfsc       STATUS,C
            incf        OverAccelH,1


Detuning_5_A
            btfsc       Counter_1,3             ;0, Division by 32
            goto        Detuning_5              ;division DONE
            bcf         STATUS,C
            incf        Counter_1               ;Increment Counter_1 resgister
            rrf         OverAccelH,1
            rrf         OverAccelL,1            ;Rotate Left, store F [Divide by 2]
            goto        Detuning_5_A

Detuning_5                                      ;Calculate adjusment due to over acceleration

            movfw       OverAccelL
            btfsc       STATUS,Z                ;0, Error>0
            goto        Detuning_7              ;1, Error=0
            movwf       Counter_1
            clrf        OverAccelH
            clrf        OverAccelL

Detuning_6                                      ;erros calculated as the number of steps belowe optimal position
            movlw       d'1'                    ;error adjustment
            addwf       OverAccelL,1
            btfsc       STATUS,C                ;0, No carry
            incf        OverAccelH,1
            decfsz      Counter_1,1             ;
            goto        Detuning_6
            return

Detuning_7                                      ;Error =0, no need for adjustment.
            return
;***********Calculate Detuning adjustment (End)********************************
;*****************Control using Phase shift (Start)*******************************************
Ctrl_Phase                          ;Control using Phase shift. Move acordenly and update current Step.
                                    ;Needed= Shift, Waveside<6>
                                    ;Output= Possible update StepH/L, Waveside2<0>, 0-> Not finished, 1->Finished

            bcf         Waveside2,0             ;Default value, Ctrl_Phase NOT finished
            btfsc       Waveside,6              ;0,Negative value
            goto        Ctrl_Phase_6            ;Positive value,

;Negative shift
Ctrl_Phase_3                                    ;Negative difference, need to move forward
            movf        ShiftH,1                ;Update Z status
            btfss       STATUS,Z                ;1, Absoulte < 256
            goto        Ctrl_Phase_5            ;Optimal more than 7 steps from current (> 256)

            movlw       d'120'                  ;Verify if phase shift is smaller than 120
            subwf       ShiftL,0                ;ShiftL - 150, store in W
            btfss       STATUS,C                ;1, ShiftL >= 150 steps.
            goto        Ctrl_Phase_NoMove       ;Absolute < 150 steps

Ctrl_Phase_4                                    ;Absolute (negative) > 120 and < 256
            call        extend                  ;Move 1 step forward and measure Phase shift
            call        MotorOFF

            goto        Ctrl_Phase_Continue     ;Calculate phase shift again

Ctrl_Phase_5                                    ;Actual Position more than 7 steps below optimal (negative) (>256)
            call        extend                  ;Extend 1 step
            call        extend                  ;Extend 1 step
            call        MotorOFF

            goto        Ctrl_Phase_Continue     ;Calculate phase shift again

;Positive shift
Ctrl_Phase_6                                    ;Positive difference, need to move backwards

            movf        ShiftH,1                ;Update Z status
            btfss       STATUS,Z                ;1, Absoulte < 256
            goto        Ctrl_Phase_8            ;Optimal more than 3 steps from current      (> 256)

            movlw       d'100'                  ;Verify if phase shift is smaller than 100
            subwf       ShiftL,0                ;ShiftL - 100, store in W
            btfss       STATUS,C                ;1, ShiftL >= 100 steps.
            goto        Ctrl_Phase_NoMove       ;Absolute < 100 steps
```

```
Ctrl_Phase_7                                    ;Absolute (Positive) > 63 and < 256
;           call        retract                 ;Move 1 step backward and measure Phase shift
;           call        MotorOFF
;           goto        Ctrl_Phase_Continue                 ;Calculate phase shift again

Ctrl_Phase_8                                    ;Actual Position above optimal (positive) (>255)
;           decf        ShiftH,0                ;AbsoluteH - 1, store W
;           btfss       STATUS,Z                ;1, Absolute < 512 and > 256 (Positive)
;           goto        Ctrl_Phase_9            ; Absolute > 511 (Positive)

            call        retract                 ;Move 1 step backward
            call        retract                 ;Move 1 step backward
            call        MotorOFF

            goto        Ctrl_Phase_Continue     ;Calculate phase shift again

Ctrl_Phase_9                                    ; Absolute > 511 (Positive)
            call        retract                 ;Move 1 step backward
            call        retract                 ;Move 1 step backward
            call        retract                 ;Move 1 step backward
            call        retract                 ;Move 1 step backward
            call        retract                 ;Move 1 step backward
            call        retract                 ;Move 1 step backward
            call        retract                 ;Move 1 step backward
            call        MotorOFF
            goto        Ctrl_Phase_Continue     ;Calculate phase shift again


Ctrl_Phase_NoMove

            call        Freqmeter               ;USING LM2903
                                                ;Measure frequency from signal at CCP1
                                                ;input= <NONE>
                                                ;output= FreqH/L

            call        Optimum                 ;Calculate the optimal position
                                                ;Input= FreqH/L
                                                ;Output= OptStepL
                                                ;Waveside<4>= 1 -> Ok, 0 -> Calculation error (measure not valid)
            btfss       Waveside,4              ;1,No error in calculation
            goto        Ctrl_Phase_NoMove
            clrf        StepH                   ;Step High
            movfw       OptStepL
            movwf       StepL                   ;Step Low
            bsf         Waveside2,0             ;Ctrl_Phase FINISHED
            return


Ctrl_Phase_Continue

            call        low_routine             ;Sleep ROUTINE
            return                              ;[TEST]

;*****************Control using Phase shift (End)*******************************************
;***********************Actuator DRIVER (Start)*********************************************
;EXTENSION
Extension
extend1
            call        extend
            btfss       PORTD,1                 ;Is the continuos switch pressed(pressed=0)?
            goto        OneStepExtend           ;No, one step taken.

            btfsc       PORTD,3                 ;Is the Extension switch still pressed?
            goto        extend1                 ;Continue extending

OneStepExtend
            call        MotorOFF                ;turn OFF all Mosfet

OneStepExtend2
            movlw       d'100'
            call        delay_1msec_TimesW_4MHz
            btfsc       PORTD,3                 ;Is the Extension switch still pressed?
            goto        OneStepExtend2          ;wait

            ;goto       WaitForConver_0         ;Return for next acitivity: Freqmeter, extention or retractions?
            return

;RETRACTION
Retraction
retract1
            call        retract

            btfss       PORTD,1                 ;Is the continuos switch pressed(pressed=0)?
            goto        OneStepRetract          ;No, one step taken.

            btfsc       PORTD,2                 ;Is the Retraction switch still pressed?
            goto        retract1                ;keep retracting

OneStepRetract
            call        MotorOFF                ;turn OFF all Mosfet

OneStepRetract2
            movlw       d'100'
            call        delay_1msec_TimesW_4MHz
            btfsc       PORTD,2                 ;Is the Retraction switch still pressed?
            goto        OneStepRetract2         ;wait
```

```
            return
;************************Actuator DRIVER (End)**********************************************
;*************************Extend motor (Start)*************************
extend
            bcf         Waveside,1              ;Defines speed Waveside<1> (0= retract, 1= extend)
            bsf         STATUS,C                ;set Carry flag
            btfss       TravelStep,0            ;Skip if set, Is the step 1 the next?
            goto        GiveStep1               ;Step 1

            btfss       TravelStep,1            ;Skip if clear, Is the step 2 the next?
            goto        GiveStep2               ;Step2

            btfss       TravelStep,2            ;Skip if clear, Is the step 3 the next?
            goto        GiveStep3               ;Step3

            btfss       TravelStep,3            ;Skip if clear, Is the step 4 the next?
            goto        GiveStep4               ;Step4

            clrf        TravelStep              ;Clear the value of TravelStep (Error case) no suitable next step
            goto        loopForward             ;Error case

GiveStep1
            rlf         TravelStep,1            ;rotate Left, store the value in TravelStep
            call        step1
            goto        loopForward

GiveStep2
            rlf         TravelStep,1            ;rotate Left, store the value in TravelStep
            call        step2
            goto        loopForward

GiveStep3
            rlf         TravelStep,1            ;rotate Left, store the value in TravelStep
            call        step3
            goto        loopForward

GiveStep4
            clrf        TravelStep              ;Clear TravelStep
            call        step4
            goto        loopForward

loopForward
            incf        StepL,1                 ;Increment Step counter, store F
            btfsc       STATUS,Z                ;0, StepL+1 =0. (Overflow)
            incf        StepH                   ;Increment StepH due to overflow

            return
;*************************Extend motor (End)*************************
;*************************Retract motor (Start)*************************
retract
;           bsf         PORTA,2                 ;(TEST)

            bsf         Waveside,1              ;Defines speed Waveside<1> (0= retract, 1= extend)
            bcf         STATUS,C                ;clear Carry flag
            btfss       TravelStep,0            ;Skip if set, Is the current step 4?
            goto        RetractStep3            ;Yes, Next Step 3

            btfss       TravelStep,1            ;Skip if set, Is the current step 1?
            goto        RetractStep4            ;Yes, Next Step 4

            btfss       TravelStep,2            ;Skip if set, Is the current step 2?
            goto        RetractStep1            ;Yes, Next Step 1

            btfss       TravelStep,3            ;Skip if set, Is the current step 3?
            goto        RetractStep2            ;Yes, Next Step 2

            clrf        TravelStep              ;Clear the value of TravelStep (Error case) no suitable next step
            goto        loopBackward ;Error case

RetractStep3
            movlw       b'00000111'             ;move status:Step3 to W
            movwf       TravelStep              ;move status: Step 3 to TravelStep
            call        step3
            goto        loopBackward

RetractStep4
            rrf         TravelStep,1            ;rotate rigth, store the value in TravelStep
            call        step4
            goto        loopBackward

RetractStep1
            rrf         TravelStep,1            ;rotate rigth, store the value in TravelStep
            call        step1
            goto        loopBackward

RetractStep2
            rrf         TravelStep,1            ;rotate rigth, store the value in TravelStep
            call        step2
            goto        loopBackward

loopBackward
            movfw       StepL                   ;Update Z flag
            btfsc       STATUS,Z                ;0,StepL NOT= 0.
            decf        StepH
            decf        StepL
            return
```

```
;************************Retract motor (End)************************
;************************STEPPER MOTOR Sequence (Start)************************
;PORTB.7    ->          Q1
;PORTB.6    ->          Q4
;PORTB.5    ->          Q2
;PORTB.4    ->          Q3
;PORTB.3    ->          Q5
;PORTB.2    ->          Q8
;PORTB.1    ->          Q6
;PORTB.0    ->          Q7

step1                                                       ;10011001
            bsf         PORTB,7                 ; High (Turn-off P-Mosfet Q1)
            bcf         PORTB,6                 ; Low (Turn-off N-Mosfet Q4)
            nop

            bcf         PORTB,5                 ; Low (Turn-on P-Mosfet Q2)
            bsf         PORTB,4                 ; High (Turn-on N-Mosfet Q3)

            bsf         PORTB,3                 ; High (Turn-off P-Mosfet Q5)
            bcf         PORTB,2                 ; Low (Turn-off N-Mosfet Q8)
            nop

            bcf         PORTB,1                 ; Low (Turn-on P-Mosfet Q6)
            bsf         PORTB,0                 ; High (Turn-on N-Mosfet Q7)

            call        Speed
            return

step2                                           ;01101001
            bsf         PORTB,5                 ; High (Turn-off P-Mosfet Q2)
            bcf         PORTB,4                 ; Low (Turn-off N-Mosfet Q3)
            nop

            bcf         PORTB,7                 ; Low (Turn-on P-Mosfet Q1)
            bsf         PORTB,6                 ; High (Turn-on N-Mosfet Q4)

            bsf         PORTB,3                 ; High (Turn-off P-Mosfet Q5)
            bcf         PORTB,2                 ; Low (Turn-off N-Mosfet Q8)
            nop

            bcf         PORTB,1                 ; Low (Turn-on P-Mosfet Q6)
            bsf         PORTB,0                 ; High (Turn-on N-Mosfet Q7)

            call        Speed
            return

step3                                                       ;01100110
            bsf         PORTB,5                 ; High (Turn-off P-Mosfet Q2)
            bcf         PORTB,4                 ; Low (Turn-off N-Mosfet Q3)
            nop

            bcf         PORTB,7                 ; Low (Turn-on P-Mosfet Q1)
            bsf         PORTB,6                 ; High (Turn-on N-Mosfet Q4)

            bsf         PORTB,1                 ; High (Turn-off P-Mosfet Q6)
            bcf         PORTB,0                 ; Low (Turn-off N-Mosfet Q7)
            nop

            bcf         PORTB,3                 ; Low (Turn-on P-Mosfet Q5)
            bsf         PORTB,2                 ; High (Turn-on N-Mosfet Q8)

            call        Speed
            return

step4                                                       ;10010110
            bsf         PORTB,7                 ; High (Turn-off P-Mosfet Q1)
            bcf         PORTB,6                 ; Low (Turn-off N-Mosfet Q4)
            nop

            bcf         PORTB,5                 ; Low (Turn-on P-Mosfet Q2)
            bsf         PORTB,4                 ; High (Turn-on N-Mosfet Q3)

            bsf         PORTB,1                 ; High (Turn-off P-Mosfet Q6)
            bcf         PORTB,0                 ; Low (Turn-off N-Mosfet Q7)
            nop

            bcf         PORTB,3                 ; Low (Turn-on P-Mosfet Q5)
            bsf         PORTB,2                 ; High (Turn-on N-Mosfet Q8)

            call        Speed
            return
;************************STEPPER MOTOR Sequence (End)************************
;************************Actuator Speed (Start)************************
Speed                   ;Waveside<1> (0= retract, 1= extend)

Speed_1                 ;extend, max speed 200 steps/sec

            call        Delay_2.5msec_4MHz      ;Delay for
            call        Delay_2.5msec_4MHz      ;200 steps/sec
            return
;************************Actuator Speed (End)************************

;*********Routine to turn-off the H-Bridges and send to ground actuator conections (Start)******************
MotorOFF
            bsf         PORTB,7                 ; High (Turn-off P-Mosfet Q1)
            bsf         PORTB,5                 ; High (Turn-off P-Mosfet Q2)
```

```
                bsf     PORTB,3                 ; High (Turn-off P-Mosfet Q5)
                bsf     PORTB,1                 ; High (Turn-off P-Mosfet Q6)

                nop

                bcf     PORTB,6                 ; Low (Turn-off N-Mosfet Q4)
                bcf     PORTB,4                 ; Low (Turn-off N-Mosfet Q3)
                bcf     PORTB,0                 ; Low (Turn-off N-Mosfet Q7)
                bcf     PORTB,2                 ; Low (Turn-off N-Mosfet Q8)
                return
;*********Routine to turn-off the H-Bridges and send to ground actuator conections (End)******************
;****************************Calculate absolute difference (Start)*************************************
Order                   ;Order the samplings, higher and lower and calculate absolute diference
                        ;Input: ASampH, ASampL, BSampH, BSampL
                        ;Output: AbsoluteH, AbsoluteL, Waveside<0>
                        ;Waveside<0> =1 if       (ASamp < BSamp) Increasing
                        ;Waveside<0> =0 if       (ASampH > BSampH) OR (ASampL => BSampL) Decreasing

                movfw   BSampH                  ;Register with value of second sampling
                subwf   ASampH,0                ;subtract W form f (f-W)(ASampH(OLD) - BSampH(NEW)) store result in W
                btfsc   STATUS,C                ;0,(ASampH < BSampH)
                goto    TestLSB                 ;(ASampH => BSampH)
                goto    Second_First            ;(ASampH < BSampH)

TestLSB
                btfss   STATUS,Z                ;1,(ASampH = ASampH)
                goto    First_Second            ;0,(ASampH > ASampH)
                movfw   BSampL
                subwf   ASampL,0                ;subtract W form f (f-W)(ASampL(OLD) - BSampL(NEW)) store result in W
                btfsc   STATUS,C                ;0,(ASampL < BSampL)
                goto    First_Second            ;ASampL => BSampL

Second_First                                    ;(ASamp < BSamp) Increasing
                bsf     Waveside,0              ;Wave its increasing its value
                movfw   BSampL
                movwf   Value1L
                movfw   BSampH
                movwf   Value1H

                movfw   ASampL
                movwf   Value2L
                movfw   ASampH
                movwf   Value2H
                goto    absolute

First_Second            ;(ASampH > BSampH) OR (ASampL => BSampL) Decreasing
                bcf     Waveside,0              ;Wave its decreasing its value
                movfw   ASampL
                movwf   Value1L
                movfw   ASampH
                movwf   Value1H

                movfw   BSampL
                movwf   Value2L
                movfw   BSampH
                movwf   Value2H

absolute                ;16-bits substraction (Value1 - Value2)
                        ;Input: Value1H, Value1L, Value2H, Value2L
                        ;Output: AbsoluteH, AbsoluteL
                movfw   Value2L
                subwf   Value1L,0               ;subtract (f-w) (Value1L - Value2L)
                movwf   AbsoluteL
                btfsc   STATUS,C                ;0, (Value1L < Value2L)
                goto    Noborrow
                decf    Value1H,1               ;Decrement by 1., store in f

Noborrow
                movfw   Value2H
                subwf   Value1H,0               ;subtract (f-w) (Value1H - Value2H), store in W
                movwf   AbsoluteH
                return
;****************************Calculate absolute difference (End)*************************************
;************************ADC conversion (Start)****************************************************
ADCconversion           ;Returns Analog-to-Digital conversion in <ResultHigh> and <ResultLow> registers.
                        ;Input: Waveside<3,2>
                        ;Waveside                <3          2>
                        ;AN0                      0          0
                        ;AN1                      0          1
                        ;Vref                     1          X
                        ;Output: ResultHigh, ResultLow

                btfss   Waveside,3              ;Waveside<3> (1-> Vref, 0->AN0 or AN1)
                goto    ADCconversion_2         ;AN0 or AN1
                bcf     Waveside,3              ;Erase flag for Vref.
                movlw   b'01111101'             ;ADCS=Fosc/8;Channel:Fixed Ref 0.6V,Enable ADC
                movwf   ADCON0
                goto    ADCconversion_1

ADCconversion_2
                movlw   b'01000101'             ;ADCS=Fosc/8;Channel:AN1,Enable ADC
                movwf   ADCON0

                btfss   Waveside,2              ;1, AN1 selected
                bcf     ADCON0,2                ;Channel AN0

ADCconversion_1
```

```
            call        AcqTime                 ;Acquisition time delay
            bsf         ADCON0,GO               ;start conversion
            btfsc       ADCON0,GO               ;Is conversion done?
            goto        $-1                     ;No-> test again

            bcf         ADCON0,ADON                         ;Disable ADC, reduces current consumption
            movf        ADRESH,W                ;Move higher 8 bits to W
            movwf       ResultHigh              ;Store higher 8 bits
            bcf         STATUS,RP1              ;Bank1
            bsf         STATUS,RP0              ;
            movf        ADRESL,W                ;Move lower 8 bits to W;
            bcf         STATUS,RP1              ;Bank0
            bcf         STATUS,RP0              ;
            movwf       ResultLow               ;Store lower 8 bits

            return

AcqTime                                                                 ;Acquistion time delay
            nop
            nop
            nop
            nop
            nop
            nop
            return

;************************ADC conversion (End)*******************************************************
;***********************Convert 16-bit to 4 digit BCD (Start)***************************************
TwoBitesToBCD                           ;Converts 16-bit binary number to 4 digit BCD and send to LCD
;                                                           ;Input: NumH, NumL (binary number)
;                                                           ;Output: TenK, Thou, Hund,Tens, Ones.

;http://www.piclist.com/techref/microchip/math/radix/b2bu-16b5d.htm
                        clrf        TenK         ;B4
                        clrf        Thou        ;B3
                        clrf        Hund         ;B2
                        clrf        Tens       ;B1
                        clrf        Ones        ;B0

                        swapf       NumH,w      ;w  = A2*16+A3
    andlw   0x0F    ;w  = A3                    *** PERSONALLY, I'D REPLACE THESE 2
    addlw   0xF0            ;w  = A3-16    *** LINES WITH "IORLW b'11110000B' " -AW
    movwf   Thou            ;B3 = A3-16
    addwf   Thou,f          ;B3 = 2*(A3-16) = 2A3 - 32
    addlw   .226            ;w  = A3-16 - 30 = A3-46
    movwf   Hund            ;B2 = A3-46
    addlw   .50             ;w  = A3-46 + 50 = A3+4
    movwf   Ones            ;B0 = A3+4

    movf    NumH,w          ;w  = A3*16+A2
    andlw   0x0F            ;w  = A2
    addwf   Hund,f          ;B2 = A3-46 + A2 = A3+A2-46
    addwf   Hund,f          ;B2 = A3+A2-46  + A2 = A3+2A2-46
    addwf   Ones,f          ;B0 = A3+4 + A2 = A3+A2+4
    addlw   .233            ;w  = A2 - 23
    movwf   Tens            ;B1 = A2-23
    addwf   Tens,f          ;B1 = 2*(A2-23)
    addwf   Tens,f          ;B1 = 3*(A2-23) = 3A2-69 (Doh! thanks NG)

    swapf   NumL,w          ;w  = A0*16+A1
    andlw   0x0F            ;w  = A1
    addwf   Tens,f          ;B1 = 3A2-69 + A1 = 3A2+A1-69 range -69...-9
    addwf   Ones,f          ;B0 = A3+A2+4 + A1 = A3+A2+A1+4 and Carry = 0 (thanks NG)

    rlf     Tens,f          ;B1 = 2*(3A2+A1-69) + C = 6A2+2A1-138 and Carry is now 1 as tens register had to be negitive
    rlf     Ones,f          ;B0 = 2*(A3+A2+A1+4) + C = 2A3+2A2+2A1+9 (+9 not +8 due to the carry from prev line, Thanks NG)
    comf    Ones,f          ;B0 = ~(2A3+2A2+2A1+9) = -2A3-2A2-2A1-10 (ones complement plus 1 is twos complement. Thanks SD)
    rlf     Ones,f          ;B0 = 2*(-2A3-2A2-2A1-10) = -4A3-4A2-4A1-20

    movf    NumL,w          ;w  = A1*16+A0
    andlw   0x0F            ;w  = A0
    addwf   Ones,f          ;B0 = -4A3-4A2-4A1-20 + A0 = A0-4(A3+A2+A1)-20 range -215...-5 Carry=0
    rlf     Thou,f          ;B3 = 2*(2A3 - 32) = 4A3 - 64

    movlw   0x07            ;w  = 7
    movwf   TenK            ;B4 = 7
    movlw   .10             ;w  = 10
Lb1:                                    ;do
    addwf   Ones,f          ; B0 += 10
    decf    Tens,f          ; B1 -= 1
    btfss   3,0
     goto   Lb1             ; while B0 < 0
Lb2:                                    ;do
    addwf   Tens,f          ; B1 += 10
    decf    Hund,f          ; B2 -= 1
    btfss   3,0
     goto   Lb2             ; while B1 < 0
Lb3:                                    ;do
    addwf   Hund,f          ; B2 += 10
    decf    Thou,f          ; B3 -= 1
    btfss   3,0
     goto   Lb3             ; while B2 < 0
Lb4:                                    ;do
    addwf   Thou,f          ; B3 += 10
    decf    TenK,f          ; B4 -= 1
    btfss   3,0
     goto   Lb4             ; while B3 < 0
```

```
                        retlw   0
;**********************Convert 16-bit to 4 digit BCD (End)**************************************
;**********************Division X_Int/Y= X_Int (Start)**************************************
;Division routine X_Int/Y= X_Int (This routine takes 229 cycles to be completed irrespective of the dividend or divisor values)
Div16by8                                                    ;Input: X_IntH, X_IntL, Y
                                                            ;Output: X_IntH, X_IntL
            movlw       d'16'
            movwf       Counter
  movf      Y,W                     ;keep Y value in accumulator
  clrf      Y                       ;and use Y register as temporary

Div16by8_1
            rlf         X_IntL, f   ;shift next msb into temporary
  rlf       X_IntH, f
  rlf       Y, f
  rlf       Counter, f  ;carry has 9th bit of temporary, copy carry to counter

  subwf     Y, f                    ;substract Y (in w) from temporary

            skpnc                   ;if no borrow, set Counter.0
  bsf       Counter, 0

  btfss     Counter, 0              ;if Counter.0 clear (borrow) restore temporary
  addwf     Y, f

  clrc                  ;restore counter
  rrf       Counter, f
                                                                                    ;at this point carry is the next bit of result
            decfsz      Counter, f              ;repeat 16 times to find integer part
  goto      Div16by8_1
                        ;shift last integer bit
  rlf       X_IntL, f
  rlf       X_IntH, f

            return
;**********************Division X_Int/Y= X_Int (End)**************************************
;*****************************DELAY ROUTINES (Start)****************************************
; Calls the delay 1ms routine the number of times specified by the W register @ 4MHz
delay_1msec_TimesW_4MHz
            movwf       R_DEL2
delay_1msec_TimesW_4MHz_0
            call        delay_1ms_4MHz
            decfsz      R_DEL2, F
            goto        delay_1msec_TimesW_4MHz_0
            return

;------------------------100usec-----------------------------------
Delay_100usec_4MHz                                  ;94 cycles
            movlw       0x1F
            movwf       d1
Delay_100usec_4MHz_0
            decfsz      d1, f
            goto        Delay_100usec_4MHz_0                        ;2 cycles
            goto        $+1                                 ;4 cycles (including call)
            return
;------------------------1msec-----------------------------------
;Delay routine 1msec @ 4Mhz
delay_1ms_4MHz
            movlw       d'248'
            movwf       R_DEL1
delay_1ms_loop
            nop
            decfsz      R_DEL1, F
            goto        delay_1ms_loop
            return

;------------------------1.6msec-----------------------------------
;Delay routine 1.6msec at 4MHz
Delay_1.6ms_4MHz                                    ;1593 cycles
            movlw       0x3E
            movwf       d1
            movlw       0x02
            movwf       d2
Delay_1.6ms_4MHz_0
            decfsz      d1, f
            goto        $+2
            decfsz      d2, f
            goto        Delay_1.6ms_4MHz_0                          ;3 cycles
            goto        $+1
            nop                                     ;4 cycles (including call)
            return
;------------------------2.5msec-----------------------------------
;Delay routine 2.5msec at 4MHz
Delay_2.5msec_4MHz                  ;@ 4MHz (2493 cycles)
            movlw       0xF2
            movwf       d1
            movlw       0x02
            movwf       d2
Delay_2.5msec_4MHz_0
            decfsz      d1, f
            goto        $+2
            decfsz      d2, f
            goto        Delay_2.5msec_4MHz_0                        ;3 cycles
            goto        $+1
            nop                                                     ;4 cycles (including call)
            return
;------------------------3msec-----------------------------------
```

```
;Delay routine 3msec at 4MHz
Delay_3msec_4MHz                ;@4MHz (2993 cycles)
        movlw   0x56
        movwf   d1
        movlw   0x03
        movwf   d2
Delay_3msec_4MHz_0
        decfsz  d1, f
        goto    $+2
        decfsz  d2, f
        goto    Delay_3msec_4MHz_0      ;3 cycles
        goto    $+1
        nop                                             ;4 cycles (including call)
        return
;------------------------3.3msec-----------------------------------
Delay_3.3msec_4MHz              ;3293 cycles
        movlw   0x92
        movwf   d1
        movlw   0x03
        movwf   d2
Delay_3.3msec_4MHz_0
        decfsz  d1, f
        goto    $+2
        decfsz  d2, f
        goto    Delay_3.3msec_4MHz_0            ;3 cycles
        goto    $+1
        nop                     ;4 cycles (including call)
        return
;------------------------10msec-----------------------------------
;Delay routine 10msec at 4MHz
Delay_10msec_4MHz               ;9993 cycles
        movlw   0xCE
        movwf   d1
        movlw   0x08
        movwf   d2
Delay_10msec_4MHz_0
        decfsz  d1, f
        goto    $+2
        decfsz  d2, f
        goto    Delay_10msec_4MHz_0             ;3 cycles
        goto    $+1
        nop                     ;4 cycles (including call)
        return

;------------------------1sec-----------------------------------
;Delay routine 1sec at 4MHz
Delay_1sec_4MHz                 ;@4MHz (999990 cycles)
        movlw   0x07
        movwf   d1
        movlw   0x2F
        movwf   d2
        movlw   0x03
        movwf   d3
Delay_1sec_4MHz_0
        decfsz  d1, f
        goto    $+2
        decfsz  d2, f
        goto    $+2
        decfsz  d3, f
        goto    Delay_1sec_4MHz_0       ;6 cycles
        goto    $+1
        goto    $+1
        goto    $+1                     ;4 cycles (including call)
        return
;****************************DELAY ROUTINES (End)****************************************
```

Bibliography

[1] S. P. Beeby, M. J. Tudor, and N. M. White, "Energy harvesting vibration sources for microsystems applications," *Measurement Science and Technology*, vol. 17, pp. 175-195, 2006.

[2] D. Zhu, M. J. Tudor, and S. P. Beeby, "Strategies for increasing the operating frequency range of vibration energy harvesters: a review," *Measurement Science and Technology*, vol. 21, pp. 1-29, 2010.

[3] D. Zhu, S. Roberts, M. J. Tudor, and S. P. Beeby, "Design and experimental characterization of a tunable vibration-based electromagnetic micro-generator," *Sensors and Actuators A: Physical*, vol. 158 (2), pp. 284-293, 2010.

[4] S. Beeby and N. M. White, *Energy Harvesting for Autonomous Systems*: artech house, 2010.

[5] S. R. Platt, S. Farritor, K. Garvin, and H. A. H. H. Haider, "The use of piezoelectric ceramics for electric power generation within orthopedic implants," *IEEE/ASME Transactions on Mechatronics*, vol. 10, pp. 455-461, 2005.

[6] E. Romero, R. O. Warrington, and M. R. Neuman, "Energy scavenging sources for biomedical sensors," *Physiological Measurement*, vol. 30, pp. R35-R62, 2009.

[7] D. Zhu, S. Roberts, J. Tudor, and S. Beeby, "A self powered tag for wireless structure health monitoring in aeronautical applications," in *Technical Digest PowerMEMS 2009*, 1-4 December. Washington DC., 2009, pp. 201-204.

[8] N. Elvin, A. Elvin, and D. H. Choi, "A self-powered damage detection sensor," *Journal of Strain Analysis for Engineering Design*, vol. 38, pp. 115-124, 2003.

[9] J. A. Paradiso and T. Starner, "Energy scavenging for mobile and wireless electronics," *Pervasive Computing, IEEE*, vol. 4, pp. 18-27, 2005.

[10] I. Stark, "Invited Talk: Thermal Energy Harvesting with Thermo Life," *International Workshop on Wearable and Implantable Body Sensor Networks, 2006*, pp. 19-22, 2006.

[11] M. Ferrari, V. Ferrari, M. Guizzetti, D. Marioli, and A. Taroni, "Characterization of Thermoelectric Modules for Powering Autonomous Sensors," *Instrumentation and Measurement Technology Conference Proceedings, 2007*, pp. 1-6, 2007.

[12] L. Mateu, C. Codrea, N. Lucas, M. Pollak, and P. Spies, "Human Body Energy Harvesting Thermogenerator for Sensing Applications," *International Conference on Sensor Technologies and Applications, 2007. SensorComm 2007*, pp. 366-372, 2007.

[13] A. Ricci, M. Grisanti, I. De Munari, and P. Ciapolini, "Design of a Low-Power Digital Core for Passive UHF RFID Transponder," *Conference on*

Digital System Design: Architectures, Methods and Tools, 2006. 9th EUROMICRO pp. 561-568, 2006.

[14] D. Rancourt, T. Ahmadreza, and L. G. Fréchette, "Evaluation of Centimeter-Scale Micro Wind Mills: Aerodynamics and Electromagnetic Power Generation," in *Technical Digest PowerMEMS 2007*, Freiburg, Germany, 2007, pp. 93-96.

[15] L. Greenemeier. (March 10, 2008, April 15). *It Came From the Sea--Renewable Energy, That Is*. Available: http://www.sciam.com/article.cfm?id=tidal-wave-renewable-energy

[16] P. D. Mitcheson, E. M. Yeatman, G. Kondala Rao, A. S. Holmes, and T. C. Green, "Energy Harvesting From Human and Machine Motion for Wireless Electronic Devices," *Proceedings of the IEEE*, vol. 96, pp. 1457-1486, 2008.

[17] E. P. James, M. J. Tudor, S. P. Beeby, N. R. Harris, P. Glynne-Jones, J. N. Ross, and N. M. White, "An investigation of self-powered systems for condition monitoring applications," *Sensors and Actuators A: Physical*, vol. 110, pp. 171-176, 2004.

[18] C. B. Williams and R. B. Yates, "Analysis of a micro-electric generator for microsystems," *Sensors and Actuators A: Physical*, vol. 52, pp. 8-11, 1996.

[19] S. Beeby, M. Tudor, R. Torah, S. Roberts, T. O'Donnell, and S. Roy, "Experimental comparison of macro and micro scale electromagnetic vibration powered generators," *Microsystem Technologies*, vol. 13, pp. 1647-1653, 2007.

[20] S. P. Beeby, R. N. Torah, M. J. Tudor, P. Glynne-Jones, T. O'Donnell, C. R. Saha, and S. Roy, "A micro electromagnetic generator for vibration energy harvesting," *Journal of Micromechanics and Microengineering*, vol. 17, pp. 1257-1265, 2007.

[21] S. M. Shahruz, "Design of mechanical band-pass filters for energy scavenging," *Journal of Sound and Vibration*, vol. 292, pp. 987-998, 2006.

[22] M. Ferrari, V. Ferrari, M. Guizzetti, D. Marioli, and A. Taroni, "Piezoelectric multifrequency energy converter for power harvesting in autonomous microsystems," *Sensors and Actuators A: Physical*, vol. 142, pp. 329-335, 2008.

[23] I. Sari, T. Balkan, and H. Kulah, "A Wideband Electromagnetic Micro Power Generator for Wireless Microsystems," *International Solid-State Sensors, Actuators and Microsystems Conference, 2007.*, pp. 275-278, 2007.

[24] I. Sari, T. Balkan, and H. Kulah, "An electromagnetic micro power generator for wideband environmental vibrations," *Sensors and Actuators A: Physical*, vol. 145-146, pp. 405-413, 2008.

[25] I. Sari, T. Balkan, and H. Kulah, "An electromagnetic micro energy harvester based on an array of parylene cantilevers," *Journal of Micromechanics and Microengineering*, vol. 19, p. 105023, 2009.

[26] J. Liu, H. Fang, Z. Xu, X. Mao, X. Shen, D. Chen, H. Liao, and B. Cai, "A MEMS-based piezoelectric power generator array for vibration energy harvesting," *Microelectronics Journal*, vol. 39, pp. 802-806, 2008.

[27] S. Qi, R. Shuttleworth, S. O. Oyadiji, and J. Wright, "Design of a multiresonant beam for broadband piezoelectric energy harvesting," *Smart Materials and Structures*, vol. 19, p. 094009, 2010.

[28] M. S. M. Soliman, E. M. Abdel-Rahman, E. F. El-Saadany, and R. R. Mansour, "A wideband vibration-based energy harvester," *Journal of Micromechanics and Microengineering,* vol. 18, pp. 1-8, 2008.

[29] M. Soliman, E. M. Abdel-Rahman, E. F. El-Saadany, and R. R. Mansour, "A Design Procedure for Wideband Micropower Generators," *Microelectromechanical Systems, Journal of,* vol. 18, pp. 1288-1299, 2009.

[30] K. Dogheche, B. Cavallier, P. Delobelle, L. Hirsinger, S. Ballandras, E. Cattan, D. Remiens, M. Marzencki, B. Charlot, and S. Basrour, "Piezoelectric micro-machined ultrasonic transducer (pMUT) for energy harvesting," *Ultrasonics Symposium, 2005,* vol. 2, pp. 939-942, 2005.

[31] K. Dogheche, B. Cavallier, P. Delobelle, L. Hirsinger, E. Cattan, D. Miens, M. Marzencki, B. Charlot, S. Basrour, and S. Ballandras, "A bi-stable micro-machined piezoelectric transducer for mechanical to electrical energy transformation," *Integrated Ferroelectrics,* vol. 80, pp. 305-315, 2006.

[32] R. Ramlan, M. J. Brennan, and B. R. Mace, "Nonlinear bistable mechanism for energy harvesting devices," *Proceedings of EURODYN 2008,* pp. 1-12, 2008.

[33] R. Ramlan, M. J. Brennan, B. R. Mace, and I. Kovacic, "Potential benefits of a non-linear stiffness in an energy harvesting device," *Nonlinear Dynamics,* vol. 59, pp. 545-558, 2010.

[34] R. Ramlan, M. J. Brennan, B. R. Mace, and I. Kovaic, "An investigation into the benefits of using a nonlinear stiffness in an energy harvesting device," *PhD review report. Institute of Sound and Vibration Research, University of Southampton.,* 2008.

[35] B. Andò, S. Baglio, C. Trigona, N. Dumas, L. Latorre, and P. Nouet, "Nonlinear mechanism in MEMS devices for energy harvesting applications," *Journal of Micromechanics and Microengineering,* vol. 20, p. 125020, 2010.

[36] S. P. Beeby, G. Ensell, M. Kraft, and N. White, *MEMS mechanical sensors*. Boston: Artech House, 2004.

[37] S. G. Burrow, L. R. Clare, A. Carrella, and D. Barton, "Vibration energy harvesters with non-linear compliance," *Active and Passive Smart Structures and Integrated Systems 2008,* vol. 6928, pp. 1-10, 2008.

[38] J. J. Yao and N. C. MacDonald, "A micromachined, single-crystal silicon, tunable resonator," *Journal of Micromechanics and Microengineering,* vol. 5, pp. 257-264, 1995.

[39] W. T. Thomson, *Theory of vibration with applications,* 3rd ed. Englewood Cliffs, N.J.: Prentice-Hall, 1988.

[40] R. Ramlan, M. J. Brennan, and B. R. Mace, "Improving the performance of an energy harvesting device using nonlinearity," *Proceedings of ISMA,* pp. 307-322, 2008.

[41] S. G. Burrow and L. R. Clare, "A Resonant Generator with Non-Linear Compliance for Energy Harvesting in High Vibrational Environments," in *IEEE International Electric Machines & Drives Conference, 2007.*, 2007, pp. 715-720.

[42] D. A. W. Barton, S. G. Burrow, and L. R. Clare, "Energy Harvesting From Vibrations With a Nonlinear Oscillator," *Journal of Vibration and Acoustics,* vol. 132, p. 021009, 2010.

[43] S. C. Stanton, C. C. McGehee, and B. P. Mann, "Reversible hysteresis for broadband magnetopiezoelastic energy harvesting," *Applied Physics Letters,* vol. 95, p. 174103, 2009.

[44] G. Sebald, H. Kuwano, D. Guyomar, and B. Ducharne, "Simulation of a Duffing oscillator for broadband piezoelectric energy harvesting," *Smart Materials and Structures,* vol. 20, p. 075022, 2011.

[45] D. S. Nguyen, E. Halvorsen, G. U. Jensen, and A. Vogl, "Fabrication and characterization of a wideband MEMS energy harvester utilizing nonlinear springs," *Journal of Micromechanics and Microengineering,* vol. 20, p. 125009, 2010.

[46] L. G. W. Tvedt, N. Duy Son, and E. Halvorsen, "Nonlinear Behavior of an Electrostatic Energy Harvester Under Wide- and Narrowband Excitation," *Microelectromechanical Systems, Journal of,* vol. 19, pp. 305-316, 2010.

[47] F. Cottone, H. Vocca, and L. Gammaitoni, "Nonlinear Energy Harvesting," *Physical Review Letters,* vol. 102, pp. 1-4, 2009.

[48] A. Erturk, J. Hoffmann, and D. J. Inman, "A piezomagnetoelastic structure for broadband vibration energy harvesting," *Applied Physics Letters,* vol. 94, p. 3, June 2009.

[49] W. Wu, Y. Chen, B. Lee, J. He, and Y. Peng, "Tunable resonant frequency power harvesting devices," *Smart Structures and Materials 2006: Damping and Isolation,* vol. 6169, pp. 1-8, 2006.

[50] W. Wen-Jong, C. Yi-Fan, C. Yu-Yin, W. Chao-Sheng, and C. Yun-Hsuan, "Smart Wireless Sensor Network Powered by Random Ambient Vibrations," in *IEEE International Conference on Systems, Man and Cybernetics*, 2006, pp. 2701-2708.

[51] C. Peters, D. Maurath, W. Schock, and Y. Manoli, "Novel electrically tunable mehcanical resonator for energy harvesting," in *Technical Digest PowerMEMS 2008*, Sendai, Japan, 2008.

[52] C. Peters, D. Maurath, W. Schock, F. Mezger, and Y. Manoli, "A closed-loop wide-range tunable mechanical resonator for energy harvesting systems," *Journal of Micromechanics and Microengineering,* vol. 19, pp. 1-9, September 2009.

[53] M. Wischke, M. Masur, F. Goldschmidtboeing, and P. Woias, "Electromagnetic vibration harvester with piezoelectrically tunable resonance frequency," *Journal of Micromechanics and Microengineering,* vol. 20, 2010.

[54] M. Lallart, S. R. Anton, and D. J. Inman, "Frequency Self-tuning Scheme for Broadband Vibration Energy Harvesting," *Journal of Intelligent Material Systems and Structures*, vol. 21, pp. 897-906, 2010.

[55] A. Cammarano, S. G. Burrow, D. A. W. Barton, A. Carrella, and L. R. Clare, "Tuning a resonant energy harvester using a generalized electrical load," *Smart Materials and Structures*, vol. 19, 2010.

[56] C. Cabuz, K. Fukatsu, H. Hashimoto, S. Shoji, T. Kurabayashi, K. Minami, and M. Esashi, "Fine frequency tuning in resonant sensors," *IEEE Workshop on Micro Electro Mechanical Systems, 1994, MEMS '94*, pp. 245-250, 1994.

[57] G. Piazza, R. Abdolvand, and F. Ayazi, "Voltage-tunable piezoelectrically-transduced single-crystal silicon resonators on SOI substrate," *IEEE The*

Sixteenth Annual International Conference on Micro Electro Mechanical Systems, 2003. MEMS-03, pp. 149-152, 2003.

[58] D. Scheibner, J. Mehner, D. Reuter, U. Kotarsky, T. Gessner, and W. Dotzel, "Characterization and self-test of electrostatically tunable resonators for frequency selective vibration measurements," *Sensors and Actuators A: Physical,* vol. 111, pp. 93-99, 2004.

[59] E. S. Leland and P. K. Wright, "Resonance tuning of piezoelectric vibration energy scavenging generators using compressive axial preload," *Smart Materials and Structures,* vol. 15, pp. 1413-1420, 2006.

[60] V. R. Challa, M. G. Prasad, Y. Shi, and F. T. Fisher, "A vibration energy harvesting device with bidirectional resonance frequency tunability," *Smart Materials and Structures,* vol. 17, pp. 1-10, 2008.

[61] C. Eichhorn, F. Goldschmidtboeing, and P. Woias, "A Frequency Tunable Piezoelectric Energy Converter Based on a Cantilever Beam," in *Technical Digest PowerMEMS 2008,* Sendai, Japan, 2008, pp. 309-312.

[62] C. Eichhorn, F. Goldschmidtboeing, and P. Woias, "Bidirectional frequency tuning of a piezoelectric energy converter based on a cantilever beam," *Journal of Micromechanics and Microengineering,* vol. 19, p. 6, 2009.

[63] X. Wu, J. Lin, S. Kato, K. Zhang, T. Ren, and L. Liu, "A frequency adjustable vibration energy harvester," in *Technical Digest PowerMEMS 2008,* Sendai, Japan, 2008, pp. 245-248.

[64] D. J. Morris, J. M. Youngsman, M. J. Anderson, and D. F. Bahr, "A resonant frequency tunable, extensional mode piezoelectric vibration harvesting mechanism," *Smart Materials and Structures,* vol. 17, 2008.

[65] L. Ji-Tzuoh, W. Jones, B. Alphenaar, X. Yang, and D. Alphenaar, "Passive magnetic coupling to enhance piezoelectric cantilever response in energy scavenging applications," *17th IEEE International Symposium on the Applications of Ferroelectrics,* pp. 1-2, 2008.

[66] D. Zhu, S. Roberts, M. J. Tudor, and S. P. Beeby, "Closed Loop Frequency Tuning of a Vibration-Based Micro-Generator," in *Technical Digest PowerMEMS 2008,* Sendai, Japan, 2008, pp. 229-232.

[67] M. O. Mansour, M. H. Arafa, and S. M. Megahed, "Resonator with magnetically adjustable natural frequency for vibration energy harvesting," *Sensors and Actuators A: Physical,* vol. 163, pp. 297-303, 2010.

[68] P. Mitcheson, T. Green, and E. Yeatman, "Power processing circuits for electromagnetic, electrostatic and piezoelectric inertial energy scavengers," *Microsystem Technologies,* vol. 13, pp. 1629-1635, 2007.

[69] L. R. Clare and S. G. Burrow, "Power conditioning for energy harvesting," *Active and Passive Smart Structures and Integrated Systems 2008,* vol. 6928, pp. 1-13, 2008.

[70] R. D'hulst, T. Sterken, R. Puers, and J. Driesen, "Requirements for Power Electronics used for Energy Harvesting Devices," in *Technical Digest PowerMEMS 2005,* Tokyo, Japan, 2005, pp. 53-56.

[71] J. F. Dickson, "On-chip high-voltage generation in MNOS integrated circuits using an improved voltage multiplier technique," *Solid-State Circuits, IEEE Journal of,* vol. 11, pp. 374-378, 1976.

[72] F. Pan and T. Samaddar, *Charge pump circuit design*. New York: McGraw-Hill, 2006.

[73] J. S. Brugler, "Theoretical performance of voltage multiplier circuits," *IEEE Journal of Solid-State Circuits*, vol. 6, pp. 132-135, 1971.

[74] R. N. Torah, M. J. Tudor, K. Patel, I. N. Garcia, and S. P. Beeby, "Autonomous Low Power Microsystem Powered by Vibration Energy Harvesting," in *IEEESensors 2007*, Atlanta, US, 2007, pp. 264-267.

[75] C. Saha, T. O'Donnell, J. Godsell, L. Carlioz, N. Wang, P. Mccloskey, S. Beeby, J. Tudor, and R. Torah, "Step-up converter for electromagnetic vibrational energy scavenger," in *Dans Symposium on Design, Test, Integration and Packaging of MEMS/MOEMS - DTIP 2007*, Stresa, Italy, 2008.

[76] D. Maurath, M. Ortmanns, and Y. Manoli, "Adaptive power extraction from micro generators with implicit voltage up-conversion," in *Technical Digest PowerMEMS 2007*, Freiburg, Germany, 2007, pp. 351-354.

[77] D. Maurath, M. Ortmanns, and Y. Manoli, "High efficiency, low-voltage and self-adjusting charge pump with enhanced impedance matching," *51st Midwest Symposium on Circuits and Systems*, pp. 189-192, 2008.

[78] M. D. and M. Y., "CMOS-Integrated adaptive load matching interface with an integrated load matching detector," in *Technical Digest PowerMEMS 2009*, Washington DC, USA, 2009, pp. 217-220.

[79] D. Maurath and Y. Manoli, "A self-adaptive switched-capacitor voltage converter with dynamic input load control for energy harvesting," in *ESSCIRC, 2009. ESSCIRC '09. Proceedings of*, 2009, pp. 284-287.

[80] T. Taithongchai and E. Leelarasmee, "Adaptive electromagnetic energy harvesting circuit for wireless sensor application," in *6th International Conference on Electrical Engineering/Electronics, Computer, Telecommunications and Information Technology*, 2009, pp. 278-281.

[81] S. Dwari and L. Parsa, "Efficient low voltage direct AC/DC converters for self-powered wireless sensor nodes and mobile electronics," in *IEEE 30th International Telecommunications Energy Conference*, 2008, pp. 1-7.

[82] C. Xinping, C. Wen-Jen, K. Ya-Chin, and A. Y.-K. L. Yi-Kuen Lee, "Electromagnetic Energy Harvesting Circuit With Feedforward and Feedback DC–DC PWM Boost Converter for Vibration Power Generator System," *IEEE Transactions on Power Electronics*, vol. 22, pp. 679-685, 2007.

[83] G. K. Ottman, H. F. Hofmann, A. C. Bhatt, and G. A. A. L. G. A. Lesieutre, "Adaptive piezoelectric energy harvesting circuit for wireless remote power supply," *IEEE Transactions on Power Electronics*, vol. 17, pp. 669-676, 2002.

[84] G. K. Ottman, H. F. Hofmann, and G. A. Lesieutre, "Optimized piezoelectric energy harvesting circuit using step-down converter in discontinuous conduction mode," *Power Electronics, IEEE Transactions on*, vol. 18, pp. 696-703, 2003.

[85] N. Kong, T. Cochran, H. Dong Sam, L. Hung-Chih, and D. J. Inman, "A self-powered power management circuit for energy harvested by a piezoelectric cantilever," in *Applied Power Electronics Conference and Exposition (APEC), 2010 Twenty-Fifth Annual IEEE*, 2010, pp. 2154-2160.

[86] S. Xu, K. D. T. Ngo, T. Nishida, G. Chung, and A. Sharma, "Converter and controller for micro-power energy harvesting," in *Applied Power Electronics*

Conference and Exposition, 2005. APEC 2005. Twentieth Annual IEEE, 2005, pp. 226-230 Vol. 1.

[87] C. Richard, D. Guyomar, D. Audigier, and G. Ching, *Semi-passive damping using continuous switching of a piezoelectric device* vol. 3672: SPIE, 1999.

[88] A. Badel, A. Benayad, E. Lefeuvre, L. Lebrun, C. Richards, and D. Guyomar, "Single crystals and nonlinear process for outstanding vibration-powered electrical generators," *Ultrasonics, Ferroelectrics and Frequency Control, IEEE Transactions on,* vol. 53, pp. 673-684, 2006.

[89] M. Lallart and D. Guyomar, "An optimized self-powered switching circuit for non-linear energy harvesting with low voltage output," *Smart Materials and Structures,* p. 035030, 2008.

[90] E. Lefeuvre, A. Badel, C. Richard, L. Petit, and D. Guyomar, "A comparison between several vibration-powered piezoelectric generators for standalone systems," *Sensors and Actuators A: Physical,* vol. 126, pp. 405-416, 2006.

[91] D. Guyomar, A. Badel, E. Lefeuvre, and C. Richard, "Toward energy harvesting using active materials and conversion improvement by nonlinear processing," *IEEE Transactions on Ultrasonics, Ferroelectrics and Frequency Control,* vol. 52, pp. 584-595, 2005.

[92] Mitcheson P D and Tzern T T, "Power Management Electronics," in *Energy Harvesting for Autonomous Systems*, Beeby S P and N. M. White, Eds., ed: Artech House Publishers, 2010, pp. 159-209.

[93] M. Lallart, L. Garbuio, L. Petit, C. Richard, and D. Guyomar, "Double synchronized switch harvesting (DSSH): a new energy harvesting scheme for efficient energy extraction," *IEEE Transactions on Ultrasonics, Ferroelectrics and Frequency Control,* vol. 55, pp. 2119-2130, 2008.

[94] E. Lefeuvre, D. Audigier, C. Richard, and D. A. G. D. Guyomar, "Buck-Boost Converter for Sensorless Power Optimization of Piezoelectric Energy Harvester," *IEEE Transactions on Power Electronics*, vol. 22, pp. 2018-2025, 2007.

[95] M. Belleville, E. Cantatore, and H. Fanet, "Energy autonomous systems : future trends in devices, technology, and systems," CATRENE. Working Group on Energy Autonomous Systems 2009.

[96] *Vibration Energy Scavenging ('VIBES').* Available: http://www.vibes.ecs.soton.ac.uk/

[97] S. W. Arms, C. P. Townsend, D. L. Churchill, J. H. Galbreath, and S. W. Mundell, "Power management for energy harvesting wireless sensors," *Smart Structures and Materials 2005: Smart Electronics, Mems, Biomems, and Nanotechnology,* vol. 5763, pp. 267-275, 2005.

[98] A. Chandrakasan, R. Min, M. Bhardwaj, S. Cho, and A. Wang, "Power Aware Wireless Microsensor Systems," *Proceeding of the 32nd European Solid-State Device Research Conference, 2002,* pp. 37-44, 2002.

[99] *HaydonKerk Motion Solutions 1500 Series linear stepper motor datasheet.* Available: http://www.hsi-inc.com/ accessed 12/Dec/2008

[100] F. Simjee and P. H. Chou, "Everlast: Long-life, Supercapacitor-operated Wireless Sensor Node," *Proceedings of the 2006 International Symposium on Low Power Electronics and Design, 2006.*, pp. 197-202, 2006.

[101] *Panasonic Gold Capacitors Technical Guide*. Available: http://www.panasonic.com/industrial/components/pdf/goldcap_tech-guide_052505.pdf

[102] *CAP-XX Ltd.* Available: http://www.cap-xx.com/index.php

[103] *A Holistic Approach to Energy Harvesting Electronics*. Available: http://www.holistic.ecs.soton.ac.uk/

[104] M. J. Brennan, "Some recent developments in adaptive tuned vibration absorbers/neutralisers," *Shock and Vibration*, vol. 13, pp. 531-543, 2006.

[105] "PIC16F882/883/884/886/887 Data Sheet," *Microchip Technology Inc.*, 2008.

[106] "MPLAB IDE User's Guide with MPLAB Editor and MPLAB SIM Simulator," ed: Microchip Technology Inc., 2009, p. 352.

[107] N. G. Stephen, "On energy harvesting from ambient vibration," *Journal of Sound and Vibration*, vol. 293, pp. 409-425, 2006.

[108] J. N. Ross, *The essence of power electronics*. London ; New York: Prentice Hall, 1997.

[109] *MSP430 Wireless Development Tool*. Available: http://www.ti.com/tool/ez430-rf2500

[110] K. Rao, P. D. Mitcheson, and T. C. Green, "Imperial College Energy-Harvesting Simulator."